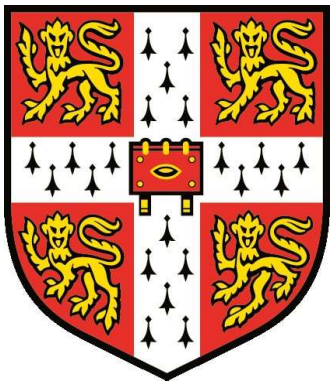
The effect of Alzheimer's disease on cortical microcircuits

Juliette Hélène Lanskey



King's College

University of Cambridge

This thesis is submitted for the degree of Doctor of Philosophy

April 2024

Preface

This thesis is the result of my own work and includes nothing which is the outcome of work done in collaboration except as declared in the preface and specified in the text. It is not substantially the same as any work that has already been submitted, or is being concurrently submitted, for any degree, diploma or other qualification at the University of Cambridge or any other University or similar institution except as declared in the preface and specified in the text. It does not exceed the prescribed word limit for the relevant Degree Committee.

The data used for Chapter 3, Chapter 4, Chapter 5 and Chapter 6 were collected as part of collaborative research studies.

A manuscript related to chapter 2 is published as:

Lanskey, J. H., Kocagoncu, E., Quinn, A. J., Cheng, Y. J., Karadag, M., Pitt, J., Lowe, S., Perkinton, M., Raymont, V., Singh, K. D., Woolrich, M., Nobre, A. C., Henson, R. N., & Rowe, J. B. (2022). New Therapeutics in Alzheimer's Disease Longitudinal Cohort study (NTAD): study protocol. BMJ Open, 12(12), e055135. https://doi.org/10.1136/BMJOPEN-2021-055135

A manuscript related to chapter 4 has been posted to medRxiv as:

Lanskey, J. H., Jafarian, A., Karadag, M., Kocagoncu, E., Williams, R., Yadav, P., Quinn, A. J., Pitt, J., Thayanandan, T., Lowe, S., Perkinton, M., Timmers, M., Raymont, V., Singh, K. D., Woolrich, M., Nobre, A. C., Henson, R. N., Rowe, J. B., (2024) The effect of Alzheimer's disease and its progression on pyramidal cell gain and connectivity.

A manuscript related to chapter 5 is currently in preparation as:

Lanskey, J. H., Jafarian, A., Karadag, M., Kocagoncu, E., Nobre, A. C., Raymont, V., Singh, K. D., Woolrich, M., Henson, R. N., Rowe, J. B., (2024) NMDA-channel kinetics of people living with Alzheimer's disease.

A manuscript related to chapter 6 is currently in preparation as:

Lanskey, J. H., Jafarian, A., Hughes, L., Karadag, M., Kocagoncu, E., Rouse, M., Adams, N., Naessens, M., Singh, K. D., Henson, R. N., Rowe, J. B., (2024) Memantine and Alzheimer's disease effects on NMDA-receptor blockade: non-invasive *in vivo* insights from magnetoencephalography.

Abstract

There is a pressing need to facilitate and accelerate new treatments for Alzheimer's disease. An improved mechanistic understanding of the human disease will facilitate new treatments. Human pathophysiological biomarkers sensitive to treatment and disease mechanisms will help accelerate such new treatments. To this end, biophysically-informed dynamic causal models can support inferences around laminar and cell-specific disease effects from human non-invasive imaging. This thesis aims to use dynamic causal models to elucidate cellular-level effects of Alzheimer's disease on cognition to (i) improve our understanding of disease mechanisms and (ii) identify mechanistically-informative biomarkers for interventional studies.

The objectives of my thesis are to: (i) assess the reliability and sensitivity of magnetoencephalography evoked responses from a mismatch negativity paradigm to the severity and progression of Alzheimer's disease and to employ dynamic causal modelling to (ii) reproduce these neurophysiological responses, (iii) test hypotheses of cellular-level disease effects in people living with Alzheimer's disease based on preclinical- and *post mortem*-derived findings and (iv) to investigate how Alzheimer's disease, its severity and progression affect cells, neurotransmitter systems and cortical networks underlying cognition.

This thesis first details the study protocol used for the data collection of the primary study used in this thesis (the New Therapeutics in Alzheimer's disease study, NTAD, PMCID: PMC9756184). NTAD is a multi-site project which aims to assess magnetoencephalography as a potential biomarker platform for experimental medicine studies of novel compounds. To this end, NTAD includes clinical, cognitive and neuroimaging measures from participants with mild cognitive impairment or early dementia from Alzheimer's disease and neurologically-healthy control participants. The analyses herein use baseline, test-retest and 16-month follow up data from the Cambridge NTAD cohort.

Group comparisons of the NTAD Cambridge cohort confirmed clinical, cognitive and anatomical changes typical of mild cognitive impairment and early Alzheimer's dementia. For magnetoencephalography, sensor-level analyses demonstrated attenuated mismatch negativity responses from 140ms to 160ms for people with Alzheimer's disease. Mismatch negativity responses were more attenuated when disease was more severe (lower Mini-Mental State

Examination scores) and after annual follow up (follow up versus baseline). An absolute, intraclass correlation model of the test-retest mismatch negativity amplitude illustrated excellent reliability. To be suitable as a biomarker platform, magnetoencephalography must be reliable and sensitive to disease. Magnetoencephalography biomarkers should ideally also be informative about disease mechanisms at the level of cortical microcircuits and their cells or receptors. The cortical generators underlying the neurophysiological deficit are assessed in chapters 4, 5 and 6.

Chapter 4 tests the hypothesis that Alzheimer's disease affects the gain and connectivity of pyramidal cells. The analysis used in this chapter inverts a dynamic causal model[1] with pyramidal cell gain and pyramidal cell extrinsic connectivity parameters to evoked magnetoencephalographic responses to the mismatch negativity task. I confirm that superficial pyramidal cell gain modulation and extrinsic connectivity between pyramidal cells are reduced in Alzheimer's disease and reduce further over time.

Chapter 5 reports how Alzheimer's disease affects channel time constants and channel-mediated signalling. I inverted dynamic causal models with ion channel parameters to magnetoencephalographic responses to the mismatch negativity task. This analysis confirms that abnormal NMDA-channel function explains the neurophysiological deficit, more than AMPA or GABA channel changes. Alzheimer's disease progressively changes NMDA channel time constants in primary auditory and inferior frontal regions.

Chapter 6 examines the ability of dynamic causal models to identify the mechanism of action of a currently licenced medication for Alzheimer's disease, memantine. To do this, I use magnetoencephalography data recorded during mismatch negativity paradigms from (1) neurologically-healthy people from a double-blind placebo-controlled crossover study of the NMDA antagonist memantine and (2) people with Alzheimer's disease and controls from the Cambridge NTAD study. I first tested where memantine acts in the canonical microcircuit by inverting dynamic causal models to evoked responses from healthy controls on placebo versus memantine. Next, I assessed how the strength of this blockade affects cognitive function and whether it is affected by Alzheimer's disease progression. I confirm in humans that memantine increases and Alzheimer's disease decreases NMDA-receptor inhibition.

[1] Model inversion estimates the model parameters that describe neural activity underlying scalp responses.

The biomarkers identified in this thesis are particularly important to the field as they quantify cellular-level effects of disease mechanisms on cognition. These biomarkers could consequently be used by experimental medicine studies to evaluate drug effects on pyramidal cell and NMDA channel function that underlie neurophysiological deficits. Future studies could similarly tailor biologically-informed models to identify novel targets-of-interest and assess their relationship with disease severity and progression. Therapeutic target-engagement and effect on cognition could then be measured to determine the potential of novel therapeutics. The techniques used and biomarkers identified in this thesis, that quantify cellular properties of an individual, could inform personalised treatment plans in clinic. Future studies could determine whether these techniques can accurately determine which therapeutics, or therapeutic combination, are most beneficial to a patient. These techniques could similarly be applied to identify cellular-level disease effects underlying performance in other cognitive tasks. For example, in the NTAD study, magnetoencephalography was recorded in tasks assessing episodic memory and paired associates learning. These cognitive domains are affected early in the course of Alzheimer's disease. As such, disease mechanisms underlying poorer performance in these tasks may be early markers of cognitive involvement in Alzheimer's disease. Future studies could therefore apply the techniques illustrated in this thesis to identify biomarkers that provide insight into disease mechanisms affecting cognitive performance in other domains.

In conclusion, this thesis uses mechanistic modelling to identify disease effects on the cortical microcircuit that can explain the observed neurophysiological deficit. In line with preclinical and pathological findings, the mechanistic modelling confirmed hypotheses that in Alzheimer's disease there is reduced pyramidal cell connectivity, impaired NMDA-channel kinetics and opposing effects on the cortical microcircuit of disease and its therapeutics.

Acknowledgements

I am immensely grateful to the large number of people who have helped me with this work.

Thank you to Professor James Rowe who struck the perfect balance between giving me the tools to learn and freedom to develop my scientific skills. He has been a constant source of inspiration, knowledge and invaluable support. Thank you to my advisor, Professor Rik Henson, whose swift and sharp advice vastly improved my analyses. I have benefited hugely from the teachings and advice of Dr Amirhossein Jafarian. He provided the foundation to not only learn about, but to develop a keen interest in dynamic causal modelling. Thank you to the NTAD team for all their help with the NTAD study which forms an integral part of this thesis. I am especially grateful to Melek Karadag for her help with participant recruitment and data collection. Thank you to the participants for the time and dedication they generously gave to this research, without whom advancing dementia research would be impossible. It has been an honour to work with them towards this aim.

There have been a great number of people I have had the pleasure of working with and learning from including every member of the Rowe lab group, internal and external dynamic causal modelling experts, and colleagues and friends from the MRC Cognition and Brain Sciences unit. The benefits of working in the inspiring environments of the MRC Cognition and Brain Sciences unit and King's College Cambridge were made especially poignant when access was restricted by Covid-19 lockdowns. Thank you to the Medical Research Council who funded my PhD studentship.

I am, and always will be, grateful for the limitless support my family has given me. Thank you, especially, to my parents. Even more valuable than their academic insight, has been their unwavering support. Thank you to my siblings, Rachel and Luke, for keeping me company through life's many adventures. This thesis has been inspired as much by books and papers as from personal experience over these past few years. I am immensely grateful for all the fire-side teas with Granny, with Grandpa always in our hearts; Australian ice-creams with Grandma and Granddad; and wind-swept walks and talks with my wider family and friends.

I am especially grateful to my husband, Colin, for being beside me through it all. Thank you.

Table of Contents

Preface i
Abstract ii
Acknowledgements v
Table of Contents vi
List of Figures viii
List of Tables ix
List of Supplementary Figures x
List of Supplementary Tables xi
Abbreviations xii
Chapter 1 | General introduction 1
1.1 Canonical and emerging concepts of Alzheimer's disease research 2
1.2 The neurophysiology of Alzheimer's disease 6
1.3 The mismatch negativity task 9
1.4 Effect of Alzheimer's disease on cortical microcircuits 13
1.5 Dynamic causal modelling 14
1.6 Aims of the thesis 19
Chapter 2 | The New Therapeutics in Alzheimer's Disease Longitudinal Cohort study (NTAD): study protocol 22
2.1 Introduction 23
2.2 Methods 26
2.3 Study procedures 30
2.4 Ethics and dissemination 42
Chapter 3 | Describing the NTAD Cambridge cohort 43
3.1 Introduction 44
3.2 Methodology 46
3.3 Results 49
3.4 Discussion 60
Chapter 4 | The effect of Alzheimer's disease and its progression on pyramidal cell gain and connectivity 65
4.1 Introduction 67
4.2 Materials and methods 69
4.3 Results 75
4.4 Discussion 79
Appendix A: Supplementary materials for Chapter 4 87
Chapter 5 | NMDA-channel kinetics of people living with Alzheimer's disease 96
5.1 Introduction 97
5.2 Materials and methods 98

5.3 Results 103
5.4 Discussion 107
Appendix B: Supplementary materials for Chapter 5 113

Chapter 6 | Memantine and Alzheimer's disease effects on NMDA-receptor blockade: non-invasive *in vivo* insights from magnetoencephalography 117
6.1 Introduction 118
6.2 Methods 119
6.3 Results 125
6.4 Discussion 129
Appendix C: Supplementary materials for Chapter 6 134

Chapter 7 | General Discussion 138
7.1 Summary of the principal findings 139
7.2 Basic measures of Alzheimer's disease 143
7.3 Dynamic causal modelling for assessment of cortical microcircuits 145
7.4 Effect of Alzheimer's disease on pyramidal cell connectivity and NMDA channels 147
7.5 Mechanistically-informative biomarkers for clinical trials 150
7.6 General limitations and future directions 151
7.7 Concluding remarks 154

Bibliography 155

List of Figures

Figure 1.1 Pathological changes occur prior to cognitive decline in Alzheimer's disease. 5
Figure 1.2 The roving auditory mismatch negativity paradigm. 11
Figure 1.3 Generative model of brain function. 16
Figure 2.1 Participant flow chart 27
Figure 2.2 Study effect sizes by sample size 29
Figure 2.3 Timeline summary of study procedures 31
Figure 2.4 NTAD magneto/electroencephalography tasks 38
Figure 3.1 Clinical test scores for people with Alzheimer's disease compared to controls. 51
Figure 3.2 Alzheimer's pathology for controls versus people with Alzheimer's disease at baseline 52
Figure 3.3 Correlations between fluidic and CSF biomarkers for controls and patients 53
Figure 3.4 Scree plot showing percentage of variance explained by principal components 54
Figure 3.5 Principal component scores for controls and patients at baseline, and patients at follow up. 55
Figure 3.6 Alzheimer's disease progressively affects total brain volume. 55
Figure 3.7 Voxel-based morphometry of T1-weighted MRI images 56
Figure 4.1 Scalp responses to the mismatch negativity task. 76
Figure 4.2 Defining the model structure. 77
Figure 4.3 Gain of the superficial pyramidal cell self-inhibition and the effect of disease and progression. 78
Figure 4.4 The effect of disease presence and progression on extrinsic superficial and deep pyramidal cell connectivity. 79
Figure 5.1 The conductance based dynamic causal model with NMDA parameters. 100
Figure 5.2 Model fits 101
Figure 5.3 Mismatch negativity waveforms. 104
Figure 5.4 Relative free energy of PEB models with AMPA, GABA or NMDA parameters 105
Figure 5.5 Model space over which Bayesian model comparisons were run. 106
Figure 5.6 Results from the Bayesian model comparison and averaging. 107
Figure 6.1 Mismatch negativity responses 126
Figure 6.2 The generative canonical microcircuit conductance model with NMDA channel blockade parameters and the mechanism of memantine. 127
Figure 6.3 NMDA channel blockade is affected by Alzheimer's disease in right parietal cortex 129

List of Tables

Table 2.1 Group inclusion criteria and general exclusion criteria.....28
Table 2.2 Blood sample processing guidelines 32
Table 2.3 Order of neuropsychological assessments.....37
Table 2.4 Order and parameters of MRI sequences. 42
Table 3.1 Participant demographics and screening data 50
Table 3.2 Loadings of principal components of the neuropsychological data. 54
Table 3.3 Grey matter atrophy of participants with Alzheimer's disease compared to controls. 57
Table 3.4 Grey matter atrophy associated with patient neuropsychological severity.....59
Table 3.5 Grey matter atrophy of participants with Alzheimer's disease at 16-month follow up compared to baseline. 59
Table 4.1 Participant demographics and clinical data 75
Table 5.1 Participant demographics and screening data. 103
Table 6.1 Memantine-placebo control participant demographics. 120
Table 6.2 NTAD patient participant demographics.....120

List of Supplementary Figures

Supplementary Figure A.1 Predicted (grey) and observed (teal) evoked responses to the deviant tone for each subject at baseline 90
Supplementary Figure A.2 Predicted (grey) and observed (teal) evoked responses to the deviant tone at longitudinal follow up. 90
Supplementary Figure A.3 Kernel density distribution of correlation coefficients for observed and predicted evoked responses of all sessions and groups and a rug plot with individual points. 90
Supplementary Figure A.4 Regional comparisons of PEB models of superficial pyramidal cell gain modulation. 91
Supplementary Figure A.5 Regional comparisons of PEB models including connections between pyramidal cells of different regions. 92
Supplementary Figure A.6 The effect of disease and its progression on the intrinsic repetition effect. 93
Supplementary Figure A.7 The effect of disease and its progression on extrinsic repetition effects 94
Supplementary Figure A.8 Model comparison of PEB models with intrinsic or extrinsic parameters. 94
Supplementary Figure A.9 Group PEB comparisons controlling for age. 95
Supplementary Figure B.1 Defining the model structure. 113
Supplementary Figure B.2 Kernel density distribution and rug plot of correlation coefficients for observed and predicted evoked responses. 114
Supplementary Figure B.3 Relative free energy of PEB models with AMPA, GABA or NMDA parameters with patients versus controls taking no dementia medication 115
Supplementary Figure B.4 Results from the Bayesian model comparison and averaging with patients versus controls taking no dementia medication. 115
Supplementary Figure C.1 Outliers excluded from sensor level analyses 135
Supplementary Figure C.2 The mismatch response for NTAD participants at baseline. 135
Supplementary Figure C.3 Model fits for the healthy controls from the memantine-placebo study .. 136
Supplementary Figure C.4 Model fits for NTAD patient group 136
Supplementary Figure C.5 Model fits for the healthy controls from the NTAD study 137
Supplementary Figure C.6 The effect of age and group on the NMDA blockade parameter 137

List of Supplementary Tables

Supplementary Table A.1 Parameters of interest from the canonical microcircuit dynamic causal model. 95
Supplementary Table C.1 NTAD control participant demographics..... 134

Abbreviations

A1	Primary Auditory Cortex
ACE-R	Addenbrooke's Cognitive Examination Revised
AD	Alzheimer's Disease
BF	Bayes Factor
CDR	Clinical Dementia Rating
CSF	Cerebrospinal Fluid
DCM	Dynamic Causal Model
EEG	Electroencephalography
F	Free energy
IFG	Inferior Frontal Gyrus
IPC	Inferior Parietal Cortex
MCI	Mild Cognitive Impairment
MEG	Magnetoencephalography
MMN	Mismatch Negativity
MMSE	Mini-Mental State Examination
NTAD	New Therapeutics in Alzheimer's Disease Study
PEB	Parametric Empirical Bayes
PET	Positron emission tomography
PC1	First principal component score
Pp	Posterior parameter probability
STG	Superior Temporal Gyrus
SUVR	Standardized Uptake Value Ratio

1 | General introduction

With 50 million people living with Alzheimer's disease (Scheltens *et al.*, 2021), there is an urgent need for effective treatments that slow or prevent disease progression. There are significant bottlenecks in clinical trials with few effective treatments despite nearly 40 billion pounds (Cummings *et al.*, 2022) and 40 years (Schneider *et al.*, 2014) spent on drug development. To aid clinical trials, better tools are needed to measure the pathophysiological mechanisms of Alzheimer's disease. Such tools will provide evidence of how effective candidate treatments are at targeting disease mechanisms that underlie dementia. This thesis aims to understand and quantify how Alzheimer's disease affects cortical microcircuits, in humans, *in vivo*.

In this chapter, I introduce canonical and emerging concepts of Alzheimer's disease research and the benchmarks needed for future biomarker platforms. I review resting and task-based electroencephalography (EEG) and magnetoencephalography (MEG) studies of Alzheimer's disease. I then describe why I chose to analyse neurophysiological responses to the mismatch negativity task: I detail its suitability for clinical trials, the effect of Alzheimer's disease on mismatch negativity responses and cognitive and cortical mechanisms that may underlie the mismatch negativity. Next, I describe how Alzheimer's disease affects cortical microcircuits, according to animal and *post mortem* findings. I introduce dynamic causal modelling, which aims to quantify disease effects on human, cortical microcircuits *in vivo*. Finally, I outline the thesis aims and structure.

1.1 Canonical and emerging concepts of Alzheimer's disease research

In 1906, Alzheimer's disease was first described by Alois Alzheimer as an 'eigenartige' (strange) illness (Alzheimer, 1907) associated with distinctive extracellular plaques and intracellular neurofibrillary tangles in the brain. The molecular bases of plaques and tangles were later defined as beta-amyloid (Glenner and Wong, 1984) and tau (Kosik *et al.*, 1986). Beta-amyloid plaques and tau tangles are now considered hallmarks of Alzheimer's disease. The subsequent amyloid hypothesis proposed that amyloid is the cause of dementia due to Alzheimer's disease (Hardy and Allsop, 1991). The amyloid plaques also cause an inflammatory response, progressively increasing neuronal injury and disruption to cellular processes. The amyloid-mediated processes in turn trigger hyperphosphorylation, misfolding and aggregation of tau protein. Together, these events lead to neuronal dysfunction and death resulting in cognitive decline and dementia (Hardy and Allsop, 1991; Karran and De Strooper, 2022). The four highest-risk genes of Alzheimer's disease all relate to beta-amyloid production or accumulation. The commonest genetic variant associated with sporadic Alzheimer's disease is apolipoprotein E allele epsilon 4 (APOE4, Saunders 1993). ApoE is involved in beta-amyloid clearance and this process is impaired for APOE4 carriers (Raulin *et al.*, 2022). Genetic mutations of the amyloid precursor protein (APP, Goate, 2006), presenilin 1 (PSEN1) and 2 (PSEN2) cause familial Alzheimer's disease (Rogaev *et al.*, 1995). Whether for production (APP) or processing (PSEN1 and PSEN2) of amyloid precursor proteins, mutations of these genes lead to overexpression of beta-amyloid (Weggen and Beher, 2012).

The amyloid hypothesis puts forward amyloid as the fundamental cause of Alzheimer's disease and its dementia. However, other factors are happening in parallel to beta-amyloid accumulation (Scheltens *et al.*, 2021), including ageing (Lu *et al.*, 2014), neuroinflammation (Venegas *et al.*, 2017) and vascular change (Montagne *et al.*, 2020). Indeed, while genes related to amyloid account for the highest risk associated with Alzheimer's disease, genes associated with the immune response, metabolism, lipid dysfunction, cholesterol, endocytosis and vascular factors also contribute to disease risk (Hardy *et al.*, 2014; Di Marco *et al.*, 2015; Van Cauwenberghe *et al.*, 2016; Naj and Schellenberg, 2017; Bennett *et al.*, 2018; Verheijen and Sleegers, 2018). A polygenic risk score can be calculated based on the presence or absence of these risk alleles, which is able to distinguish between people with and without Alzheimer's disease with around 80% accuracy (Escott-Price *et al.*, 2015). In addition to risk alleles, there are protective genes that reduce the risk of Alzheimer's disease. These include the APOE ε2

allele (Genin *et al.*, 2011) and a mutation of APP (Jonsson *et al.*, 2012). There are also genes with protective effects that regulate neuroinflammation, lipid metabolism, cellular trafficking and synaptic function (Seto *et al.*, 2021). These offer insights into mechanisms that therapeutics can target to potentially protect cognition.

Beta-amyloid is a precursor to the spread of tau pathology in Alzheimer's disease (Price and Morris, 1999; Price *et al.*, 2009; Wang *et al.*, 2016; Hanseeuw *et al.*, 2019; Long and Holtzman, 2019; Pontecorvo *et al.*, 2019) and facilitates its toxic effects (Tomidokoro *et al.*, 2001; Götz *et al.*, 2019). The spread of tau pathology across the brain has a clear link with cognitive decline (Arriagada *et al.*, 1992; Pontecorvo *et al.*, 2017; Adams *et al.*, 2019) and clinical presentations of Alzheimer's disease (Ossenkoppele *et al.*, 2016). Indeed, impairment of cognitive domains mirror tau insult to brain regions underlying domain-specific function, e.g. episodic memory, medial temporal lobe; executive functions, frontoparietal regions; and visuospatial functions, occipitotemporal regions (Bejanin *et al.*, 2017). Tau has direct and atrophy-mediated effects on cognitive domains (Bejanin *et al.*, 2017).

Cognitive decline has long been associated with neurodegeneration (Fox and Schott, 2004). Relatively late in the disease pathogenesis, advanced stages of neurodegeneration can be measured non-invasively by brain imaging of grey matter atrophy**.** Atrophy of the hippocampus and entorhinal cortex is particularly severe in Alzheimer's disease (van Hoesen *et al.*, 1991; Knight *et al.*, 2016). The parietal cortex is also affected relatively early in the clinical stages of the illness, with atrophy (Knight *et al.*, 2016) and amyloid pathology (Villeneuve *et al.*, 2015; Busche and Hyman, 2020).

Biomarker evidence can be categorised according to these three hallmarks of Alzheimer's disease; amyloid, tau and neurodegeneration (as A, T, N; Jack *et al.*, 2018). Amyloid and tau provide first-tier evidence which can be used for Alzheimer's disease diagnosis and staging (Therriault *et al.*, 2024). Biomarkers for the amyloid and tau hallmarks, and other measures of Alzheimer's disease like inflammation, can be obtained from cerebrospinal fluid (Maji *et al.*, 2010) and PET imaging (Bucci *et al.*, 2021). Recent work has further shown the potential of blood-based biomarkers (Ashton *et al.*, 2024), which mirror established biomarkers and are more accessible than PET or CSF biomarkers (Hudd *et al.*, 2019).

Diagnostic concepts have also evolved over time. In the 1980s, the diagnosis of Alzheimer's disease developed from being based purely on histopathology to being based on medical history

and neurological examination (McKhann *et al.*, 1984; Knopman *et al.*, 2019). In 1984, clinical diagnostic criteria for Alzheimer's disease were established to define 'probable' Alzheimer's disease (McKhann *et al.*, 1984). This definition only included people with dementia (defined as progressive cognitive impairment interfering with daily functioning). The term 'mild cognitive impairment' was consequently used to define people who had cognitive impairment with normal daily function (Morris *et al.*, 2001). In 2011, revised criteria recommended incorporating biomarker evidence when determining the certainty that 'mild cognitive impairment' or dementia was due to Alzheimer's disease (Albert *et al.*, 2011; McKhann *et al.*, 2011). This focus on biomarkers was further developed within the ATN research framework in 2018 (Jack *et al.*, 2018). In 2023, a steering committee convened by the Alzheimer's Association drafted revised diagnostic criteria (Alzheimer's Association, 2023). These current guidelines recommend defining and staging Alzheimer's disease biologically, using core biomarkers, rather than using the previous syndromic descriptions of 'cognitively unimpaired', 'mild cognitive impairment' and 'dementia' (Jack *et al.*, 2018; Scheltens *et al.*, 2021). This is because Alzheimer's disease can be considered a continuum with preclinical and clinical stages. Continuous biomarkers are more suitable for measuring continuous disease severity (Jack *et al.*, 2018). Additionally, neuropathological changes are proposed to occur and progress years before symptom onset (see Figure 1.1) allowing definition of presymptomatic disease severity. Methods established for autopsy-staging, typically as Braak stages 0-6, can be approximated by *in vivo* brain imaging markers (Jack *et al.*, 2010; Therriault *et al.*, 2024).

One reason for defining Alzheimer's disease severity using biomarker evidence, rather than later-onset clinical symptoms, is to identify Alzheimer's disease in its earliest stages. This is when treatments may have the best chance of delaying and reducing clinical symptoms. People with 'early-stage' clinical symptoms of Alzheimer's disease (Mintun *et al.*, 2021; Budd Haeberlein *et al.*, 2022) usually already have relatively severe pathological changes. This has been proposed as a contributor to the weak or absent benefits from clinical trials of anti-amyloid therapies (Therriault *et al.*, 2024). *Post mortem* examination of a patient treated with the anti-amyloid therapy, aducanumab, revealed continuing and severe pathological insult by tau, at Braak stages V-VI (Plowey *et al.*, 2022). This was despite successful amyloid clearance. As clinical symptoms occur many years after disease onset (see Figure 1.1), such treatments may have been administered at a sub-optimal time (Tian Hui Kwan *et al.*, 2021).

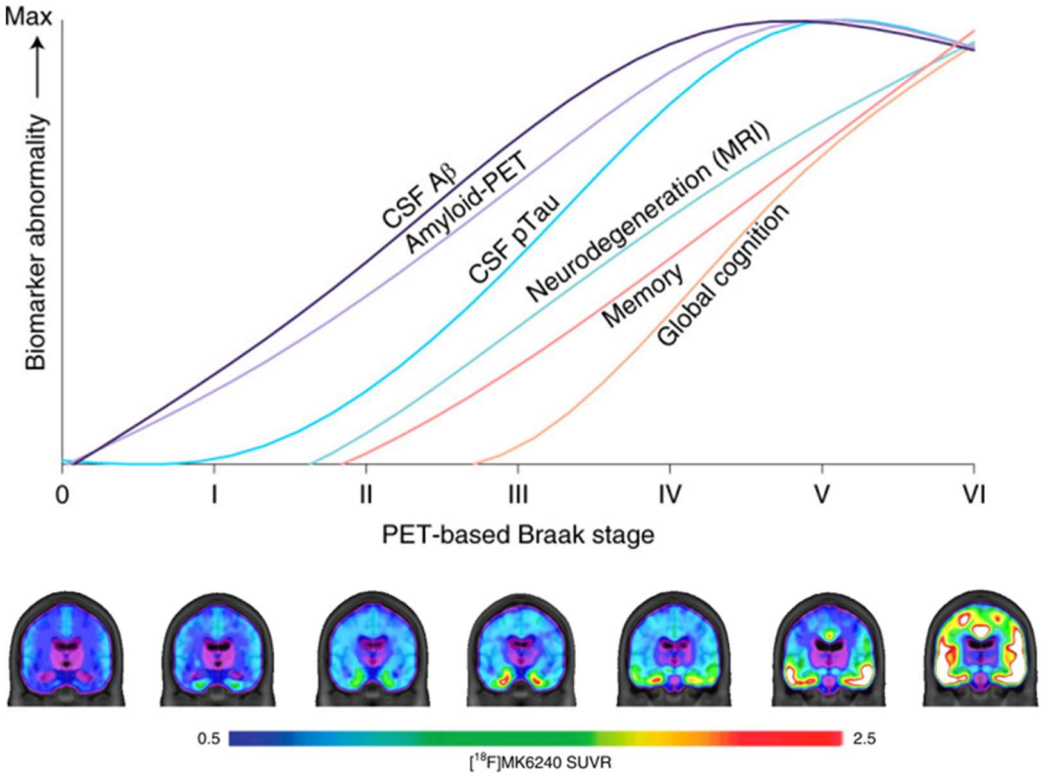


Figure 1.1 Pathological changes occur prior to cognitive decline in Alzheimer's disease.
Pathological changes can be used to stage the disease similarly to established methods used at autopsy. CSF, cerebrospinal fluid; Aβ, amyloid-β; PET, positron emission tomography; SUVR, standardised uptake value ratio. Adapted from (Therriault et al., 2022) CC BY 4.0 (https://creativecommons.org/licenses/by/4.0/).

In 2022, aducanumab was the first drug licenced to treat Alzheimer's disease since 2003 and the first licenced with the intention of modifying the course of the underlying disease. In 2023, lecanemab was also granted FDA approval. Both agents target and remove amyloid. Prior to the approval of aducanumab, licensed therapeutics were symptomatic. The majority targeted the cholinergic systems that are severely affected in Alzheimer's disease (Davies and Maloney, 1976). Current clinical trials are assessing new symptomatic treatments that aim to enhance cognition primarily by targeting neurotransmitter receptors (Cummings *et al.*, 2023). However, around 80% of current clinical trials are assessing disease-modifying treatments, rather than purely symptomatic treatments (Cummings *et al.*, 2023). Targets of the disease-modifying drugs in current phase 1, 2, and 3 clinical trials include amyloid, tau, inflammation, synaptic plasticity, and circuits and metabolism (Cummings *et al.*, 2023). While these therapeutics may not directly target cognitive mechanisms of dementia, they will hopefully target driving disease mechanisms that lead to cognitive decline. For example, amyloid and tau reduce synapse

density and function (Shankar *et al.*, 2007; Mijalkov *et al.*, 2021). Synaptic loss is strongly associated with cognitive impairments (Kashyap *et al.*, 2019). By modifying neuropathological changes, cognitive and clinical symptoms might be delayed or prevented.

The purpose of earlier-phase trials is to explore novel therapeutic mechanisms and to support 'proof of concept' (Cummings *et al.*, 2023). High-profile and expensive failures of clinical trials of Alzheimer's disease treatments (Cummings *et al.*, 2017; Mehta *et al.*, 2017) illustrate the need for better go/no-go evidence at earlier stages of drug development, especially in the transition from laboratory to early-phase human studies where attrition and costs increase markedly (Friedman *et al.*, 2021).

Given the high burden and increasing incidence of Alzheimer's disease, better go/no-go evidence is needed to accelerate clinical trials and reduce their risk and cost. This led to the creation of the New Therapeutics in Alzheimer's disease (NTAD) consortium, within the Dementias Platform UK. NTAD aims to derisk drug development by testing MEG as a potential biomarker platform for experimental medicine studies of novel compounds. This longitudinal study with human participants evaluates MEG biomarkers of disease mechanisms.

There are benchmarks that a biomarker platform must meet. First, the biomarkers must be sensitive to the presence of Alzheimer's disease, its severity and its progression. It should also be reliable in test-retest assessments to ensure any change with drug or time can be detected with high sensitivity (reliability is directly linked to power, in repeated measures designs). The assessments should be applicable and feasible. A good biomarker is also well-tolerated by participants, safe and scalable at least to the degree required for early phase trials. Finally, though optional, the biomarker should ideally also reveal disease and cognitive mechanisms underlying dementia.

1.2 The neurophysiology of Alzheimer's disease

Alzheimer's disease affects populations of synaptically-connected neurons and their neurophysiology. This underlies the potential of MEG to detect the effects of Alzheimer's disease, as follows. Action potentials are the propagation of changes in membrane potential down the axon (Hodgkin and Huxley, 1939). Action potentials allow neurones to transmit information to another. These primary currents occur within a neurone and generate a perpendicular magnetic field. The primary current causes secondary, extracellular currents that

are conducted via a convoluted path to the scalp (López-Sanz *et al.*, 2019). When multiple pyramidal cells fire together, the electric and magnetic fields (of secondary and primary currents, respectively) are detectable by MEG or EEG. Therefore, MEG and EEG measure neuronal activity and are sensitive to pathological changes to neuronal activity.

Since the discovery of the electroencephalogram by Hans Berger (Berger, 1934), EEG studies have illustrated the neurophysiological consequences of Alzheimer's disease. These include a loss of alpha power (Letemendia and Pampiglione, 1958; Gordon and Sim, 1967) and beta rhythms (Weiner and Schuster, 1956; Letemendia and Pampiglione, 1958) and increase in theta and delta rhythms (Coben *et al.*, 1983, 1985; Brenner *et al.*, 1986; Giaquinto and Nolfe, 1986). These EEG measures correlate with dementia severity (Shanmugham *et al.*, 1989; Lejko *et al.*, 2020), cognitive decline (Hata *et al.*, 2016; Baik *et al.*, 2022) and disease progression (Coben *et al.*, 1985). More recent EEG studies have illustrated network disruption (Jeong, 2004), predictive of whether cognitive impairment is due to Alzheimer's disease (Tait *et al.*, 2019). EEG studies have also shown differences in evoked responses between people with and without Alzheimer's disease (Olichney *et al.*, 2008; Chapman *et al.*, 2011; Horvath *et al.*, 2018; Rossini *et al.*, 2020), including in visual (Parra *et al.*, 2012; Jiang *et al.*, 2015; Stothart *et al.*, 2021) and auditory (Bennys *et al.*, 2007; Lee *et al.*, 2013; Howe *et al.*, 2014; Hedges *et al.*, 2016) oddball tasks.

MEG measures the magnetic fields generated by neuronal activity, particularly the flux generated by dendritic currents following post synaptic depolarisation. MEG is more sensitive to tangential sources, typically found in sulci, while EEG is more sensitive to radial sources (Lopes da Silva, 2013; Piastra et al., 2021). However, the relative positioning and distance of sensors to grey matter on superficial versus deep part of gyri or sulci mitigates the differential sensitivity of EEG and MEG to depth and orientation effects (Hillebrand and Barnes, 2002). Currently, EEG is more portable than MEG, and has the potential for home-based measurements (Blackman *et al.*, 2023). MEG fields are less distorted or smoothed by the CSF or skull boundaries, and provide better spatial resolution (Lopes da Silva, 2013) with generally better signal to noise than EEG for cortex (López-Sanz *et al.*, 2019).

MEG analyses have also demonstrated changes to frequency bands associated with Alzheimer's disease. These studies confirm the association of Alzheimer's disease with reduced power of higher frequency signals (Huang *et al.*, 2000; Stam *et al.*, 2002, 2006; De

Haan *et al.*, 2008; Sami *et al.*, 2018) and increased power of lower frequency signals (Huang *et al.*, 2000; Fernández *et al.*, 2002; Engels *et al.*, 2017). This shift towards lower frequencies may in part reflect the cholinergic deficit (Maestú *et al.*, 2015; López-Sanz *et al.*, 2019) and reduced synaptic function (Hindriks and van Putten, 2013). The frequency shift is particularly prominent in parietal, temporal and occipital regions (Engels *et al.*, 2017).

Alzheimer's disease has a specific physiological signature (Sami *et al.*, 2018). In addition to the shift in power for different frequencies, people with Alzheimer's disease have less complex (Gómez *et al.*, 2006; Fernández *et al.*, 2010) and more predictable brain signals than controls (Poza *et al.*, 2007; Escudero *et al.*, 2008). Functional connectivity changes measured with MEG are often reported in temporal and parietal regions (Garcés *et al.*, 2014; Engels *et al.*, 2017; Koelewijn *et al.*, 2017; Buzi *et al.*, 2023) and are associated with genetic dementia risk (Cuesta *et al.*, 2015; Koelewijn *et al.*, 2019), pathological (Canuet *et al.*, 2015; Kocagoncu *et al.*, 2020) and cognitive impairments (Ranasinghe *et al.*, 2014). The distribution of change also correlates with the syndrome – bitemporal deficits in typical amnestic Alzheimer's disease, and parietal deficits in posterior cortical atrophy (Sami *et al.*, 2018). Prior to symptom onset, MEG also detects disrupted functional connectivity (López-Sanz *et al.*, 2018), associated with amyloid pathology (Nakamura *et al.*, 2017) and the APOE4 risk allele (Cuesta *et al.*, 2015).

Task-based MEG studies are particularly useful in assessing neurophysiological changes associated with cognitive decline in Alzheimer's disease. Hippocampal-dependent paired associates learning is impaired by Alzheimer's disease (Blackwell *et al.*, 2004; De Rover *et al.*, 2011) and associated with reduced MEG responses (Kocagoncu *et al.*, 2022). Attention is an early non-memory domain affected by Alzheimer's disease (Perry and Hodges, 1999) and MEG has revealed that people with reduced performance on attention tasks exhibit reduced theta oscillations in frontoparietal and cingulate cortices (López-Sanz *et al.*, 2018). One of the most common domains assessed with task-based MEG of Alzheimer's disease is working memory (Casagrande *et al.*, 2023). MEG studies of working memory tasks have reported reduced early induced oscillatory responses for people with mild cognitive impairment (Ahmadlou *et al.*, 2014) and Alzheimer's disease (Kurimoto *et al.*, 2012), in proportion to task performance (Serrano *et al.*, 2020). Later responses (>300ms) are also reduced in Alzheimer's disease during working memory tasks (Maestú *et al.*, 2004).

These studies illustrate that MEG is sensitive to Alzheimer's disease and correlates with disease severity. Importantly, MEG reflects pathological effects on neuronal activity. Task-based MEG directly measures neuronal activity underlying cognitive tasks. The main analyses of this thesis in chapters 4, 5 and 6 reveal disease effects on neuronal activity to a mismatch negativity task.

Alzheimer's disease is associated with attenuated 'mismatch negativity' responses, which I focus on in the next section.

1.3 The mismatch negativity task

Discriminable changes to a repetitive auditory stimulus elicit the mismatch negativity response. There are different types of discriminable change: frequency, intensity, duration, location and gap. The classic mismatch negativity paradigm includes a sequence of repeating 'standard' tones which are infrequently interrupted by 'deviant' stimuli of the same type (e.g. frequency deviants). During the 'Optimum-1' paradigm, 5 different types of deviant alternate with a standard tone (Näätänen *et al.*, 2004). The roving mismatch negativity paradigm is designed to elicit error responses to deviant stimuli followed by rapid plasticity as predictions are updated upon repetition of this deviant stimulus (Friston, 2005; Kiebel *et al.*, 2007). During the roving auditory mismatch negativity task which I use, participants hear tones which repeat at the same frequency within blocks and different frequencies between blocks (see Figure 1.2a). During these mismatch negativity paradigms, evoked responses are larger to deviant than repeated tones between the 'mismatch negativity' time window (from around 140 to 160ms after stimulus onset, Moran *et al.*, 2013). Subtracting the deviant response from a repeated response gives the mismatch negativity waveform (see Figure 1.2b).

The mismatch negativity is affected by Alzheimer's disease, with differences between cognitively-healthy adults and people with a diagnosis of mild cognitive impairment (Ji *et al.*, 2015; Papadaniil *et al.*, 2016; Gao *et al.*, 2018; Laptinskaya *et al.*, 2018) or Alzheimer's disease (Savolainen *et al.*, 2001; Cheng *et al.*, 2012; Hsiao *et al.*, 2014; Papadaniil *et al.*, 2016; Jiang *et al.*, 2017). The mismatch negativity also reflects disease severity, with increased tau (Gjini *et al.*, 2022) and beta-amyloid (Kim *et al.*, 2020) attenuating the mismatch negativity response. The mismatch negativity response of people with a diagnosis of mild cognitive impairment or Alzheimer's disease is also associated with episodic memory (Gao *et al.*, 2018; Laptinskaya *et*

al., 2018), verbal learning (Mowszowski *et al.*, 2012), self-reported disability (Mowszowski *et al.*, 2012) and cognitive training (Mowszowski *et al.*, 2014).

The mismatch negativity task has several advantages for the study of Alzheimer's disease, and for use in early-phase clinical trials. First, the mismatch negativity paradigm is an easy task for participants to complete. Participants need only passively listen to the task, with minimal instructions or training required and no performance confounds. The generation of the mismatch negativity response is automatic. Indeed, the mismatch negativity task is such a robust neurophysiological signature that elements of the response are detectable in people who are unconscious (Bekinschtein *et al.*, 2009). This is ideal for dementia studies to avoid training and performance confounds and to achieve high compliance with people at any disease stage. This task also largely overcomes the educational and cultural biases of other neuropsychological measures that require verbal or written interactions (Stothart *et al.*, 2021). There is also a direct animal task homologue which can inform the cognitive mechanisms underlying mismatch negativity generation (Schöbi *et al.*, 2021).

A heuristic biomarker does not need to give insights into cognitive mechanisms; nevertheless, such insights are an advantage. The roving mismatch negativity can be explained within a predictive coding framework (Garrido *et al.*, 2009*a*; Wacongne *et al.*, 2011). The changing amplitude of evoked responses in the mismatch negativity time window (see Figure 1.2c) over successive repetitions (with short interstimulus intervals) reflects short term plasticity of cortical microcircuits as participants learn and adapt to the changing stimulus (Garrido *et al.*, 2009*a*). Deviant tones elicit a large neurophysiological response, reflecting the network's 'surprise' to this unpredicted tone yielding a large prediction error. Prediction errors are sent up the hierarchy from hierarchically lower to higher regions (Bastos *et al.*, 2012). These are called bottom-up connections or forward connections. Bottom-up prediction errors update the predictions of hierarchically higher regions. Predictions sent from hierarchically higher to lower regions are termed top-down / backward connections (Bastos *et al.*, 2012).

The magnitude of the prediction error reflects discrepancies between predictions from higher levels with the lower area's sensory input. The iterative updating of predictions by prediction errors enables learning. Predictions become more accurate with stimulus repetition which leads to smaller prediction errors indexed by attenuated neurophysiological signatures (Garrido *et al.*, 2009*a*).

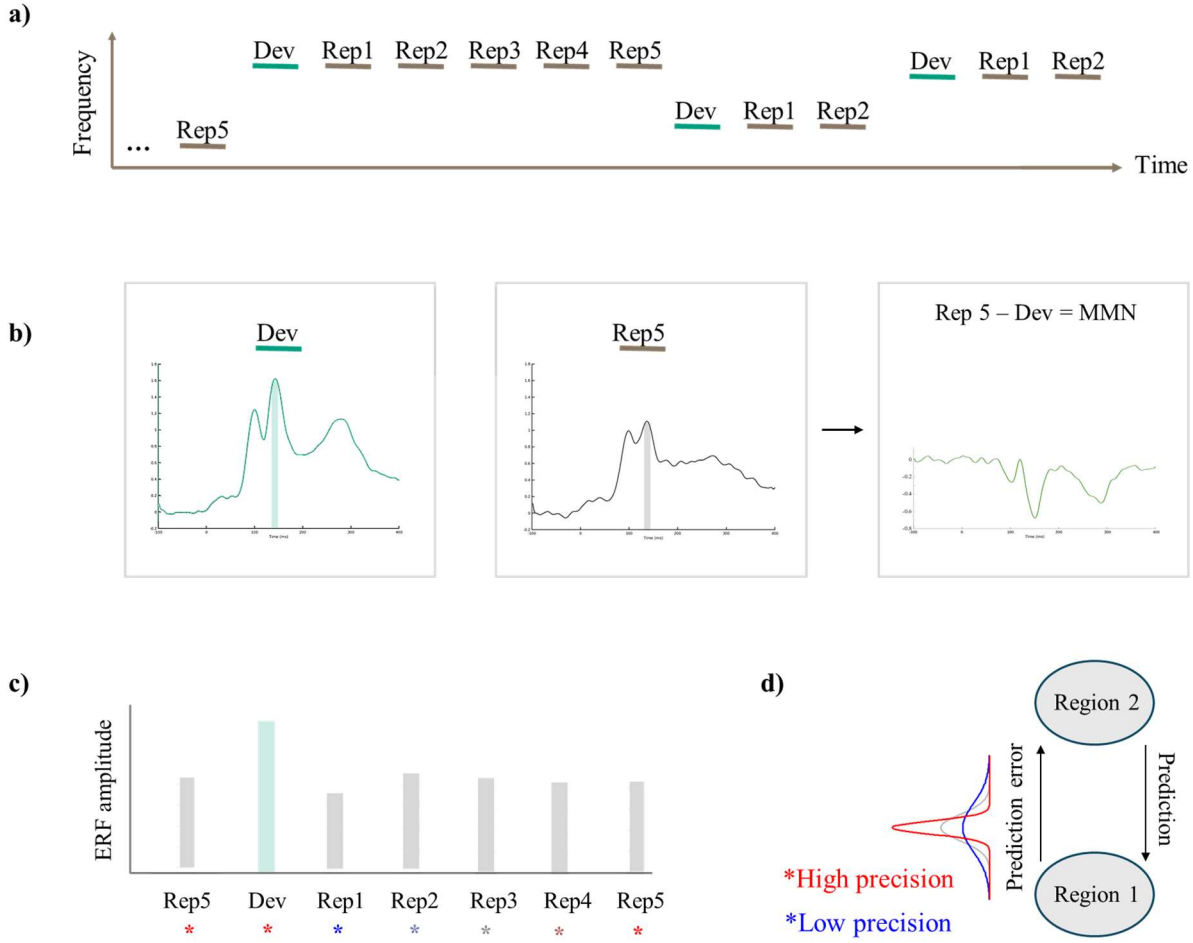


Figure 1.2 The roving auditory mismatch negativity paradigm.
a) Participants hear tones which repeat at the same frequency within blocks and change frequency between blocks. The number of tones within a block varies unpredictably. The 'deviant' tone is the first tone of a new block (teal), which becomes 'standard' (black) upon repetition. **b)** MEG responses are larger for deviant than repeated responses. Subtracting the larger deviant response from the smaller repeated response gives the mismatch negativity waveform (green) with a peak around 150ms. **c)** Mean amplitudes of evoked responses in this mismatch negativity 'peak' window (140-160ms) follow a pattern where responses are large to deviant tones and drop immediately to the first repeated tone before slowly recovering moderately. **d)** The task can be explained within a predictive coding framework. Hierarchically higher regions (region 2) send predictions about the tone frequency to hierarchically lower regions (region 1). The lower region compares the predictions to its incoming sensory information and sends prediction errors back up the hierarchy (back to region 2). As a tone repeats at the same frequency, it becomes predictable. This means the prediction error is smaller. The more certain the network is of its predictions, the higher the precision on the subsequent prediction error. This means, repetition 5 has high precision (red) and a low prediction error. The deviant repetition maintains the high precision of the previous tone but generates a large prediction error. The high precision boosts the large prediction error giving a large scalp response. This network, no longer certain of its predictions, reduces precision for the first repetition which attenuates responses. The precision increases as the tone becomes more predictable while the magnitude of the prediction error decreases with repetition.

The magnitude of the mismatch response reflects the precision of the prediction error (Garrido *et al.*, 2009*a*; Moran *et al.*, 2013). The precision of prediction error relays contextual effects of top-down predictions (Friston, 2005, Garrido *et al.*, 2009*a*). As predictions become more accurate, the network becomes more confident in its predictions such that precision of subsequent prediction errors is increased (Auksztulewicz and Friston, 2016). With tone repetition, precision increases. The deviant tone retains the high precision of the preceding repeated tone. This high precision enhances an already-large prediction error signal. With such a large prediction error, the network becomes uncertain of its predictions and reduces precision of subsequent prediction errors (attenuating the neurophysiological response). With tone repetition, confidence in predictions, and therefore precision of prediction errors, recovers as a new 'standard' tone is learnt (please see Figure 1.2).

The network underlying mismatch negativity responses involves a well-established network of primary auditory, superior temporal and inferior frontal regions (Garrido *et al.*, 2008; Phillips *et al.*, 2015). The parietal cortex is also involved (Lappe *et al.*, 2013; Cope *et al.*, 2022). Previous studies have established that primary auditory cortices are low in the hierarchy. These low regions are activated by sensory information (Witon *et al.*, 2020). This leads to involvement of hierarchically higher regions (e.g. superior temporal and inferior frontal regions) which may modulate prediction errors via precision enhancement (Witon *et al.*, 2020). While not being obligatory for mismatch negativity generation, attention enhances the response through improved precision of prediction errors (Chennu *et al.*, 2013).

The mismatch negativity can be framed within a predictive coding context, although it is consistent with other hierarchical information processing networks without recourse to predictive coding. An advantage of the predictive coding hypothesis is its direct association with mechanisms and functions of specific cell-types and layers of cortical microcircuits and the difference between forward and backward connectivity.

This thesis explores how changes to the function of these cortical microcircuits by Alzheimer's disease underlies attenuation of mismatch negativity responses. The next section explores how the cortical microcircuit is affected by Alzheimer's disease.

1.4 Effect of Alzheimer's disease on cortical microcircuits

Information flows through neurones within microcircuits of the cortical column (Douglas and Martin, 1991). These microcircuits have laminar and cellular-specific connections regulating information flow. For example, signalling of pyramidal cells depends on whether they are in superficial versus deep layers of a cortical column (Douglas and Martin, 1991). Intrinsic and extrinsic connectivity within and between cortical column microcircuits are critical for cognitive function (Bastos *et al.*, 2012). Alzheimer's disease has diverse effects that disrupt this cellular connectivity and the strength of synaptic connections.

An early feature of preclinical models of Alzheimer's disease are short-term plasticity changes (Lee *et al.*, 2012), which correlate with memory encoding (Chakroborty *et al.*, 2019) and occur prior to cell death (Selkoe, 2002). Beta-amyloid and tau disrupt synaptic transmission (Spires-Jones and Hyman, 2014) and cause synaptic loss (Tzioras *et al.*, 2022). Reduced synaptic density is strongly correlated with cognitive impairment (Terry *et al.*, 1991), with the burden and distribution of tau closely relating to cognitive decline (Nelson *et al.*, 2012; Malpetti *et al.*, 2020; Tanner *et al.*, 2022) and the clinical phenotype (Ossenkoppele *et al.*, 2016). In addition to synaptic loss, this cognitive effect is partly caused by the disruption by Alzheimer's pathology to axon and dendrite trajectories, dendritic spines and dendritic dearborization (Allard *et al.*, 2012; Merino-Serrais *et al.*, 2013; Spires-Jones and Hyman, 2014; Mijalkov *et al.*, 2021).

Pyramidal cells are particularly affected by Alzheimer's disease (Lacor *et al.*, 2007; Braak and Tredici, 2018). Pyramidal cells are the primary source of extrinsic connectivity between cortical microcircuits of different regions. They are consequently critical for receiving and sending information. Even subtle changes to pyramidal cell morphology can dramatically impair generation and propagation of action potentials in response to synaptic input (Ferrante *et al.*, 2013). Alzheimer's disease pathology reduces the number of electrophysiologically active pyramidal cell synapses (Shankar *et al.*, 2007), is synaptotoxic and alters pyramidal cell morphology (Lacor *et al.*, 2007; Mijalkov *et al.*, 2021) disrupting pyramidal cell connectivity (Lison *et al.*, 2014). Transgenic models have illustrated that disrupted pyramidal cell activity and synaptic degeneration (Oakley *et al.*, 2006) occur prior to pyramidal cell death (Lison *et al.*, 2014). *Post mortem* human studies report loss of superficial and deep pyramidal cells in people with Alzheimer's disease pathology proportionate to tau burden (Hof *et al.*, 1990).

Pyramidal cell connectivity within and between cortical microcircuits is also affected by neurotransmitter imbalances. Rodent studies have shown that cholinergic deficits affect the gain of superficial pyramidal cells (Schöbi *et al.*, 2021). Indeed, licenced cholinergic treatments for Alzheimer's disease oppose this effect on superficial pyramidal cells (Moran *et al.*, 2013).

Neuronal activity regulates beta-amyloid production (Kamenetz *et al.*, 2003). In health, this is part of a negative feedback mechanism to regulate neuronal activity. In Alzheimer's disease, impaired regulation of beta-amyloid leads to aberrant neuronal activity, including hypo- and hyper-active neurones (Busche *et al.*, 2008), and epileptiform activity illustrated through EEG of hippocampal networks of mice (Palop and Mucke, 2010). This is consistent with increased presence of amyloid in people with epilepsy (Mackenzie and Miller, 1994) and increased risk of seizures in people with Alzheimer's disease (Amatniek *et al.*, 2006). Mouse models with destabilised network activity have reduced glutamatergic synaptic transmission, with reduced levels of AMPA and NMDA receptors (Palop *et al.*, 2007).

NMDA channels are critical for synaptic function (Hunt and Castillo, 2012). NMDA channels are affected by Alzheimer's pathology (Ortiz-Sanz *et al.*, 2022; Dong *et al.*, 2023). Modulation of NMDA receptors by Alzheimer's disease pathology causes synaptic depression (Kamenetz *et al.*, 2003) and pyramidal cell spine loss (Shankar *et al.*, 2007). These direct and indirect effects of NMDA-receptor changes by Alzheimer's disease pathology may underlie disruption to human cognitive processes reliant on NMDA-receptor function, such as memory updating (Yang *et al.*, 2023).

It is important to note that preclinical models are reductionist and, despite construct validation for cross-species pathogenic mechanisms, caution must be taken when using them to interpret disease effects (Scheltens *et al.*, 2021). One of the original contributions of this thesis is to bridge the understanding from preclinical to human mechanisms of Alzheimer's disease effects on cortical microcircuits and examine how they relate to cognitive dysfunction and progression.

1.5 Dynamic causal modelling

Identification of cellular mechanisms of disease in people living with Alzheimer's disease can be achieved with biophysically-informed generative models, informed by functional neuroimaging (e.g. MEG). Dynamic causal models offer one such method to identify the cellular mechanisms generating an individual's MEG data. These imaging-informed models

can reveal therapeutic mechanisms (galantamine: Moran *et al.*, 2013; ketamine: Rosch *et al.*, 2019; tiagabine: Adams *et al.*, 2020) and disease-effects (channelopathies: Gilbert *et al.*, 2016; anti-NMDA receptor encephalitis: Symmonds *et al.*, 2018) non-invasively in humans.

Dynamic causal modelling is a generative modelling framework that estimates the model parameters of neural networks as causes of the experimental observations. Information flows within and between the canonical microcircuits of dynamic causal models. This activity generates scalp responses which can be compared with the recorded data to iteratively update parameters of the model's cortical microcircuits. The regulation of information flow through the circuitry of a dynamic causal model is based on biological microcircuits (Bastos *et al.*, 2012). For example, the canonical microcircuit convolution model is based on the cat primary visual cortex and is illustrated in Figure 1.3a. As such, information flow through the dynamic causal model reflects information flow through a cortical network. Here, I describe signal flow through a general dynamic causal model network of cortical microcircuits. The dynamics are governed by model-specific parameters and equations as detailed in the empirical chapters.

Experimental inputs enter the system to regions receiving driving input (specified by a user-defined 'C' matrix). Spiny stellate cells are the only population to receive external, driving inputs; however, other cellular populations (inhibitory interneurons, superficial and deep pyramidal cells) receive inputs from extrinsic and intrinsic neuronal populations (see Figure 1.3a). These include inputs from extrinsic regions (mediated by extrinsic connectivity, according to user-defined 'A' matrices, which are modulated by external inputs, according to user-defined 'B' matrices) and intrinsic inputs (mediated by intrinsic connectivity parameters). The summation of all inputs (intrinsic, extrinsic and experimental firing inputs) form the presynaptic firing rate.

Each cellular population has hidden states described by differential equations that model their depolarisation to presynaptic firing rates (Friston *et al.*, 2019). As such, presynaptic inputs change the postsynaptic potential of the receiving neuronal population. Postsynaptic membrane potentials generate firing rates (average action potential). The resulting firing rate is weighted by the extrinsic or intrinsic connectivity parameters of the efferent connection. The efferent connection becomes an input to another cellular population and so the neuronal dynamics of each cellular population within the entire system are perturbed by the external input.

These neuronal dynamics propagate to sensor space according to a lead field model (see Figure 1.3). This allows the dynamic causal model to generate evoked responses to the experimental inputs at the scalp level. The generated response is compared to the participant's recorded (observed) response. The model parameters are iteratively updated to gradually improve the accuracy of the generated response with respect to the participant's recorded response. This iterative optimisation of the model parameters uses a variational Laplace scheme, which approximates posterior parameters of the model using variational Bayes with the Laplace assumption that parameters have a fixed Gaussian distribution (Friston *et al.*, 2007). Variational Laplace estimates parameters and their model evidence, i.e. the free energy of the model, which is a lower bound for the log model evidence ($Y|m$). Free energy describes the difference between how accurate the predictions of the model are with the complexity of the model. The variational Laplace inversion iteratively updates model parameters until the free energy (approximating the model evidence) is maximised.

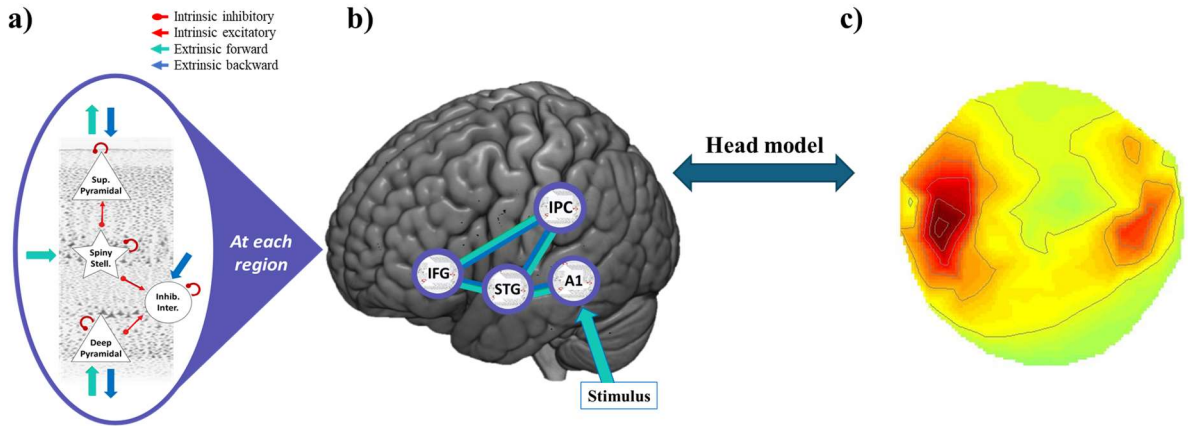


Figure 1.3 Generative model of brain function.
Dynamic causal models comprise **a)** cortical microcircuits* connected within a cortical hierarchy. An example of a single regions cortical microcircuit is circled in purple. It receives and sends connections to hierarchically higher and lower regions. Models can be a single region, or **b)** a network of regions. The user specifies regions and how they are connected. **c)** The model generates and is informed by predicted and observed MEG responses, respectively. *NB: model parameters are dependent on model specification and may differ to the microcircuit shown here. Sup, superficial; stell., stellate; inter., interneurons; inhib., inhibitory; l, left; r, right; A1, primary auditory cortex; STG, superior temporal gyrus; IFG, inferior frontal gyrus; IPC, inferior parietal cortex

There is extensive evidence supporting dynamic causal modelling in terms of its face validity (Friston *et al.*, 2003; Chumbley *et al.*, 2007; Stephan *et al.*, 2008), construct validity (Penny *et al.*, 2004; Lee *et al.*, 2006; Razi *et al.*, 2015; Phillips *et al.*, 2016; Symmonds *et al.*, 2018) and

predictive validity (David *et al.*, 2008*b*, *a*, Moran *et al.*, 2011*b*, 2014; Shaw *et al.*, 2019; Adams *et al.*, 2020, Jafarian *et al.*, 2023*a*). The free energy of a dynamic causal model is used for model comparisons and is reliable (Rowe *et al.*, 2010, Jafarian *et al.*, 2023*a*). It is important to note that while free energy is reliable, the Bayesian model comparison may not accurately identify the correct model that generated the data (Litvak *et al.*, 2019) and no model is perfect.

Several methods have been developed that allow group comparisons of dynamic causal model metrics. These methods include mixed analysis of variance models (Neufang *et al.*, 2011), group Bayes factors (Garrido *et al.*, 2007), and random model effects (Stephan *et al.*, 2009). In complex, non-linear dynamical systems with high covariance among parameters, the use of individual parameters as dependent variables is problematic. They are in breach of assumptions of independence between measures from different subjects. Given this, parametric empirical Bayes (PEB) analysis is recommended (Friston *et al.*, 2016). PEB considers the variance of parameters and reduces conditional dependencies of parameters (Jafarian *et al.*, 2023*a*). At the second-level, parametric empirical Bayes uses empirical priors informed by the researcher's hypothesis for model inversion. Parametric empirical Bayes consequently reduces conditional dependency of parameters and includes informative priors leading to improved reliability (Jafarian *et al.*, 2023*a*).

Dynamic causal modelling of fMRI data has been used to assess effective connectivity changes underlying poorer task performance for people with Alzheimer's disease. When participants with Alzheimer's disease perform visual tasks, they have reduced intrinsic and modulatory connectivity of the visual cortex (Rytsar *et al.*, 2011) and reduced parietal and frontal effective connectivity (Neufang *et al.*, 2011). When people with amnestic mild cognitive impairment perform a motor task, they have reduced effective connectivity between the right and left sensorimotor cortex (Agosta *et al.*, 2010). Dynamic causal models of resting-state fMRI are also sensitive to disease progression. Effective connectivity is reduced in Alzheimer's disease and further reduces with disease progression (Mohammadian *et al.*, 2023). Dynamic causal models of resting-state fMRI reflect disease severity; prefrontal and cingulate connectivity partially predict mini-mental state examination and clinical dementia rating scores for people with Alzheimer's disease (Huang *et al.*, 2022).

Using electrophysiological data (Kiebel *et al.*, 2008), dynamic causal models have addressed questions relating to the effects of experiments at the synaptic level (Gilbert *et al.*, 2016; Shaw

et al., 2020, Jafarian *et al.*, 2023*b*) and the role of forward and backward connections in cortical hierarchies (Boly *et al.*, 2011; Auksztulewicz and Friston, 2015). Dynamic causal models of electrophysiological data have been used to illustrate therapeutic effects on cortical microcircuits (Moran *et al.*, 2013; Rosch *et al.*, 2019; Adams *et al.*, 2020, 2021; Gilbert *et al.*, 2021). In the dementia literature, dynamic causal modelling of electrophysiological data has revealed physiological signatures of frontotemporal dementia, with reduced interactions between frequency bands in the prefrontal cortex and enhanced gamma connectivity between the pre-supplementary motor area and primary motor cortex (Hughes *et al.*, 2018*a*)**.** Laminar-specific changes relating to frontotemporal dementia have also been shown (Shaw *et al.*, 2019, 2021), which are affected by synaptic density (Adams *et al.*, 2023). Dynamic causal models have illustrated that 'top-down' connectivity (from hierarchically higher to lower regions) during a mismatch negativity task is altered in people with frontotemporal dementia, primary progressive aphasias, posterior cortical atrophy and Alzheimer's disease (Cope *et al.*, 2022).

In Alzheimer's disease research, Penny and colleagues (Penny *et al.*, 2018) used Parametric empirical Bayes (PEB) to assess differences in EEG dynamic causal model parameters of two cognitively-normal groups, one group had the PSEN1 gene mutation, which causes familial Alzheimer's disease, and the other group did not have the mutation. They found presentation of incongruent pairs of stimuli strengthened the pathway from the right inferotemporal cortex to left medial temporal lobe for the group with the PSEN1 mutation but not the group without the PSEN1 mutation. This finding is consistent with previous reports of left hippocampal hyperactivation in people with preclinical Alzheimer's disease (Mondadori *et al.*, 2006; Quiroz *et al.*, 2010). During a visual recognition task, dynamic causal modelling of EEG revealed reduced temporo-frontal connectivity for people with Alzheimer's disease and slower signal transmission from frontal regions in an implicit priming task which correlated with task performance (Tyrer *et al.*, 2020). Deviant stimuli of a mismatch negativity task led to increased forward connections and decreased backward connections in people with tau pathology (Gjini *et al.*, 2022). Dynamic causal models of MEG mismatch negativity data have also illustrated altered parietal and frontal connectivity of people with Alzheimer's disease (Cope *et al.*, 2022).

In conclusion, there is a wealth of literature describing the effects of Alzheimer's disease on neurophysiology (Rathore *et al.*, 2017; Maestú *et al.*, 2019)**.** Dynamic causal modelling can identify disease mechanisms at the cortical microcircuit level that explain such effects (Shaw *et al.*, 2019). Despite this, there are few studies that employ dynamic causal modelling to

understand how Alzheimer's disease affects cell classes and neurotransmitters underlying these neurophysiological deficits. My work addresses this knowledge gap.

1.6 Aims of the thesis

This thesis leverages preclinical and *post mortem* findings of disease effects to form and test hypotheses about how cortical microcircuits are affected in people living with Alzheimer's disease. Dynamic causal modelling enables biologically meaningful inferences of disease mechanisms from micro to macro levels of the brain. This thesis aims to use dynamic causal modelling informed by MEG data to investigate cellular-level effects of Alzheimer's disease on cognition to: (i) better understand mechanisms of Alzheimer's disease underlying cognitive decline and (ii) identify mechanistically-informative biomarkers of disease and its progression for use by interventional studies. I report two experimental studies, chapters 4 and 5, which assess the effect of Alzheimer's disease and its progression in humans, *in vivo*, on (1) pyramidal cells and (2) NMDA channel kinetics and signalling. A third experimental study, chapter 6, examines how memantine, a treatment for Alzheimer's disease, and Alzheimer's disease severity and progression affect NMDA-channel blockade.

I set four objectives for this thesis: (i) to demonstrate the effect of Alzheimer's disease, its severity and progression on a MEG-derived biomarker (the amplitude of the mismatch negativity) and to assess the reliability of this measure. I use dynamic causal modelling to (ii) generate neurophysiological signatures of Alzheimer's disease, (iii) test hypotheses based on preclinical models and *post mortem* analyses of the effects of Alzheimer's disease or Alzheimer's-disease therapeutics on cortical microcircuits; and (iv) assess how cellular and network parameters are affected by Alzheimer's disease, its severity and progression. Chapters 4, 5 and 6 address these thesis objectives using sensor-level analyses (objective i) and dynamic causal modelling (objectives ii, iii and iv) of mismatch negativity responses primarily with data from the Cambridge NTAD study. Chapters 2 and 3 therefore provide key background information about the Cambridge NTAD study data.

Chapter 2 describes the design and data types for the 'New Therapeutics in Alzheimer's disease' (NTAD) study. It provides information on the protocol followed for data collection of the Cambridge NTAD cohort whose data are used to address the thesis objectives. This chapter details the recruitment of people with amyloid-positive mild-cognitive impairment or early-

stage Alzheimer's disease and cognitively-healthy people. This chapter also describes the collection of clinical, cognitive and imaging (including MEG and MRI) data which was collected at baseline and 1 year. A subset of participants with mild cognitive impairment or Alzheimer's disease completed a retest MEG scan 2 weeks after baseline.

Chapter 3 summarises the NTAD Cambridge cohort's clinical, cognitive and MRI data. The aim of this chapter is not to find novel biomarkers but to characterise data features typically used to define Alzheimer's disease. I report clinical, cognitive and MRI differences between people with and without Alzheimer's disease and how these measures change with disease severity and progression. I set these characteristics within the context of typical findings from previous studies of people with Alzheimer's disease.

Data from the NTAD Cambridge cohort are used to address the thesis objectives in chapters 4, 5 and 6. These chapters assess the reliability and disease-sensitivity of mismatch negativity amplitudes and assess the cortical generators underlying the neurophysiological deficits.

Chapter 4 assesses how pyramidal cell connectivity is affected by Alzheimer's disease. I use convolution-based dynamic causal models (see the Statistical Parametric Mapping function 'spm_fx_cmc.m' for model specification) informed by mismatch negativity MEG data from the Cambridge NTAD cohort. Based on pre-clinical models and effects of cholinesterase inhibitors, I test the hypothesis that Alzheimer's disease affects superficial pyramidal cell gain and extrinsic connectivity between pyramidal cells of different regions. I also assess how disease progression affects these features.

Chapter 5 examines how Alzheimer's disease affects NMDA-channel kinetics. I invert conductance-based dynamic causal models (see 'spm_fx_cmm_NMDA.m') to the mismatch negativity MEG responses. Given preclinical findings, I predict that NMDA-channels will be important for explaining attenuation of the mismatch response. I investigate how Alzheimer's disease and its progression affects NMDA-channel time constants and NMDA-mediated signalling.

Chapter 6 is the final experimental chapter of this thesis and investigates how memantine and Alzheimer's disease affect NMDA channel blockade. For this analysis, I adapt a conductance-based dynamic causal model ('spm_fx_cmm_NMDA.m') to assess NMDA-channel blockade. First, I test the effect of memantine on NMDA-receptor blockade. I use MEG data recorded during a mismatch negativity paradigm from neurologically-healthy people from a double-

blind, placebo-controlled crossover memantine study. Secondly, I test the effect of Alzheimer's disease severity and progression on NMDA-channel blockade. I use roving mismatch negativity MEG data from the Cambridge NTAD cohort. I predict that Alzheimer's disease and memantine will have opposing effects on NMDA-receptor inhibition.

Chapter 7 summarises and integrates the principal findings of this thesis. This chapter reviews the contribution of this thesis to improving our understanding of the effects of Alzheimer's disease on the cortical microcircuit and illustrates the potential of MEG and dynamic causal modelling as a platform for future disease-modifying therapeutics.

2 | The New Therapeutics in Alzheimer's Disease Longitudinal Cohort study (NTAD): study protocol

A manuscript related to this chapter is published as:

Lanskey, J. H., Kocagoncu, E., Quinn, A. J., Cheng, Y.-J., Karadag, M., Pitt, J., Lowe, S., Perkinton, M., Raymont, V., Singh, K. D., Woolrich, M., Nobre, A. C., Henson, R. N., & Rowe, J. B. (2022). New Therapeutics in Alzheimer's Disease Longitudinal Cohort study (NTAD): study protocol. BMJ Open, 12(12), e055135. https://doi.org/10.1136/BMJOPEN-2021-055135

Abstract: This chapter describes the New Therapeutics in Alzheimer's Disease study (NTAD) protocol to acquire longitudinal MEG and EEG data in people with biomarker-positive mild cognitive impairment or early Alzheimer's disease. NTAD aims to identify a biomarker set from magneto/electroencephalography that is sensitive to disease and progression over 1 year. The study will recruit 100 people with amyloid-positive mild cognitive impairment or early-stage Alzheimer's disease and 30 healthy controls aged between 50 and 85 years. Measurements of the clinical, cognitive and imaging data (magnetoencephalography, electroencephalography and MRI) of all participants will be taken at baseline. These measurements will be repeated after approximately 1 year on participants with Alzheimer's disease or mild cognitive impairment, and clinical and cognitive assessment of these participants will be repeated again after approximately 2 years. To assess reliability of magneto/electroencephalographic changes, a subset of 30 participants with mild cognitive impairment or early-stage Alzheimer's disease will also undergo repeat magneto/electroencephalography 2 weeks after baseline. Baseline and longitudinal changes in neurophysiology are the primary analyses of interest. Additional outputs will include atrophy and cognitive change and estimated numbers needed to treat each arm of simulated clinical trials of a future disease-modifying therapy.

2.1 Introduction

With 44 million people living worldwide with dementia, treatments to slow or stop disease progression are urgently needed. Alzheimer's disease is the most common dementia but despite rapid advances in therapeutics within preclinical models (LaFerla and Green, 2012; Drummond and Wisniewski, 2017), clinical trials remain expensive, slow and challenging (Cummings *et al.*, 2014; Anderson *et al.*, 2017; Yiannopoulou *et al.*, 2019) with high-profile failures (Mehta *et al.*, 2017). Significant bottlenecks exist in early-phase trials, where efficacy rates are low and costs rapidly escalate. To bridge the gap between animal models and the human disease, better tools are needed to quantify pathogenic and pathophysiological mechanisms in patients, *in vivo* providing evidence to pursue or discontinue trials of a candidate treatment. These tools should be safe, scalable and able to support early-phase trials over a short duration and viable budget.

Brain imaging is widely used to diagnose dementia and measure pathology in clinical trials. There are diverse imaging methods with differential sensitivity to brain structure, chemistry, pathology and function. For example, magnetic resonance imaging (MRI) is commonly used to measure structural changes related to Alzheimer's disease (Frisoni *et al.*, 2010), such as entorhinal cortex (Holland *et al.*, 2012) and hippocampus volumes (Leung *et al.*, 2010). Positron emission tomography (PET) can quantify and localise Alzheimer pathology through the use of ligands that bind to the aggregated tau protein (Ossenkoppele *et al.*, 2016; Passamonti *et al.*, 2017, 2018; Cope *et al.*, 2018; Leuzy *et al.*, 2019), beta-amyloid plaques (Cai *et al.*, 2006) and neuroinflammation (Bevan-Jones *et al.*, 2017).

Loss of synapses and synaptic plasticity is an early feature of Alzheimer's disease (Palop and Mucke, 2010; Koffie *et al.*, 2011; Kashyap *et al.*, 2019). Indeed, cognitive decline may be more directly related to loss of synapses or synaptic plasticity than to atrophy (De Wilde *et al.*, 2016; Henstridge *et al.*, 2018). As synaptic changes occur early in Alzheimer's disease (De Wilde *et al.*, 2016), synaptic measures could be sensitive to the earliest precursors of cognitive involvement. This accords with preclinical models in transgenic mice where network physiology and cognition are impaired before tangles or cell death (Menkes-Caspi *et al.*, 2015).

In contrast to preclinical models and *post mortem* analysis, there are limited options to assess synaptic function in humans, *in vivo*. While PET imaging now offers ligands that indirectly quantify synaptic density, electroencephalography (EEG) and magnetoencephalography

(MEG) measure neurophysiological properties dependent on synaptic integrity and function. MEG can identify synaptic and local circuit impairments (Pinotsis *et al.*, 2013; Adams *et al.*, 2020) and their impact on network dynamics in Alzheimer's Disease (Sami *et al.*, 2018; Sitnikova *et al.*, 2018; Hughes *et al.*, 2019; Puttaert *et al.*, 2020), frontotemporal dementia (Hughes *et al.*, 2011, 2015, 2018*b*; Hughes and Rowe, 2013; Adams *et al.*, 2020), and Lewy-body disease (van Dellen *et al.*, 2015). MEG and EEG (M/EEG) therefore have potential to support and de-risk clinical trials of novel compounds. To enable M/EEG as a viable biomarker in clinical trials, one must assess longitudinal M/EEG and test-retest reliability.

The New Therapeutics for Alzheimer's Disease (NTAD) study aims to identify viable M/EEG biomarkers for clinical trials. NTAD is a multicentre study established by the Dementias Platform UK and supported by the Medical Research Council, Alzheimer's Research UK and industry partners.

2.1.1 Research Aims

The primary objective is to identify a biomarker set from neurophysiological M/EEG sensitive to the presence and progression of Alzheimer's disease. Such a neurophysiological biomarker, or biomarker set, should be related to cognitive function, have high test-retest reliability and track disease progression over the duration of clinical trials. Sensitivity to disease progression should ideally outperform current widely used biomarkers such as MRI and cognitive tests.

The secondary objective is to identify a biomarker set that can predict disease progression, explain individual differences in the future disease trajectory and variation in cognitive decline over time.

2.1.2 Analysis

Investigators across sites will identify harmonised M/EEG pre-processing pipelines to reduce analytical variance. Following standardised pre-processing, investigators will address the study aims with multiple analytical approaches. Investigators are encouraged to pre-register specific analyses. Analyses will follow an overarching framework:

Stage 0 (descriptive) analysis will describe demographics; APOE genotype; blood-based, fluidic biomarkers; neurocognitive profiles and regional brain atrophy. This serves to confirm the expected patterns of cognitive decline and atrophy typical of people with mild cognitive

impairment and early Alzheimer's disease and to enable comparison of the NTAD cohort across sites and with other study populations.

Stage 1 (baseline) analyses will identify reliable and sensitive baseline, disease-related M/EEG parameters in terms of (i) the sensitivity of cross-sectional M/EEG parameters to group differences, (ii) the correlation of cross-sectional M/EEG parameters to baseline cognition, atrophy and fluidic markers and (iii) the test-retest reliability of M/EEG parameters.

Stage 2 (longitudinal) analyses will assess the sensitivity of selected neurophysiological markers to longitudinal change by assessing how they change over ~12 months. Investigators shall compare their sensitivity (as accuracy and effect sizes) to disease progression with MRI and cognitive measures. Mediation modelling will determine how longitudinal changes in brain structure and neurophysiology explain cognitive changes. Where data are pooled across sites, site location will be included as a model factor.

Stage 3 (predictive) analyses aim to identify baseline parameters that predict disease progression and identify the optimal parameter, or parameter set, that provide parsimonious or unique predictive information.

Parameters at stages 1-3 include: (i) summary statistics of evoked and induced responses for each task; (ii) summary statistics of the spectral density in resting-state recordings; (iii) data-driven connectivity metrics, including those derived from Hidden Markov modelling (Woolrich *et al.*, 2013; Baker *et al.*, 2014; Vidaurre *et al.*, 2016); and (iv) parameters of model-based analyses of evoked responses and spectral densities using dynamic causal modelling (Adams *et al.*, 2020, 2021; Shaw *et al.*, 2020).

DNA will allow determination of genotype, including common genetic variants; and post-hoc identification of rare, autosomal dominant cases which may have distinctive physiology and phenotype. *Post-hoc* exploratory analyses will examine the relationship between cognitive and imaging biomarkers as a function of (i) variations in tau haplotype, (ii) polymorphisms of genes related to plasticity, (iii) Alzheimer's disease risk alleles (e.g. apolipoprotein e4), (iv) polygenic risk scores of Alzheimer's disease and (v) plasma tau levels. RNA is collected to enable post-hoc transcriptomics. These are exploratory genetic options, whereas participation and the principal analyses are not genetically determined. With data sharing, new analytical methods may be applied.

2.2 Methods

2.2.1 Study Design

This is a repeated-measures, observational-design study with 130 participants tested at two sites: Cambridge University and Oxford University, each in partnership with local NHS Hospital Trusts. The planned start and end dates are 01/06/2018 and 01/07/2023. The protocol includes two stages (Figure 2.1). The first, cross-sectional stage consists of baseline and test-retest sessions. Baseline sessions are comprised of clinical and neuropsychological assessments, an MRI scan and an M/EEG scan. For the test-retest session, a subset of patients returns for a second M/EEG approximately two weeks after the first. Patients proceed to stage 2, with repeat assessment at 12 months (including M/EEG and MRI, clinical and neuropsychology) and 24-months (clinical and neuropsychological reassessments).

2.2.2 Participant recruitment and selection

Participants are aged between 50 and 85 years with similar numbers of men and women, with symptomatic mild cognitive impairment or early dementia due to Alzheimer's disease (n=100) or normal cognition (n=30, Figure 2.1). Potential participants are identified by a staged screening process. First, approved clinical staff undertake electronic screening of records held by regional memory clinics or NIHR Join Dementia Research, or research team members review electronic records of people who previously consented to data retention on a contact list regarding dementia research opportunities. A participant information sheet detailing the study procedures is provided to candidate participants and a study partner who regularly sees the participant and is willing to complete assessments. Candidate participants answer a series of questions derived from the inclusion and exclusion criteria (Table 2.1) during a telephone-based screening call.

The still potentially eligible participants are invited to on-site screening (see below). For those with Alzheimer's disease or mild cognitive impairment, clinical letters are sought from their memory assessment service, in addition to within-study assessments. This final screening appointment allows further assessment of eligibility, against exclusion and inclusion criteria (Table 2.1) and Alzheimer biomarker status. Any uncertainty regarding eligibility is discussed with the principal investigator for the relevant site. Eligible people proceed to Stage 1.

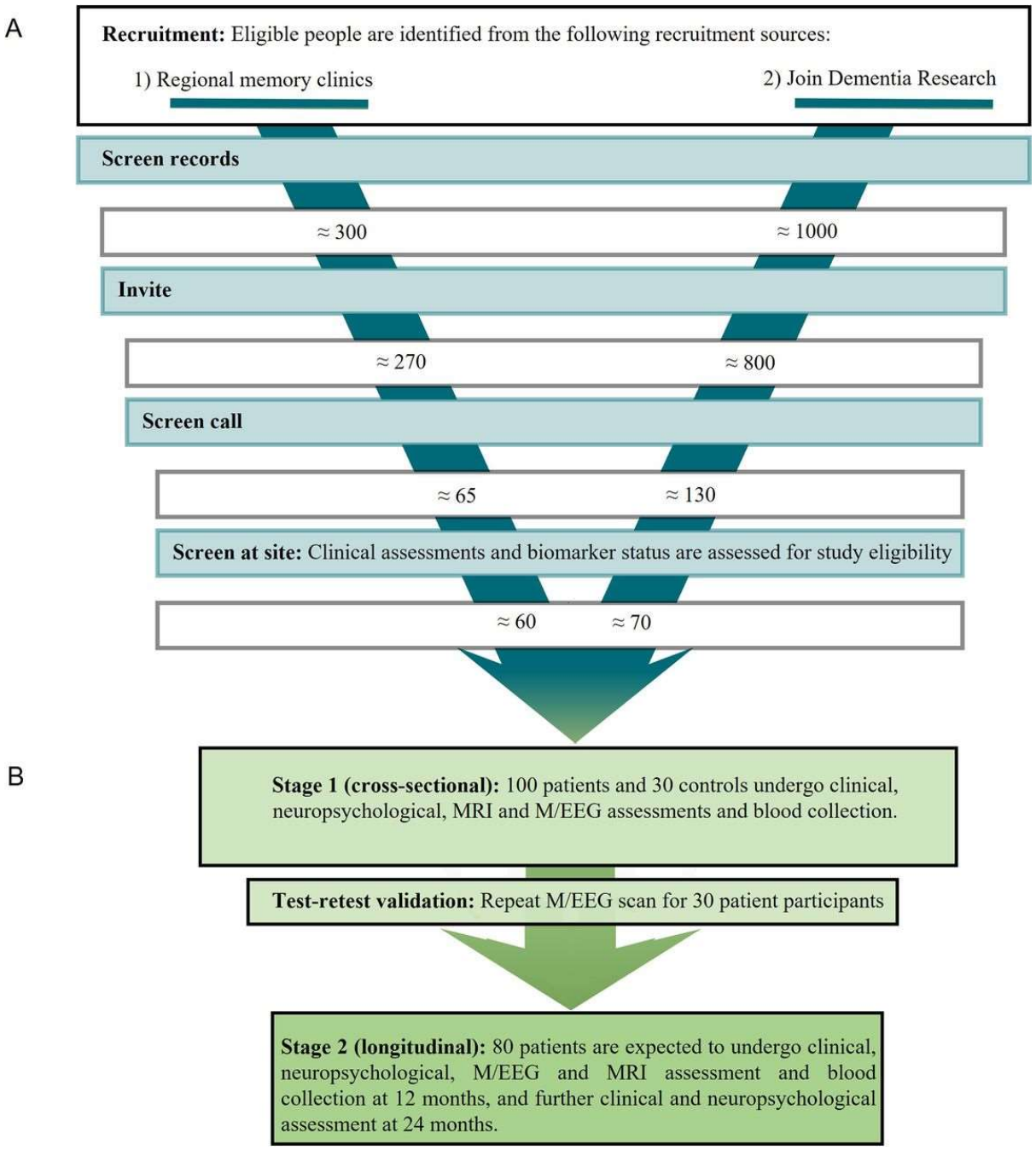


Figure 2.1 Participant flow chart.
a) Recruitment strategy: Electronic screening of records from regional memory clinics and Join Dementia Research generates approximately 300 potential patient and 1000 potential patient and control participants who are invited to telephone screening. People who remain eligible are screened further on-site to identify 100 patient and 30 control participants. **b)** Study stages: Stage 1 consists of the cross-sectional baseline assessments and, for 30 patients, a repeat of the M/EEG assessment two weeks after the first. Only patients continue to the longitudinal stage 2 of the study, with repeat assessments 12 and 24 months after baseline. Attrition of 20% is expected at stage 2. M/EEG=Magnetoencephalography combined with electroencephalography imaging, MRI=Magnetic resonance imaging

Group inclusion criteria	
Patients	Controls
Diagnosis of MCI or AD#	No neurological diagnosis
CDR = 0.5 – 1	CDR = 0
Positive AD biomarker status (CSF or PET)	Known AD biomarker status (CSF or PET)
MMSE > 18	MMSE > 24
50-85 years	50-85 years
General exclusion criteria (patients and controls)	
Significant neurological disease, other than Alzheimer's disease, that may affect cognition or ability to complete the study	
Presence of any significant psychiatric disorder that could affect participation (American Psychiatric Association, 2013)	
Any clinically important abnormality that could compromise study participation	
A clinically significant illness, medical or surgical procedure, or trauma within 30 days prior to screening or baseline	
Known or suspected systemic infection	
Medications affecting cognition, unless on a stable dose for >30 days prior to baseline	
Rosen Modified Hachinski Ischaemic score ≥ 4	
History of seizure, except febrile seizures or single provoked seizure	
Head trauma resulting in protracted loss of consciousness, or serious infectious disease affecting the brain, within five years of screening and baseline	
Participation in a clinical trial of an investigational medicinal product	
Impairment of vision or hearing that could affect study participation	
Formal education ≤ 7 years	
Lack of mental capacity or other ability to consent	
Inability to read and write fluently in English	
Inability to walk 10 metres independently*	
Contraindications to blood sampling	
Contraindications to lumbar puncture (e.g. spinal deformations) and amyloid PET scan	
Contraindication to MRI (including, but not limited to, claustrophobia; pregnancy; MRI-incompatible pacemakers and other MR-incompatible, implanted medical devices)	
Metallic implants in the body that affect MEG recordings, as judged by the Investigator	

Table 2.1 Group inclusion criteria and general exclusion criteria.
MCI=Mild Cognitive Impairment, AD=Alzheimer's Disease, MMSE=Mini Mental State Examination, CDR=Clinical Dementia Rating. # according to (Albert et al., 2011) or (McKhann et al., 2011). * Ten metre walking is required for practicality and safety during the scanning sessions to avoid the use of walking aids which may have metallic constituents.

2.2.3 Sample Size and Power

Previously published studies have detected the presence and progression of Alzheimer's disease or mild cognitive impairment with under 100 participants using MRI (Holland *et al.*, 2009). The study aims to identify MEG measures that are at least as sensitive as MRI. For longitudinal analysis, MEG (Fernández *et al.*, 2006; Pusil *et al.*, 2019, Xu *et al.*, 2021*b*) and EEG (Papaliagkas *et al.*, 2008, 2011; Lai *et al.*, 2010; Bennys *et al.*, 2011; Chapman *et al.*, 2011; Fruehwirt *et al.*, 2019) have been used over 11-36 months with 20-130 participants. Mandal and colleagues (2018) summarise the accuracies of MEG measures to distinguish Alzheimer's disease from controls: 30/34 MEG measures had areas under the curve >0.64 approximating under Gaussian assumptions to Cohen's d>0.5 (Salgado, 2018).

Power analyses were conducted in G*power (Erdfelder *et al.*, 2009). For the cross-sectional NTAD data with 130 participants, for power of 80% and α=0.05, a one-tailed test should detect (i) medium, group-wise effect sizes of >0.5 and (ii) correlations with disease severity of >0.25. With 20% attrition in follow up (n=80) and α=0.05, longitudinal analyses of disease progression would have 80% power to detect within-sample effect size >0.28 (Figure 2.2).

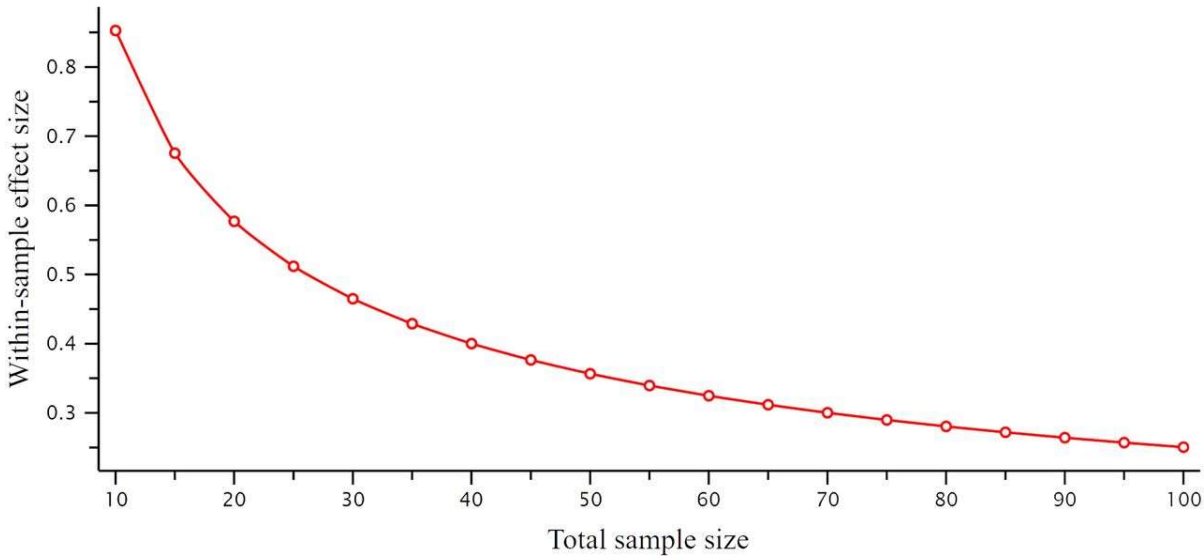


Figure 2.2 Study effect sizes by sample size.
Effect sizes required to detect longitudinal correlations with disease severity at different attrition rates (resulting in reduced longitudinal sample size) with 80% power and α=0.05.

2.3 Study Procedures

2.3.1 Overview of protocol stages

Screening

Potential participants are identified from electronic records and screened further via telephone call (see 'Participant recruitment and selection' section). Prospective participants who remain eligible are invited to an in-person screening appointment. Any further questions they have are answered before they provide written, informed consent. After written, informed consent, a medically-qualified clinician administers the clinical interview, clinical dementia rating and Hachinski ischemic scale. In the context of this study, medically qualified means having at least MRCP part II qualifications and in ST3+ level specialty training (neurology or psychiatry), or completion of neurology or psychiatry specialist training. The remaining clinical assessments are completed by a member of the research team and include physiology and blood sampling. All research team members have current Good Clinical Practice training. If Alzheimer biomarker status is unknown from recent clinical or research assessments, participants proceed to either cerebrospinal fluid examination or amyloid PET imaging according to participant preference and eligibility. For patients, where a participant's positive amyloid status has been confirmed previously, a positive result enables participation, a negative result excludes participation. For controls, the Alzheimer biomarker status must be known to proceed but, given their CDR=0, a positive test does not prevent participation.

Stage 1: Baseline

One hundred people with mild cognitive impairment or Alzheimer's disease and 30 neurologically normal people proceed to baseline assessment. Participants undergo structured neuropsychological assessment, an M/EEG scan and MRI imaging of brain structure and function over two sessions (or three by preference).

Stage 1: Two-week M/EEG retest

Thirty people from the patient group (i.e. mild cognitive impairment or Alzheimer's disease) repeat the M/EEG scan between two and four weeks after the first scan. Invitations are prioritised to people who can most readily attend the additional session (e.g. considering distance) until the target sample size is reached.

Stage 2: Annual follow-up 1

Participants in the patient group repeat the clinical and neuropsychological assessments, M/EEG scan, MRI scan and blood collection at 12 months after baseline.

Stage 2: Annual follow-up 2

Clinical and neuropsychological assessments are repeated at 24 months for participants in the patient group.

The study timeline is illustrated in Figure 2.3.

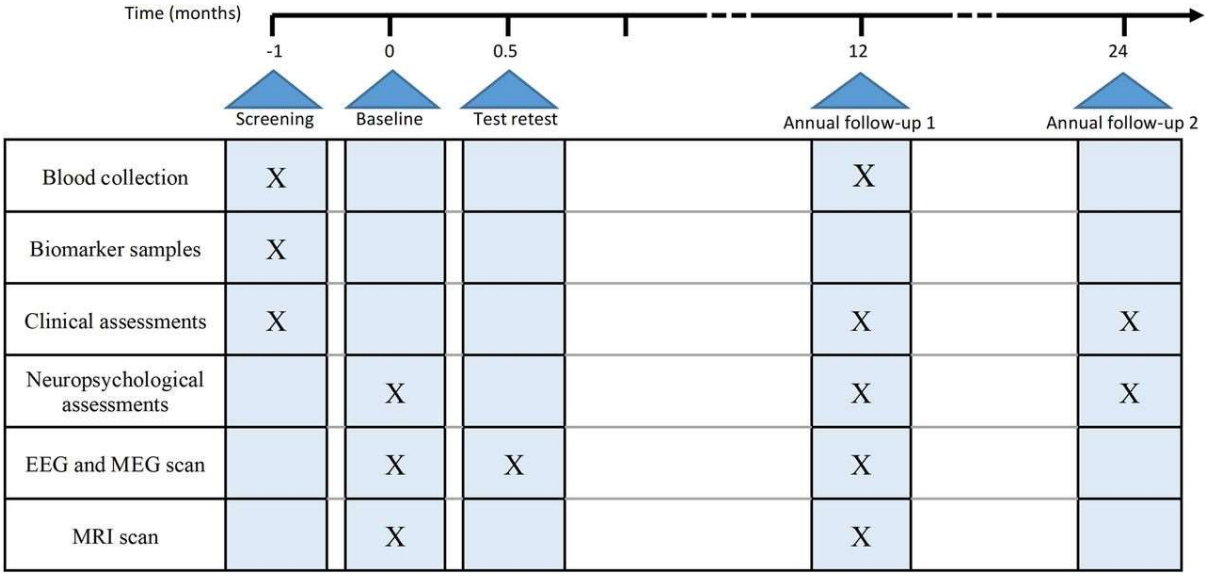


Figure 2.3 Timeline summary of study procedures.
EEG, electroencephalography; MEG, magnetoencephalography.

2.3.2 Blood Samples

Participants are asked to consume only water for two hours prior to blood collection. At baseline and follow up, blood is drawn in the following order: 2.7ml in Sodium Citrate Tubes (plasma), 5ml in Serum Separator Tubes (serum), 10ml in EDTA tubes (DNA), 10ml in EDTA tubes (plasma and buffy coat) and 2x2.5ml in PAXgene tubes (RNA). Once filled, the EDTA and PAXgene tubes are inverted 10 times. From April 2021, 4.9ml of blood is collected in S-monovette tubes for SARS-CoV-2 serology. Samples are processed and frozen according to the guidelines in Table 2.2.

Plasma	The sample in the sodium citrate tube is centrifuged at 2000g for 10 minutes at room temperature. The plasma is aliquoted into 1.4 ml matrix tubes and stored at -80°C.
Serum	At least 30 minutes after blood collection, the sample in the serum separator tube is centrifuged at 2000g for 10 min at room temperature. The serum is aliquoted into 1.4ml matrix tubes and stored at -80°C. Similarly, the sample in the S-monovette tube is centrifuged at 2000g for 10 minutes at room temperature at least 30 minutes after collection. The sample is aliquoted into 2ml Sarstedt tubes.
DNA	The first EDTA tube is frozen as soon as possible and stored at -80°C for later DNA extraction and analysis.
Plasma and buffy coat	The second EDTA tube is centrifuged immediately at 2500g for 15 minutes at room temperature. The plasma and buffy coat are aliquoted into separate 1.4 ml matrix tubes and stored at -80°C.
RNA	PAXgene tubes are stored at room temperature for 2 hours before being frozen upright at -20°C for 24 hours and then stored at -80°C.

Table 2.2 Blood sample processing guidelines

2.3.3 Biomarkers for Alzheimer disease pathology

Clinical criteria are insufficient to reliably diagnose the presence of Alzheimer's disease pathology (Monsell *et al.*, 2015; Ossenkoppele *et al.*, 2015). Additional biomarker evidence are sought, using either cerebrospinal fluid or PET imaging according to participant preference and eligibility (McKhann *et al.*, 2011).

Cerebrospinal fluid

Cerebrospinal fluid is obtained by lumbar puncture and collected in polypropylene tubes. Within one hour of collection, cerebrospinal fluid is centrifuged, separated and the supernatant frozen to −80°C for later batched analysis using a chemiluminescent enzyme immunoassay for total tau, phosphorylated tau and amyloid beta 1-42 levels. Positive amyloid status is indicated by a total tau to amyloid beta 1-42 ratio >1, and amyloid beta 1-42 concentration <450pg/ml. pTau181 concentration is recorded from April 2021.

Amyloid PET

Participants receive a 300 MBq bolus injection of florbetaben and are scanned 80-100 minutes post-injection on a GE Signa PET/MR scanner at the Wolfson Brain Imaging Centre, Cambridge or a GE D710 PET/CT scanner at the Churchill Hospital, Oxford. The centiloid method is used to classify the florbetaben scans as amyloid positive with centiloid >1.19 (Sabri *et al.*, 2015; Rowe *et al.*, 2017).

2.3.4 Clinical Assessments

Clinical assessments are completed at a clinical research centre in one or two sessions.

Clinical Interview

A study clinician interviews the participant and study partner. Clinicians follow a structured interview that covers socio-demographic factors, including age and years of education; lifestyle factors; family history of dementia; medical history, including information on significant medical conditions with date of onset; and concomitant medication usage, with details about dosage and duration.

Addenbrooke's Cognitive Examination

The revised Addenbrooke's Cognitive Examination evaluates orientation, memory, verbal fluency, language and visuo-spatial domains (Mioshi *et al.*, 2006). It is administered and scored according to the Administration and Scoring Guide (2006). Alternate versions at each visit reduce practice effects.

Mini-Mental State Examination

The Mini-Mental State Examination is acquired (Folstein *et al.*, 1975).

Clinical Dementia Rating

The Clinical Dementia Rating quantifies dementia severity through a structured interview (Hughes *et al.*, 1982; Morris, 1993; Washington University Alzheimer's Disease Research Center, 1999). Interviewers rate participant impairments in 6 categories: memory, orientation, judgment and problem solving, community affairs, home and hobbies and personal care. The global CDR is derived from these ratings (Morris, 1993).

Hachinski Ischaemic Score

The Rosen modification of the Hachinski Ischaemic Score seeks to differentiate between primary progressive dementias, including Alzheimer's disease and multi-infarct dementia (Rosen *et al.*, 1980). A study clinician uses information from medical history, physical and neurological examination and medical records to determine the score. Scores below 4 indicate a low likelihood of vascular disease as the cause of dementia.

Self-reported questionnaires

Participants complete the 30-item Geriatric Depression Scale (Ishihara and Terada, 2011), 40-item Spielberger State-Trait Anxiety Inventory (Spielberger *et al.*, 1970), and 11-item

Pittsburgh Sleep Quality Index (Buysse *et al.*, 1989). Study partners complete the 30-item Amsterdam Instrumental Activity of Daily Living Questionnaire (short version, Jutten *et al.*, 2017) and Mild Behavioral Impairment Checklist (Ismail *et al.*, 2017).

Physiological measures

Height, weight, hip-waist ratio, blood pressure, pulse rate and temperature are measured for participants using a stadiometer, electronic weight scales and stretch-resistant tape.

2.3.5 Neuropsychological Assessment

The neuropsychological test battery closely resembles the Deep and Frequent Phenotyping study (Koychev *et al.*, 2019) and IMI-European Prevention of Alzheimer's Disease (Ritchie *et al.*, 2017; Solomon *et al.*, 2018), including the preclinical Alzheimer cognitive composite (Donohue *et al.*, 2014). Assessments take place in a private, testing room in one session with breaks as needed (Table 2.3).

Repeatable Battery for the Assessment of Neuropsychological Status (RBANS)

RBANS measures cognitive decline in 5 domains: immediate memory, visuospatial, language, attention and delayed memory (Randolph *et al.*, 1998). Participants receive alternate forms at repeated assessments. The immediate memory index comprises the *list learning subtest*, with immediate recall of 10-items over 4 trials and the *story memory subtest*, with immediate recall of a 12-item story over two trials. The visuospatial index comprises the *figure copy subtest*, which involves copying a geometric figure and the 10-item, *line orientation subtest*. The language index comprises the 10-item, *picture naming subtest* and the *semantic fluency subtest*, where participants name as many exemplars of the given semantic category as possible in 60 seconds. The attention index comprises the *digit span forwards subtest*, involving immediate repetition of increasing digit strings and the *coding subtest*, scored as the total number of correctly coded numbers generated using an item-to-number code within 90 seconds. The delayed memory index comprises the *list recall subtest*, involving free recall of the list learning task; *list recognition*, where participants decide whether a word was included in the list learning task; *story recall*, where participants freely recall the story memory task; and *figure recall*, where participants draw from memory the figure presented in the figure copy task.

Digit Span Backwards

Digit span backwards, from the Wechsler adult intelligent scale (Wechsler, 1981), is used in conjunction with RBANS digit span forwards. It follows the RBANS digit span format but participants are asked to immediately repeat in reverse order.

Free and Cued Selective Reminding Test

The Free and Cued Selective Reminding Test assesses episodic memory and distinguishes retrieval from storage deficits (Grober *et al.*, 2018). Sixteen pictured items are encoded during the initial learning phase, where participants identify and name items responding to unique semantic cues. After a short delay, participants freely recall all items. Interviewers prompt for each item not recalled using the unique semantic cues from the learning phase. Participants receive alternate forms at repeated assessments.

Logical Memory

Logical Memory, taken from the Wechsler memory scale (third edition), assesses episodic memory (Wechsler, 1999). Participants immediately recall short stories they have been read. After a 30-minute delay with intervening tests, participants freely recall the stories and answer yes or no questions testing story recognition.

National Adult Reading Test

The national adult reading test (second edition) estimates premorbid intelligence from printed, irregular words (Nelson and Willison, 1991).

Digit Symbol Substitution

The digit symbol substitution from the Wechsler Adult Intelligence Scale assesses processing speed and attention (Wechsler, 1981). Participants have 90 seconds to code as many correct symbols as possible corresponding to presented numbers by using the given number-to-symbol code.

Trails Making Test B

The Trails Making Test B assesses executive function, attention and processing speed (Bowie and Harvey, 2006). Following a practice sample to ensure task comprehension, participants are presented with 25 encircled numbers on a page which they connect by alternating between numbers and letters. The time it takes to complete the sample and any errors made are recorded.

Cambridge Neuropsychological Test Automated Battery

The tablet-based Cambridge Neuropsychological Test Automated Battery assesses processing speed, episodic memory, attention, working memory and executive function (Cambridge Cognition, 2019). The reaction time task (simple and five choice variant) assesses processing speed. Participants hold down a response button and release this to respond to on-screen targets. The paired-associates learning task (standard variant) assesses episodic memory. Participants learn associations between patterns and their locations. An initial learning stage precedes immediate recall. The rapid visual processing task (3 target variant) assesses attention. Single digits appear on the screen. Participants respond when they see a string matching target sequences. The spatial working memory task (standard variant) assesses working memory and executive function. Participants search inside on-screen boxes to find and collect tokens. Tokens never appear in the same box twice.

Four Mountains Task

The tablet-based four mountains task assesses allocentric spatial processing (Hartley *et al.*, 2007). During a learning phase, participants learns the topographical layout of 4 mountains presented in a computer-generated landscape. Following a delay, participants are presented with four alternative images and identify the target image matching the topographical mountain layout of the learning-phase image, but with potentially altered colours, textures and points of view.

Order of assessments	**Duration (minutes)**
1. List learning (RBANS subtest) 2. Story memory (RBANS subtest) 3. Figure Copy (RBANS subtest) 4. Line orientation (RBANS subtest) 5. Picture naming (RBANS subtest) 6. Semantic fluency (RBANS subtest) 7. Digit span forwards (RBANS subtest) 8. Digit span backwards 9. Coding (RBANS subtest) 10. List recall (RBANS subtest) 11. List recognition (RBANS subtest) 12. Story recall (RBANS subtest) 13. Figure recall (RBANS subtest)	≈ 40

Break	≈ 15
14. Free and cued selective reminding test (PACC) 15. Logical memory part 1 (PACC) 16. National adult reading test 17. Digit symbol substitution (PACC) 18. Trails B 19. Logical memory part 2 (PACC)	≈ 45
Break	≈ 15
20. Reaction time task (CANTAB subtest) 21. Paired associates learning (CANTAB subtest) 22. Rapid visual processing (CANTAB subtest) 23. Spatial working memory (CANTAB subtest) 24. Four mountains task	≈ 30

Table 2.3 Order of neuropsychological assessments.
RBANS=Repeatable Battery for the Assessment of Neuropsychological Status, PACC=Preclinical Alzheimer Cognitive Composite, CANTAB = Cambridge Neuropsychological Test Automated Battery

2.3.6 Neurophysiology (M/EEG)

M/EEG data are collected simultaneously at 1000Hz in a magnetically-shielded room. At Cambridge, data are collected using the Elekta VectorView system from 2017 to December 2019, with 204 planar gradiometers, 102 magnetometers and an EEG 70-channel EasyCap. Stage 1 scans and the first 12 follow-up scans used the same scanner. The MEGIN Triux Neo M/EEG scanner is used from March 2020 onwards with the same sensor configuration as the VectorView and a 64-channel EasyCap. At Oxford, the MEGIN Triux Neo M/EEG scanner and an EasyCap 60 channel BrainCap for MEG with an augmented 10/20 layout are used for all data collection.

The Polhemus digitisation system records the position of the standard fiducial points, >300 additional head points, five head position indicator coils and EEG electrodes. Head position indicator coils measure head position within the MEG helmet. Electrodes on the right clavicle and left lower rib record electrocardiogram data. Electrodes above and below the left eye and on bilateral canthi record vertical and horizontal electrooculogram data. Reference and ground electrodes are placed on the left side of the nose and left cheek, respectively. During the seated scan, participants rest or perform simple tasks, responding through a button box. Participants wear non-magnetic earphones with sound delivered though plastic tubes and, if necessary, non-

magnetic glasses. Prior to M/EEG, a Snellen eye test and pure tone audiometry assess sight and hearing thresholds.

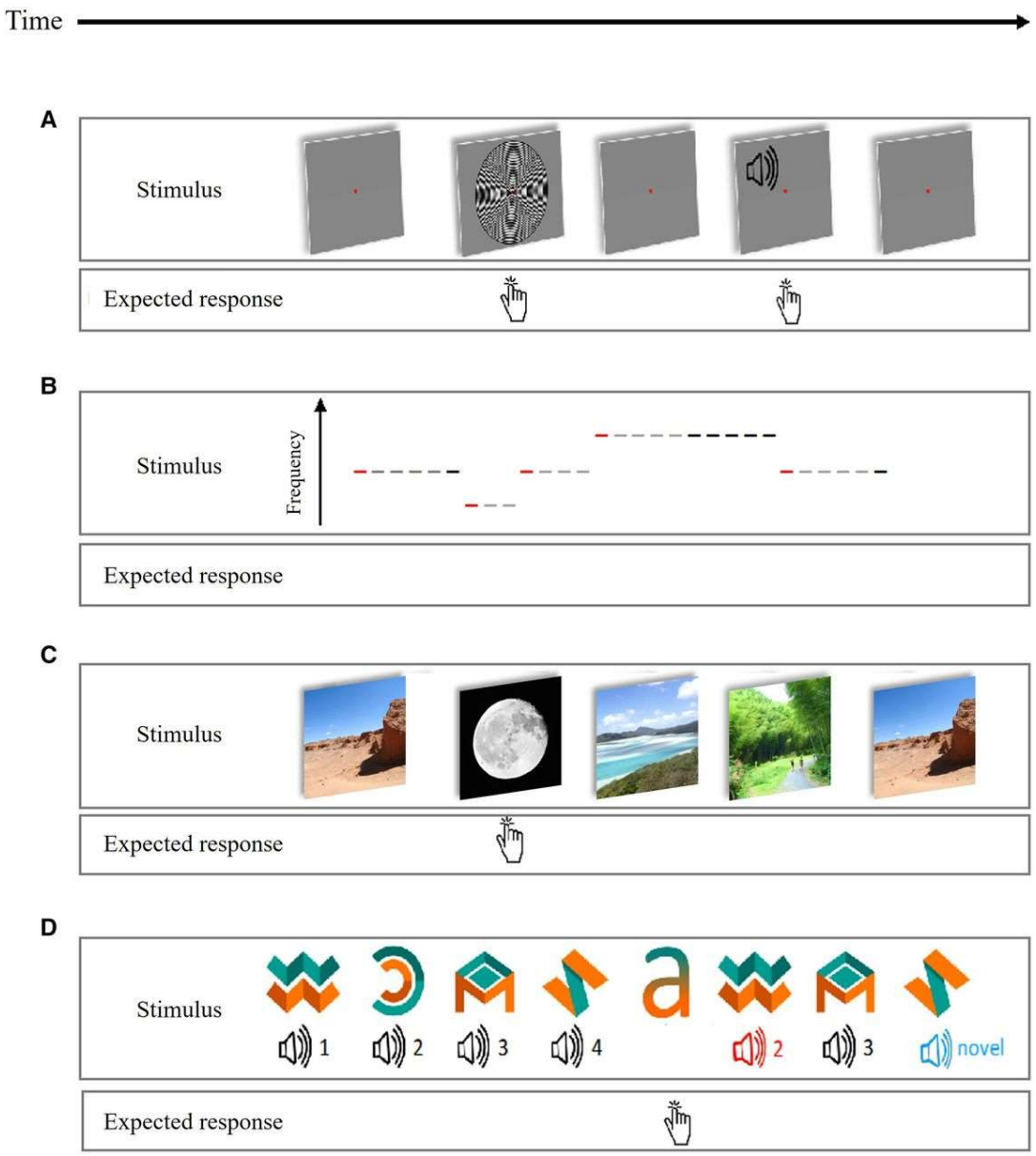


Figure 2.4 NTAD magneto/electroencephalography tasks
a) Audio-visual task: Participants visually fixate on a red dot and press a button whenever they hear or see something. **b)** Mismatch-negativity task: Participants passively watch a nature documentary while listening to tones through the earpieces. Red dashes represent deviant tones and black dashes represent standard tones (from the sixth repetition). **c)** Scene repetition task: Participants view scenes and press the button when they see a scene containing a moon. Each non-target scene repeats once during the task. **d)** Cross-modal oddball task: Participants view object-tone pairs consisting of 4 learnt (standard) pairs (the standard sounds are black in the figure); associative-deviant, object-tone pairs (the associative deviant sound is coloured red in the figure); and standard objects presented with novel tones (the novel deviant tones are blue in the figure). Participants press a button when they see the letter 'a'.

Tasks are carried out in the following order.

Simple audio-visual task

Participants fixate on a red, central fixation dot and quickly respond to each auditory or visual stimuli with a button press (Figure 2.4a). Auditory tones (n=100) of 300Hz, 600Hz or 1200Hz are presented for 300ms after a blank interval of 1000ms. Visual stimuli are concentric black and white circles that appear for 300ms after 3000ms. Filler trials (n=30) containing only the red fixation dot are included. Visual and auditory trials are randomly intermixed. Ten initial practice trials familiarise participants to the task.

Auditory Mismatch-negativity Task

The roving auditory mismatch negativity task elicits error responses to deviant tones followed by rapid plasticity as predictions are updated upon repetition of the deviant stimulus (Friston, 2005; Kiebel *et al.*, 2007). Participants passively watch a muted nature documentary. Through earpieces, they hear binaural, in-phase sinusoidal tones >60dB above the average auditory threshold with durations of 100ms and 500ms stimulus onset asynchrony. Tone frequencies are the same within but different between blocks. Blocks range from 400 to 800Hz. The number of tones per blocks varies from 3 to 11 according to a truncated exponential distribution (Figure 2.4b).

Scene-Repetition Task

In this passive memory test, participants view a series of complex scenes (landscapes and cityscapes) and press a button only when scenes contain a moon (n=26, different moon images). Target scenes containing a moon ensure attention but are not of interest; the main interest is differences between initial and repeated presentations of non-target scenes. Each scene is presented for 800ms and preceded by a fixation cross of 200ms on average (100-300ms). Scenes are pseudo-randomly intermixed with the constraint that 10 initial 'burn-in' complex scenes, with 2 moon target scenes, precede 256 complex scenes presented twice with 14-93 (median=42) intervening scenes between the first and repeat presentation (Figure 2.4c).

Cross-modal Oddball Task

The task assesses hippocampal-dependent, paired-associates learning (Blackwell *et al.*, 2004; De Rover *et al.*, 2011). Trials comprise of a 700ms visual, abstract "object" and a 400ms sound, starting 300ms after trial onset. Inter-stimulus intervals average 300ms. During the initial training period (80 trials), participants learn associations between four standard pairs of visual

objects and sounds. The main task has 770 bimodal trials and 40 unimodal trials, randomly intermixed. Bimodal trials consist of: standard, learnt object-sound pairs (n=670); standard objects paired with novel sounds (n=50); and mismatched pairs, where the object and sound are from different standard pairs (n=50). Unimodal trials ensure the task is attended, participants press a button when they see the letter 'a' (Figure 2.4d). A 10-item assessment follows the task, participants hear a standard sound and report which of four presented objects the sound was paired with most often during the task.

Eyes-open Resting State

Participants are presented with a central fixation cross and instructed to clear their mind, relax, think of nothing specific and focus on the fixation cross for 5 minutes.

Eyes-closed Resting State

Participants are instructed to clear their mind, relax, think of nothing specific and close their eyes but stay awake.

2.3.7 Magnetic Resonance Imaging

MRI sequences use 3T Siemens PRISMA scanners at the Cambridge MRC Cognition and Brain Science Unit and Oxford Centre for Human Brain Activity (Table 2.4).

T1-weighted	The 3D T1-weighted structural image is acquired using the Generalized Autocalibrating Partially Parallel Acquisitions (GRAPPA) technique applied to a high-resolution Magnetization Prepared Rapid Gradient Echo (MPRAGE) sequence with the following parameters: TE=2.91ms, TR = 2300.00ms, TI=900.00ms, flip angle =9 degrees, acquisition matrix =256 x 240, voxel size =1.00mm isotropic, number of slices =176, slice thickness =1mm, acquisition time =5 minutes and 12 seconds
T2 FLAIR	The 3D FLAIR structural image is acquired using the following parameters: TE=394.00ms, TR =5000.00ms, TI =1650.00ms, flip angle =120 degrees, acquisition matrix =256 x 256, voxel size =1.00mm isotropic, number of slices =192, slice thickness =1.00mm, acquisition time =5 minutes and 7 seconds
T2*-weighted	The T2*-weighted structural image is acquired using the following parameters: TE =20.00ms, TR =640.00ms, Flip angle =20 degrees,

	acquisition matrix =256 x 256, number of slices =47, slice thickness =3.00mm, Voxel size =0.90x0.90x3.00mm, Acquisition time =4 minutes and 7 seconds
T2-weighted with fat saturation	The T2-weighted image with fat saturation is acquired with the following parameters: TE =78.00ms, TR =4000.00ms, flip angle =150 degrees, acquisition matrix =256x232, number of slices =47, slice thickness=3.00mm, voxel size =0.90x0.90x3.00mm, acquisition time =3 minutes and 26 seconds
Diffusion Weighted Imaging	The Diffusion-Weighted Images are acquired with a spin-echo echo-planar sequence. B-values of 0, 300, 700 and 2000 s/mm^2 were used with 116 diffusion gradient directions obtained via MRTrix3 (Tournier *et al.*, 2019). The number of signal averages was 12, 8, 32, and 64 for b-values of 0, 300, 700 and 2000, respectively. The acquisition is run in the transverse orientation without any angulation. Other scan parameters include: TR=3800ms; TE=85.00ms, voxel size=2.50mm isotropic, acquisition matrix =96x96, number of slices=64, slice thickness =2.50mm, acquisition time=8 minutes and 45 seconds
Quantitative Susceptibility Mapping	The quantitative susceptibility mapping correlates with Aβ-amyloid iron density and is acquired with a 3D Gradient Echo sequence with multiple echoes and flow compensation in the readout and slice directions. (TE 1=5.20ms, TE 2=10.4ms, TE 3 =15.6ms, TE 4 =20.8ms, TE 5=26.0ms; TR =31.0ms, flip angle =15 degrees, acquisition matrix =256x192, number of slices =160 (per TE), slice thickness =1.00mm, voxel size =1.00mm isotropic, acquisition time =5 minutes 10 seconds.
Resting state eyes open	For the resting-state scan, the participants are presented with a fixation cross and asked to maintain fixation throughout the task. Echo planar images are acquired with 200 volumes with the following parameters: TE=30.00ms, TR=1500.00ms, flip angle =90 degrees, acquisition matrix =64x64, number of slices =54, slice thickness =3.00mm, voxel size = 3.00mm isotropic, acquisition time =5 minutes 50 seconds
Hippocampal subfields	The high-resolution, hippocampal subfield images are acquired with T2-weighted, turbo spin echo sequences and run with the following parameters:

	TE=50.00ms, TR=8020.00ms, flip angle =122 degrees, acquisition matrix =448x448, number of slices =30, slice thickness =2.00mm, voxel size =0.4x0.4x2.0mm, acquisition time =8 minutes 11 seconds.
Arterial Spin Labelling	3D Arterial Spin Labelling images are acquired using a flow-sensitive alternating inversion recovery spin-echo pulsed sequence with Q2-TIPS bolus saturation in the transverse plane with the following parameters: TR=4000.00ms; TE =13.20ms; flip angle =130 degrees, labelling duration =800ms, post-labelling delay =2000ms, acquisition matrix =64x60; slices per slab =32, slice thickness =4.50mm, voxel size =1.85x1.85x4.50mm, acquisition time =6 minutes 46 seconds.

Table 2.4 Order and parameters of MRI sequences.
FLAIR=Fluid Attenuated Inversion Recovery, TE=Echo time, TR=Repetition time, TI=Inversion time

2.4 Ethics and Dissemination

The study received a favourable opinion from the East of England – Cambridge Central Research Ethics Committee (REC reference 18/EE/0042). Imaging data and clinical severity scores are hosted by Dementias Platform UK Imaging Platform (https://portal.dementiasplatform.uk), using XNAT (https://www.xnat.org). Data will be made available with a managed access process through Dementias Platform UK, with constraints to preserve confidentiality and privacy.

3 | Describing the NTAD Cambridge cohort

Abstract: In this chapter, I report differences between baseline groups (patients versus controls) and patient sessions (baseline versus follow up) using standard biomarkers (of clinical severity, pathology, cognition, and brain volume). I confirm that the group of NTAD Cambridge participants have data features typical of people with mild cognitive impairment and early dementia due to Alzheimer's disease.

3.1 Introduction

The purpose of this chapter is to characterise the NTAD Cambridge cohort's clinical, cognitive and MRI data using conventional measures. Novel MEG and model-based markers are considered in later chapters. Four data domains are evaluated:

1 Clinical: Clinical assessments, including the clinical dementia rating (CDR) and mini-mental state examination (MMSE), are commonly used as clinical trial endpoints (Tampi *et al.*, 2021). They are sensitive to progression of Alzheimer's disease (Lansdall *et al.*, 2023). The CDR is widely used in research and clinics to stage dementia severity from very mild (0.5), mild (1), moderate (2), to severe (3; Hughes *et al.*, 1982). The CDR global score increases from 'mild' to a higher score for around 65% of people with Alzheimer's disease after 36 months (Williams *et al.*, 2013). The MMSE is used frequently for clinical trials of Alzheimer's disease as a secondary endpoint (Tampi *et al.*, 2021). Over 36 months, MMSE total scores can be expected to decrease by ~2 points with minimal functional deterioration, or by ~7 points with moderate deterioration in people with Alzheimer's disease (Lansdall *et al.*, 2023). However, MMSE is insensitive to detect decline in people with presymptomatic Alzheimer's disease due to ceiling effects (Evans *et al.*, 2018). A drug would have to be unrealistically effective for MMSE scores to be sensitive enough to detect therapeutic effects in people with early mild cognitive impairment due to Alzheimer's disease (Evans *et al.*, 2018).

2. Pathology: In the earliest stages of disease, where treatment may have most long-term benefit, cognitive assessments are insensitive to detect dementia progression (US Food and Drug Administration, 2022). The US Food and Drug Administration (FDA) approved the candidate treatment aducanumab based principally on amyloid-PET endpoints, despite failing to show significant neuropsychological benefit (US Food and Drug Administration, 2021). Alzheimer pathology can be localised and quantified using positron emission tomography (PET) with ligands that bind to the aggregated tau protein (Ossenkoppele *et al.*, 2016; Passamonti *et al.*, 2017, 2018; Cope *et al.*, 2018; Leuzy *et al.*, 2019), beta-amyloid plaques (Cai *et al.*, 2006), synapses (Venkataraman *et al.*, 2021) or neuroinflammation (Bevan-Jones *et al.*, 2017). People with presymptomatic or early-stage Alzheimer's disease have increased beta-amyloid deposition, with the amyloid-PET standardised uptake value ratio (SUVR) increasing by ~0.05 per year. The rate of amyloid deposition plateaus as disease progresses to 0.03 SUVR per year for people with dementia due to Alzheimer's disease (Villemagne *et al.*, 2013). More

recently, blood biomarkers, such as p-tau217 and p-tau181, have been developed for sensitivity to Alzheimer's disease and its progression, in proportion to the beta-amyloid burden (Coomans *et al.*, 2023; Ashton *et al.*, 2024). P-tau 181 is sensitive to disease and its progression at preclinical (amyloid-positive, cognitively normal participants) and prodromal (amyloid-positive, mild cognitive impairment) stages of Alzheimer's disease with annual increases in p-tau 181 levels of 0.5 pg/ml (Chen *et al.*, 2021). P-tau217 is particularly promising, with strong associations with amyloid-PET signals (Thijssen *et al.*, 2021). P-tau217 is also sensitive to Alzheimer's disease presence and its progression at pre-clinical Alzheimer's disease stages (Ashton *et al.*, 2024), with levels increasing by ~0.1 pg/ml/year (Ashton *et al.*, 2024).

3. Neuropsychology: The NTAD neuropsychological battery includes the Addenbrooke's Cognitive Examination Revised (ACE-R), the Repeatable Battery for the Assessment of Neurological Status (RBANs) and the Preclinical Alzheimer Cognitive Composite (PACC) batteries. These tests are commonly used to quantify cognitive decline in Alzheimer's disease (Lanskey *et al.*, 2022). The ACE-R and RBANS assess multiple cognitive domains and were designed to capture the range of cognitive impairment due to dementia (Randolph *et al.*, 1998; Mioshi *et al.*, 2006). The ACE-R has excellent sensitivity to Alzheimer's disease (Larner, 2007) and the score significantly reduces with disease progression (Hsieh *et al.*, 2012; Malpetti *et al.*, 2020), by ~4 points per year (Hsieh *et al.*, 2012). RBANS total scores significantly reduce for people with Alzheimer's disease compared to controls (Duff *et al.*, 2008), and significantly reduce over follow up for people with moderate Alzheimer's disease (by ~4 points per year, Teng *et al.*, 2021). The PACC assesses memory, executive function and orientation and was designed to be a primary endpoint measure for clinical trials of Alzheimer's disease (Donohue *et al.*, 2014). PACC scores of amyloid-positive, cognitively-normal people decline significantly more than amyloid-negative, cognitively-normal people over 24 months (Donohue *et al.*, 2014). While memory is the cognitive domain with greatest decline in early stages of Alzheimer's disease pathogenesis (e.g. for controls with a positive amyloid status), as disease progresses other non-memory domains have relatively higher decline e.g. for people with a diagnosis of Alzheimer's disease (Villemagne *et al.*, 2013).

4. Structural imaging. Clinical trials often use MRI-based neuroimaging to quantify the presence and progression of atrophy. Structural changes caused by Alzheimer's disease can be readily measured with MRI (Frisoni *et al.*, 2010; Knight *et al.*, 2016), such as entorhinal (Holland *et al.*, 2012) and hippocampal atrophy (Leung *et al.*, 2010). Cognitively normal

people with low amyloid levels have hippocampal atrophy of around -0.03 cm^3/year, while people with presymptomatic Alzheimer's disease have hippocampal atrophy of -0.05 cm^3/year; and people with a clinical diagnosis of mild cognitive impairment or Alzheimer's disease and high amyloid levels have hippocampal atrophy of -0.10 cm^3/year (Villemagne *et al.*, 2013). Falling total brain volume or rising ventricular volume are also used as a primary outcome of clinical trials (Kehoe *et al.*, 2021). Total brain volume reduces by around 20 mL/year for people with mild to moderate Alzheimer's disease (Kehoe *et al.*, 2021).

Note that in view of the selection criteria set out in Chapter 2, the patient and control groups are expected to be markedly different to each other on the standard clinical, cognitive, neuropsychological and imaging tests: as such, many of the simple descriptive values presented in this chapter are merely confirmatory. However, they establish the profile of phenotype and severity of the NTAD participants' disease with which to contextualise and compare the novel assessments in later chapters.

I expected the cohort's data to reproduce typical findings of cognitive decline, medial temporal lobe atrophy (Visser *et al.*, 2002), neuropsychological impairment typical of Alzheimer's disease (Weintraub *et al.*, 2012) and Alzheimer pathology, detectable with positron emission tomography (PET, Bullich *et al.*, 2021), cerebrospinal fluid (CSF, Fagan *et al.*, 2007), p-tau181 (Coomans *et al.*, 2023) and p-tau217 (Ashton *et al.*, 2024).

I also describe the baseline demographic data of people who withdrew from the longitudinal assessments and whether their baseline demographics differed significantly from the people who completed the 16-month follow up to describe any bias introduced.

3.2 Methodology

3.2.1 Patient Characteristics

This chapter presents demographic, clinical, cognitive and MRI data from the 50 people with a diagnosis of Alzheimer's disease or mild cognitive impairment with a positive amyloid status (Alzheimer's disease) and 15 healthy control participants from the Cambridge NTAD cohort.

Independent Student's t-tests and Bayesian t-tests were used for continuous data, or chi-squared tests for categorical data, to identify differences at baseline between (1) participants with

symptomatic Alzheimer's disease and control participants and (2) people who completed follow up and who withdrew.

3.2.2 Clinical data analysis

For the clinical data analysis, two people were excluded whose diagnosis of mild cognitive impairment or Alzheimer's disease changed to a non-Alzheimer dementia during follow up. Independent (patient versus control groups) or paired-sample (patients at baseline versus 16-month follow up sessions) Student's t-tests and Bayesian t-tests were used to compare means between groups and sessions for MMSE and ACE-R scores. To calculate the average annual rate of decline for people with Alzheimer's disease, the annualised decrease in points per participant was calculated (as 365*value/days between baseline and follow up) and averaged across participants.

3.2.3 Pathology markers

Independent (groups) or paired-sample (sessions) Student's and Bayesian t-tests were used to compare means for p-tau217 and p-tau181 levels, SUVR from amyloid-PET and CSF measures. Effect sizes were calculated using Cohen's d. To see how the relatively new blood measures correlated with standard measures, pairwise Pearson's correlations were run on complete observations of the following pathological measures: PET SUVR, CSF tau/amyloid-beta 1-42 ratio, CSF phosphorylated tau, CSF total tau, CSF amyloid-beta 1-42, p-tau181 and p-tau217.

3.2.4 Neuropsychology: principal component analysis

Three people with Alzheimer's disease were excluded who did not complete the neuropsychology battery (n=1) and/or had a change of diagnosis (n=2). The following variables were used in the principal component analysis: the ACE-R total score; the PACC score (defined as the sum of the normalised total recall score from the Free and Cued Selective Reminding Test, FCSRT, delayed recall score from the logical memory subtest from the Wechsler Memory Scale, the digit symbol substitution test score and the MMSE total score); RBANS total score; the time taken to complete the Trials B sample; the sum of the digit span forward and backward scores; the total number of errors made on the National Adult Reading Test; the recommended metrics from the Cambridge Neuropsychological Test Automated Battery (CANTAB) battery as detailed in Table 3.2 (Please see Chapter 2 for further details).

I used the patient data at baseline to determine the principal components of cognitive and behavioural change. I used the MICE package (Multivariate Imputation via Chained Equation) in R to impute the missing patient, baseline data (19.2%). I scaled and centred the patient, baseline data and then I used R's *prcomp* function to determine the principal components. The principal component analysis was conducted without varimax rotation.

Principal component scores for control participants and participants with symptomatic Alzheimer's disease at 16-month follow up were calculated using the factor loadings from the baseline, patient principal component analysis. First, the MICE package was used to impute missing data for each group and session separately. For neurologically healthy people, 3.59% of data was missing; for people with Alzheimer's disease at 16-month follow up, 44.2% of data was missing. I scaled the data of controls and patients at 16-month follow up using the centring and scaling parameters obtained from patients at baseline.

The standardised scores for each participant at each session were multiplied with the first principal component's factor loadings from the baseline, patient principal component analysis and summed to give principal component scores. I used independent sample or paired sample Student's t-tests and Bayesian t-tests to assess differences between principal component scores of patients and controls at baseline. I used paired frequentist and Bayesian t-tests to assess differences in principal component scores for patients at baseline versus follow-up sessions. Effect sizes were calculated using Cohen's d.

3.2.5 Structural Imaging analysis: Voxel-based morphometry

The T1-weighted images were analysed using Statistical Parametric Mapping toolbox (SPM12, The Wellcome Trust Centre for Neuroimaging, UCL, UK). First, the images were segmented into grey matter, white matter and cerebrospinal fluid (Ashburner and Friston, 2005). Next, the DARTEL algorithm was used to create a group template (Ashburner, 2007) registered to MNI space. This was used to generate Jacobian-scaled grey matter images in MNI space for each subject which were smoothed with an 8 mm FWHM Gaussian kernel. To calculate total brain volume, I summed grey and white matter for each participant. To calculate total intracranial volume, I summed cerebrospinal fluid and grey and white matter. Independent and paired Student's and Bayesian t-tests were used to compare total brain volume between groups at baseline (patients vs controls) and sessions (patients at baseline versus follow up). Effect sizes were calculated using Cohen's d.

To compare the grey matter volumes of patients and controls, an independent two-sample t-test within SPM's general linear model was performed on the grey matter images. A multiple regression analysis was also performed on the grey matter images that included scores from the first principal component of the neuropsychological scores, age and the intercept in the design matrix. Both analyses used absolute masking with a threshold of 0.2, total intracranial volumes for proportional scaling, age as a covariate of no interest and false discovery rate (FDR) correction applied at $p < .05$.

I ran a longitudinal pairwise regression to align baseline and follow-up scans within participant. For the pairwise longitudinal registration, I specified the time (in years) between scans for each participant and used default values for the noise estimate ('NaN'), warping regularisation (0, 0, 100, 25, 100) and bias regularisation (1000000). This generated a mid-point average image for each person, which was segmented using default settings, and a Jacobian difference image which was multiplied with the segmented average grey matter image for each participant and normalised. Then, I ran a voxel-wise, one sample t-test on the resulting images and applied FDR correction for multiple comparisons at $p < .05$.

3.3 Results

3.3.1 Participant demographics

Participant demographics and screening data are shown in Table 3.1. There were no significant differences between the control and baseline patient groups for sex, education, handedness or Hachinski ischaemic score; there was a significant difference for age, with patients older than controls. There were significant differences for MMSE, ACE-R, CDR, PET and CSF.

	Controls	AD Baseline	AD Retest	AD Follow up	AD withdrew	Controls vs AD	Follow up vs withdrew
Sex (Male:Female)	9:6	25:25	6:9	19:17	6:8	χ^2=0.15, p=.70	χ^2=0.10, p=.75
Handedness (Right:Left:Both)	12:3:0	45:4:1	14:0:1	32:3:1	13:1:0	χ^2=1.97, p=.37	χ^2=0.42, p=.81
Education (yrs)	16.2 (±3.38)	14.2 (±3.86)	14.0 (±4.55)	14.5 (±4.16)	13.3 (±2.87)	t=1.96, p=.06, BF=1.11	t= -1.20, p=.24, BF= = 0.47
Baseline Age (yrs)	65.3 (±7.03)	73.5 (±7.32)	74.4 (±7.19)	72.6 (±7.78)	75.9 (±5.53)	t=-3.96, p<.001, BF=93.2	t= 1.67, p=.10, BF=0.70
Baseline CDR	0 (±0)	0.65 (±0.23)	0.53 (±0.23)	0.63 (±0.23)	0.7 (±0.26)	χ^2=61, p<.001	χ^2=0.13, p=.72
Baseline MMSE	29.4 (±0.74)	24.9 (±3.42)	26.1 (±2.94)	24.9 (±3.09)	24.7 (±4.27)	t=8.56, p<.001, BF=3601	t= -0.18, p=.86, BF=0.31
Baseline ACE-R	92.8 (±4.97)	73.9 (±13.7)	78.9, (±10.14)	74.7 (±11.4)	71.7 (±18.6)	t=8.16, p<.001, BF= 6682	t=-0.56, p=.58, BF = 0.37
Baseline HIS	0.07 (±0.26)	0.54 (±0.79)	0.73 (±0.96)	0.5 (±0.79)	0.6 (±0.84)	χ^2=5.54, p=.14	χ^2=1.28, p=.73
Baseline PET† (SUVR)	1.08 (± 0.23)	1.68 (±0.20)	1.79 (±0.21)	1.71 (±0.19)	1.60 (±0.20)	t=-4.18, p=.04, BF=264	t= -1.31, p =.22, BF = 0.75
Baseline CSF† (tau/Abeta 1-42)	0.38 (±0.23)	2.10 (±1.25)	2.62 (±1.45)	1.97 (±1.28)	2.40 (±1.21)	t = -6.33, p<.001, BF= 75.8	t = 0.76, p = .46, BF = 0.49
Taking dementia medication (%)	0	52.0	40.0	52.8	50.0	χ^2=10.9, p<.001	χ^2=0.00, p=1

Table 3.1 Participant demographics and screening data

Values are given as mean (SD). AD, people with symptomatic Alzheimer's disease, CDR, clinical dementia rating; MMSE, mini-mental state examination; ACE-R, Addenbrooke's cognitive examination revised; HIS, Hachinski ischaemic score, PET, positron emission tomography; SUVR, standardised uptake value ratio; CSF, cerebrospinal fluid; BF, Bayes factor. †Amyloid status was assessed using CSF or PET. For amyloid-PET, 3/15 controls and 25/50 patients; for CSF, 9/15 controls, 24/50 patients. Amyloid status was determined from previous studies for the remaining participants.

3.3.2 Clinical tests

For the clinical data, there were expected differences between controls and patients for MMSE and the ACE-R total score (see Table 3.1), with large effect sizes (MMSE: d=1.49; ACE-R: d=1.54). ACE-R subdomains significantly differed between patients and controls for attention and orientation (t=5.89, p<.001, BF=45.7, d=1.07), memory (t=10.9, p<.001, BF=13044350, d = 2.19), language (t=4.78, p<.001, BF=6.82, d =0.84), and visuospatial domains (t=4.10, p<.001, BF=3.04, d = 0.72); however, fluency was not significantly different between groups (t=2.03, p=0.05, BF=0.43, d = 1.53).

MMSE scores were lower at follow up than baseline (t = 4.21, p<.001, BF=149, d = 0.53). ACE-R total scores were lower at follow up (t=3.27, p=.002, BF=14.3, d=0.59). The ACE-R subdomains that were impaired for people with Alzheimer's disease at baseline compared to control participants, became further impaired at follow up for attention and orientation (t=4.53, p<.001, BF=347, d = 0.49), memory (t=2.08, p=.04, BF=1.23, d = 0.28), language (t=3.59, p=.001, BF=30.8, d =0.36) and visuospatial domains (t=3.88, p<.001, BF=64.5, d = 0.40). Fluency was not significantly lower at follow up than baseline (t=1.73, p=0.09, BF= 0.70, d = 0.28). MMSE score changed by an average rate of -1.97 points/year and ACE-R total score by -5.47 points/year. The ACE-R subdomains changed by -1.48 points/year (-8.23 %/year) for attention and orientation, -0.96 points/year (-3.68 %/year) for memory, -0.50 points/year (-3.54 %/year) for fluency, -1.54 points/year (-5.93 %/year) for language, and -0.99 points/year (-6.22 %/year) for visuospatial domains.

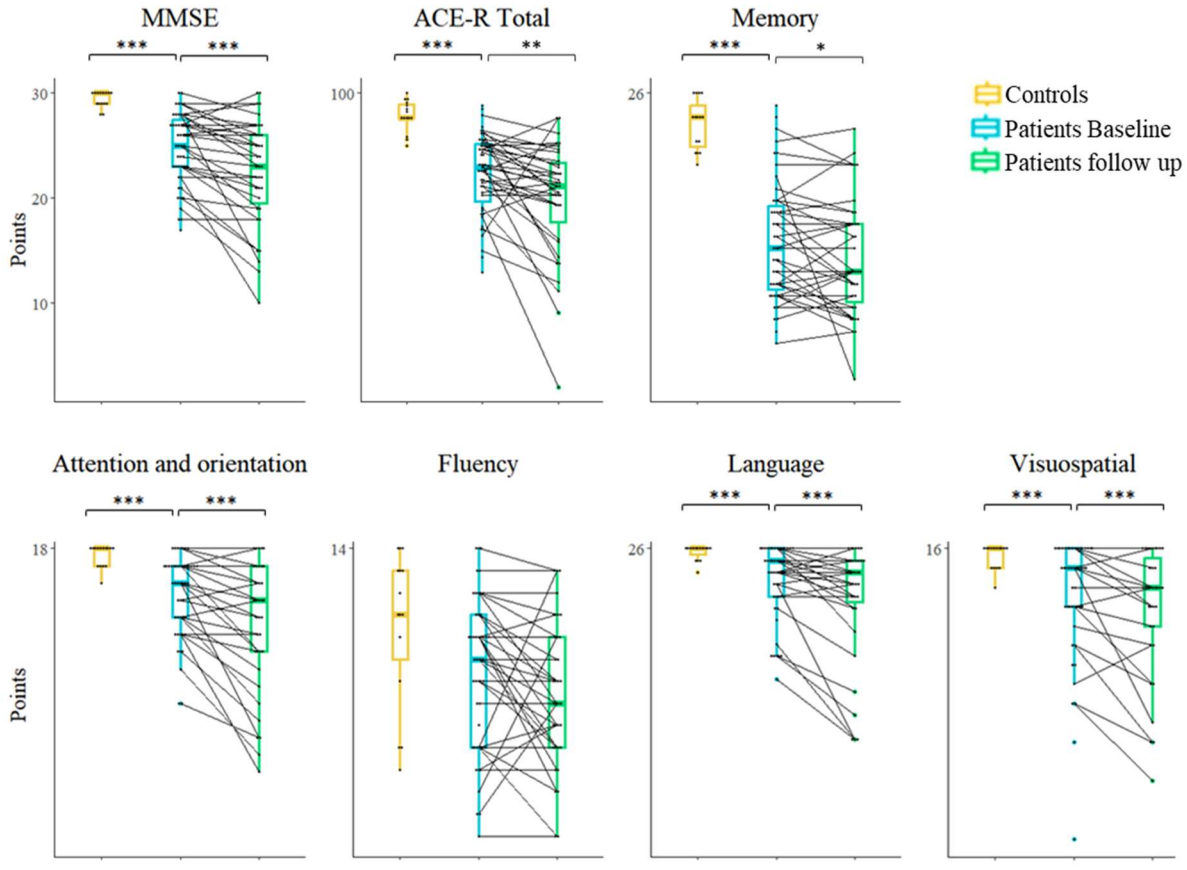


Figure 3.1 Clinical test scores for people with Alzheimer's disease compared to controls.
Participants with Alzheimer's disease performed worse than controls and worse at follow up for MMSE and ACE-R total scores and ACE-R subdomains (Memory, Attention and orientation, Language and Visuospatial). ACE-R, Addenbrooke's Cognitive Examination Revised; MMSE, mini-mental state examination. *p<.05, **p<.01, ***p<.001

3.3.3 Clinical features

CSF and blood biomarkers were, as expected, higher for people with Alzheimer's disease compared to controls at baseline (see Figure 3.2). There were differences in p-tau181 levels (t = -6.13, p<.001, BF = 26739), p-tau217 levels (t = -8.42, p<.001, BF= 7628), amyloid PET SUVR (t=-4.18, p=.04, BF=264), CSF tau/amyloid beta 1-42 (t = -6.33, p<.001, BF= 75.8), CSF amyloid beta 1-42 (t = 3.58, p=.006, BF = 521), CSF total tau (t = -4.76, p<.001, BF = 14.8) and CSF p-tau (t = -4.35, p<.001, BF = 6.79). Effect sizes were large for all measures. Effect sizes were largest for amyloid-PET (d = 2.96) followed by CSF amyloid-beta 1-42 (d = 1.99), p-tau181 (d = 1.69), CSF tau/amyloid beta 1-42 (d = 1.59), p-tau217 (d = 1.57), CSF total tau (d = 1.34) and CSF p-tau (d = 1.17).

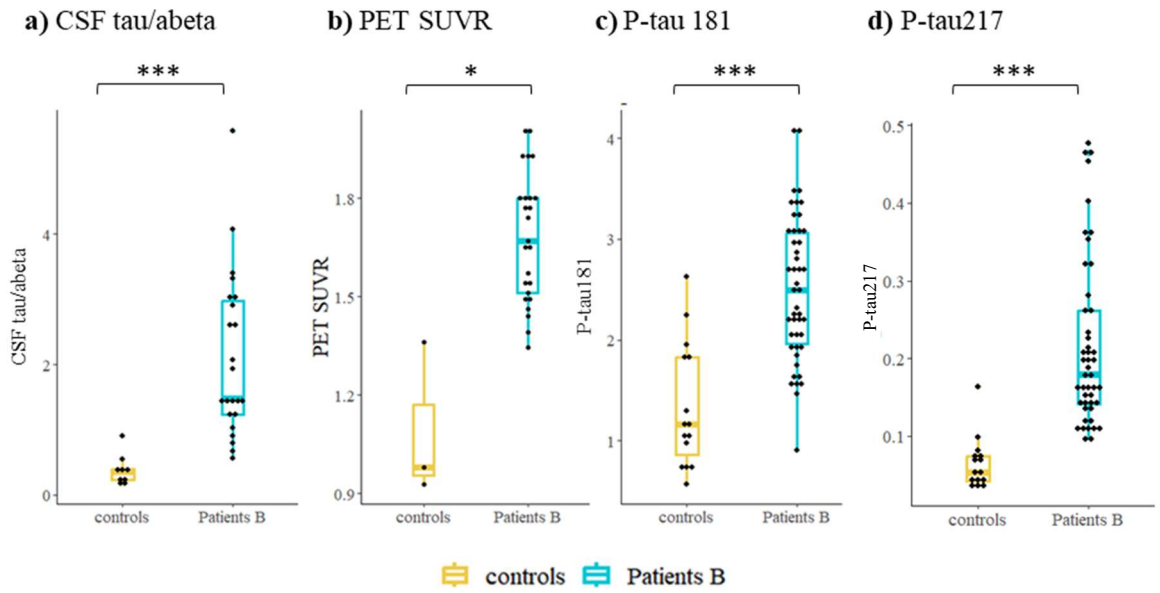


Figure 3.2 Alzheimer's pathology for controls versus people with Alzheimer's disease at baseline. Participants with Alzheimer's disease had higher measures of Alzheimer's disease pathology measured with **a)** CSF, **b)** PET, **c)** p-tau181 and **d)** p-tau217. CSF, cerebrospinal fluid; PET, positron emission tomography; SUVR, standardised uptake value ratio. *p<.05, ***p<.001

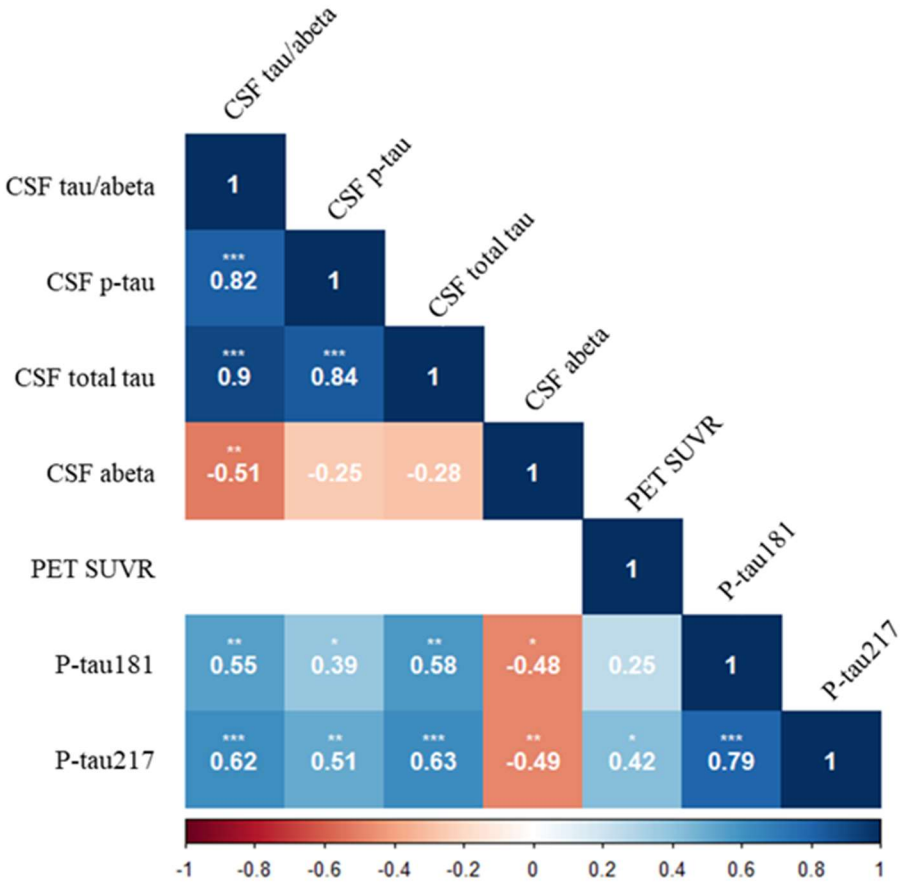


Figure 3.3 Correlations between fluidic and CSF biomarkers for controls and patients.
Pairwise Pearson's correlation coefficients are shown. Participants completed either lumbar puncture or amyloid-PET. CSF, cerebrospinal fluid; abeta, amyloid beta 1-42; PET, positron emission tomography; SUVR, standardised uptake value ratio. *p<.05, **p<.01, ***p<.001

3.3.4 Principal component analysis of neuropsychology

The first three components identified by the principal component analysis are shown in Table 3.2 and explain 66.7% of the data variance (for variances explained by each component, please see Figure 3.4).

There was a significant difference for the first principal component (PC1) scores between patients and controls (t = -10.9, p<.001, BF = 138654480, d = -2.38). PC1 scores also significantly differed for people with Alzheimer's disease at follow up compared to baseline (t = -2.47, p=.01, BF = 2.51, d = 0.35). PC2 scores were significantly different between patients and controls at baseline (t = 4.54, p<.001, BF = 818, d = 1.37) and for patients at baseline versus follow-up sessions (t=-2.58, p=.01, BF = 3.13, d = 0.44). PC3 scores did not differ significantly between groups or between sessions.

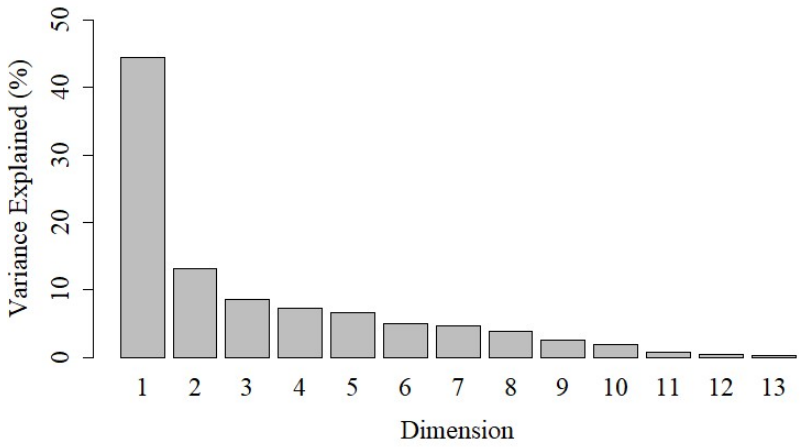


Figure 3.4 Scree plot showing percentage of variance explained by principal components.
The principal component analysis was of neuropsychology data from people with Alzheimer's disease at baseline.

	PC1	PC2	PC3
Eigenvalue	**5.79**	**1.70**	**1.12**
Variance explained	**44.5**	**13.1**	**8.63**
ACE-R	**-0.34**	-0.14	0.09
PACC	**-0.37**	0.09	0.10
RBANS	**-0.38**	-0.02	0.11
Trails B	0.29	-0.09	0.08
Digit span total	-0.27	**-0.36**	0.02
NART errors	0.19	0.17	-0.11
PAL first mem	-0.24	**0.52**	**-0.33**
PAL tea	0.28	**-0.50**	0.24
RTI	0.20	**0.34**	**0.37**
RVPA	**-0.32**	-0.03	0.20
RVPlatency	0.28	0.29	-0.09
SWMberrors	0.21	-0.10	-0.06
SWMstrategy	0.01	-0.29	**-0.77**

Table 3.2 Loadings of principal components of the neuropsychological data.
Loadings are based on the principal component analysis, which was conducted without varimax rotation. Component loadings > 0.3 are highlighted. PC – principal component; ACE-R – Addenbrooke's Cognitive Examination Revised; PACC – Preclinical Alzheimer's cognitive composite; RBANS – Repeatable battery for the Assessment of Neurological Status; Trails B - Trails B time to completion; NART – National Adult Reading Test errors; PALfirst mem – paired associates learning (PAL) first memory score; PAL tea – PAL total errors adjusted; RTI - reaction time; RVPA- rapid visual processing (RVP) A prime; SWMberrors – spatial working memory (SWM) between errors; SWMstrategy – spatial working memory strategy

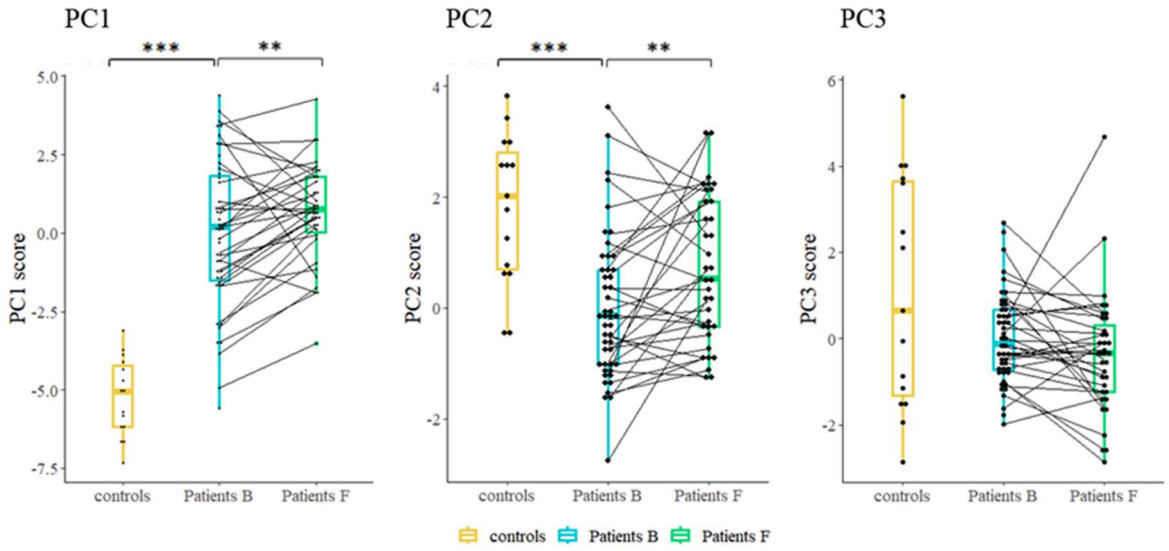


Figure 3.5 Principal component scores for controls and patients at baseline, and patients at follow up.
PC, Principal Component, B, Baseline, F, follow up. **p<.01, ***p<.00. Note the "improvement" in PC2 which may be due to practice effects on the PAL task.

3.3.5 Voxel-based morphometry

There were significant differences in total brain volume for people with versus without Alzheimer's disease (t = 4.42, p < .001, BF = 10404, d = 1.59) and for people with Alzheimer's disease at baseline versus 16-month follow up (t = 8.53, p < .001, BF = 19234125, d = 0.4).

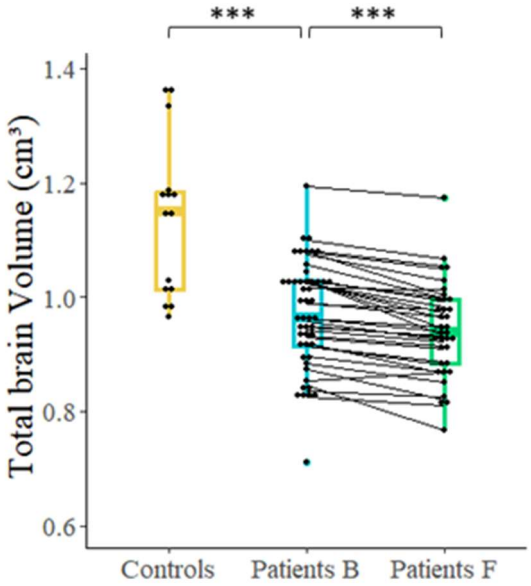


Figure 3.6 Alzheimer's disease progressively affects total brain volume.
Total brain volume is shown for healthy controls (yellow) and people with Alzheimer's disease at baseline (blue) and follow-up (green) sessions. B, baseline; F, follow up.

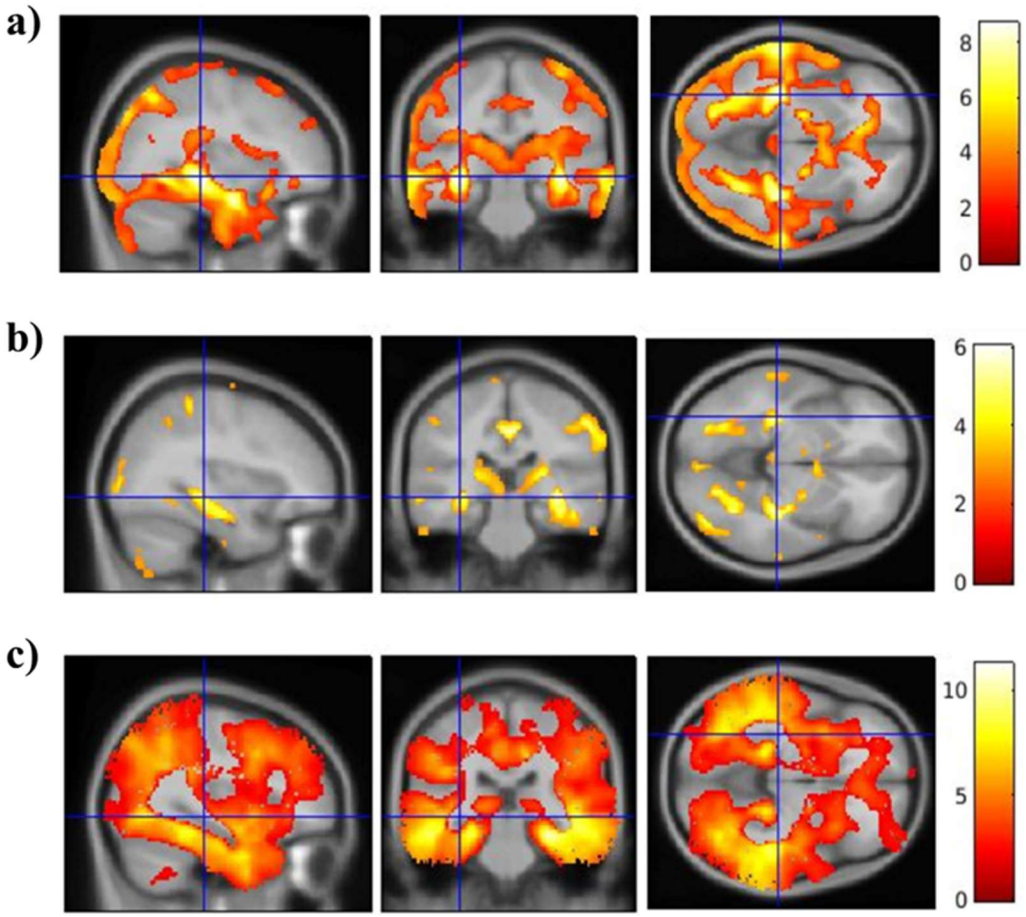


Figure 3.7 Voxel-based morphometry of T1-weighted MRI images
Atrophy is shown for people with Alzheimer's disease **a)** compared to control participants, **b)** that correlates with disease severity as measured using the neuropsychological PC1 score and **c)** at follow-up compared to baseline sessions. For all images, the crosshair is centred on the most significant coordinate from patients versus controls at -34.5, -28.5, -6 (MNI coordinates) in the left hippocampus. For all images, a false discovery rate correction was applied at p <.05.

In the contrast of people with Alzheimer's disease compared to neurologically-healthy people, grey matter volume decreased for patients at regions including the hippocampus (see Figure 3.7a and Table 3.3). The neuropsychological score calculated using the first principal component also significantly correlated with grey matter atrophy in regions including the hippocampus (see Figure 3.7b and Table 3.4). The second and first principal components did not significantly correlate with grey matter (with FDR correction applied at p< .05). With disease progression over 16 months there was significant grey matter atrophy in widespread temporoparietal regions including the hippocampus (see Figure 3.7c and Table 3.5).

Cluster size (voxels)	MNI coordinates			Nearest AAL Region	T	p (FDR-corrected)
	x	y	z			
183718	-34	-28	-6	Hippocampus_L	8.73	<.001
	-34	-4	-22	Hippocampus_L	8.26	<.001
	39	-22	-12	Hippocampus_R	8.25	<.001
338	-12	-56	-36	Cerebelum_9_L	3.81	0.002
	-18	-40	-39	Cerebelum_10_L	3.11	0.008
1001	-46	45	26	Frontal_Mid_L	3.76	0.002
	-45	56	9	Frontal_Mid_L	3.57	0.003
	-38	48	32	Frontal_Mid_L	3.11	0.008
184	-45	-14	38	Postcentral_L	3.67	0.002
	-51	-9	27	Postcentral_L	2.39	0.035
319	10	-52	-34	Cerebelum_9_R	3.43	0.004
	21	-46	-42	Cerebelum_8_R	3.22	0.006
986	50	16	51	Frontal_Mid_R	3.41	0.004
	44	6	60	Frontal_Mid_R	3.26	0.006
	56	18	40	Frontal_Inf_Oper_R	2.8	0.016
254	46	26	21	Frontal_Inf_Tri_R	3.15	0.007
	39	34	18	Frontal_Inf_Tri_R	2.62	0.022
56	-20	63	26	Frontal_Sup_L	3.07	0.009
248	0	8	46	Supp_Motor_Area_L	2.97	0.011
	4	15	39	Cingulum_Mid_R	2.93	0.012
70	63	20	14	Frontal_Inf_Oper_R	2.93	0.012
44	15	-62	-2	Lingual_R	2.9	0.013
121	68	6	21	Precentral_R	2.87	0.013
	66	6	32	Precentral_R	2.64	0.022
91	-58	38	8	Frontal_Inf_Tri_L	2.79	0.016
149	39	3	33	Precentral_R	2.78	0.016
48	60	4	45	Precentral_R	2.74	0.018
202	-40	36	46	Frontal_Mid_L	2.68	0.020
	-46	33	40	Frontal_Mid_L	2.66	0.021
53	-26	46	15	Frontal_Mid_L	2.62	0.023
23	-24	69	-2	Frontal_Sup_Orb_L	2.58	0.024
22	-22	-14	57	Precentral_L	2.56	0.025
38	2	-63	-10	Vermis_6	2.55	0.026
68	30	-45	33	Angular_R	2.48	0.029
	32	-42	26	Angular_R	2.43	0.033
20	32	-24	56	Precentral_R	2.48	0.030
14	-2	-54	-72	Cerebelum_9_L	2.44	0.032
12	-20	36	24	Frontal_Mid_L	2.43	0.033
5	-10	39	34	Frontal_Sup_Medial_L	2.28	0.044
2	45	-12	34	Postcentral_R	2.24	0.047
2	69	-27	26	SupraMarginal_R	2.23	0.047

Table 3.3 Grey matter atrophy of participants with Alzheimer's disease compared to controls. Montreal Neurological Institute (MNI) coordinates are shown with FDR correction < 0.05. The table shows the top 3 local maxima (highest T score) >8mm apart in each cluster. AAL, Automated anatomical labelling; MNI, Montreal Neurological Institute; FDR, false discovery rate

Cluster size (Voxels)	MNI coordinates			Nearest AAL Region	T	p (FDR-corrected)
	x	y	z			
21394	32	-10	-14	Hippocampus_R	6.05	0.002
	38	-22	-16	Hippocampus_R	6	0.002
	18	-10	-18	Hippocampus_R	5.93	0.002
4908	2	-27	40	Cingulum_Mid_R	5.76	0.002
	2	-36	39	Cingulum_Mid_R	5.67	0.002
	-2	-52	30	Cingulum_Post_L	4.55	0.005
3996	57	-32	45	SupraMarginal_R	5.63	0.002
	57	-21	46	Postcentral_R	5.23	0.002
	56	-44	38	SupraMarginal_R	5.08	0.003
2188	-27	-81	-9	Occipital_Inf_L	4.8	0.004
	-28	-70	-4	Fusiform_L	4.67	0.004
	0	-88	-12	Calcarine_L	3.88	0.014
1138	-30	-39	57	Postcentral_L	4.75	0.004
	-38	-52	50	Parietal_Inf_L	4.27	0.008
	-52	-33	52	Postcentral_L	3.77	0.017
364	0	40	26	Cingulum_Ant_L	4.6	0.005
	0	30	36	Cingulum_Mid_L	3.14	0.036
726	27	10	10	Putamen_R	4.47	0.006
196	27	-94	4	Occipital_Mid_R	4.3	0.007
1470	-22	-78	-50	Cerebelum_7b_L	4.09	0.010
677	-33	-90	2	Occipital_Mid_L	4.05	0.011
	-30	-92	10	Occipital_Mid_L	3.62	0.020
	-9	-94	21	Occipital_Sup_L	3.45	0.025
294	33	-62	48	Angular_R	3.98	0.012
	28	-51	48	Parietal_Inf_R	3.05	0.039
295	-63	-30	-8	Temporal_Mid_L	3.89	0.014
	-63	-21	-9	Temporal_Mid_L	3.75	0.017
97	2	16	44	Cingulum_Mid_R	3.81	0.016
224	33	-4	48	Precentral_R	3.79	0.016
	39	3	52	Precentral_R	3.28	0.030
1605	26	-75	-54	Cerebelum_8_R	3.69	0.019
	18	-82	-42	Cerebelum_Crus2_R	3.63	0.020
	10	-81	-48	Cerebelum_Crus2_R	3.49	0.024
197	15	-56	-3	Lingual_R	3.66	0.019
138	-26	-72	34	Occipital_Mid_L	3.63	0.020
144	-62	-26	-28	Temporal_Inf_L	3.61	0.020
50	6	51	8	Frontal_Sup_Medial_R	3.58	0.021
37	56	12	-24	Temporal_Pole_Mid_R	3.52	0.023
84	48	-12	62	Precentral_R	3.51	0.023
80	45	-40	0	Temporal_Mid_R	3.51	0.023
318	33	-8	72	Frontal_Sup_R	3.47	0.024
	15	-10	75	Frontal_Sup_R	3.43	0.026
368	-6	-2	68	Supp_Motor_Area_L	3.43	0.025
	-20	4	72	Frontal_Sup_L	3.36	0.028
	-2	6	66	Supp_Motor_Area_L	3.11	0.037
84	-10	-42	74	Precuneus_L	3.42	0.026
	-20	-39	70	Postcentral_L	3.11	0.037
54	66	-26	-8	Temporal_Mid_R	3.4	0.026
103	51	14	-10	Temporal_Pole_Sup_R	3.39	0.027
	54	2	-2	Temporal_Sup_R	3.37	0.027
87	-60	-15	6	Temporal_Sup_L	3.38	0.027
	-52	-26	8	Temporal_Sup_L	2.95	0.044
57	-39	15	9	Insula_L	3.34	0.028
77	22	-90	22	Occipital_Sup_R	3.28	0.030
127	8	-68	-60	Cerebelum_8_R	3.26	0.031
43	-44	-14	60	Precentral_L	3.25	0.031
98	14	30	58	Frontal_Sup_R	3.25	0.031
30	-18	-8	22	Caudate_L	3.21	0.033
94	-46	-36	26	SupraMarginal_L	3.21	0.033
	-51	-42	28	SupraMarginal_L	3.07	0.038
28	15	44	51	Frontal_Sup_R	3.19	0.034

25	-32	-9	74	Precentral_L	3.14	0.035
41	-54	-30	15	Temporal_Sup_L	3.13	0.036
24	27	-50	68	Parietal_Sup_R	3.12	0.036
14	-30	22	54	Frontal_Mid_L	3.11	0.037
39	-48	-20	-33	Temporal_Inf_L	3.11	0.037
8	18	20	45	Frontal_Sup_R	3.07	0.039
15	-9	-28	76	Paracentral_Lobule_L	3.05	0.039
14	22	45	18	Frontal_Sup_R	3.02	0.040
9	64	2	30	Precentral_R	3.02	0.040
47	-44	-60	16	Temporal_Mid_L	3.01	0.041
23	42	3	-18	Temporal_Pole_Sup_R	3	0.041
14	48	-57	-44	Cerebelum_Crus2_R	2.98	0.042
15	-24	6	12	Putamen_L	2.96	0.043
9	-8	-66	-56	Cerebelum_8_L	2.95	0.044
23	-36	-14	-39	Fusiform_L	2.95	0.044
5	-26	-8	20	Putamen_L	2.94	0.044
7	-58	12	10	Frontal_Inf_Oper_L	2.93	0.045
7	63	-6	-18	Temporal_Mid_R	2.91	0.046
6	-60	-57	21	Temporal_Mid_L	2.91	0.046
12	-32	-45	-21	Fusiform_L	2.9	0.046
2	60	-44	-18	Temporal_Inf_R	2.89	0.047
3	-45	-46	-27	Cerebelum_Crus1_L	2.89	0.047
3	-10	-64	62	Precuneus_L	2.88	0.047
1	45	10	-6	Insula_R	2.87	0.048
3	58	-50	8	Temporal_Mid_R	2.85	0.049
3	-45	-81	-10	Occipital_Inf_L	2.85	0.049
1	54	-62	21	Temporal_Mid_R	2.85	0.049
1	-42	-3	-9	Temporal_Sup_L	2.83	0.050
1	-12	-57	6	Calcarine_L	2.83	0.050

Table 3.4 Grey matter atrophy associated with patient neuropsychological severity.
Patient neuropsychological severity is measured using the first principal component score. Montreal Neurological Institute (MNI) coordinates are shown with FDR correction < 0.05. The table shows the top 3 local maxima (highest T score) >8mm apart in each cluster. AAL, Automated anatomical labelling; MNI, Montreal Neurological Institute; FDR, false discovery rate

Cluster size (Voxels)	MNI coordinates			Nearest AAL Region	T	p (FDR-corrected)
	x	y	z			
361609	20	-3	-28	ParaHippocampal_R	11.28	<.001
	30	-32	-18	Fusiform_R	10.94	<.001
	48	-20	-20	Temporal_Inf_R	9.60	<.001
1	-58	-78	-14	Occipital_Inf_L	3.34	0.003
1598	-18	-57	-44	Cerebelum_8_L	3.21	0.004
	-33	-54	-45	Cerebelum_8_L	2.33	0.026
671	38	-45	-48	Cerebelum_8_R	2.79	0.010
1	-36	52	40	Frontal_Mid_L	2.73	0.012
183	40	32	-16	Frontal_Inf_Orb_R	2.67	0.013
1	42	-39	75	Postcentral_R	2.56	0.017
1	-72	-34	39	SupraMarginal_L	2.54	0.017
1	-42	-42	74	Postcentral_L	2.29	0.028
93	36	-70	-54	Cerebelum_7b_R	2.17	0.036
6	-12	-75	-28	Cerebelum_Crus1_L	2.03	0.047
1	-52	-84	-18	Occipital_Inf_L	2.02	0.048

Table 3.5 Grey matter atrophy of participants with Alzheimer's disease at 16-month follow up compared to baseline.
Montreal Neurological Institute (MNI) coordinates are shown with FDR <.05 correction. The table shows the top 3 local maxima (highest T score) >8mm apart in each cluster. AAL, Automated anatomical labelling; MNI, Montreal Neurological Institute; FDR, false discovery rate

3.4 Discussion

This chapter confirms that the group of participants with symptomatic Alzheimer's disease have data features typical of people with sporadic, late-onset Alzheimer's disease compared to control participants. People with Alzheimer's disease performed worse than neurologically-healthy people on clinical tests including the MMSE, CDR and ACE-R, with large effects sizes ($1<d<2$), and performance deteriorated during follow up with small to moderate effects sizes ($0.1<d<0.5$). Participants with Alzheimer's disease had higher markers of beta-amyloid pathology, measured using amyloid-PET, CSF, p-tau181 or p-tau217. Neuropsychology performance, described by the first principal component of neuropsychology scores, worsened during follow up. There was significant grey-matter atrophy for the group of people with Alzheimer's disease, including in medial temporal regions, which correlated with disease severity and progression. However, the patient group was on average 8 years older than the control group, which may confound the between-group comparisons.

1. Clinical tests: People with Alzheimer's disease performed worse on MMSE and CDR tests. On follow up, MMSE scores were lower for participants with Alzheimer's disease (Figure 3.7). The annual rate of decline was -2 points in line with the rate of decline for people with Alzheimer's disease (Stanley *et al.*, 2019; Lansdall *et al.*, 2023).

For the ACE-R subdomains, there were significant differences for all domains apart from fluency for participants with Alzheimer's disease versus control participants and for participants with Alzheimer's disease at baseline versus 16-month follow up. Memory was especially impaired for participants with Alzheimer's disease compared to control participants, as expected given the early impact of disease pathology on regions important to memory function (Grober *et al.*, 1999). This accords with early Alzheimer's disease staging, where memory deficits should be most pronounced (Villemagne *et al.*, 2013). While memory is affected at early-disease stages, other domains become increasingly involved as the disease progresses (Henneges *et al.*, 2016). Attention is often the first, non-memory cognitive domain to be affected by Alzheimer's disease (Perry and Hodges, 1999) and orientation is also often affected earlier in disease than other domains (Henneges *et al.*, 2016). Indeed, attention and orientation was found to be the most affected by disease progression in the Cambridge NTAD Alzheimer's disease cohort (with the greatest percent decline per year and largest Cohen's d).

The ACE-R total score declined by 5.47 points per year, similar to previous reports of around 4 point decline (Hsieh *et al.*, 2012).

2. Pathology: People with Alzheimer's disease had increased markers of beta-amyloid pathology. I assessed pathological severity using the blood measures p-tau181 and p-tau217 and CSF or amyloid-PET. All levels were higher for people with Alzheimer's disease than controls (see Figure 3.2). Continuous biomarkers, such as these, are encouraged for diagnosis and staging of Alzheimer's disease (Therriault *et al.*, 2022). All measures of pathology had large effect sizes ($d>0.8$). Compared to p-tau181, p-tau217 was more strongly correlated with CSF and PET measures of beta-amyloid pathology (see Figure 3.3). Previous studies have reported that p-tau217 better mirrors classical biomarkers than p-tau181 (Thijssen *et al.*, 2021; Xiao *et al.*, 2023; Mendes *et al.*, 2024). The moderate to strong ($0.4<r<0.79$) correlations of blood markers with CSF and PET markers accords with recent evidence that the novel blood measures mirror established biomarkers (Hudd *et al.*, 2019; Coomans *et al.*, 2023; Ashton *et al.*, 2024). This is encouraging given their lower cost and greater tolerability in comparison to PET or lumbar puncture.

3. Neuropsychology: The principal component analysis of the neuropsychological scores for participants with Alzheimer's disease identified a first component which explained 43.1% of the variance. Participants with Alzheimer's disease at baseline had higher PC1 scores than control participants, and their PC1 score further increased at follow up compared to baseline. The neuropsychological batteries ACE-R, PACC and RBANs had the highest loadings of the first principal component. These batteries are widely used to describe cognitive severity in Alzheimer's disease and are very sensitive to Alzheimer's disease and its progression (Larner, 2007; Donohue *et al.*, 2014; Teng *et al.*, 2021). I consequently confirm that the severity of Alzheimer's disease in the patient Cambridge NTAD cohort was best described by neuropsychological test sets designed to assess domains affected by early dementia due to Alzheimer's disease.

The second principal component explained 13% of the variance. It was significantly lower for people with Alzheimer's disease compared to healthy controls at baseline; however, it was higher at follow-up than baseline sessions for people with Alzheimer's disease. The unexpected longitudinal direction of effect could be due to practice effects (Calamia *et al.*, 2012). Indeed, the CANTAB paired associates learning task had the highest loadings onto the component and

has practice effects in people with mild cognitive impairment or Alzheimer's disease (Gonçalves *et al.*, 2016; Cacciamani *et al.*, 2018). The third principal component scores were not significantly different between groups or sessions. Spatial working memory strategy scores had a major loading onto the third principal component. For this task, a participant with unusual PC3 score progression scored similarly at baseline and 2-year follow up but performed better at the 1-year follow up (this score was an 'outlier', 2 standard deviations better than average, though not a recording error).

4. MRI: The most significantly affected regions with grey matter volume loss by Alzheimer's disease are medial temporal lobes (Murphy *et al.*, 1993; Kaye *et al.*, 1997; Jack *et al.*, 1998; Laakso *et al.*, 1999; Thompson *et al.*, 2003; Billette *et al.*, 2022). In NTAD, the left hippocampus had the greatest amount of grey matter loss for participants with Alzheimer's disease compared to controls, followed by the right hippocampus. The correlation of PC1 scores with grey matter atrophy identified grey matter loss associated with disease severity in regions including the hippocampus. The longitudinal assessment of grey matter loss revealed moderate atrophy, also in the hippocampus. Loss of hippocampal volume occurs early in the course of Alzheimer's disease, progressively interfering with memory function (Jahn, 2013), and is associated with cognitive performance (Rao *et al.*, 2022). Temporal lobe changes may be a useful outcome measure for clinical trials (Holland *et al.*, 2009). In addition to accelerated hippocampal atrophy in Alzheimer's disease (~4.3 times greater than controls), whole brain atrophy rates are ~2.4 times greater in people with Alzheimer's disease than controls (Leung *et al.*, 2013). I confirmed a reduction in total brain volume with disease and its progression. Given that total brain volume decreases with disease progression, it is often used as a primary outcome marker in clinical trials (Kehoe *et al.*, 2021).

While early studies demonstrated hippocampal loss and whole-brain atrophy, voxel-based techniques have since detailed the regional spreading of atrophy (Sluimer *et al.*, 2009), beginning in medial temporal lobes and fusiform gyrus, then spreading to posterior temporal, parietal and frontal lobes (Whitwell, 2010). This pattern of grey matter loss mirrors the progression of neurofibrillary tangles (Thompson *et al.*, 2003) and cell loss (Baron *et al.*, 2001). Accordingly, NTAD data confirmed grey-matter loss in widespread temporal, limbic, occipital, parietal and frontal cortices for participants with Alzheimer's disease (see Figure 3.7).

Cell loss is a relatively late event in the pathogenesis of Alzheimer's disease (Niikura *et al.*, 2006) and there are techniques that may be more sensitive to the earliest stages of cognitive involvement in dementia, such as techniques sensitive to tissue biochemical or microstructure changes (Knight *et al.*, 2016, 2019; Lanskey *et al.*, 2018; Wearn *et al.*, 2020) or, as later chapters will show, techniques sensitive to neurophysiological changes dependent on synaptic and microcircuit integrity.

Cohen's d effect sizes indicated that the strongest effects between groups were for amyloid-PET SUVRs. Amyloid-PET has previously been shown to outperform other Alzheimer's biomarkers (Vandenberghe *et al.*, 2013; Ramusino *et al.*, 2020). The first principal component of neuropsychology scores had the next strongest effect size, followed by ACE-R memory scores, CSF amyloid beta 1-42, p-tau 181 and then total brain volume. All biomarkers of Alzheimer's disease that I assessed (PET, CSF, blood and MRI) had stronger effect sizes than MMSE or ACE-R total scores. As pathological changes occur prior to cognitive decline (Therriault *et al.*, 2022), I expected amyloid-PET and CSF amyloid-beta and MRI to have stronger effect sizes than memory and PC1 scores (see Figure 1.1). Nevertheless, memory scores and PC1 scores were less sensitive to disease progression than MRI. Memory measures may have reached a ceiling effect, being able to discriminate people with Alzheimer's disease from controls but being less sensitive to disease as it spreads beyond memory-related brain regions. Clinical trials are recommended, for this reason, not to use cognitive scores to measure disease progression (US Food and Drug Administration, 2022). Use of biomarkers is advised (Scheltens *et al.*, 2021; Therriault *et al.*, 2024). While I analysed no longitudinal data for blood, PET or CSF, previous studies have illustrated that PET has higher effect sizes for disease progression than MRI (Ortner *et al.*, 2019). MMSE and ACE-R total scores had large progression effect sizes, typical of people with Alzheimer's disease (Stanley *et al.*, 2019; Lansdall *et al.*, 2023).

There are several limitations to this study. The attrition rate of 28% may limit inferences made from the longitudinal analyses; however, I found no significant differences in demographic or clinical data between people who withdrew and who completed follow up. It is nevertheless important to consider differences between the study population and the general population when interpreting study findings (Grill and Karlawish, 2010). Participants were recruited from local clinical services and volunteer panels. This may not reflect national diversity. Follow-up assessments were originally intended to be at 12-months post baseline; however, lockdowns

associated with the covid-19 pandemic delayed follow-up assessments. Groups were defined by their clinical diagnoses, though these were supported by amyloid status determined using CSF assays and PET. There is no *post mortem* pathological confirmation of disease. Some participants were taking medication which affects cognition. The numbers of people with mild cognitive impairment or Alzheimer's disease taking stable doses of dementia treatments were as follows: donepezil (n=19), memantine (n=3), galantamine (n=2) and rivastigmine (n=2). There was a significant difference in age between groups. I included this as a regressor in the voxel-based morphometry analyses. Future analyses should control for age when possible. There are more sensitive analytical techniques than I used. I used data from the Cambridge site only for this thesis (not the Oxford site). Analyses, such as the principal component analysis which included 13 variables, may have more stable results with a larger sample size. There were missing data, requiring imputation for the principal component analysis, which may have affected results.

In summary, this chapter sets out the NTAD study population and confirms features typical of people with mild to moderate stages of symptomatic Alzheimer's disease. People in the Alzheimer's disease group had typical clinical signs of Alzheimer's disease, with higher markers of amyloid pathology and poorer performance on clinical and cognitive assessments, and grey matter loss in regions including the hippocampi. These features became more pronounced with disease progression. As such, I conclude this cohort is a good representation of people with late-onset, amnestic Alzheimer's disease.

4 | The effect of Alzheimer's disease and its progression on pyramidal cell gain and connectivity

A manuscript related to this chapter has been posted to medRxiv as:

Lanskey, J. H., Jafarian, A., Karadag, M., Kocagoncu, E., Williams, R., Yadav, P., Quinn, A. J., Pitt, J., Thayanandan, T., Lowe, S., Perkinton, M., Timmers, M., Raymont, V., Singh, K. D., Woolrich, M., Nobre, A. C., Henson, R. N., Rowe, J. B., (2024) The effect of Alzheimer's disease and its progression on pyramidal cell gain and connectivity.

The code used is available at: https://github.com/jlansk/dcm_cmc_ntad

Abstract: Alzheimer's disease affects cognitive neurophysiology by loss of neurones, synapses and neurotransmitters. An improved mechanistic understanding of the human disease will facilitate new treatments. To this end, biophysically-informed dynamic causal models can support inferences around laminar and cell-specific disease effects from human non-invasive imaging. Based on pre-clinical models and effects of cholinesterase inhibitors, I hypothesised that Alzheimer's disease would affect the modulation of superficial pyramidal cell gain and extrinsic connectivity between pyramidal cells of different regions in hierarchical cognitive networks. Magnetoencephalography was recorded during an auditory mismatch negativity task from healthy adults (n=14) and people with symptomatic Alzheimer's disease (n=45, amyloid-biomarker positive) at baseline and after 16 months. Fourteen people from the symptomatic group had repeat magnetoencephalography at two weeks to assess test-retest reliability. Sensor-level data were analysed using t-tests of the mismatch negativity amplitude from 140ms to 160ms. The repetition effect was assessed with repeated-measures analysis of covariance, using the average evoked response in the mismatch negativity time window as the repeated measure. An absolute, intraclass correlation model of the test-retest data assessed mismatch negativity amplitude reliability. Dynamic causal models were then fitted to the evoked responses over

500ms. Second-level parametric empirical Bayes across participants examined the effect of (1) group, patients vs controls, and (2) progression, baseline vs follow up, on the model parameters reflecting pyramidal cell gain modulation and extrinsic connectivity. There was a significant effect of both disease and progression on the mismatch negativity amplitude (patients vs controls, T=-1.80, p=0.04; patient baseline vs follow up, T=-2.72, p=.005), which had excellent reliability (ICC=0.95, p<.001). Parametric empirical Bayes revealed strong evidence (posterior probability>95%) that Alzheimer's disease reduced extrinsic connectivity and superficial pyramidal cell gain modulation, which was reduced further at follow up assessment. The mechanistic modelling confirmed the hypothesis that reduced superficial pyramidal cell gain modulation and extrinsic connectivity can explain the observed neurophysiological effect of Alzheimer's disease. This approach to non-invasive magnetoencephalography data may be used for experimental medicine studies of candidate treatments, and bridge clinical to preclinical models of drug efficacy.

4.1 Introduction

Developing effective treatments for Alzheimer's disease remains a major challenge (Anderson *et al.*, 2017). Effective treatments should target the disease mechanisms behind the neurophysiological and cognitive deficits (Yiannopoulou *et al.*, 2019). To develop these treatments *in vivo,* human assays that quantify the causes of neurophysiological change are needed (Drummond and Wisniewski, 2017). Here, the sensitivity of the inversion between magnetoencephalography (MEG) and generative models of human neurophysiology to the presence and progression of Alzheimer's disease is tested. This approach allows human, *in vivo* characterisation of neural dynamics by cortical layer and cell type from non-invasive neuroimaging (Friston *et al.*, 2003).

This chapter focusses on the impact of Alzheimer's disease on the connectivity of pyramidal cells. Pyramidal cells in superficial layers of cortex are modulated by currently licenced cholinergic treatments for dementia (Moran *et al.*, 2013). For example, galantamine modulates activity of superficial pyramidal cells, leading to changes in neurophysiological responses to rapidly changing stimuli. In rodent models, cholinergic agonists and antagonists have opposing dose-dependent effects on superficial pyramidal cell gain modulation (Schöbi *et al.*, 2021). The hippocampus, which has early and significant involvement in the course of Alzheimer's disease, may be involved in inhibiting and disinhibiting superficial pyramidal cells through regulation of acetylcholine (Barron *et al.*, 2020).

Pyramidal cells are directly affected by the molecular hallmarks of Alzheimer's disease: extracellular beta-amyloid plaques (Braak and Braak, 1997) and intraneuronal tau tangles (Braak and Braak, 1991; Thangavel *et al.*, 2008). Tau aggregates develop in pyramidal cells and can spread between pyramidal cells (Braak and Tredici, 2018). Variance in the distribution and burden of tauopathy in Alzheimer's disease is closely associated with the clinical phenotype (Ossenkoppele et al., 2016), cognitive deficit (Nelson et al., 2012) and rate of cognitive decline (Malpetti *et al.*, 2020; Tanner *et al.*, 2022). The effect of aggregated tau on cognition in part results from synaptic toxicity and dendritic dearborization of pyramidal cells (Allard *et al.*, 2012; Merino-Serrais *et al.*, 2013; Mijalkov *et al.*, 2021).

Identification of pyramidal cell function in humans, *in vivo,* can be achieved by invasive electrocorticography, usually in people undergoing evaluation of epilepsy. This is not practical as a basis for research and drug development in the context of Alzheimer's disease. An

alternative approach is the inversion between functional neuroimaging (e.g., electro- and magneto-encephalography, E/MEG) and biophysical models of the cortex. This approach has been used to study the effects of anti-NMDA autoimmune encephalopathy (Symmonds et al., 2018), inherited channelopathies (Gilbert et al., 2016), ageing (Moran et al., 2014), pathophysiology of non-Alzheimer dementias (Shaw *et al.*, 2019; Adams *et al.*, 2020, 2021, 2023) and confirmatory studies of drug interventions (Moran *et al.*, 2013; Adams *et al.*, 2021).

Here, generative models with non-invasive human MEG are used to test the hypothesis that Alzheimer's disease affects pyramidal cell gain and connectivity, which influence the neurophysiological response to unexpected inputs. This is done in the context of a sensory mismatch negativity paradigm, in which participants automatically learn and adapt to changing auditory stimulus frequency. This learning reflects short-term plasticity (Garrido *et al.*, 2009*a*) and is achieved by iterative updating of top-down predictions by bottom-up prediction errors (Auksztulewicz and Friston, 2016). As top-down predictions of a repeated stimulus become more accurate with short-term learning, prediction errors (and their neurophysiological correlate) reduce. With repetition, the network becomes more precise in its predictions such that prediction errors acquire greater precision (Auksztulewicz and Friston, 2016). An initial deviant stimulus retains the high precision of the previous standard, thereby enhancing the signal of the large prediction error (i.e., a large magnitude error made with high precision). Following such a large prediction error, the precision (c.f., the confidence, in lay terms) in the model is reduced, such that the subsequent prediction error is less precise and generates an attenuated mismatch response.

The precision of prediction errors is proposed to be encoded by the gain modulation of superficial pyramidal cells (Moran *et al.*, 2013; Schöbi *et al.*, 2021), while prediction error is proposed to be mediated by superficial pyramidal cell forward connections (Auksztulewicz and Friston, 2016). In Alzheimer's disease, this mechanism is disrupted with changes including reductions in precision and prediction error signalling (Kocagoncu *et al.*, 2021). Indeed, novelty encoding (Bastin *et al.*, 2019) and auditory predictions (Pérez-González *et al.*, 2022) are disrupted in Alzheimer's disease, particularly in parietal and medial temporal cortices (Billette *et al.*, 2022; Pérez-González *et al.*, 2022). This deficit would not only impair learning, but also signal processing and perception in a noisy environment, as observed in Alzheimer's disease (Pérez-González *et al.*, 2022).

The overarching hypothesis is that the observed physiological effect of Alzheimer's disease on the mismatch negativity response is explained by reduced gain modulation of superficial pyramidal cells and reduced effectiveness of extrinsic connectivity between pyramidal cell populations of connected regions. I test two specific predictions: (1) symptomatic Alzheimer's disease, in the form of amyloid-positive mild cognitive impairment and mild Alzheimer-type dementia, is associated with reduced gain modulation of superficial pyramidal cells and reduced extrinsic connectivity between pyramidal cells; (2) the same features of the cortical microcircuit change with disease progression.

4.2 Materials and methods

4.2.1 Participants

Data were drawn from the New Therapeutics in Alzheimer's Disease (NTAD) multicentre longitudinal observational study (Lanskey *et al.*, 2022). The study included neurologically-normal, control participants and participants with a clinical diagnosis of Alzheimer's disease or mild cognitive impairment. Participants completed (i) amyloid screening through either positron emission tomography or cerebrospinal fluid collection, a positive amyloid status enabled study participation for prospective patient participants; (ii) a battery of clinical and neuropsychological assessments; and (iii) neuroimaging, comprising MRI and E/MEG protocols. People in the control group completed screening and baseline assessments only, while people in the patient group completed additional, longitudinal assessments as follows: clinical and neuropsychological assessments were completed at three timepoints with ~16 months between sessions; blood collection, E/MEG and MRI were completed at baseline and again at ~16 months. An additional E/MEG scan was completed two-weeks after baseline for a subset of people from the patient group (see Lanskey *et al.*, 2022 for further details).

For the current analysis, the MEG, MRI and demographic baseline data from participants who completed the mismatch negativity MEG recording are used. Of the 50 people with mild cognitive impairment or Alzheimer's disease who completed the NTAD baseline MEG scan at the Cambridge site, two people were excluded who did not complete the mismatch negativity task as the earphones did not fit comfortably, two people whose diagnosis was revised during follow up and one due to data recording technical issues at baseline. Of the 15 people with mild cognitive impairment or Alzheimer's disease who completed the test-retest MEG scans at the

Cambridge site, one person was excluded from the analysis because of trigger-failures on the retest session. One control participant was amyloid-positive and excluded from the current analysis. The resulting participant numbers comprised 45 people with Alzheimer's disease or mild cognitive impairment with a positive amyloid status and 14 neurologically-normal control participants with a negative amyloid status. For the test-retest analysis, the subset of 14 participants from the test-retest subgroup of participants with Alzheimer's disease were used. Clinical and cognitive data for participants are given in Table 4.1. Independent Student's t-tests and Bayesian t-tests were used for continuous data, or chi-squared tests for categorical data, to identify differences at baseline between participants with Alzheimer's disease and controls.

4.2.2 Task

A passive roving mismatch negativity task was used (Adams *et al.*, 2020) while the participants passively watched a muted nature documentary (from BBC One's Frozen Planet). The auditory mismatch negativity task elicits responses to unexpected 'oddball' stimuli followed by rapid plasticity as predictions are updated upon repetition of the new stimulus (Friston, 2005; Kiebel et al., 2007). Through non-magnetic earpieces, the participants hear blocks of short sinusoidal tones binaurally in phase, 60dB above the average auditory threshold. The tones are presented for 100ms at 500ms intervals with frequencies in the range 400 to 800Hz varying in 50Hz steps. The frequency of successive tones is the same within blocks but changes between blocks. The number of repeated tones per block varied from 3 to 11. Consequently, the first tone of each block represents a deviant tone, which becomes a new standard tone upon repetition.

4.2.3 Imaging acquisition

MEG data were collected on the ElektaVectorView system and MEGIN Triux Neo scanner. Both scanners were configured with 204 planar gradiometers and 102 magnetometers. The position of five head position indicator coils, standard fiducial points and over 300 additional head points were recorded using the Polhemus digitization system. ECG data was recorded by an electrode on the right clavicle and a second electrode on the left, lower rib. A reference electrode recorded from the left side of the nose and the ground electrode was placed on the left cheek. Electrodes on bilateral canthi and below and above the left eye recorded electro-oculogram data.

T1-weighted MRI was recorded from each participant with a 3T Siemens PRISMA scanner using a magnetisation prepared rapid gradient echo (MPRAGE) sequence (echo time, 2.91ms;

inversion time, 900ms; repetition time, 2300ms; flip angle, 9 degrees; voxel size, 1mm isotropic; slice thickness, 1mm; slice number, 176; acquisition matrix, 256×240).

4.2.4 Data analyses

Pre-processing

Pre-processing followed the NTAD study pre-processing pipeline. MaxFilter v2.2 software (Elekta Neuromag) was used on the raw data to automatically detect bad channels, perform temporal signal space separation, and correct for head movement. Independent component analysis was performed using the EEGLAB toolbox (Delorme and Makeig, 2004) to detect and remove artefactual components that correlated with EOG and ECG timeseries using cardiac spatial and normative blink templates. The residual timeseries were subsequently reconstructed for further preprocessing using SPM12 (r7771). Data were bandpass filtered between 0.01Hz and 40Hz and epoched from -100ms to 500ms relative to stimulus onset (0ms). OSL's artefact rejection algorithm (github.com/OHBA-analysis/osl-core) was used to remove residual bad channels and trials. Robust averaging was used to average epochs for deviant and repeated trials, with conditions weighted separately. A final low-pass filter was applied to the data to correct for potential high frequencies introduced during robust averaging.

Sensor space analysis

For the sensor space analysis, planar gradiometers were combined by calculating their root mean square. The mean response across planar gradiometers was calculated for each subject, for each trial type, for each session separately (baseline, two-weeks and annual follow up). The repetition effect was assessed with a repeated-measures ANCOVA, using the average evoked response in the mismatch negativity time window (140-160ms, Moran *et al.*, 2013) with tone repetition number (deviant, repetition 1, repetition 2, repetition 3, repetition 4 and repetition 5) as the repeated measure, group (controls versus patients) for the between-subject measure and age as the covariate. The difference waveform for each subject was also assessed; the response to the deviant tone was subtracted from the response to the first stimulus repetition. The average amplitude of this difference waveform from 140 to 160ms was calculated. An independent sample t-test was used to compare means of the mismatch negativity amplitude between groups and Cohen's d determined the effect size. Group average waveforms were plotted after averaging difference waveforms across participants of each group.

For the longitudinal patient data, the difference in means between baseline and follow-up sessions was assessed using a t-test and the effect size was assessed using Cohen's d. The repetition effect was assessed with a repeated-measures ANOVA, using the average evoked response in the mismatch negativity time window (140-160ms, Moran *et al.*, 2013) with tone repetition number (deviant, repetition 1, repetition 2, repetition 3, repetition 4 and repetition 5) and session (baseline versus follow up) as repeated measures.

Test-retest reliability of the baseline and two-week data was estimated using an absolute, intra-class correlation model (Koo and Li, 2016). With similar means, the intra-class correlation coefficient is numerically equivalent to the product moment correlation (estimated as Pearson's correlation coefficient).

First level network modelling

I used dynamic causal modelling with laminar-specific parameters to determine the effect of Alzheimer's disease on the neurophysiological generators. A canonical microcircuit model for evoked responses was used (Bastos *et al.*, 2012; Pinotsis *et al.*, 2013) comprising of four cell populations at each of 8 cortical regions (see Figure 4.2): bilateral primary auditory cortex (left MNI coordinates: -42, -22, 7; right MNI coordinates: 46, -14, 8), bilateral superior temporal gyrus (left: -61, -32, +8; right: +59, -25, +8), bilateral inferior frontal gyrus (left: -46, +20, +8; right: +46, +20, +8), and bilateral inferior parietal cortex (left: -58, -27, +30; right: +59, -41, +30). Six of these regions are based on a series of prior studies with healthy adults and those with non-Alzheimer dementia (Garrido *et al.*, 2008; Phillips *et al.*, 2015; Rosch *et al.*, 2019; Adams *et al.*, 2021). The network was extended to include the inferior parietal cortex (Lappe *et al.*, 2013), given the impact of Alzheimer's disease on parietal cortex (Jacobs *et al.*, 2012; Talwar *et al.*, 2021) and evidence of mismatch negativity responses from parietal cortex (Lappe *et al.*, 2013; Dietz *et al.*, 2014; Cope *et al.*, 2022). Multiple, alternative, symmetric model architectures were defined, each representing plausible alternative hierarchical relationships between regions and their connectivity to include the inferior parietal cortex (Figure 4.2). Given that higher regions send backward connections to, and receive forward connections from, lower regions in a hierarchical network, forward and backward connections were specified according to the following hierarchy as set out previously (Garrido *et al.*, 2008; Phillips *et al.*, 2015; Rosch *et al.*, 2019; Adams *et al.*, 2021): inferior frontal gyrus > superior temporal gyrus > primary auditory cortex. These connections were unchanging across models. All models included auditory input to primary auditory cortex and prediction/expectancy input to inferior

frontal cortex (Phillips *et al.*, 2015, 2016). Models 1 and 4 had no connections between frontal and parietal nodes. Models 2 and 5 had the inferior parietal cortex higher than the inferior frontal cortex in the cortical hierarchy. Models 3 and 6 had the inferior frontal cortex higher than parietal cortex in the cortical hierarchy. Models 1-3 had no expectancy input to parietal cortex, while models 4-6 had expectancy input to parietal cortex (Figure 4.2B). The laminar asymmetry of forward vs backward connectivity is based on the canonical microcircuit model described by Bastos and colleagues (2012).

The first 6 repetitions of tones in the mismatch negativity paradigm were modelled to identify the effect of repetition on parameters from the first tone of each block (deviant) to the 6^{th} tone (a new 'standard' for each block). In anticipation of short-term plasticity within the dynamic causal models, the changes to neural responses were modelled over successive tone repetitions as varying by (1) exponential decay or (2) exponential decay combined with phasic change (as used by Garrido and colleagues, 2009). The second set of models with both exponential and phasic change embody the hypothesis of predictive coding for sequential neural responses to stimuli, allowing extrinsic connections to show stimulus-specific adaptation with exponential decrease with repetition; while intrinsic connections show a phasic response, reducing after the deviant tone and recovering with subsequent tones thereby reflecting the precision of prediction error (Garrido *et al.*, 2009*a*; Rosch *et al.*, 2019).

The neuronal parameters for each participant's dynamic causal model were inferred from their observed response fields of gradiometers using a lead field informed by subject-specific T1 magnetic resonance images. This inversion uses the Bayesian variational Laplace method that minimizes the free energy of the model as a cost function to estimate the free energy of the model's and posterior estimates of its parameters (Friston *et al.*, 2003, 2007). Of the 14 controls and 45 patient participants included at baseline, one control and five patients had an inversion failure during model fitting and were excluded from the parametric empirical Bayes (PEB) analyses. For the longitudinal session, three patients failed to invert during model fitting and were excluded from the longitudinal PEB analyses.

Bayesian model reduction was applied to each individual's dynamic causal model to identify the most likely explanatory model for group differences (the "winning" model) from the model space. The model space included 12 canonical microcircuit models (Figure 4.2A), with 2 sets of the 6 alternative extrinsic connectivity architectures among eight regions; one set describing

the effect over sequential tones with an exponential decay and the second set, as a combination of exponential and phasic basis functions (Garrido *et al.*, 2009*a*). The free energies of reduced models were averaged (i) across all participants at baseline and (ii) separately, across all baseline and longitudinal data for patient participants. The same model had the highest model evidence for both baseline and longitudinal datasets. This model with the highest model evidence was taken forward to PEB analysis to study group differences.

The effect of Alzheimer's disease

Second-level analysis with PEB of the winning model examined how disease group (healthy control *vs* Alzheimer's disease) affected the change in generative model of successive repetitions after a change in tone frequency. I ran two analyses with PEB. For both, the PEB design matrix comprised a unitary regressor for the group mean (ones) and a regressor for group membership (zeros for control participants and ones for people with Alzheimer's disease).

The first PEB analysis tested whether individual differences in the gain of superficial pyramidal cells explains the group difference in the scalp response to the mismatch negativity task. The gain modulation parameter represents a lump sum of features such as potassium conductances and hyperpolarisation after an action potential, which act as an auto-regulation or self-inhibition of the cell population (rather than being a biological inhibitory connection per se; Moran *et al.*, 2013). A second PEB analysis tested the effect of individual differences in the extrinsic connectivity between pyramidal cells between all regions (both forward and backward connections). For both PEB models, Bayesian model comparison and averaging was performed over a model space of all parameter combinations with hemispheric symmetry and the Bayesian model average results were plotted.

The effect of Alzheimer's disease progression

For the analysis of longitudinal change, two second-level analyses were performed with PEB applied to baseline and annual follow-up data from patients. Both PEB models included a group mean regressor and a regressor specifying whether the scan was at baseline, given a value of 0, or at the annual follow up, given a value of 1. A third regressor specified the time in years between the baseline and follow-up scans for each patient (0 for baseline scans and with scores from 0.8 to 2.2 for follow-up scans mean-centred and standardised). Two such PEB models were inverted to examine the impact of disease progression on the (i) gain modulation of

superficial pyramidal cells and (ii) extrinsic connectivity between superficial and deep pyramidal cells. For each PEB model, Bayesian model comparison and averaging were performed over a reduced model space of only those parameters that had differentiated patients *versus* controls at baseline, and then the Bayesian model average results were plotted.

4.3 Results

Demographic and clinical data are shown in Table 4.1. There were no significant differences between the groups in terms of sex (χ^2=0.98, p=.32), handedness (t=1.86, p=.40), or Hachinski ischaemic score (χ^2=5.12, p=.16). Patients were on average older than controls (t=-3.80, p=<.001, BF=72). As expected, there were group differences for the mini-mental state examination (t=4.75, p<.001, BF=1163), ACE-R (t=5.02, p<.001, BF=2722), and clinical dementia rating (χ^2=55, p<.001). The baseline data of those completing two-week retest MEG, and annual follow up, were similar to the whole baseline group.

	Controls	**AD/MCI Baseline**	**AD/MCI Retest**	**AD/MCI Follow up**
Sex (Male:Female)	9:5	20:25	6:8	16:16
Handedness (Right:Left:Both)	11:3:0	40:4:1	13:0:1	28:3:1
Baseline Age (yrs)*	65.3 (±7.29)	73.8 (±7.32)	74.8 (±7.33)	73.2 (±7.89)
Baseline MMSE*	29.4 (±0.74)	24.8 (±3.52)	(26.1 (±3.05)	25.1 (±3.24)
Baseline ACE-R*	92.4 (±4.94)	74.2 (±13.1)	78.5 (±10.5)	75.7 (±11.1)
Baseline HIS	0.07 (±0.27)	0.56 (±0.8)	0.83 (±1.03)	0.53 (±0.82)
Baseline pTau-181 (pg/mL)	1.29 (±0.63)	2.59 (±0.68)	2.84 (±0.63)	2.58 (±0.69)
Baseline PET (SUVR)	0.98 (± 0)	1.68 (±0.79)	1.67 (±0.15)	1.64 (±0.42)
Baseline CSF (tau/Abeta 1-42)	0.38 (±0.21)	1.84 (±0.21)	2.21 (±0.98)	1.63 (±0.24)

Table 4.1 Participant demographics and clinical data
Values are given as mean (standard deviation) *denotes significant difference between baseline groups by frequentist and/or Bayesian statistics, as per text. Yrs, years; MMSE, mini-mental state examination; ACE-R, Addenbrooke's cognitive examination revised; HIS, Hachinski ischaemic score; PET, positron emission tomography; SUVR, standardised uptake value ratio; CSF, cerebrospinal fluid

4.3.1 Sensor-level effects of Alzheimer's disease

The amplitude of the mismatch response from 140 to 160ms was significantly reduced in patients compared to controls at baseline (t = -1.80, p = 0.04, Figure 4.1B upper panel) with a medium effect size (d = 0.55). The repeated-measures ANCOVA found a significant main effect of repetition (F(5, 280) = 38.0, p<0.001); that interacted with group (F(5, 280) = 2.48, p = 0.03), where the responses were smaller for patients particularly for early repetitions.

The patients' mismatch response was further attenuated (less negative) at annual follow up compared to patients' baseline (t = -2.72, p = .005, Figure 4.1B lower panel) with a small effect size (d=0.46). In the longitudinal repeated-measures ANOVA, there was a significant main effect of tone repetition (F(5, 155) = 20.0, p<.001) and progression (baseline versus follow up, F(1, 31) = 75.2, p < .001), which interacted with each other (F(5, 155)=16.6, p<.001). The mismatch negativity amplitude had high reliability across the baseline and two-week test-retest sessions (ICC = 0.95, p < .001, Figure 4.1C).

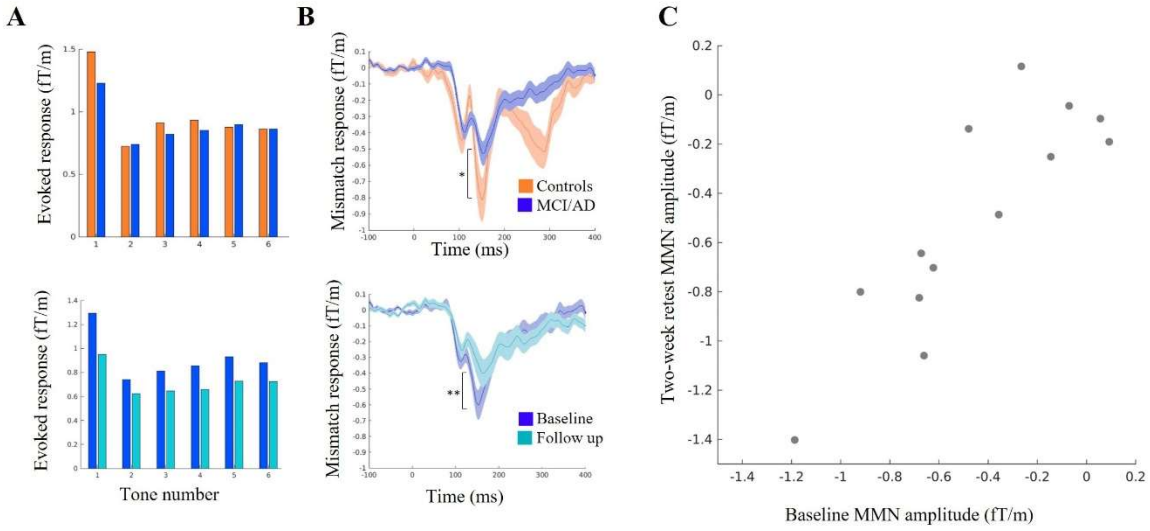


Figure 4.1 Scalp responses to the mismatch negativity task.
(a) Amplitude of the evoked scalp responses to tones 1-6, averaged across root mean square values of all gradiometers and across samples within the *a priori* mismatch negativity window from 140ms to 160ms; top panel - for baseline controls in blue and patients in orange; bottom panel - for patients at baseline in dark blue and follow up in light blue. **(b)** Average mismatch negativity waveform of repetition 1 minus deviant tones; top panel - for baseline controls in blue and patients in orange; bottom panel - for patients at baseline in dark blue and follow up in light blue. (c) Absolute intraclass correlation for the mismatch negativity calculated using the test-retest data. MCI/AD, mild cognitive impairment or Alzheimer's disease; MMN, mismatch negativity

4.3.2 Dynamic causal models

The evoked responses generated by dynamic causal models were accurate, with an average Pearson correlation between generated and observed responses of 0.88 (±1.70) and 0.84 (±0.15) for patients at baseline and follow up, respectively; and 0.85 (±0.18) for controls at baseline (see the supplementary figures for individual model fits).

The model with the highest model evidence was the same for (1) models across baseline patient and control groups (see Figure 4.2C) and (2) models across baseline and follow-up scans for

patients (see Figure 4.2D). The winning model identified the inferior frontal cortex as above the parietal cortex in the network hierarchy. The winning model had the combination of exponential and phasic basis functions changes in parameters over successive repetitions, in accordance with Garrido *et al.*, (2009*a*) and Rosch *et al.* (2019), and in line with a predictive coding framework for the mismatch negativity task rather than stimulus-specific adaptation only (Garrido *et al.*, 2009).

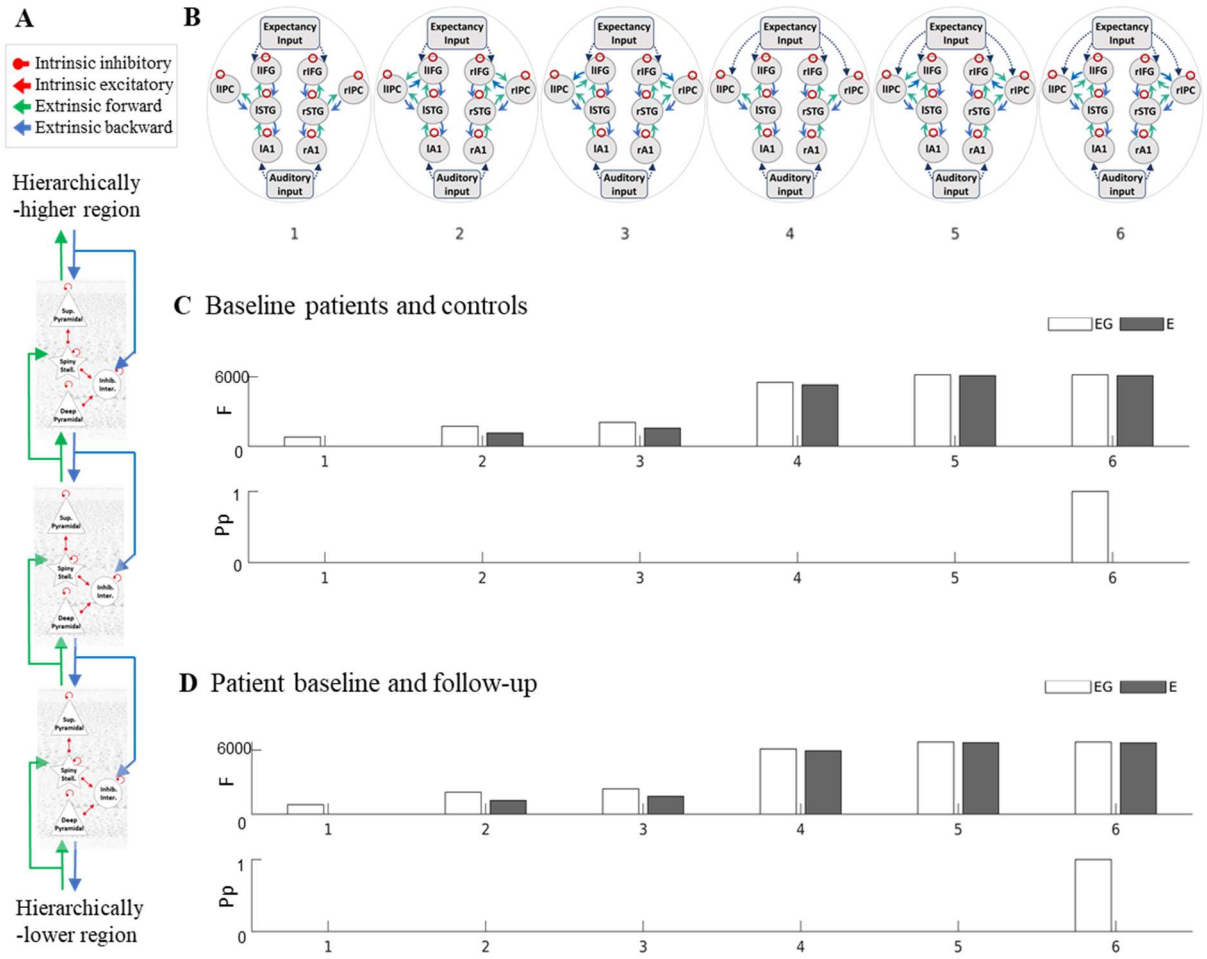


Figure 4.2 Defining the model structure.
(A) The canonical microcircuit model for evoked responses; **(B)** Model space for determining the connectivity of the inferior parietal nodes; **(C)** The free energy (top panel) and posterior probability (bottom panel) of models for the patient and control groups; **(D)** and for the patient baseline and follow-up groups. Sup, superficial; stell., stellate; inter., interneurons; inhib., inhibitory; F, free energy; Pp, posterior probability; l, left; r, right; A1, primary auditory cortex; STG, superior temporal gyrus; IFG, inferior frontal gyrus; IPC, inferior parietal cortex

4.3.3 Superficial pyramidal cell gain modulation is reduced by Alzheimer's disease

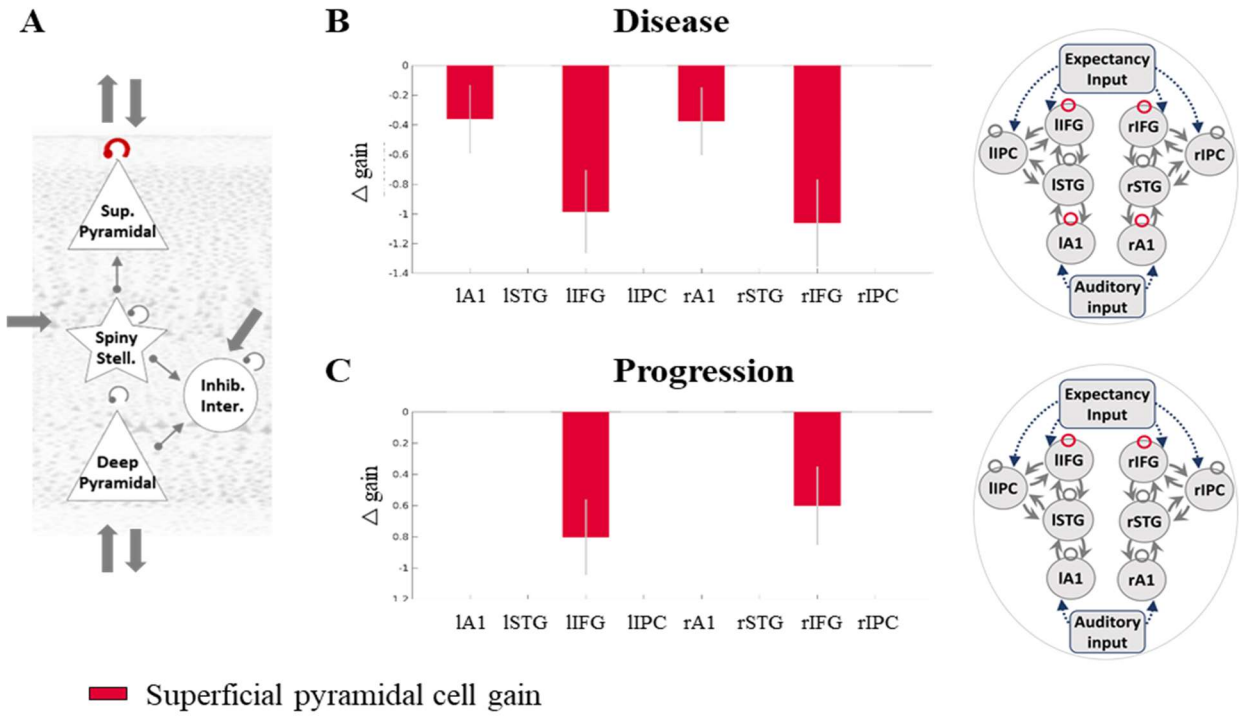


Figure 4.3 Gain of the superficial pyramidal cell self-inhibition and the effect of disease and progression.
(A) The superficial pyramidal cell self-inhibitory connection is shown in red. Regions where this connection was modulated with a posterior probability >0.95 by **(B)** disease presence and **(C)** progression are shown in the in red. Sup, superficial; stell., stellate; inter., interneurons; inhib., inhibitory; F, free energy; Pp, posterior probability; l, left; r, right; A1, primary auditory cortex; STG, superior temporal gyrus; IFG, inferior frontal gyrus; IPC, inferior parietal cortex

The analyses across all regions confirmed that Alzheimer's disease (Figure 4.3B: control versus patient PEB model) reduced the gain modulation of superficial pyramidal cells in auditory cortices and inferior frontal gyri. Disease progression also negatively modulated the gain of superficial pyramidal cell self-inhibition in the inferior frontal cortex (Figure 4.3C: patient baseline versus follow-up PEB model).

4.3.4 Extrinsic connectivity: effect of disease and progression

The analyses assessing extrinsic connectivity between superficial and deep pyramidal cells confirmed that the effect of disease was to weaken forward and backward connections. Forward connections were reduced from superior temporal to inferior frontal and inferior parietal

cortices and from inferior parietal to inferior frontal cortices; backward connections were reduced from inferior frontal to inferior parietal cortices (Figure 4.4B). The effect of disease progression was also to reduce the forward connections from superior temporal to inferior frontal cortices and from inferior parietal to inferior frontal cortices and also to reduce backward connections from inferior frontal to inferior parietal cortices (Figure 4.4C).

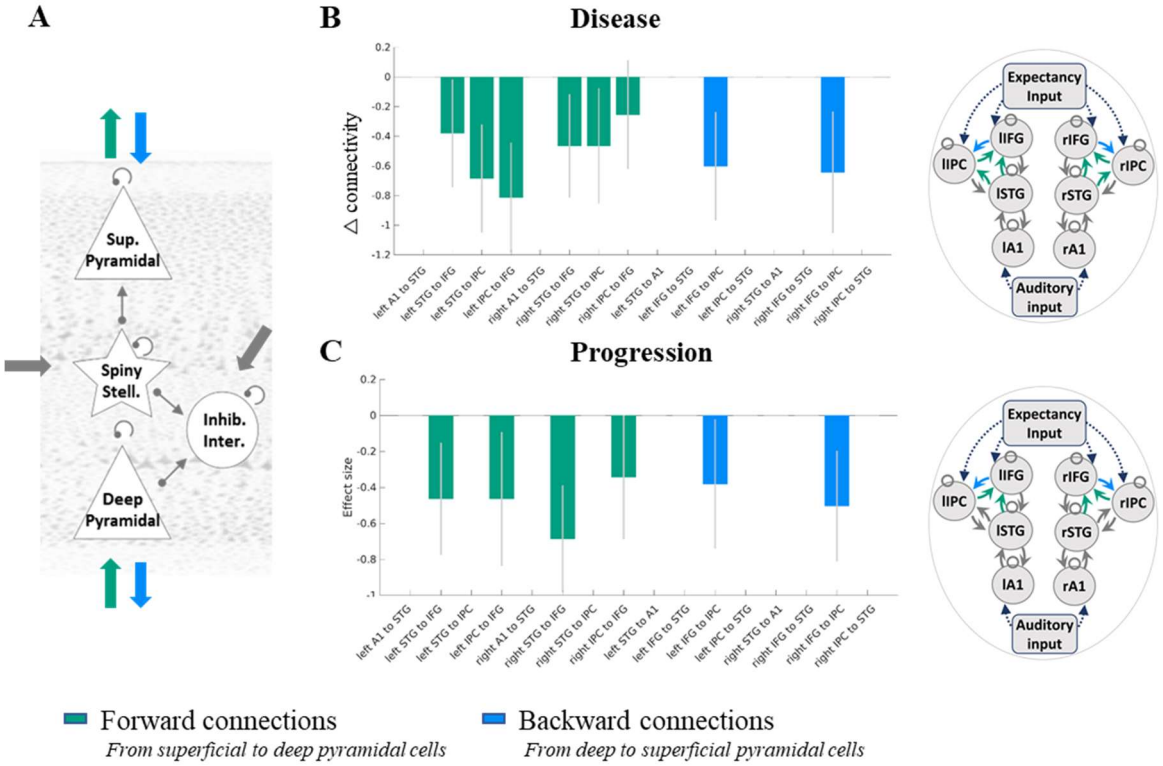


Figure 4.4 The effect of disease presence and progression on extrinsic superficial and deep pyramidal cell connectivity.

(A) The extrinsic connections from superficial pyramidal to deep pyramidal cells (green) and deep to superficial pyramidal cells (blue) are shown in the left hand diagram. Regions between which these connections were modulated with a posterior probability >0.95 are shown in green or blue for **(B)** disease: patient vs controls and **(C)** progression: baseline vs follow up. Sup, superficial; stell., stellate; inter., interneurons; inhib., inhibitory; F, free energy; Pp, posterior probability; l, left; r, right; A1, primary auditory cortex; STG, superior temporal gyrus; IFG, inferior frontal gyrus; IPC, inferior parietal cortex

4.4 Discussion

This study confirms that MEG of a simple auditory paradigm is sensitive to the presence of Alzheimer's disease and its progression over 16 months. Furthermore, the mismatch negativity amplitude was highly reliable. Dynamic causal models accurately reproduced scalp responses

to the mismatch negativity task. These models revealed the effect of Alzheimer's disease on laminar and cellular mechanisms. Critically, this study confirmed the hypothesis that the presence and progression of Alzheimer's disease change both the gain modulation of superficial pyramidal cells and extrinsic connectivity between pyramidal cells thereby reducing the mismatch negativity response compared to controls and with disease progression. Reductions in the fast phasic response of intrinsic connections (see supplementary material analysis) to tone repetition were also shown, illustrating an effect of Alzheimer's disease on short-term plasticity.

4.4.1 The mismatch negativity waveform

I propose the mismatch negativity response as an early neurocognitive marker of Alzheimer's disease. Previous mismatch negativity studies have also shown differences between healthy older adults and people with mild cognitive impairment (Ji *et al.*, 2015; Papadaniil *et al.*, 2016; Gao *et al.*, 2018; Laptinskaya *et al.*, 2018) and Alzheimer's disease (Savolainen *et al.*, 2001; Cheng *et al.*, 2012; Hsiao *et al.*, 2014; Papadaniil *et al.*, 2016; Jiang *et al.*, 2017). These studies showed differences in mismatch negativity latency (Cheng *et al.*, 2012; Ji *et al.*, 2015; Papadaniil *et al.*, 2016; Jiang *et al.*, 2017; Gao *et al.*, 2018) or amplitude (Savolainen *et al.*, 2001; Papadaniil *et al.*, 2016; Jiang *et al.*, 2017; Laptinskaya *et al.*, 2018) for people with or at risk of Alzheimer's disease compared to control participants. Although the mismatch paradigm does not directly probe episodic memory, it is correlated with episodic memory in people at risk of Alzheimer's disease (Gao *et al.*, 2018; Laptinskaya *et al.*, 2018). The majority of studies used EEG (Savolainen *et al.*, 2001; Ji *et al.*, 2015; Papadaniil *et al.*, 2016; Jiang *et al.*, 2017; Gao *et al.*, 2018; Laptinskaya *et al.*, 2018) rather than MEG (Cheng *et al.*, 2012; Hsiao *et al.*, 2014) and used the standard mismatch negativity paradigm (Savolainen *et al.*, 2001; Cheng *et al.*, 2012; Hsiao *et al.*, 2014; Ji *et al.*, 2015; Papadaniil *et al.*, 2016; Jiang *et al.*, 2017; Gao *et al.*, 2018) rather than the roving mismatch negativity paradigm used in the current study. These limitations should be considered when comparing findings with the current study. It should also be noted that only one of the studies confirmed Alzheimer's disease pathology in patients. In line with our findings of reduced mismatch respones in people wtih Alzheimer's disease and a postiive amyloid status, mismatch negativity amplitudes were reduced for people with Alzheimer's disease with pathology verified through biopsy (Savolainen *et al.*, 2001). Despite methodological differences, these studies show changes in mismatch responses for people with or at risk of Alzheimer's disease, including reduced mismatch negativity amplitudes

(Savolainen *et al.*, 2001; Papadaniil *et al.*, 2016; Jiang *et al.*, 2017; Laptinskaya *et al.*, 2018), Amyloid pathology has also been shown to reduce mismatch negativity responses of preclinical models of Alzheimer's disease (Kim *et al.*, 2020). The mismatch paradigm has important advantages as a potential platform in translational studies and for drug development. For example, it requires minimal training, can be undertaken at any stage of disease, has a direct animal task homologue, and it avoids the ambiguity in interpreting tasks on which memory performance differs between groups. The auditory mismatch is also particularly suitable for MEG, since MEG is more sensitive to superficial cortical regions than deep-brain regions, such as structures in the medial temporal lobes.

Changes to short-term plasticity are an early feature of preclinical models of Alzheimer's disease (Lee *et al.*, 2012), occurring prior to cell death (Selkoe, 2002) and in proportion to cognitive impairment (Chakroborty *et al.*, 2019). Short-term plasticity in cortical microcircuits is reflected by the task-induced physiological changes. The changing amplitude of evoked responses over successive tone repetitions (see Figure 4.2) is considered to index the precision (certainty) of the prediction error (Garrido *et al.*, 2009*a*). As proposed by Garrido and colleagues (2009a), the high precision 'surprise' in response to a deviant tone is followed by an initial reduction of precision which gradually recovers as a new standard tone is learnt. This is reflected in the decay pattern of the magnitude of amplitudes (see Figure 4.2); changes to the mismatch negativity amplitude over successive repetitions aligned with a phasic-plus-exponential-decay pattern over successive tones (see Figure 4.2). The fast, phasic response reflects short-term plasticity as the mismatch negativity network rapidly adapts to the changing auditory stimulus. Supplementary analyses showed reductions in the fast phasic response of intrinsic connections to tone repetition (see Supplementary Figure A.6) illustrating an effect of Alzheimer's disease on short-term plasticity. This finding was expected, as Alzheimer's disease pathology affects synaptic plasticity (Lacor *et al.*, 2007; Mijalkov *et al.*, 2021) and short-term plasticity changes are an early feature of preclinical models of Alzheimer's disease (Lee *et al.*, 2012) occurring prior to cell death (Selkoe, 2002). Short-term plasticity changes correlate with memory encoding (Chakroborty *et al.*, 2019) and cognitive decline (De Wilde *et al.*, 2016; Henstridge *et al.*, 2018). Given that these changes occur early in the course of Alzheimer's disease, markers of short-term plasticity could be sensitive to the earliest effects of disease on cognition. However, longitudinal analyses showed no effect of disease progression over 16 months on measures of short-term plasticity. As such, further assessment is needed to determine

whether and how short-term plasticity markers can be used by early-phase clinical trials of shorter duration.

4.4.2 Superficial pyramidal cell gain

For neurophysiological measures and their biophysical models to be useful in support of experimental medicine studies they must do more than merely differ between people with dementia and healthy adults. They should also be sensitive to disease progression and be interpretable in terms of pathological or pharmacological aspects of disease. This study focussed on the hypothesised impact of disease on superficial pyramidal cell dynamics and connectivity.

The cholinergic deficit in Alzheimer's disease is one mechanism by which the cortical generators of the neurophysiological response may differ. For example, cholinergic agonists increase (Moran *et al.*, 2013; Schöbi *et al.*, 2021) and cholinergic antagonists decrease (Schöbi *et al.*, 2021) parameters for the gain modulation of superficial pyramidal cells in the auditory cortex. Moreover. mismatch negativity responses are altered by cholinergic antagonists (Pekkonen *et al.*, 2005). Deep brain stimulation of the nucleus basalis of Meynert, a major source of cholinergic innervation of the cortex, affects repetition suppression (Dürschmid *et al.*, 2020). Based on the contrasting dose-related effects of cholinergic agonists and antagonists, I predicted an effect of disease on the gain modulation of superficial pyramidal cells. Indeed, Alzheimer's disease reduced gain modulation in primary auditory and inferior frontal cortices (see Figure 4.3), where there is a high degree of cholinergic fibre loss (Geula and Mesulam, 1996). The gain modulation of pyramidal cells is proposed to encode the precision of prediction errors (Moran *et al.*, 2013; Schöbi *et al.*, 2021). The hippocampus, affected early in the course of Alzheimer's disease, may modulate the precision of prediction errors with cholinergic regulation of regions at the top of the cortical hierarchy (see Figure 3, Barron *et al.*, 2020, and Figure 4.2, current study). The inferior frontal cortex was situated at the top of the cortical hierarchy of the model and received expectancy input from external regions, such as the hippocampus. Given the involvement of parietal cortex in Alzheimer's disease (Jacobs *et al.*, 2012; Talwar *et al.*, 2021), and that the parietal cortex also received expectancy input from external regions such as the hippocampus (see Figure 4.2), superficial pyramidal cell gain in parietal cortex may also be expected to be affected by Alzheimer's disease. The findings of this study, however, showed no evidence that Alzheimer's disease affects parietal superficial

pyramidal cell gain (though does support altered extrinsic parietal pyramidal cell connectivity, as later discussed and shown in Figure 4.4). Cholinergic innervation of frontal and primary auditory cortices is higher than parietal cortices (Geula and Mesulam, 1996). This could explain why change in gain was seen in primary auditory and frontal cortices, where the effects of cholinergic alterations due to Alzheimer's disease would consequently be most pronounced.

While the hypothesis was based on the action of cholinergic modulation on superficial pyramidal cell gain, there are other possible contributors to the change in pyramidal cell gain reported. Alzheimer's disease has a complex pathophysiology including changes to neurotransmitter systems, accumulation of tau and beta-amyloid (Braak and Braak, 1991), neuroinflammation (Venegas *et al.*, 2017) and vascular change (Montagne *et al.*, 2020). These may consequently also affect pyramidal cell connectivity. For example, NMDA receptor activity modulates, in part, the loss of pyramidal cell synapses (Shankar *et al.*, 2007) and acetylcholine release (Giovannini *et al.*, 1994; Newcomer *et al.*, 2000). As such, glutamatergic signalling could also be contributing to the reduced pyramidal cell connectivity reported. I explore this further in Chapter 5, where I formally assess how Alzheimer's disease affects glutamatergic signalling. To explore how other pathophysiological changes may be contributing to the observed pyramidal cell connectivity changes, futures studies using PET can quantify Alzheimer pathology such as the aggregated tau protein (Ossenkoppele *et al.*, 2016; Passamonti *et al.*, 2017, 2018; Cope *et al.*, 2018; Leuzy *et al.*, 2019), beta-amyloid plaques (Cai *et al.*, 2006) and neuroinflammation (Bevan-Jones *et al.*, 2017). Such measures can then be used to assess how they affect pyramidal cell connectivity and the cortical microcircuit (Adams *et al.*, 2023).

4.4.3 Extrinsic pyramidal cell connectivity

In addition to the changes of gain modulation *within* the canonical microcircuit of temporal and frontal regions, connectivity changes were illustrated *between* regions in the large-scale network of temporal, parietal, and frontal sources (Figure 4.3). Connectivity changes in large-scale networks related to Alzheimer's disease have been observed with both fMRI and M/EEG (Yu *et al.*, 2021). For example, Alzheimer's disease pathology has been associated with changes to functional connectivity of the default-mode network and/or frontoparietal network (Engels *et al.*, 2015; Klaassens *et al.*, 2017; Mandal *et al.*, 2018; Zhao *et al.*, 2019; Wales and Leung, 2021; Yang *et al.*, 2021; Fathian *et al.*, 2022; Moffat *et al.*, 2022; Zhukovsky *et al.*, 2023) and

networks responding in mismatch paradigms (Başar *et al.*, 2017; Jovicich *et al.*, 2019; Nguyen *et al.*, 2019; Cope *et al.*, 2022; Gjini *et al.*, 2022).

Pyramidal cells are the principal source of such inter-regional connectivity. The model-based analysis suggests that pyramidal cell connectivity is impaired by the presence and progression of Alzheimer's disease (see Figure 4.3 and Figure 4.4). Toxic species of aggregated tau affect pyramidal-cell dendritic complexity (Braak and Braak, 1991; Merino-Serrais *et al.*, 2013; Braak and Tredici, 2018) even before axonal aggregation (Braak and Tredici, 2018). Tau oligomers and beta-amyloid aggregates are also synaptotoxic (Lacor *et al.*, 2007; Mijalkov *et al.*, 2021). This will reduce sensitivity to incoming connections, reducing effective connectivity (Ahnaou *et al.*, 2017).

Another potential contributor to the abnormal mismatch response is synaptic loss and later pyramidal cell death. Transgenic models show disruption of pyramidal cell activity prior to cell death (Lison *et al.*, 2014) with significant degeneration of synapses (Oakley *et al.*, 2006). Human *in vivo* studies with SV2a-binding PET ligands confirm this loss of synaptic density (Venkataraman *et al.*, 2021). From *post mortem* human studies, there is substantial loss of layer 3 (superficial) and layer 5 (deep) pyramidal cells in people with Alzheimer's disease compared to controls (Hof *et al.*, 1990). This loss is proportional to the burden of tau neurofibrillary tangles (Hof *et al.*, 1990). This may explain the reduced extrinsic connectivity between superficial and deep pyramidal cells observed (Figure 4.4).

For extrinsic connections between superficial and deep pyramidal cells, connections to and from the parietal regions were especially affected (see Figure 4.4 and the regional analysis in supplementary materials, which found the PEB model including parietal connections had greater free energy than other single-region PEB models, Supplementary Figure A.5). The parietal cortex is commonly implicated in functional and structural imaging of Alzheimer's disease (Wang *et al.*, 2015). In contrast, connections to and from primary auditory cortices were not significantly affected (see Supplementary Figure A.5), in accord with the classical progression of pathology over Braak stages (Braak and Tredici, 2018).

4.4.4 Limitations

This study has several important limitations. First, the diagnostic groups were defined by clinical diagnoses, albeit supported by amyloid biomarker status determined using PET or cerebrospinal fluid assays. Further work could examine preclinical stages or phenotypic

variants. Second, a simplified anatomical model was applied based on earlier studies of the mismatch negativity response augmented by the parietal cortex because of its involvement in Alzheimer's disease. The model space was defined to suit the hypotheses; however, other models could exist which better explain the data. For example, the hippocampus and adjacent medial temporal cortex, which are affected early in the progression of Alzheimer's disease, were not included. MEG signals from the hippocampus present methodological and signal-to-nose challenges. Specialist techniques, such as rigid head moulds, optically pumped magnetometers, or long recording sessions, are not well-suited to the patient population. However, hippocampal signals may be implicit in the model in the form of the expectancy inputs to the upper layers of the current generative model. For tasks with hippocampal involvement, future studies could include the hippocampus as a hidden node in the dynamic causal model (David *et al.*, 2011). The hippocampus would thereby be included in the model despite its activity being hidden from the sensors. Model comparison could assess whether including the hippocampus as a hidden node improves the model evidence. MEG is more sensitive to tangential sources, typically found in sulci, while EEG is more sensitive to radial sources (Lopes da Silva, 2013; Piastra et al., 2021). The relative positioning and distance of sensors to grey matter on superficial versus deep part of gyri or sulci mitigates the differential sensitivity of EEG and MEG to depth and orientation effects (Hillebrand and Barnes, 2002). EEG is more portable than MEG and has the potential for home-based measurements. Given this, future studies could use EEG for larger-scale assessment of mismatch negativity amplitudes (Blackman *et al.*, 2023). A third consideration is the use of concomitant medication in the patient group; however, participants were required to be on a stable dose for at least 30 days prior to participation in the study. The impact of treatments, such as cholinesterase inhibitors, could therefore have moderated the results. However, only 4 patients were on cholinesterase inhibitors (donepezil hydrochloride) in the baseline comparison, 3 of these completed the longitudinal assessment while none in the test-retest group took cholinesterase inhibitors. I would expect such cholinesterase inhibitors to reduce (rather than exacerbate) differences between groups. Fourth, there was a significant difference in age between patient and control groups. However, supplementary PEB analyses which included age as a regressor of non-interest showed similar results (see supplementary analysis). Fifth, attrition at follow up could affect results. However, the attrition rate of 29% over an average 16-month interval is in line with previous longitudinal studies prior to COVID-19. The original study protocol planned for an interval of 12 months, in accord with many early phase clinical trials of disease-

modifying agents. However, the COVID-19 pandemic lockdowns extended the average interval. Future *in vivo*, human studies could determine whether disease-modifying treatments targeting the cholinergic deficit or tau depositions in pyramidal cells alleviate the reported findings. Future research can use new methods for incorporating information about where in the cortex the synaptic loss is located using dynamic causal modelling (Adams *et al.*, 2023, Jafarian *et al.*, 2023*b*) or *post mortem* data. The current method would also be applicable to presymptomatic people and further research is needed to determine sensitivity prior to mild cognitive impairment.

4.4.5 Conclusion

In conclusion, this chapter has shown how dynamic causal modelling of human neurophysiological non-invasive recordings is reliable and sensitive to detect the effects of Alzheimer's disease and progression of Alzheimer's disease. Specifically, this chapter confirmed changes in the pyramidal cell gain and connectivity as predicted by preclinical and *post mortem* studies. This methodology helps to bridge the gap between preclinical and clinical studies, identifying mechanistically-informative markers of disease that are sensitive to disease presence and progression. This methodology can be tailored for drug discovery pipelines. This would allow relationships between targets-of-interest and measures of disease severity and progression to be quantified. Targets-of-interest with greatest potential to improve clinical outcomes could therefore be identified. In addition, these techniques can be used to quantify engagement of novel therapeutics and determine the effect of target modulation on the severity and progression of Alzheimer's disease. Finally, in the future, personalised dynamic causal modelling may be able to assess how beneficial a treatment, or combination of treatments, may be for an individual. This would improve participant selection for clinical trials (by identifying participants who would benefit most from the experimental medicine) and could help inform personalised treatment plans in clinic. This chapter consequently illustrates a framework that can be used for future development, assessment and prescription of dementia therapeutics.

Appendix A: Supplementary materials for Chapter 4

Data availability

The code used is available at https://github.com/jlansk/dcm_cmc_ntad. Anonymised (unlinked) raw data will be made available via Dementias Platform UK, subject to managed access conditions that protect participant confidentiality and conditions of consent.

Dynamic causal modelling

In this section, I provide further detail on the biologically-informed generative model of the scalp MEG data used in this chapter.

Dynamic casual modelling entails a variational Bayes inversion of biologically-informed models to neuroimaging data under the Laplace assumption that the priors and posteriors of the unknown parameters have a Gaussian distribution (Friston *et al.*, 2003, 2007, 2019; Kiebel *et al.*, 2007). Dynamic causal modelling is used to infer the posterior densities of model parameters and the model's free energy score from features of the electrophysiological recordings, in this case, the evoked response. The negative free energy of the model provides a lower bound for the log model evidence and is the difference between the predictions of the model's accuracy and complexity. The objective of variational Laplace is to maximise the free energy score by iteratively updating and adjusting the model parameters given data features and prior information. As the model's parameters are updated, the accuracy of the predicted model's response to the observed response is gradually improved, while the inversion scheme penalises model complexity to reduce the risk of overfitting (Zeidman *et al.*, 2023). The model evidence of different models, with neuronal architectures differing according to the hypothesis being tested, can be compared to elucidate the most likely underlying causes of the observed brain response.

In this study, the neuronal model of each source is the convolution canonical microcircuit model (spm_fx_cmc.m). This model compromises an intrinsic anatomical network in each region, with inhibitory interneurons, superficial and deep pyramidal cells and spiny stellate excitatory populations as shown in Figure 4.2a. Specification of the parameters and their priors

are set at the default values (spm_cmm_nmda_priors.m). The mean, presynaptic firing rate of each population is scaled by extrinsic connectivity parameters and convolved with a synaptic impulse response function (modelled by single time constant, T, with an alpha-shaped kernel, $h(t) = \frac{t}{T}\exp(-\frac{t}{T})$) to produce the average membrane potential. The membrane potential is passed through the sigmoid transformation (denoted by σ) to give the mean firing rate (average action potentials).

Mathematically, the membrane potential in a population j within region i, $v_i^{(j)}$, can be calculated by convolving (denoted by $\otimes$) the presynaptic firing rate (the sum of all intrinsic, extrinsic, and experimental firing inputs) with a synaptic kernel as follows:

$$v_i^{(j)} = (\underbrace{\sum_k \boldsymbol{G}_{ik}^{(j)}\sigma(v_k^{(j)})}_{\text{intrinsic}} + \underbrace{\sum_{kl} \boldsymbol{A}_{jl}^{(ik)}\sigma(v_k^{(l)})}_{\text{extrinsic}} + \underbrace{\sum_m C_{jm}^{(i)}u_m}_{\text{experimental}}) \otimes h(t) \quad (1)$$

In equation 1, intrinsic connections $\boldsymbol{G}_{ik}^{(j)}$s (within region j, and from population k to i) are specified according to laminar-specific features of cortical columns. Each population is subject to self-inhibition, a proxy of self-regulation, to ensure the stability of the model. Extrinsic connectivity, denoted in equation 1 as $\boldsymbol{A}_{jl}^{(ik)}$s (from distal source k to i and from population l to j), can be bottom-up (originating from superficial pyramidal cells in a lower level and targeting spiny stellate cells and deep pyramidal cells in a higher level of a cortical hierarchy) and/or top-down (from deep pyramidal cells at high cortical levels to inhibitory interneurons and superficial pyramidal cells in the lower levels (Felleman and Van Essen, 1991; Hilgetag *et al.*, 2000). A thalamic drive is denoted by u_m, which excites spiny stellate cells (in some sources) and models the effect of experimental input (scaled by C). The model of an experimental input is a Gaussian function (with latency prior of $70 \pm 16\ ms$).

To generate simulated scalp MEG data, a network was specified with interconnected neuronal sources that are active under the experimental paradigm. The activities of the neuronal sources are approximated as equivalent current dipoles, with orientations estimated with symmetry constraints as part of the fitting of the whole model. The models were fitted to sensor data which had been reduced using singular value decomposition to eight principal modes for computational expediency. The generative model is thereby able to predict evoked responses to experimental inputs. This generative model was fitted to the scalp MEG data using the variational Laplace scheme in the SPM12 software.

Supplementary methods and results

Short-term plasticity over repetitions

To assess the effect of Alzheimer's disease on short-term plasticity, I inverted two sets of PEB models including parameters for the (i) monotonic (exponential) reduction of forward connections over sequential repetitions; and (ii) phasic repetition effect on intrinsic connections (Garrido *et al.*, 2009*a*).

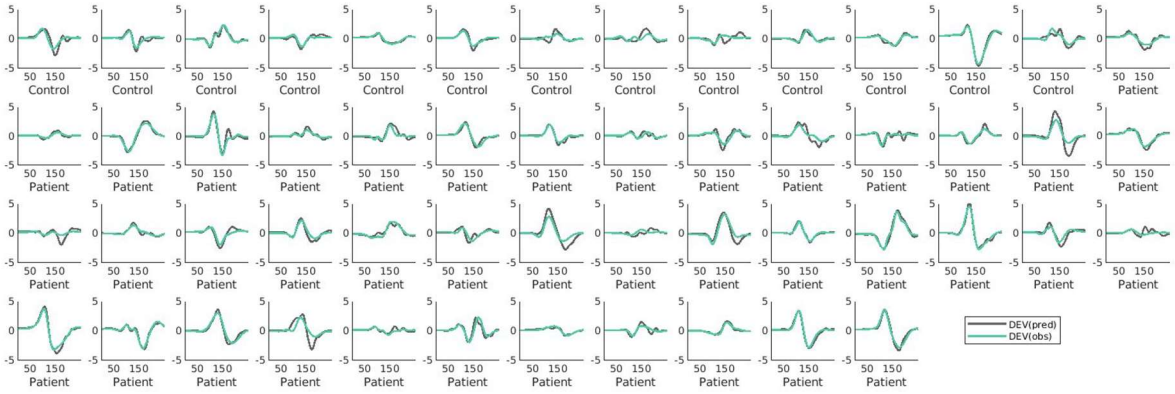
To do this, each set of parameters were optimised in PEB models comparing (i) patients and controls, using a design matrix with a first regressor of ones and second regressor of 0 for controls and 1 for patients and (ii) patients at baseline and follow up, with a first regressor of ones and a second regressor with 0 for baseline dynamic causal models and years-from-baseline for follow-up dynamic causal models. For each PEB model, Bayesian model comparison and averaging (function spm_dcm_peb_bmc) was performed over a model space of all parameter combinations with hemispheric symmetry.

Bayesian model comparison of PEB models

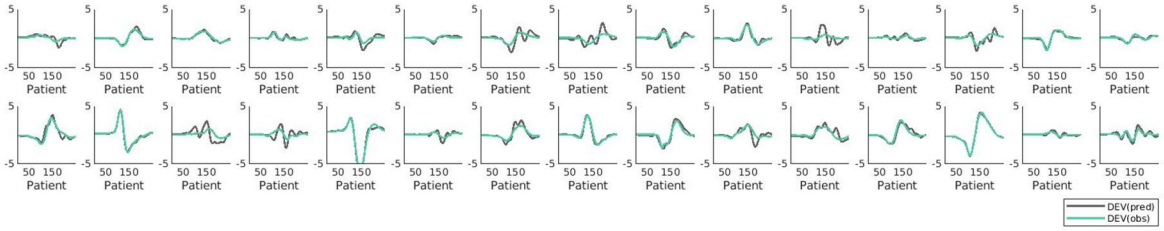
I then identified which of the intrinsic parameters (superficial pyramidal cell gain modulation versus intrinsic phasic repetition effect) and extrinsic parameters tested (connectivity between pyramidal cells versus extrinsic exponential repetition effect) best explained the effect of disease on the neurophysiological responses to the mismatch negativity task (see Supplementary Figure A.8). To do this, I calculated and plotted the difference in free energies for intrinsic (Figure 4.3 versus Supplementary Figure A.6) and extrinsic PEB models (Figure 4.4 versus Supplementary Figure A.7) of disease presence and progression.

Including age as a covariate in the baseline PEB-analyses

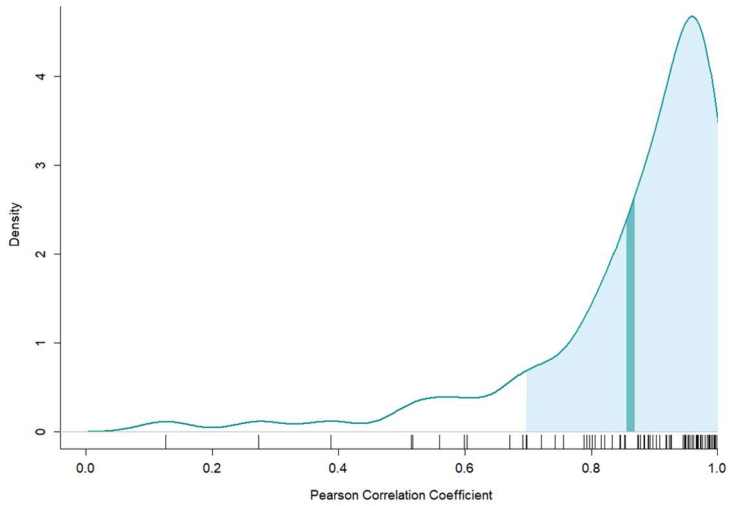
Group PEB analyses were inverted with z-scored age as the third regressor in the design matrix. The PEB included all parameters that had differentiated patients from controls at baseline. These analyses were conducted given the significant difference in age between groups. Including age as a covariate had minimal effect on the posterior estimates and their probabilities of differing between groups (patients versus controls). Age had no significant effect on these connections (see Supplementary Figure A.9).



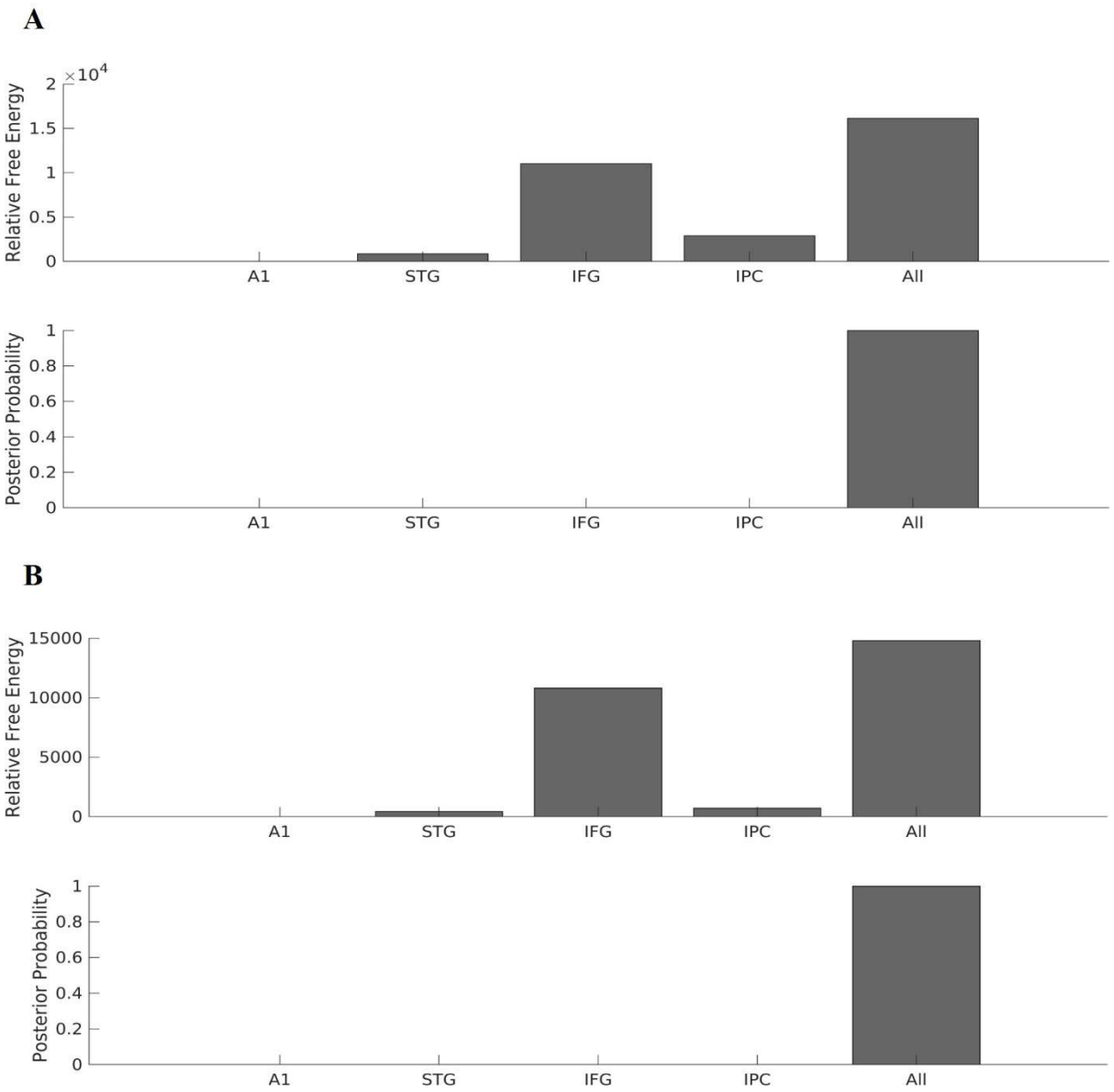
Supplementary Figure A.1 Predicted (grey) and observed (teal) evoked responses to the deviant tone for each subject at baseline



Supplementary Figure A.2 Predicted (grey) and observed (teal) evoked responses to the deviant tone at longitudinal follow up.

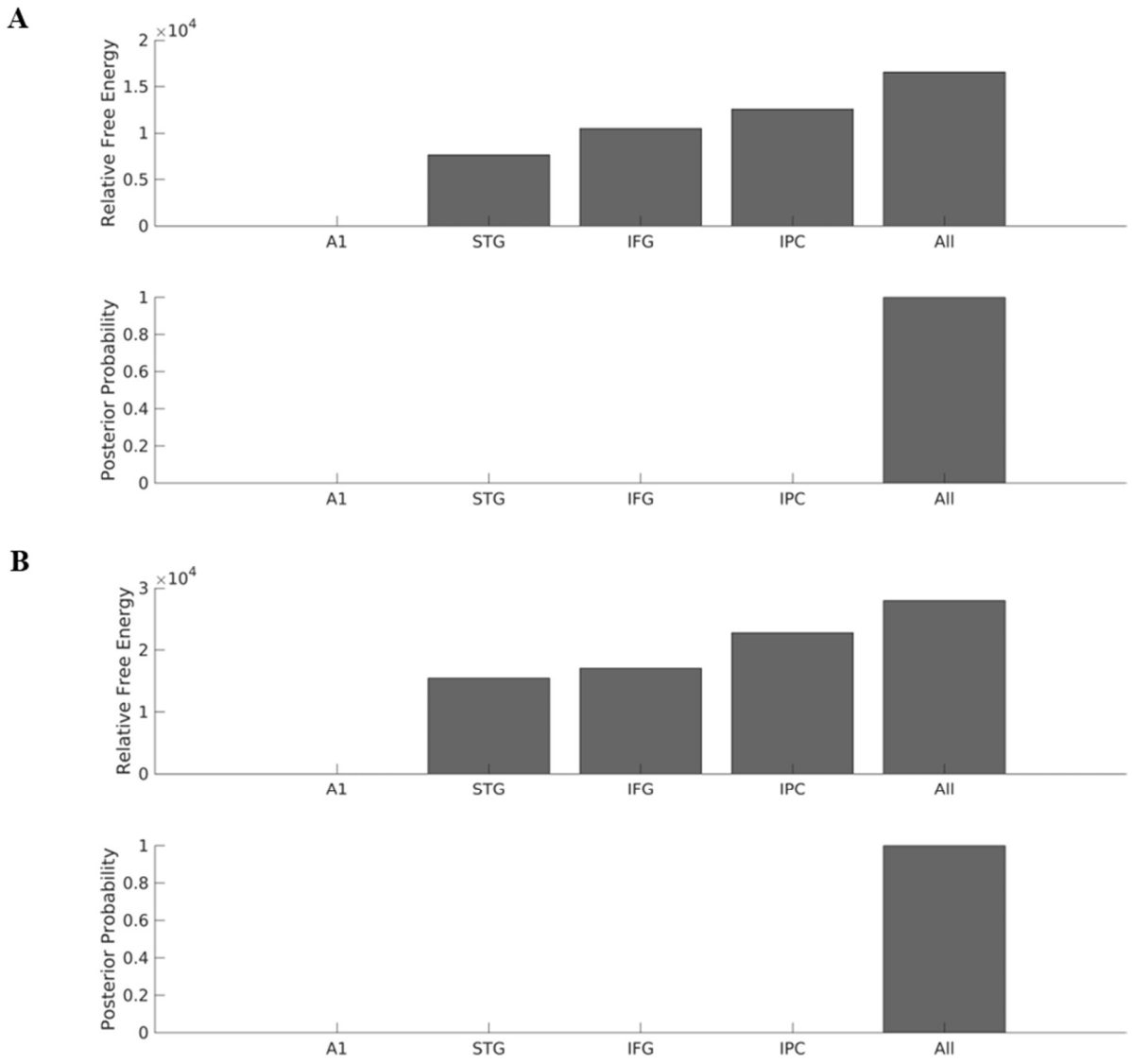


Supplementary Figure A.3 Kernel density distribution of correlation coefficients for observed and predicted evoked responses of all sessions and groups and a rug plot with individual points.
The Pearson's correlation coefficient of the predicted and observed evoked responses were calculated for each participant and each session. The kernel density distribution and rug plot of individual correlation coefficients are shown. The observed and model-generated evoked responses were highly correlated (mean Pearson's correlation = 0.86 ± 0.16).



Supplementary Figure A.4 Regional comparisons of PEB models of superficial pyramidal cell gain modulation.

Regional comparisons of PEB models with (A) controls versus patients and (B) patients at baseline versus follow up are shown. In both instances, for the models including a single region only, the model with frontal regions best explained group differences with a difference in free energy between the frontal and the next highest region, parietal, of 8137 for patient versus control PEB models (A); and 10089 for patient baseline versus follow-up PEB models (B). However, the model with all 4 regions was the winning model, with a difference in free energy between the winning and second-best model of 5121 for baseline patients versus controls (A); and 3998 for patient baseline versus follow up (B). $\triangle F$, difference in free energy; A1, primary auditory cortices; STG, superior temporal gyri; IFG, inferior frontal gyri; IPC, inferior parietal cortices.



Supplementary Figure A.5 Regional comparisons of PEB models including connections between pyramidal cells of different regions.

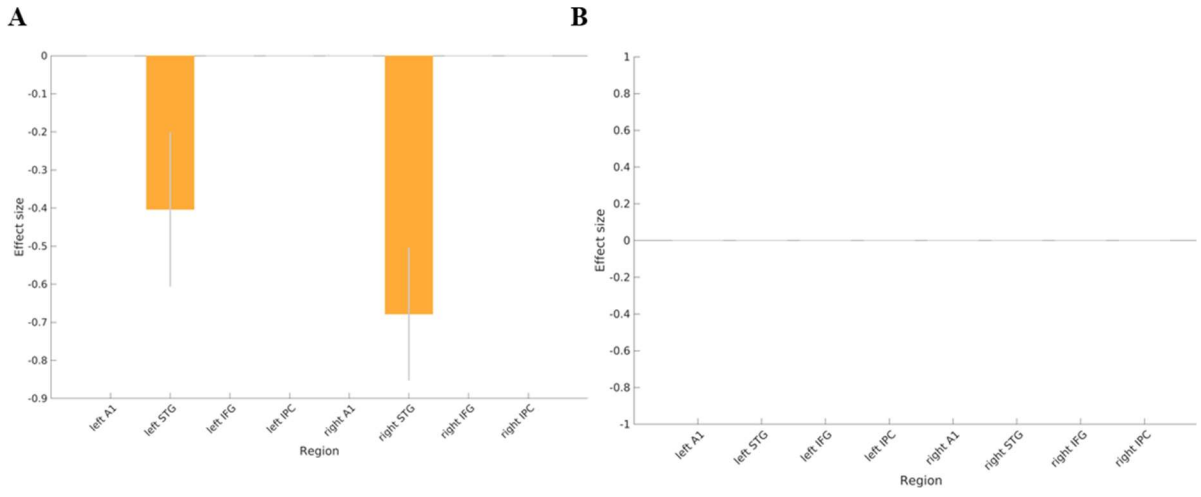
Regional comparisons of PEB models with **(A)** controls versus patients and **(B)** patients at baseline versus follow up. In both instances, for the models including connections originating and terminating from a single region, the parietal model best explained group differences in responses to the mismatch negativity task with a difference in free energy between the parietal and the next highest region, frontal, of 2077 for patient versus control PEBs (A); and of 5770 for patient baseline versus follow-up PEBs (B). However, the model with all 4 regions was the winning model, with a difference in free energy between the winning and second-best model of 3983 for baseline patients versus controls (A); and 5168 for patient baseline versus follow up (B). $\triangle F$=difference in free energy; A1=primary auditory cortices; STG = superior temporal gyri; IFG=inferior frontal gyri; IPC=inferior parietal cortices.

Short-term plasticity: effect of disease presence and progression

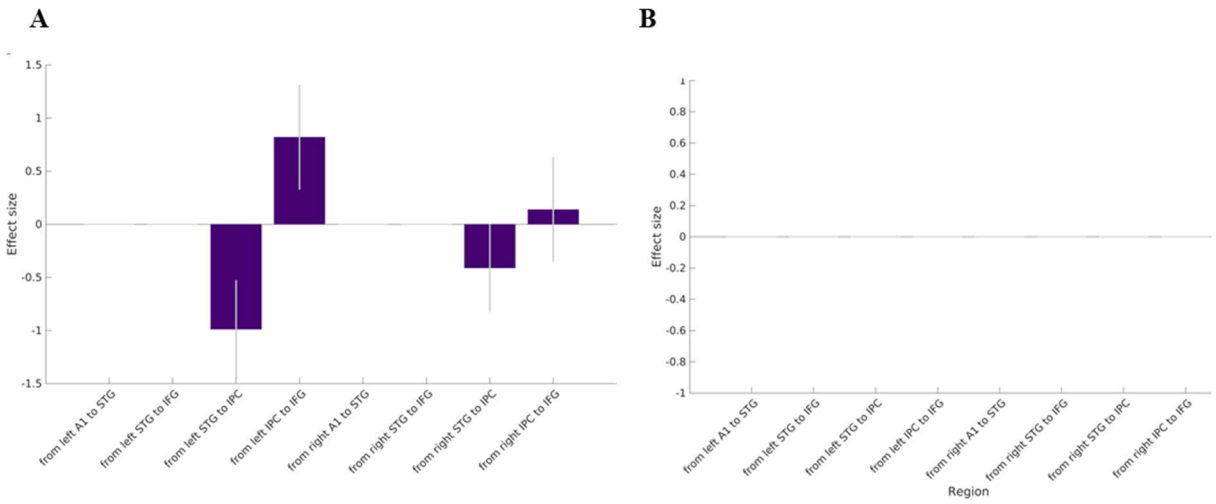
The analyses of sequential stimulus repetition effects reveals how the presence of Alzheimer's disease changes the phasic effect of stimulus repetition, with a rapid decrease and subsequent increase, in intrinsic connections and slower exponential repetition effect in extrinsic forward connectivity. The phasic response of intrinsic connections was decreased in intrinsic connections of the superior temporal cortices while the slower exponential response was decreased from superior temporal to inferior parietal cortices with an increase from left inferior parietal to inferior frontal cortices (Supplementary Figure A.6).

The PEB models optimising superficial pyramidal cell gain modulation and extrinsic connectivity between pyramidal cells were best at explaining differences between patient and control groups compared to intrinsic and extrinsic repetition effects, respectively (see upper panel of Supplementary Figure A.8).

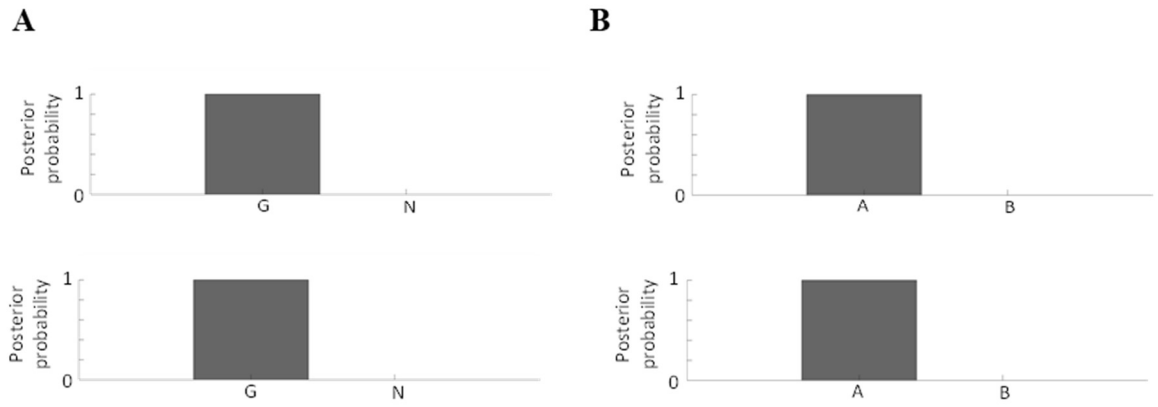
There were no significant changes to the effect of repetition with disease progression (patient baseline versus follow up); however, repetition effects on intrinsic and extrinsic connectivity were less important than the effects of superficial pyramidal cell gain modulation and extrinsic connectivity between pyramidal cells for the longitudinal analyses (see lower panel of Supplementary Figure A.8).



Supplementary Figure A.6 The effect of disease and its progression on the intrinsic repetition effect.
The rapid decrease and subsequent increase (phasic) response to tone repetition in intrinsic connections was **(A)** decreased for patients compared to controls; **(B)** had no significant change between baseline and follow up for patients.



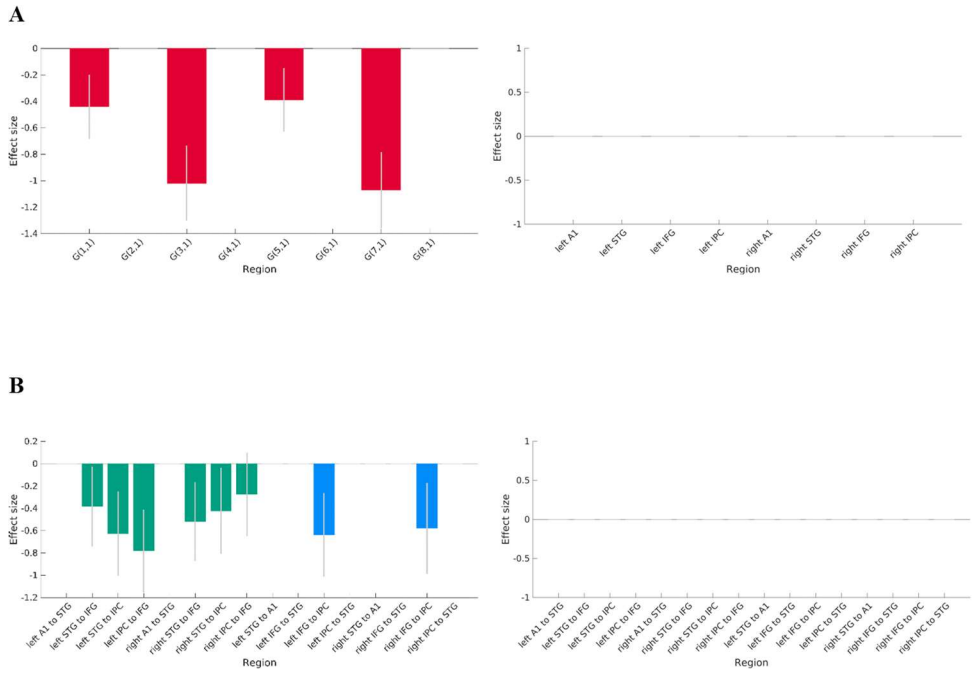
Supplementary Figure A.7 The effect of disease and its progression on extrinsic repetition effects **(A)** The slower exponential decreasing response to tone repetition of extrinsic connections was lower in people with Alzheimer's disease or MCI than controls for the connection from superior temporal to inferior parietal cortices and increased from inferior parietal to frontal cortices. **(B)** There were no significant changes to this response for patients between baseline and follow up.



Supplementary Figure A.8 Model comparison of PEB models with intrinsic or extrinsic parameters.

Posterior probability of PEB models for controls versus patients (top) and longitudinally for patients (bottom) with (A) intrinsic parameters (superficial pyramidal cell gain modulation versus phasic repetition effect) and (B) extrinsic parameters (connectivity between pyramidal cells of different regions versus the exponential repetition effect on extrinsic connections).

Group PEBs with age



Supplementary Figure A.9 Group PEB comparisons controlling for age.
Effects are shown for **controls versus patients (left)** and **age (right)** for (A) superficial pyramidal cell gain and (B) extrinsic connections between pyramidal cells of different regions

	Description	**Prior**
$G_i^{(k)}$	Gain modulation of the *i*-th neuronal population in region *k*	$p(\theta_G) = N(0, \frac{1}{16})$
$A_{kl}^{(ij)}$	Extrinsic forward and backward connectivity from population *j* in region *l* to population *i* in region *k*	$p(\theta_A) = N(0, \frac{1}{8})$
B_{klm}	Change in forward and backward extrinsic connectivity caused by the *m*-th input	$p(\theta_B) = N(0, \frac{1}{8})$
N_{jim}	Change in intrinsic connectivity caused by the *m*-th input	$p(\theta_N) = N(0, \frac{1}{8})$

Supplementary Table A.1 Parameters of interest from the canonical microcircuit dynamic causal model.
All parameters used the standard priors and parameterisation (as specified within SPM 12 https://www.fil.ion.ucl.ac.uk/spm/software/spm12/). The parameters of interest are shown.

5 | NMDA-channel kinetics of people living with Alzheimer's disease

A manuscript related to this chapter is currently in preparation as:
Lanskey, J. H., Jafarian, A., Karadag, M., Kocagoncu, E., Nobre, A. C., Raymont, V., Singh, K. D., Woolrich, M., Henson, R. N., Rowe, J. B., (2024) NMDA-channel kinetics of people living with Alzheimer's disease.

The code used is available at: https://github.com/jlansk/cmm_NMDA

Abstract: A better understanding of disease mechanisms driving cognitive change in Alzheimer's disease may identify new targets for disease-modifying treatments. NMDA-receptors are important for memory and important mediators of extrinsic connectivity. In this chapter, I examine changes to NMDA-receptor kinetics in people living with Alzheimer's disease. I invert conductance-based canonical microcircuit dynamic causal models with NMDA receptor parameters to mismatch negativity MEG responses. I confirm that abnormal NMDA-receptor function explains the neurophysiological deficit associated with Alzheimer's disease more than AMPA or GABA receptor changes. Alzheimer's disease progressively changes NMDA-channel time constants in primary auditory and inferior frontal regions. This study demonstrates the potential for dynamic causal models to support studies of novel therapeutics of Alzheimer's disease that affect NMDA-channel activity.

5.1 Introduction

With the immense health, social and economic burden of Alzheimer's disease, new treatments for symptoms are required, as well as effective disease-modifying treatments. A better mechanistic understanding of the cellular mechanisms of human cognitive impairments has the potential to identify priority targets and surrogate markers of drug effects. Here, I consider the role of glutamatergic synapses, as the major mediator of long range and intra-cortical excitatory connectivity, and the particular impact of Alzheimer's disease pathology on NMDA-receptor function (Carlson *et al.*, 1993; Lai *et al.*, 2019).

NMDA receptors play an important role in memory (Yang *et al.*, 2023), a major cognitive domain affected by Alzheimer's disease (Villemagne *et al.*, 2013; Figure 3.1). The drug memantine acts primarily on NMDA receptors and is licensed to treat cognitive decline in moderate to severe Alzheimer's disease (Wilkinson, 2012). Memantine blocks NMDA channels that are pathologically open in later disease stages (Danysz and Parsons, 2012). At early disease stages, Alzheimer's-related beta-amyloid changes proteins that moderate NMDA-channel opening times, such as PSD95 and Protein kinase C (Ortiz-Sanz *et al.*, 2022). Changes to NMDA channel opening times are predicted to influence NMDA-mediated signalling (Xu *et al.*, 2021*a*) and thereby moderate cognition (Yang *et al.*, 2023). Such changes to NMDA-channel kinetics may be followed by compensatory mechanisms that increase NMDA signalling (Newcomer *et al.*, 2000). Understanding the changes to NMDA-channel kinetics in people living with Alzheimer's disease may therefore highlight new targets for drugs and new biomarkers of drug efficacy. It also provides the opportunity to test neurobiologically-informed biophysical models of human cortical function, which can now incorporate specific ion-channel properties including NMDA-channel time constants and NMDA-mediated connectivity (Moran *et al.*, 2011*a*; Symmonds *et al.*, 2018, Jafarian *et al.*, 2023*b*).

This chapter examines changes to NMDA-channel kinetics in people living with Alzheimer's disease using generative models of cognitive physiology. Specifically, conductance-based dynamic causal models (DCMs) are used to test how Alzheimer's disease drives neurophysiological changes. Responses were recorded by magnetoencephalography (MEG) during a roving mismatch negativity task. This task is reliant on NMDA-receptor mediated iterative updating of predictions by prediction errors (Wacongne *et al.*, 2012). Responses to the mismatch events are attenuated by Alzheimer's disease and its progression (Chapter 4). To

understand the role of specific ion receptors (AMPA, GABA or NMDA), I inverted DCMs to MEG responses of participants with and without Alzheimer's disease. Given preclinical findings, I expected NMDA receptor differences to be most important for explaining differences in neurophysiological responses due to Alzheimer's disease (Carlson *et al.*, 1993; Lai *et al.*, 2019). I then determined how Alzheimer's disease and its progression affects the parameters of the NMDA receptor.

5.2 Materials and methods

5.2.1 Participants

MEG, MRI and neuropsychology data from the New Therapeutics in Alzheimer's Disease study (NTAD, Lanskey *et al.*, 2022) were used. Amyloid status of participants was determined by cerebrospinal fluid examination or positron emission tomography. Data from neurologically-healthy control participants with negative amyloid status were included (n = 14). Participants were included with amyloid-positive mild cognitive impairment or Alzheimer's disease with early dementia who completed the mismatch negativity MEG task at baseline (n=45); 32 of whom completed MEG after an average interval of 16 months. Baseline clinical and cognitive data for participants are given in Table 5.1. Independent Student's t-tests and Bayesian t-tests were used for continuous data, or chi-squared tests for categorical data, to identify differences at baseline between patients and control groups.

5.2.2 Task

Data from a roving mismatch negativity task were used (Lanskey *et al.*, 2022). During the task, participants listened passively to a train of 75ms tones presented at 400ms intervals while watching a silent nature documentary. The frequency of the tone pseudo-randomly changed after 3 to 10 repetitions. Tone frequencies ranged from 400 to 800Hz. The first (deviant) and sixth tones after each frequency change were used as deviant and standard respectively.

5.2.3 Imaging acquisition and preprocessing

MEG was recorded at the MRC Cognition and Brain Sciences unit with the Elekta Neuromag VectorView system and MEGIN Triux Neo scanner. Both scanners contained two planar gradiometers and one magnetometer at 102 sensor locations. Participant head movements were measured with five Head-Position Indicator coils that were digitised using a 3D digitizer

(Fastrak Polhemus) with >300 additional scalp surface points in relation to the standard fiducial points. An electrode on the right clavicle and a second on the left, lower rib recorded electrocardiogram data. Eye movements were measured with vertical and horizontal electrooculography. Structural T1-weighted MRI images were recorded from each participant with a 3T Siemens PRISMA scanner (3D MPRAGE sequence, echo time, 2.91ms; inversion time, 900ms; repetition time, 2300ms; flip angle, 9 degrees; voxel size, 1mm isotropic; slice thickness, 1mm; slice number, 176; acquisition matrix, 256×240). Data preprocessing followed the same NTAD preprocessing pipeline as previously reported (Chapter 4). In brief, MaxFilter v2.2 software (Elekta Neuromag) was used on the raw data. The EEGLAB toolbox was used to perform independent component analysis (Delorme and Makeig, 2004). Data were bandpass filtered between 0.01Hz and 40Hz and epoched from -100ms to 500ms. OSL's artefact rejection algorithm was used to remove residual bad trials and channels (github.com/OHBA-analysis/osl-core). Robust averaging was used to average epochs for trials, with conditions separately weighted. A final low-pass filter was applied to the data to correct for potential high frequencies introduced during robust averaging.

5.2.4 Sensor-level analysis

Planar gradiometers were combined by calculating their root mean square. For each participant, the mean response across planar gradiometers was calculated for each subject, tone and session separately. The average amplitude from 140 to 160ms of the difference waveform between the first and sixth tone was calculated. An independent-sample, one-sided, Student's t-test assessed the group difference at baseline (controls versus people with Alzheimer's disease) and a paired, one-sided, Student's t-test assessed session differences between baseline and 16-month follow up for people with Alzheimer's disease. Effect sizes were calculated using Cohen's d.

5.2.5 First-level network modelling

I used a canonical microcircuit model with NMDA channels (cmm_NMDA in SPM12 r7771; Moran *et al.*, 2011) to determine the effect of Alzheimer's disease on cortical generators of evoked responses. The model comprised of four cell populations at each of 8 cortical regions: bilateral primary auditory cortex (left: -42, -22, 7; right: 46, -14, 8), bilateral superior temporal gyrus (left: -61, -32, +8; right: +59, -25, +8), bilateral inferior frontal gyrus (left: -46, +20, +8; right: +46, +20, +8), and bilateral inferior parietal cortex (left: -58, -27, +30; right: +59, -41, +30). The connectivity of six of these regions has been studied over a series of prior works

(bilateral primary auditory cortex, superior temporal cortex and inferior frontal gyrus; Garrido *et al.*, 2008; Phillips *et al.*, 2015; Rosch *et al.*, 2019; Adams *et al.*, 2021). Regions are connected according to their level in an information-processing hierarchy; with forward connections from lower to higher regions, and backward connections from higher to lower regions. The connectivity of the parietal cortex within this network has been previously reported (Lanskey *et al.*, 2024; Chapter 4) as follows: inferior frontal gyrus > inferior parietal cortex > superior temporal gyrus > primary auditory cortex. A series of nested model architectures were defined according to Lanskey *et al.* (2024) and the corresponding 'full' model, the model with all possible connections, was inverted. Tone repetition was modelled with a design matrix of 1 for evoked responses to the first (deviant) tone and 0, for the sixth tone (repetition 5).

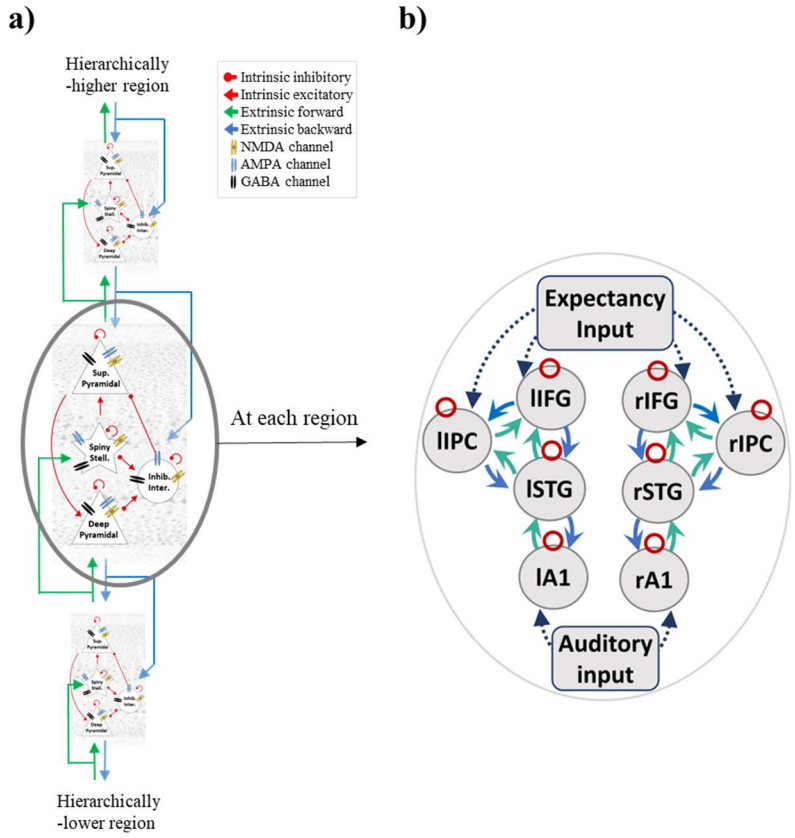


Figure 5.1 The conductance based dynamic causal model with NMDA parameters.
The model used (function: cmm_NMDA) included **a)** a canonical microcircuit with intrinsic (red), NMDA (yellow), AMPA (blue) and GABA (black) parameters at **b)** each of 8 regions connected with forward (green) and backward (blue) connections. The winning model '6' is shown.

I inverted the models for all participants at all sessions to evoked responses from 0 to 300ms. Sensor data was reduced to 8 spatial nodes and a Hanning window was applied. During model inversion, source activity was approximated as equivalent current dipoles with symmetry constraints and a lead field informed by subject-specific T1-weighted MRI images was used. Data from one control participant and one participant with symptomatic Alzheimer's disease at baseline had inversion failures and were excluded from the second-level analyses. For the longitudinal session, four people with symptomatic Alzheimer's disease had an inversion failure and were excluded from the second-level analysis.

Bayesian model reduction (function spm_dcm_bmr) was used to determine the average relative free energies of nested models across controls and patients at baseline, and patients at baseline and follow-up sessions. For controls and patients, model 6 (inferior frontal gyrus > inferior parietal cortex > superior temporal gyrus > primary auditory cortex) had highest free energy (see supplementary figure B1) in line with previous studies (Cope *et al.*, 2022; Lanskey *et al.*, 2024). This model is consequently used for PEB analyses.

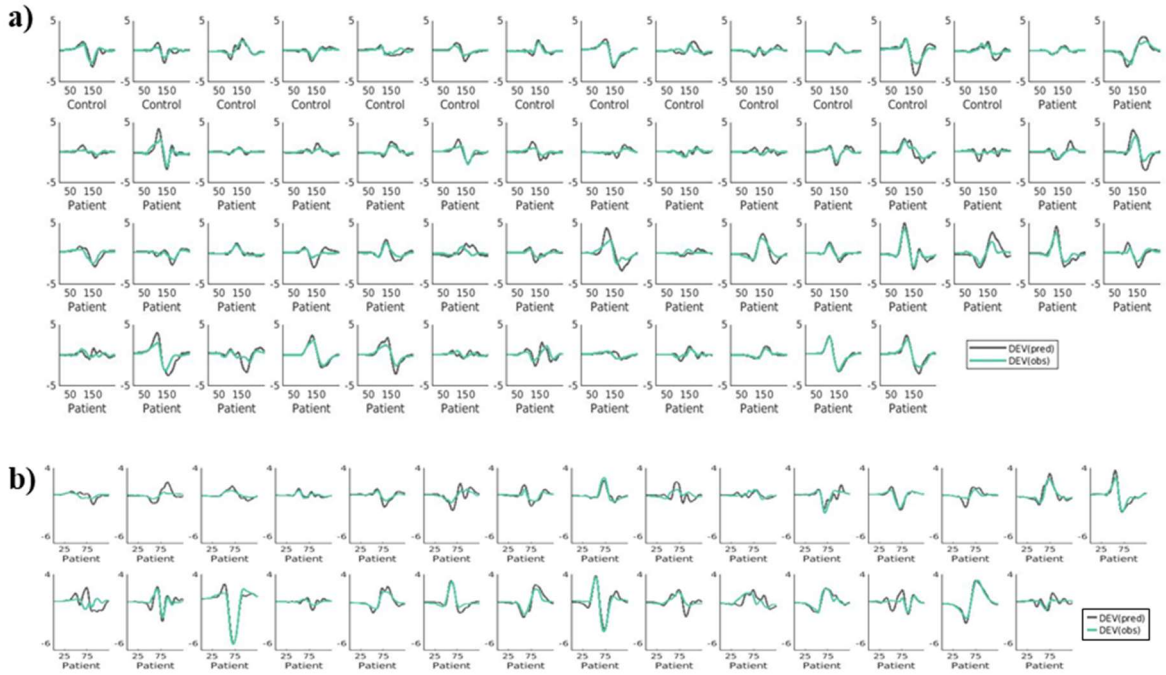


Figure 5.2 Model fits.
Observed responses (cyan) and model-generated responses (grey) to the deviant tones of the Mismatch Negativity paradigm for each participant at a) baseline and b) follow up sessions.

5.2.6 Second-level analyses

The winning DCM was taken forward to second-level analyses using parametric empirical Bayes (PEB) to compare group-effects of subsets of parameters. First, I tested which neurotransmitter system was most affected by Alzheimer's disease. The PEB models included baseline DCMs of controls and people with Alzheimer's disease. A series of PEB analyses were run with a design matrix comprising a unitary regressor of ones for the group mean and a regressor for group membership (zero for control participants and one for participants with Alzheimer's disease). A third regressor controlling for age (mean centred and scaled) was included. Each PEB had a different set of parameters explaining the group effect (1 included AMPA time constants and AMPA-mediated extrinsic connections; 2, GABA time constants; 3, NMDA time constants and NMDA-mediated extrinsic connections).

A second series of PEB analyses tested which neurotransmitter system was most affected by Alzheimer's disease progression. The PEB models included DCMs of participants with Alzheimer's disease at baseline and follow-up sessions and a design matrix comprising a unitary regressor of ones and a regressor for session (zero for baseline and one for follow up). A third regressor specified the time in years between the baseline and follow-up scans for each patient (0 for baseline scans and with scores from 0.8 to 2.2 for follow-up scans mean-centred and standardised). Each PEB model had a different set of parameters explaining the session effect (1 included AMPA time constants and AMPA-mediated extrinsic connections; 2, GABA time constants; 3, NMDA time constants and NMDA-mediated extrinsic connections. See Figure 5.5).

Bayesian model comparison and Bayesian model averaging were run for the winning PEB model from the baseline group comparison across a model space including parameters that differed in the baseline PEB with a probability > 0.95 and their hemispheric counterparts for the winning baseline group and longitudinal PEB models (given the size of the model space, imposing hemispheric symmetry across the entire model space was computationally unfeasible).

5.3 Results

5.3.1 Participant demographics

There were no significant differences between the groups for sex (χ^2=0.98, p=.32), handedness (t=1.86, p=.40) or Hachinski ischaemic score (χ^2=5.12, p=.16). There was a difference between groups in age (patients older than controls, t=-3.80, p=<.001, BF=71.67). There were expected group differences for the mini-mental state examination (t=4.75, p<.001, BF=1163), ACE-R (t=5.02, p<.001, BF=2722), clinical dementia rating (χ^2=55, p<.001), PET SUVR (t=-15.3, p<.01, BF=424), and CSF tau/amyloid-beta 1-42 (t = -6.51, p<.001, BF = 313). The baseline data of people who completed annual follow up was similar to the whole baseline group (see Table 5.1).

	Controls	**AD Baseline**	**AD Follow up**
Sex (Male:Female)	9:5	20:25	16:16
Handedness (Right:Left:Both)	11:3:0	40:4:1	28:3:1
Baseline Age (yrs)*	65.3 (±7.29)	73.8 (±7.32)	73.2 (±7.89)
Baseline MMSE*	29.4 (±0.74)	24.8 (±3.52)	25.1 (±3.24)
Baseline ACE-R*	92.4 (±4.94)	74.2 (±13.1)	75.7 (±11.1)
Baseline HIS	0.07 (±0.27)	0.56 (±0.8)	0.53 (±0.82)
Baseline pTau-181 (pg/mL)	1.29 (±0.63)	2.59 (±0.68)	2.58 (±0.69)
Baseline PET (SUVR)	0.98 (± 0)	1.68 (±0.79)	1.64 (±0.42)
Baseline CSF (tau/Abeta 1-42)	0.38 (±0.21)	1.84 (±0.21)	1.63 (±0.24)

Table 5.1 Participant demographics and screening data.
Values are given as mean (standard deviation) *denotes significant difference between baseline groups by frequentist and/or Bayesian statistics, as per text. AD, people with symptomatic Alzheimer's disease; Yrs, years; MMSE, mini-mental state examination; ACE-R, Addenbrooke's cognitive examination revised; HIS, Hachinski ischaemic score; PET, positron emission tomography; SUVR, standardised uptake value ratio; CSF, cerebrospinal fluid

5.3.2 Alzheimer's disease attenuates the mismatch negativity response

The amplitude of the mismatch negativity waveform from 140 to 160ms of people with Alzheimer's disease was significantly attenuated compared to controls (t=-1.71, p=.046, d =0.52, see Figure 5.3a) and with disease progression (baseline versus follow-up sessions; t=-2.83, p=.004, d=0.38, Figure 5.3b).

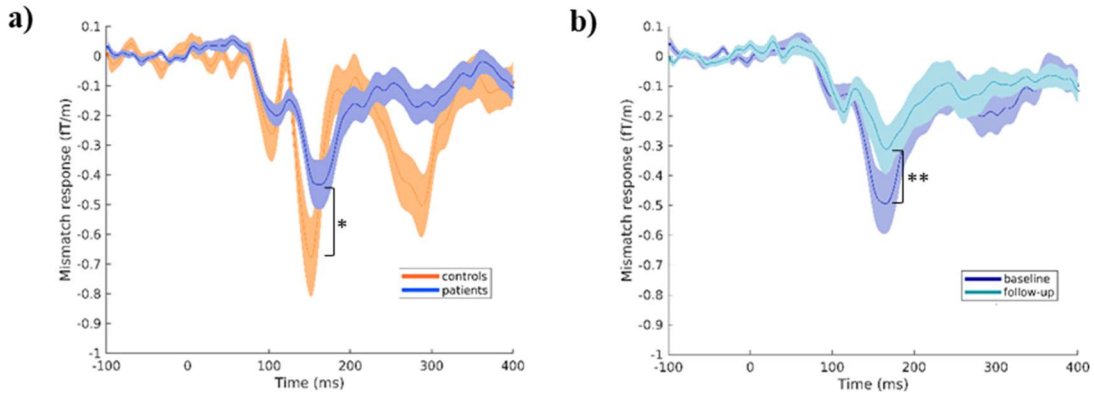


Figure 5.3 Mismatch negativity waveforms.
Average mismatch negativity waveforms **a)** at baseline for controls (orange) versus people with Alzheimer's disease (purple) and **b)** for people with Alzheimer's disease at baseline (purple) and follow-up MEG sessions (blue). *p<.05, **p<.01

5.3.3 Alzheimer's disease and its progression affect NMDA parameters

The PEB with NMDA-related parameters had the greatest probability of explaining the effect of Alzheimer's disease (baseline controls vs patients) and the effect of time (baseline versus follow up in patients) compared to PEB models with GABA or AMPA parameters (Figure 5.4).

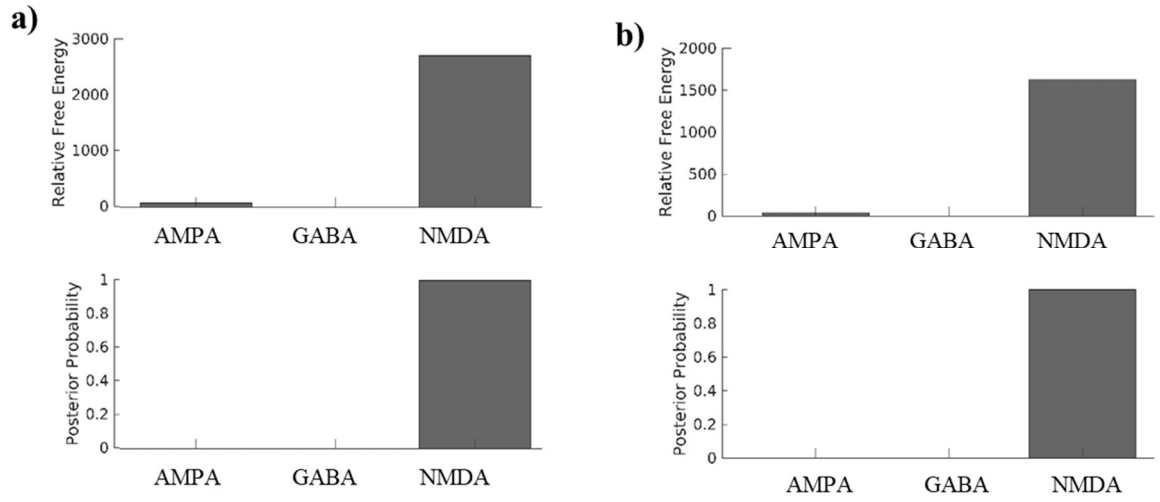


Figure 5.4 Relative free energy of PEB models with AMPA, GABA or NMDA parameters
Model comparisons for AMPA vs GABA vs NMDA PEB models with (a) patients versus controls and **b)** patients at follow up versus baseline for people with Alzheimer's disease. The AMPA model included AMPA time constants, AMPA-mediated extrinsic connections and AMPA-mediated modulatory extrinsic connectivity (T(:,1), A, and B parameters, respectively). The GABA model included GABA time constants (T(:,2) parameters). The NMDA model included NMDA time constants, NMDA-mediated extrinsic connections and NMDA-mediated modulatory extrinsic connections (T(:,3), AN, and BN parameters, respectively).

5.3.4 Alzheimer's disease progressively affects NMDA-channel time constants

Parameters that differed in the PEB of baseline patients *versus* controls with a probability > 0.95 (Figure 5.5a) defined a model space over which Bayesian model comparisons were run. These parameters and their hemispheric counterparts were used to define the model space (see Figure 5.5b). The model space included all hemispherically-symmetric combinations of the NMDA-channel time constants (parameters 1:8) and forward connections from superior temporal to inferior parietal regions (parameters 11 and 15).

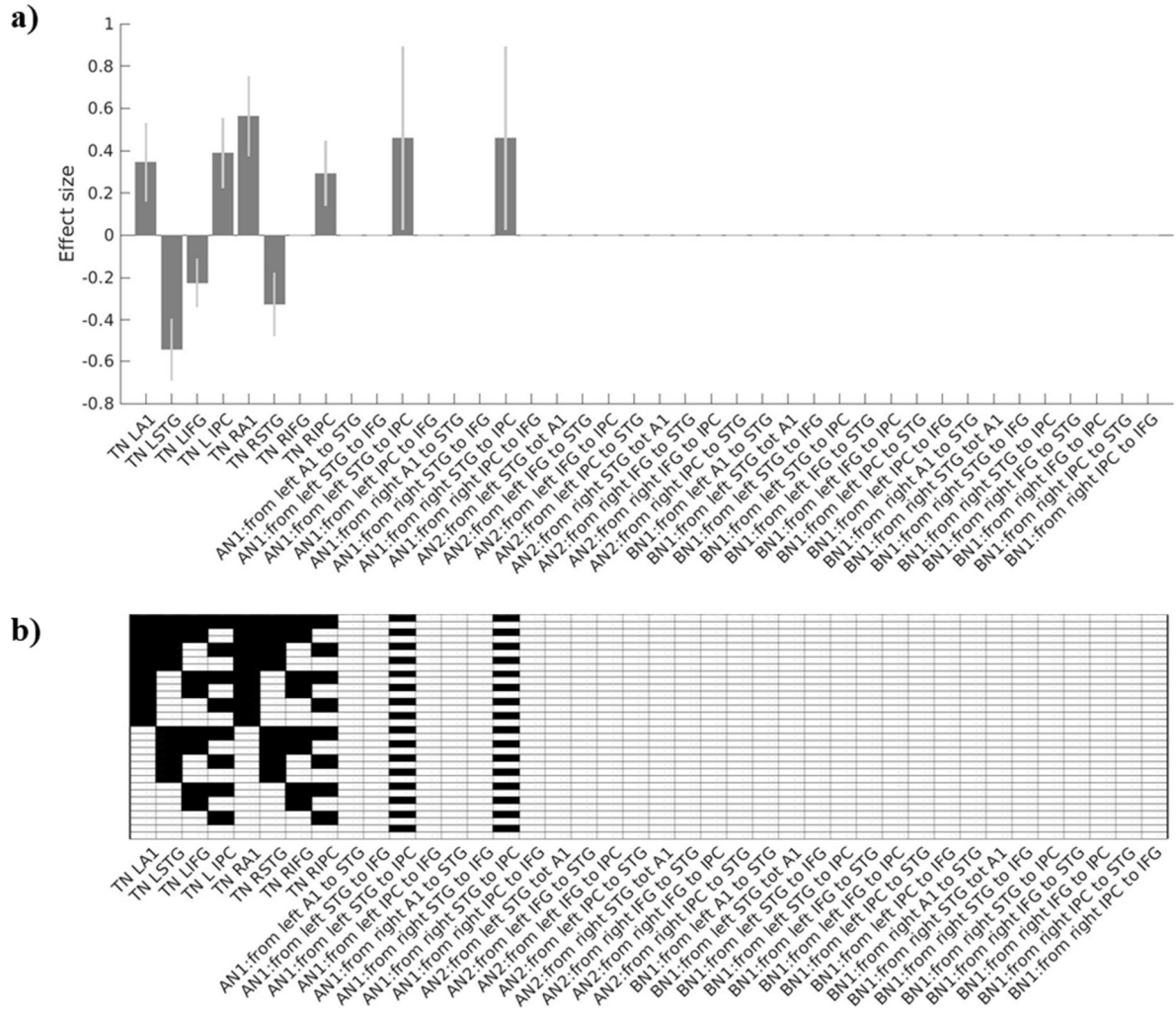


Figure 5.5 Model space over which Bayesian model comparisons were run.
a) Parameters with >.95 posterior probability in PEB analysis of people with and without Alzheimer's disease. **b)** These parameters and their hemispheric counterparts defined a hemispheric-symmetric space, shown here, to run Bayesian model comparisons over. TN, NMDA receptor time constant; AN1, NMDA-mediated forward extrinsic connectivity to repeated tones; AN2, NMDA-mediated backward extrinsic connectivity to repeated tones; BN1, modulatory effect of deviant tones on NMDA-mediated extrinsic connectivity; L, left; R, right; A1, primary auditory cortex; STG, superior temporal gyrus; IFG, inferior frontal gyrus; IPC, inferior parietal cortex

Bayesian model comparison and Bayesian model averaging showed that people with Alzheimer's disease had increased NMDA-channel time constants of inferior parietal cortices and primary auditory cortices and decreased NMDA-channel time constants of superior temporal and inferior frontal gyri (see Figure 5.6a). Alzheimer's disease progression increased NMDA-channel time constants of primary auditory cortex and decreased NMDA-channel time constants of inferior frontal gyri (see Figure 5.6b).

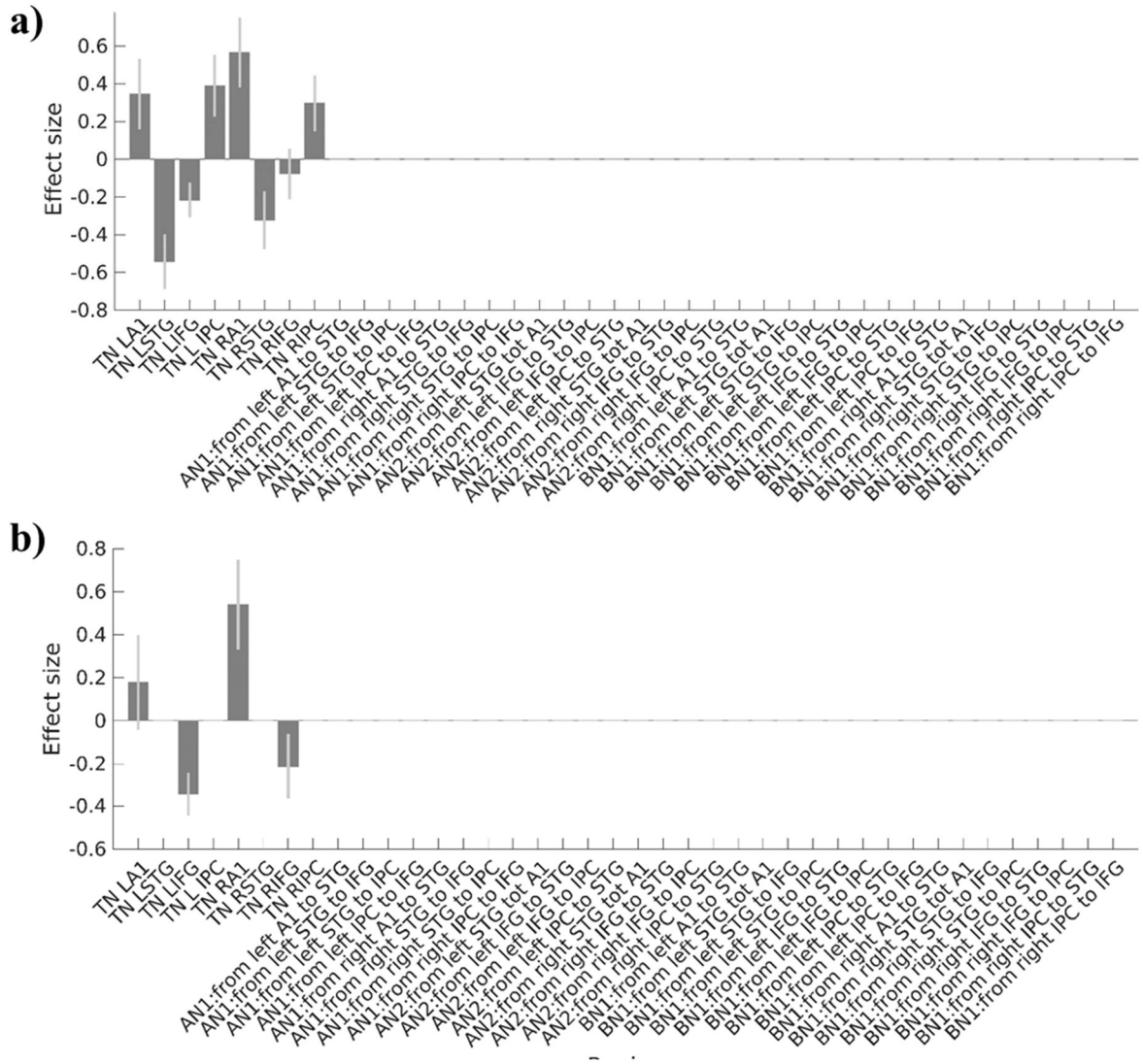


Figure 5.6 Results from the Bayesian model comparison and averaging.
Parameters are shown that differ **a)** between people with versus without Alzheimer's disease and **b)** that changed with disease progression (baseline versus 16-month follow up of people with Alzheimer's disease). TN, NMDA receptor time constant; AN1, NMDA-mediated forward extrinsic connectivity; AN2, NMDA-mediated backward extrinsic connectivity; BN1, modulatory effect of deviant tones on NMDA-mediated extrinsic connectivity; L, left; R, right; A1, primary auditory cortex; STG, superior temporal gyrus; IFG, inferior frontal gyrus; IPC, inferior parietal cortex

5.4 Discussion

The primary finding from this study is that inversion from brain imaging to generative models of human cortex reveals that people with symptomatic Alzheimer's disease have abnormal NMDA-channel time constants. There were differences in neurophysiological responses to a mismatch negativity task in people with Alzheimer's disease compared to controls and during 16 month follow up. DCMs of these MEG responses were inverted to quantify how ion-channel

receptors contribute to the neurophysiological difference. This study confirmed the hypothesis that abnormal NMDA-receptor function explains the deficit more than AMPA or GABA receptor changes. This study also confirmed that NMDA-channel time constants change with Alzheimer's disease and its progression.

The main effect of Alzheimer's disease on the mismatch negativity response is in line with previous reports (Savolainen *et al.*, 2001; Pekkonen *et al.*, 2005; Cheng *et al.*, 2012; Hsiao *et al.*, 2014; Papadaniil *et al.*, 2016; Jiang *et al.*, 2017). This study suggests that NMDA-receptor dysfunction is at least in part responsible for the attenuated responses in mismatch negativity paradigms. Indeed, Alzheimer's disease can be treated by partial NMDA-receptor antagonism by memantine, which in turn has been shown to enhances mismatch negativity responses (Koola *et al.*, 2018).

Attenuation of the mismatch negativity response by Alzheimer's disease and its progression was better explained by changes of NMDA receptor function than of AMPA or GABA receptor function. Though AMPA and GABA receptors may also be impaired in Alzheimer's disease (Chang *et al.*, 2006; Govindpani *et al.*, 2020) and play a role in temporal auditory processing (Wu *et al.*, 2004), rodent and *post mortem* studies have shown NMDA receptors are most affected (Carlson *et al.*, 1993; Lai *et al.*, 2019). *Post mortem* analysis has found that NMDA receptors are selectively-vulnerable in regions most affected by Alzheimer's disease pathology (Sze *et al.*, 2001). *Post mortem* analysis has also found that the number of NMDA receptors correlates with cognitive performance (Sze *et al.*, 2001, Xu *et al.*, 2021*a*). While AMPA receptors are also vulnerable to disease processes, their number may not directly correlate with pathology (Carlson *et al.*, 1993). These findings together support the conclusion that NMDA parameters best explain the mismatch negativity attenuation by Alzheimer's disease. While it is therefore important to focus on NMDA receptors for therapeutic interventions, the current study does not suggest there is no effect of AMPA or GABA on the neurophysiological deficit. Indeed, it may well be important for future studies to consider the interplay of these different receptor systems and how they affect excitatory-inhibitory balances. In Alzheimer's disease, impaired regulation of beta-amyloid leads to aberrant neuronal activity, including hypo- and hyper-active neurones (Busche *et al.*, 2008), and epileptiform activity illustrated through EEG of hippocampal networks of mice (Palop and Mucke, 2010). Mouse models with destabilised network activity have reduced levels of AMPA and NMDA receptors (Palop *et al.*, 2007). Alzheimer pathology, such as amyloid fibrils, may increase concentrations of glutamate leading

to overactivation of NMDA receptors. The expression of AMPA and NMDA receptors are subsequently reduced (Roselli *et al.*, 2005). Amyloid pathology has also been shown to trigger NMDA and AMPA internalisation in hippocampal neurons (Jürgensen *et al.*, 2010). Blockade of AMPA and NMDA receptors have both been shown to block effects of amyloid pathology (Louzada *et al.*, 2001). These studies illustrate the interplay of glutamatergic receptors in the pathophysiology of Alzheimer's disease. In addition to dysfunction of glutamatergic signalling, GABAergic signalling may also be affected by Alzheimer's disease (Rissman and Mobley, 2011; Paula-Lima *et al.*, 2013). Changes to glutamatergic and GABAergic signalling lead to excitatory-inhibitory imbalances which may contribute to cognitive decline (Rissman and Mobley, 2011). GABA receptors regulate NMDA receptor activity (Collingridge *et al.*, 2004) and excessive glutamate triggers GABA release (Saransaari and Oja, 1997) and increases GABA receptor levels (Rodríguez *et al.*, 2005). Given the complex interplay of these receptor systems in neuronal signalling, therapeutic combinations that target more than one system may be necessary. For example, targeting GABA and NMDA receptors together reduces excess glutamate release by amyloid pathology (Brito-Moreira *et al.*, 2011). The current study supports evidence that NMDA receptors play an important role in neurophysiological deficits caused by Alzheimer's disease; however, whether combined therapies would have maximum clinical benefit should be further explored in the future.

Previous imaging studies with dynamic causal modelling have found altered extrinsic connectivity associated with Alzheimer's disease (Penny et al., 2018; Tyrer et al., 2020, chapter 4), or with drug-mediated modulation of NMDA-receptor blockade (Moran et al., 2015; Parras et al., 2020; Shaw et al., 2020). For example, NMDA-receptor blockade increased forward connectivity (Parras et al., 2020), which may index prediction error signalling. Modulation of forward signalling of prediction errors by higher-level predictions may be mediated by NMDA receptors (Friston, 2005). The slow time constants of NMDA receptors prolong modulation of prediction errors by contextual information compared to phasic sensory information of evoked responses (Friston, 2005). Changes to NMDA receptor time constants by Alzheimer's disease, as reported here, may therefore interfere with the iterative updating of predictions by prediction error. Indeed, NMDA-receptor disruption increases interference of new with prior information impairing memory updating (Yang et al., 2023). However, this study found no conclusive evidence for altered NMDA-mediated extrinsic connectivity.

The NMDA-receptor time constant was altered in all regions for people with Alzheimer's disease compared to controls, but in different directions. Alzheimer's disease progressively increased NMDA time constants of primary auditory regions and progressively decreased NMDA time constants of inferior frontal regions. There is a complex evolution of NMDA-receptor function in the course of Alzheimer's disease. In healthy ageing, there is reduced function of NMDA receptors (Pegasiou *et al.*, 2020). Alzheimer's disease may exacerbate this ageing effect on NMDA receptor function in early disease stages (Olney *et al.*, 1997). This initial early-stage reduction in NMDA receptor function (Olney et al., 1997; Newcomer et al., 2000) is proceeded by a compensatory mild yet chronic over-activation of NMDA receptors (Hynd et al., 2004; Danysz and Parsons, 2012). At later disease stages, there are reduced levels of NMDA receptors (Ułas and Cotman, 1997). This could explain the opposing effect directions in different regions, with different degrees of pathological insult. One would expect primary auditory cortex to be relatively spared, while inferior frontal regions have increased pathology (Braak and Tredici, 2018).

Alzheimer's disease pathology affects proteins, such as protein kinase C, that decrease NMDA receptor opening times (Ortiz-Sanz *et al.*, 2022). This could explain the progressively decreasing time constants reported in the left and right inferior frontal gyri. Clinical trials are currently assessing novel treatments for Alzheimer's disease which affect protein kinase C levels or NMDA receptor activity (Cummings *et al.*, 2023). NMDA receptor function can also be facilitated by drugs which alter channel opening times (Perszyk *et al.*, 2020), though further research is needed to assess potential of such therapeutics for Alzheimer's disease treatment. This study identifies potential, mechanistically-informative biomarkers for such studies.

Until recently, effective treatments for Alzheimer's disease have been symptomatic and mainly targeted cholinergic or NMDA systems. This chapter corroborates findings that altered glutamatergic signalling underlies cognitive decline in Alzheimer's disease. Changes to the NMDA system are dynamic, with increases and decreases of NMDA receptor function at different disease stages. Evolution has had years to finesse the balance of NMDA-receptor signalling. Whether pharmaceuticals can be identified that can effectively re-establish this balance in disease is worth considering (Kemp and McKernan, 2002). Nevertheless, memantine does improve symptoms at later disease stages (Wilkinson, 2012) and clinical trials are assessing drugs that target NMDA channel activity (Cummings *et al.*, 2023). Managing the NMDA-receptor imbalance at earlier disease stages may show improvements above and

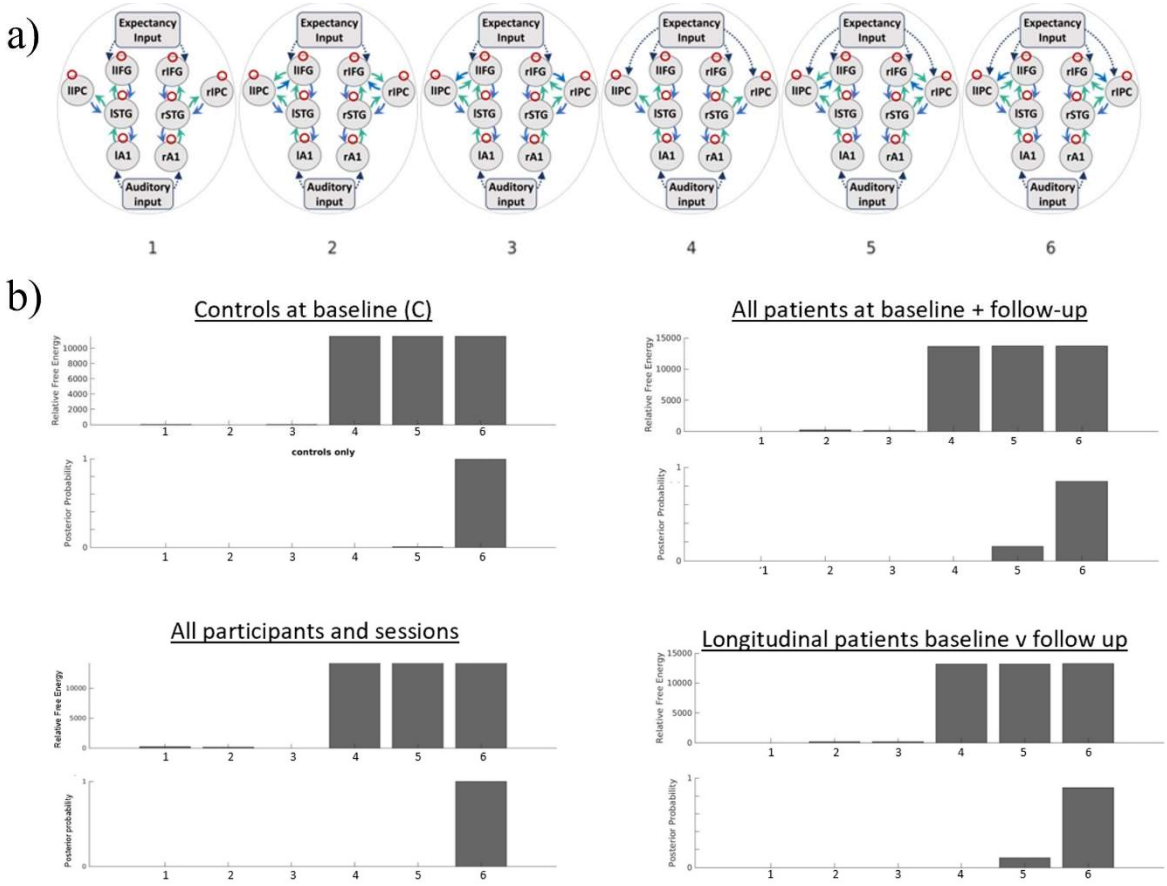
beyond those shown by memantine. Given the complex evolution of NMDA receptor dysfunction, NMDA-targeting treatments may need to be individually and progressively tailored to each stage of NMDA receptor dysfunction. Future studies can explore personalised measurement of NMDA receptor function using the methods illustrated in this paper. Once NMDA-receptor function has been established to be hyper- or hypo-functioning, an appropriate personalised treatment plan can be implemented (to either increase or decrease NMDA function, respectively). The biomarkers reported in this study may also be important for assessing suitability of participants for clinical trials of candidate NMDA receptor treatments. If the treatment reduces hyperfunction of NMDA receptors, such as memantine, dynamic causal modelling can assess whether the patient group have hyperfunctioning NMDA receptors, and vice versa. Alternatively, targeting disease processes that precede NMDA-receptor malfunction may indirectly improve the balance of NMDA-receptor function and so improve associated cognition. The neurophysiological biomarkers presented here may be more sensitive to this effect than cognitive tests.

There are several limitations to this study. First, patient participants were recruited according to clinical diagnosis of mild cognitive impairment or Alzheimer's disease. This was supported by a positive amyloid status determined by amyloid-PET imaging or cerebrospinal fluid assays, but co-morbidities cannot be excluded. Second, no model is perfect and although the anatomical and microcircuit model was based on previous work, other models may be better. The model was selected according to a series of previous work establishing the mismatch negativity network (Garrido *et al.*, 2008; Phillips *et al.*, 2015; Rosch *et al.*, 2019; Adams *et al.*, 2021). Only a couple of these studies included participants with Alzheimer's disease (Cope *et al.*, 2022; Chapter 4). There may be models better suited to assessing mismatch negativity responses in people with Alzheimer's disease. For example, the medial temporal lobe is affected early by Alzheimer's disease and may be involved in mismatch negativity responses (Billette *et al.*, 2022; Pérez-González *et al.*, 2022). The medial temporal lobe could be included as a hidden node (David *et al.*, 2011). Whether this would improve free energy of the model would need to be assessed using model space comparisons. It is important to note, however, that an exhaustive number of model architectures exist and so the model space must always be restricted. It is also important to note that no model is good enough. The human brain is complex; DCMs are extremely simple. Third, participants in the patient group took medications which could interfere with study findings (see Table 3.1). For participants with Alzheimer's

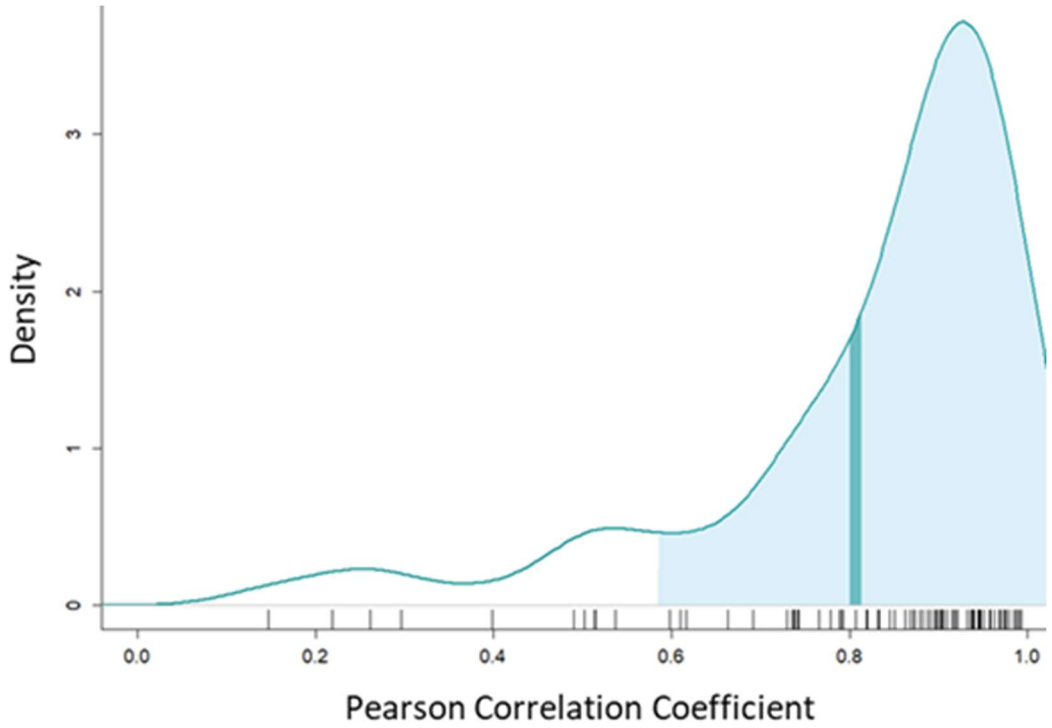
disease, 52% were taking a dementia medication. Participants were required to be on a stable dose for a minimum of 30 days prior to study participation. Nevertheless, some medications affect neurotransmitter receptors, such as memantine which blocks NMDA receptors, or cholinesterase inhibitors which may indirectly affect ion channels. For example, cholinergic modulation may affect NMDA-mediated signalling (Chen *et al.*, 2008). Consequently, dementia medications could have affected the study findings. Given the possible effect of dementia medication on ion channel properties, I repeated baseline analyses with participants taking no dementia medications only (see supplementary materials). The results were similar; however, the NMDA receptor time constants in parietal cortices were decreased rather than increased. The main findings remained: the winning PEB model included NMDA parameters (rather than GABA or AMPA parameters) and people with Alzheimer's disease had increased time constants in primary auditory cortices and decreased time constants in inferior frontal cortices (these were the only parameters to changed with disease progression). Fourth, people with mild cognitive impairment or Alzheimer's disease were significantly older than control participants. Age was consequently controlled for in the PEB analysis. Age has previously been associated with reduced NMDA receptor function (Pegasiou *et al.*, 2020). While age was controlled for in the analysis, this may contribute towards increased time constants in regions such as the primary auditory cortex less affected by Alzheimer's pathology. Finally, attrition of 29% at 16-month follow up may have affected the results, and was higher than expected due in part to the ongoing Covid pandemic and extended interval (16 months rather than 12 months). This may have biased longitudinal results towards or away from more severe disease progression. However, there were no significant differences in clinical data or demographics between people who completed follow up and who withdrew from the study (see Table 4.1).

In conclusion, this study has shown progressive changes to NMDA-channel kinetics by Alzheimer's disease. Responses to the mismatch negativity task were attenuated and this deficit was reproduced with dynamic causal modelling. While NMDA-channels may be a potential target for novel therapeutics of Alzheimer's disease, the value of this study goes further, in demonstrating the potential for detailed biophysical models to support experimental medicine studies and early-phase trials.

Appendix B: Supplementary materials for Chapter 5



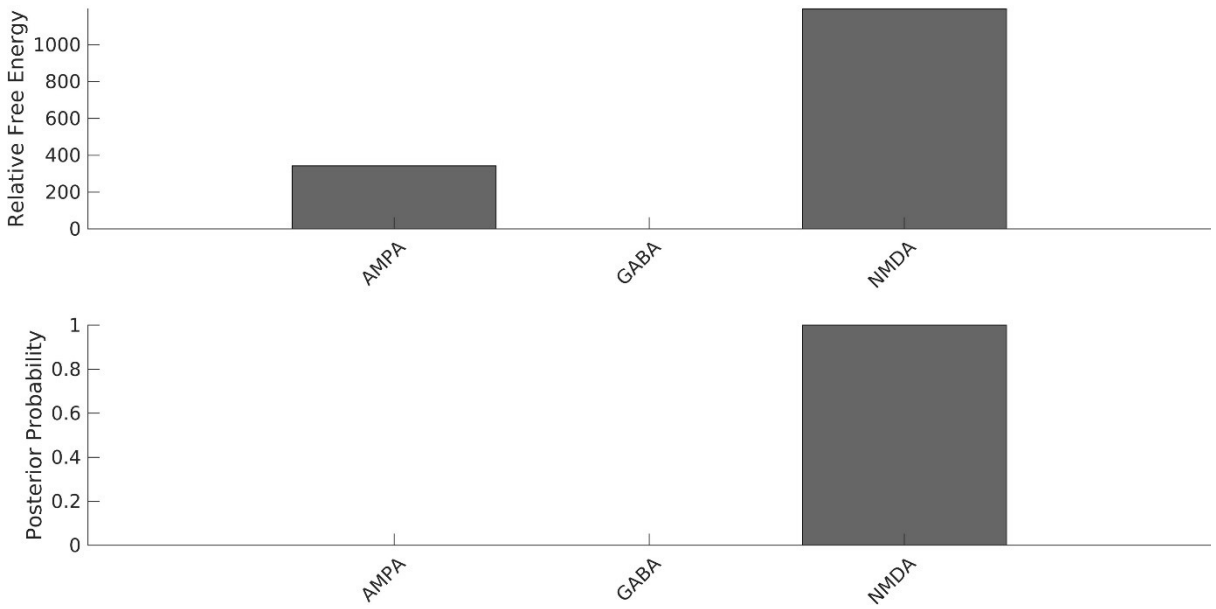
Supplementary Figure B.1 Defining the model structure.
a) Model space, with different model architectures defined in models 1-6. Model 6 is used for the PEB analyses in this study. **b)** Relative average free energies of models for participants are shown. Red, intrinsic connections; green, forward connections; blue, backward connections; l, left; r, right; A1, primary auditory cortex; STG, superior temporal gyrus; IPC, inferior parietal cortex; IFG, inferior frontal gyrus.



Supplementary Figure B.2 Kernel density distribution and rug plot of correlation coefficients for observed and predicted evoked responses.
The Pearson's correlation coefficient of the predicted and observed evoked responses were calculated for each participant and each session. The kernel density distribution and rug plot of correlation coefficients are shown. The observed and model-generated evoked responses were highly correlated (mean Pearson's correlation = 0.81 ± 0.22).

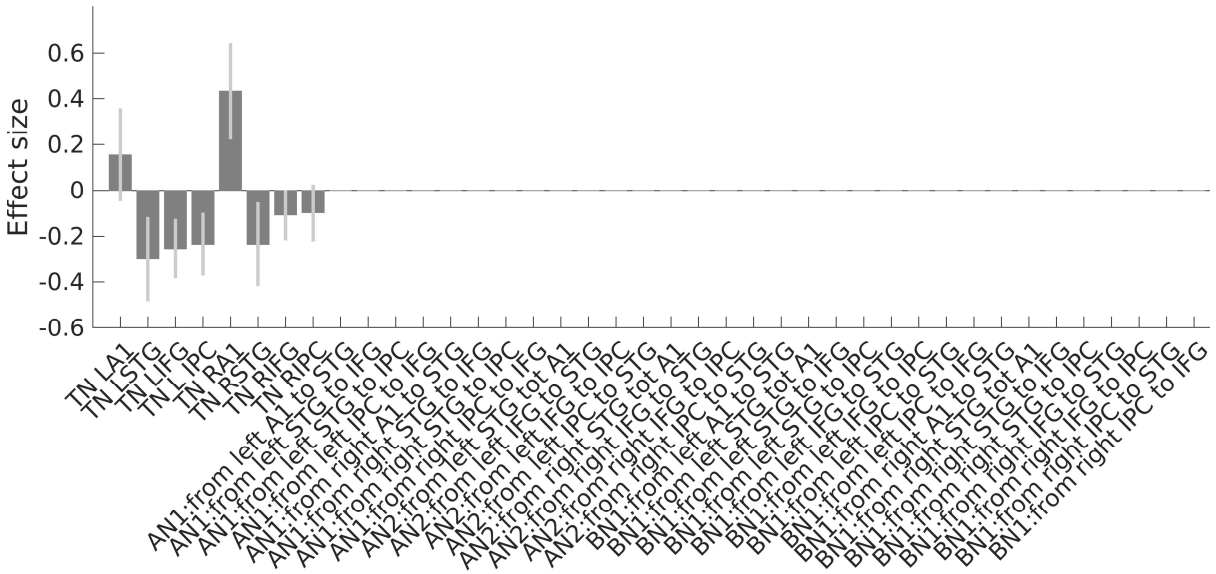
Repeating PEB analyses with participants taking no dementia medication

To assess the effect of Alzheimer's disease on receptor parameters without possible interference from dementia medications, I repeated the PEB analyses including only people taking no dementia medications. Of the 44 patients with successfully inverted baseline DCMs (one patient's DCM failed to invert), 22 were taking no dementia medication and included in the supplementary analysis. The PEB pipeline was repeated with these participants (see methodology section 5.2.6) giving the following results.



Supplementary Figure B.3 Relative free energy of PEB models with AMPA, GABA or NMDA parameters with patients versus controls taking no dementia medication

The AMPA model included AMPA time constants, AMPA-mediated extrinsic connections and AMPA-mediated modulatory extrinsic connectivity (T(:,1), A, and B parameters, respectively). The GABA model included GABA time constants (T(:,2) parameters). The NMDA model included NMDA time constants, NMDA-mediated extrinsic connections and NMDA-mediated modulatory extrinsic connections (T(:,3), AN, and BN parameters, respectively).



Supplementary Figure B.4 Results from the Bayesian model comparison and averaging with patients versus controls taking no dementia medication.

Parameters are shown that differ between people with versus without Alzheimer's disease who were on no dementia medication. TN, NMDA receptor time constant; AN1, NMDA-mediated forward extrinsic connectivity; AN2, NMDA-mediated backward extrinsic connectivity; BN1, modulatory effect of deviant tones on NMDA-mediated extrinsic connectivity; L, left; R, right; A1, primary auditory cortex; STG, superior temporal gyrus; IFG, inferior frontal gyrus; IPC, inferior parietal cortex

The results for people taking no dementia medication were similar for the main group comparison. The PEB model with NMDA parameters had the greatest Free energy and was therefore the best model for explaining differences in the neurophysiological deficit between groups. Time constants were increased in the left auditory cortex, and decreased in all other regions. The time constant of the parietal cortex was in the opposite direction to the whole group analysis. However, the time constants of other regions were affected in the same direction as the main analysis. The primary auditory cortex and inferior frontal cortex (which were the only regions affected longitudinally, and therefore the best candidates as potential biomarkers) were affected in the same direction as the main group analysis. The increased time constant in primary auditory regions and decreased time constant of inferior frontal regions may reflect the different levels of pathology in these regions. The primary auditory cortex would be expected to be relatively spared in early Alzheimer's disease.

6 | Memantine and Alzheimer's disease effects on NMDA-receptor blockade: non-invasive *in vivo* insights from magnetoencephalography

A manuscript related to this chapter is currently in preparation as:

Lanskey, J. H., Jafarian, A., Hughes, L., Karadag, M., Kocagoncu, E., Rouse, M., Adams, N., Naessens, M., Singh, K. D., Henson, R. N., Rowe, J. B., (2024) Memantine and Alzheimer's disease effects on NMDA-receptor blockade: non-invasive *in vivo* insights from magnetoencephalography

The code used is available at: https://github.com/jlansk/NMDA_blockade

Abstract: To accelerate new treatments for Alzheimer's disease, there is the need for human pathophysiological biomarkers that are sensitive to treatment and disease mechanisms. In this chapter, I assess biophysical models of non-invasive human MEG imaging to test the pharmacological and disease modulation of NMDA-receptor inhibition. MEG was recorded during mismatch negativity paradigms from (1) neurologically-healthy people on memantine/placebo (n=19); (2) people with Alzheimer's disease at baseline and 16-months (n=42, amyloid-biomarker positive). Optimised dynamic causal models inferred voltage-dependent NMDA-receptor blockade from the MEG data, using Parametric empirical Bayes to test group effects. The mismatch negativity amplitude was attenuated when Alzheimer's disease was more severe (lower mini-mental state examination scores) and after follow up (follow up versus baseline). Alzheimer's disease reduced NMDA-receptor inhibition in proportion to severity and over time. Memantine increased NMDA-receptor inhibition, compared to placebo. In line with preclinical studies, this study confirms in humans that memantine and Alzheimer's disease have opposing effects on NMDA-receptor inhibition. The ability to infer such receptor dynamics and pharmacology from non-invasive physiological recordings has wide applications, including to assess novel drugs of interest, whether candidate symptomatic or disease-modifying treatments.

6.1 Introduction

Early in the pathogenesis of Alzheimer's disease, there is impairment and loss of synapses (Tzioras *et al.*, 2022). Synaptic density is closely related to cognitive impairment (Terry *et al.*, 1991), and the maintenance and restoration of synaptic health is an area of therapeutic interest. Voltage-dependent NMDA type glutamatergic receptors are critical to synaptic function and implicated in the pathogenesis of Alzheimer's disease. NMDA-receptors are subject to voltage-dependent blockade by magnesium ions (Lau and Zukin, 2007). The magnesium inhibition of NMDA-receptors is reduced in Alzheimer's disease, with reduced magnesium occupation of the NMDA-receptor channel pore even at low levels of depolarisation (Parsons *et al.*, 2007; Liu *et al.*, 2019). This leads to over-activation of NMDA receptors, with excess calcium influx disruptive to cognition (Danysz and Parsons, 2003). Since 2004, the drug memantine has been licenced to treat moderate to severe Alzheimer's disease (Wilkinson, 2012; Folch *et al.*, 2018). Memantine's principal mode of action is to block NMDA-receptor channels when they are pathologically open at low-levels of depolarisation, without affecting the neurotransmission when the post-synaptic membrane is sufficiently depolarised (Parsons *et al.*, 2007).

NMDA-channel kinetics (Iacobucci and Popescu, 2017) and the impact of Alzheimer's disease on the voltage dependency of NMDA receptors (Danysz and Parsons, 2012) have been studied extensively in tissue cultures (Song *et al.*, 2018), animal studies (Rozumna *et al.*, 2023) and *post mortem* data (Palmer and Gershon, 1990; Gilling *et al.*, 2009; Mazzo *et al.*, 2016). This provides a test case for the development of biophysical models suitable for use in early phase trials for people with, or at risk of, Alzheimer's disease. In particular, a technique called dynamic causal modelling can be exploited to reveal disease effects and therapeutic mechanisms non-invasively in humans to the level of cell-classes and neurotransmitters (Friston *et al.*, 2019; Rosch *et al.*, 2019; Shaw *et al.*, 2019; Adams *et al.*, 2023). Dynamic causal modelling identifies cellular mechanisms underlying neurophysiological responses, such as magneto- and encephalographic observations (Garrido *et al.*, 2009*a*; Bastos *et al.*, 2012). The generation of evoked responses in response, to say, unexpected stimuli, relies on an intact NMDA transmission within and between nodes in neural information processing hierarchies (Wacongne *et al.*, 2012). This effect is dose-dependently blocked by NMDA-receptor pore blockers (Tikhonravov *et al.*, 2008).

In Alzheimer's disease, it is proposed that increased intracellular calcium at rest (due to NMDA receptor dysfunction) (Mazzo *et al.*, 2016) increases background calcium ion 'noise', leading to impaired synaptic signal detection (Danysz and Parsons, 2012). Indeed, the evoked mismatch negativity response amplitude is reduced in Alzheimer's disease (Lanskey *et al.*, 2024). This creates the opportunity to model *in vivo* the generators of evoked responses, and validate the dynamic causal modelling approach. Specifically, one can establish predictive validity of the models, via the effects of Alzheimer's disease on cortical generators and the effects of drugs, like memantine, that act on NMDA-receptors.

In this chapter, I therefore examined the effect of memantine and the effect of Alzheimer's disease on the DCM parameters representing NMDA-receptor blockade. I compare changes in NMDA-receptor dynamics related to drug in healthy controls, and cognition and disease progression in people with symptomatic Alzheimer's disease (beta-amyloid positive, with amnestic mild cognitive impairment or early dementia). In doing so, this study confirms sensitivity of MEG and dynamic causal modelling to both the severity and progression of Alzheimer's disease. Data from two separate studies were used: (1) a randomised placebo-controlled double-blinded crossover study of memantine in healthy controls; and (2) a longitudinal study of people with Alzheimer's disease. The following hypotheses were tested: 1a) the mechanism of action of memantine is blockade of NMDA-receptors; 1b) memantine increases the blockade of NMDA channels; 2a) the mismatch negativity amplitude is reduced in Alzheimer's disease, more so with disease severity and progression; 2b) NMDA blockade inferred from dynamic causal models (DCMs) is lower in people with more severe Alzheimer's disease (e.g. lower MMSE) and 2c) progression of Alzheimer's disease reduces the inferred blockade of NMDA channels (baseline versus follow up).

6.2 Methods

The study has two principal parts. The first part is a randomised, placebo-controlled double-blind crossover study with healthy controls (Perry *et al.*, 2022). The second part is a longitudinal study of people with Alzheimer's disease, including its prodromal state of mild cognitive impairment (Lanskey *et al.*, 2022).

6.2.1 Participants

For the placebo-memantine crossover study (Perry *et al.*, 2022), nineteen neurologically healthy people completed two MEG sessions, two weeks apart where they received either (1) placebo or (2) 10mg oral memantine. The MEG scan was completed three hours after drug administration, in line with estimated peak concentration. See Table 6.1.

Sex (Male:Female)	**Handedness (Right:Left:Both)**	**Age (yrs)***	**Education (yrs)**	**Baseline MMSE***
14:5	1:0:0	67.1 (±7.29)	15.5 (±3.27)	29.6 (±0.50)

Table 6.1 Memantine-placebo control participant demographics.
Yrs, years; MMSE, Mini-Mental State Examination

From the New Therapeutics in Alzheimer's disease study (Lanskey *et al.*, 2022), MRI, MEG and cognitive data were included from people with amyloid-positive mild cognitive impairment or Alzheimer's disease dementia, who completed the mismatch negativity MEG scan at baseline (n=50). Two people were excluded who did not complete the mismatch negativity task because the earphones did not fit comfortably, two people whose diagnosis was revised during follow up and one person due to data recording technical issues. Three people with Alzheimer's disease were taking memantine and excluded from the study (final n=42). MRI, MEG and cognitive data were also included from 30 people with mild cognitive impairment or Alzheimer's disease who completed a follow-up scan at an average of 16 months after the baseline MEG scan.

Sex (M:F)	**Handedness (R:L:B)**	**Age (yrs)***	**Education (yrs)**	**Baseline MMSE***	**Baseline PET (SUVR)**	**Baseline CSF (tau/A-beta 1-42)**
23:24	41:4:1	73.3 (±7.36)	14.2 (±3.82)	24.9 (±3.5)	1.66 (± 0.19)	2.14 (±1.27)

Table 6.2 NTAD patient participant demographics.
M, male; F, female; R, right; L, left; B, ambidextrous; MMSE, mini-mental state examination; PET, positron emission tomography; SUVR, standardized uptake value ratio; CSF, cerebrospinal fluid; Yrs, years; MMSE, Mini-Mental State Examination

6.2.2 Data collection

For the memantine-placebo study (Perry *et al.*, 2022), magnetoencephalography (MEG) data were recorded three hours after drug or placebo administration while participants listened passively to a 3x5 minute roving mismatch negativity paradigm. Tones repeated at frequencies of 400 to 800Hz with 75ms duration at 500ms intervals. After 3 to 10 repetitions, the tone frequency changed pseudorandomly (with an approximate Poisson distribution). MEG was recorded with the Elekta VectorView system, configured with 204 planar gradiometers and 102 magnetometers at 102 locations. Eye movements and head position were measured with vertical and horizontal electrooculography and 5 head position indicator coils, respectively. Nasion and pre-auricular fiducial points were measured with a 3D digitizer (Fastrak Polhemus Inc., Colchester, VA), with over 60 additional scalp surface points.

For the NTAD study (Lanskey *et al.*, 2022), MEG data were recorded while participants listened passively to a 2x5 minute roving mismatch negativity paradigm. Tones repeated at frequencies of 400 to 800Hz varying in 50Hz steps with 75ms duration at 500ms intervals. After 3 to 10 repetitions, the tone frequency changed. MEG was recorded with the Elekta VectorView system and MEGIN Triux Neo scanner, with 204 planar gradiometers and 102 magnetometers at 102 locations. Electrocardiogram data was recorded with 2 electrodes on the right clavicle and left, lower rib; electrooculography data with an electrode below and above the left eye and on bilateral canthi; and head position with five head position indicator coils, standard fiducial points and over 500 additional scalp surface points with a 3D digitizer (Fastrak Polhemus Inc., Colchester, VA).

T1-weighted MRI was recorded from each participant with a 3T Siemens PRISMA scanner using a magnetisation prepared rapid gradient echo (MPRAGE) sequence.

6.2.3 Preprocessing

Preprocessing of data from both studies followed the same pipeline as previously reported (Chapter 4). In brief, MaxFilter v2.2 software was used. Independent component analysis of data using the EEGLAB toolbox was performed (Delorme and Makeig, 2004). Data were then bandpass filtered between 0.01Hz and 40Hz and epoched from -100ms to 500ms. OSL's artefact rejection algorithm removed residual bad trials and channels. Robust averaging averaged epochs for trials, with conditions separately weighted. A final low-pass filter corrected for potential high frequencies introduced during robust averaging.

6.2.4 Sensor level analysis

For each participant with mild cognitive impairment or Alzheimer's disease from the included NTAD participants, data from combined planar gradiometers to the repeated tones (tones 2 to 11) were subtracted from the first (deviant) tone, giving mismatch negativity waveforms for each participant for each session (baseline and follow-up recordings). Based on prior studies of the MMN, the average amplitudes between 140 to 160ms was calculated for each waveform (Moran *et al.*, 2013; Chapter 4; Chapter 5), for each participant, at each session. Two participants were excluded from further sensor level analyses as their mean mismatch negativity amplitudes were three scaled median absolute deviations from the median at both baseline and follow-up sessions (The MathWorks Inc, 2023). One outlier had a low MMSE of 18, the second outlier had a high MMSE of 27 and both outliers had low mismatch negativity amplitudes. Supplementary data include plots showing these outliers' mismatch negativity amplitudes. The average amplitude across waveforms was calculated for each participant.

A two-sample t-test was used to assess change in average amplitude between baseline and follow-up MEG scans. A linear regression was fitted to the average amplitude and baseline MMSE scores.

6.2.5 First-level dynamic causal modelling

A variant of the conductance-based canonical microcircuit model was developed (cmm_NMDA in SPM12 version 7771). The standard cmm_NMDA model has spiny stellate, superficial pyramidal, inhibitory interneurons, and deep pyramidal cells in three layers of the cortical column as shown in Figure 6.2a. The dynamics of each neuronal population are governed by a Morris–Lecar model, which can be thought of as a reduction of the Hodgkin and Huxley's squid axon model (Moran *et al.*, 2011a) as follows:

$$\frac{dV}{dt} = \frac{1}{C}[g_L(V_L - V) + g_{AMPA}(V_{AMPA} - V) + g_{GABA}(V_{GABA} - V) + g_{NMDA}\, m(V)(V_{NMDA} - V)] + u,$$

$$\frac{dg_*}{dt} = \frac{1}{\tau_*}\left(\sum_{k=sp,inh,dp,ss} S_k\, \sigma_k - g_*\right) + u, \quad *= [L_c, AMPA, GABA, NMDA] \qquad (1)$$

In Equation 1, V is the membrane potential; $g_*(L, NMDA, AMPA, GABA)$, the conductance of ion channels; u, thalamic input given by a hump shape function; C is the membrane

capacitance; L_c is a passive leak current, τ_* are time constants for the ion channels, V_* are the reversal equilibrium potential of the ion channels. σ_k is the afferent presynaptic firings from a population k, which is scaled by S_k, intrinsic and extrinsic connectivity.

Each region can interact with distal regions via forward connections (from superficial pyramidal cells to spiny stellate and deep pyramidal cells) and backward connections (from deep pyramidal cells to superficial pyramidal and inhibitory interneurones).

NMDA channels are both ligand-gated and voltage-gated, requiring both the binding of glutamate and removal of the magnesium blockade by a large transmembrane potential to open. The removal of the magnesium blockade is given by the function:

$$m(V) = \frac{1.5}{1 + 0.33\ exp\ (-0.06V)} \quad (2)$$

The model was adapted by including a parameter for NMDA channel blockade (blk_{NMDA}) able to vary during model inversion as follows:

$$\alpha_{NMDA} = \exp\ (blk_{nmda})$$

$$m(V) = \frac{1.50265}{1 + 0.33 \exp\ (-0.06\alpha_{NMDA}V)} \quad (3)$$

There is a single NMDA channel block parameter for each region in the model representing the blockade of all NMDA channels in the region.

Left and right inferior parietal cortices from the mismatch negativity network are included (Lappe *et al.*, 2013; Cope *et al.*, 2022; Chapter 4; Chapter 5). These are part of a wider network with sources including primary auditory, superior temporal, inferior frontal and inferior parietal regions (Garrido *et al.*, 2009*b*). However, given the complexity of the neuronal models and their estimation, only the inferior parietal cortex is considered, given its importance in Alzheimer's disease (Jacobs *et al.*, 2012; Talwar *et al.*, 2021) and mismatch negativity generation (Lappe *et al.*, 2013; Cope *et al.*, 2022). This reduces the complexity of the model inversion (Garrido *et al.*, 2009*a*) and offers a more parsimonious network for investigating NMDA blockade dysfunction. Each of the two regions receive thalamic input and have self-connections that are altered by repetition (deviant versus repetition 5) (Tyrer *et al.*, 2020).

There is no lateral connection between the parietal cortices. This minimal network allows analyses to investigate the dysfunctions of NMDA channel blockade in Alzheimer's disease.

The model was inverted from evoked responses to the first and sixth tones (deviant and repetition 5) from the mismatch negativity task for each participant at each session. The sensor data were reduced to eight spatial modes from 0ms to 300ms post-stimulus onset and a Hanning window applied. Source activity was approximated during DCM fitting as equivalent current dipoles with symmetry constraints. This method has previously been applied to a simplified (reduced number of sources) DCM network to generate MMN responses (Garrido *et al.*, 2009*a*). Subject-specific T1-weighted images informed the lead field. The model is fitted by iterative updating parameters to improve the fit of the model's generated response to the observed response, with a trade-off of complexity and accuracy until the parameters maximise free energy (Friston *et al.*, 2019). This furnishes a unique set of model parameters for each participant at each session that can be compared with second-level analyses.

6.2.6 Second-level analysis

A hierarchical regression model, namely Parametric empirical Bayes (PEB), was used that takes both posterior parameter estimates and covariances of parameters to the second level (Zeidman *et al.*, 2019). At the first level of the PEB, DCMs explain how neural activity causes individual evoked responses with all parameters fixed apart from the parameters of interest (see below). The parameters of interest are modelled at the second level with a general linear model. The second level uses a hierarchical variational Bayesian inversion that constrains posterior parameter estimates by the user-specified regressors to improve model evidence. Hypotheses can be tested by comparing the free energy of PEB models with different combinations of parameters explaining the second-level effect.

Second-level analysis for memantine versus placebo in control participants

Second-level group PEB analyses were performed with different sets of parameters to test biological hypotheses about the effect of memantine. These parameter sets were: 1) GABA time constants, 2) AMPA time constants, 3) NMDA time constants, 4) NMDA channel blockade and 5) intrinsic connectivity. Separate models were run in which only one of these parameter sets was free to vary, plus a sixth model 6) in which they were all allowed to vary. Each PEB included a constant term and a regressor capturing group (memantine versus placebo). The free

energies of the PEB models were converted to posterior probabilities with the softmax function to identify the likely PEB model whose parameters best explained the effect of memantine.

Second-level analysis of NMDA channel blockade in Alzheimer's disease

To explore the pathological effect of Alzheimer's disease, second level PEB analyses were tested with the winning NMDA channel blockade parameters in the Alzheimer's disease group. A PEB model was tested in which the mean-centred MMSE values were added as a regressor (along with the constant term). The PEB posterior estimate of the expected value of NMDA channel blockade parameters that differed from 0 with a posterior probability >0.95 were extracted for each person with Alzheimer's disease and plotted against their MMSE score.

Finally, a longitudinal PEB analysis was also performed on DCMs from people with Alzheimer's disease, to assess how NMDA channel blockade changes with disease progression, with constant and session (baseline versus follow up) as regressors. A third regressor specified the time in years between the baseline and follow-up scans for each patient (0 for baseline scans and with scores from 0.8 to 2.2 for follow-up scans mean-centred and standardised). PEB posterior estimates of the NMDA blockade parameter that differed from 0 with a posterior probability >0.95 were extracted and plotted against session.

6.3 Results

6.3.1 Mismatch negativity effects of memantine and Alzheimer's disease

Mismatch negativity waveforms were calculated as the difference between responses to deviant and repeated tones. T-tests assessed differences in the average mismatch negativity amplitude over the a priori interval 140 to 160ms (Moran *et al.*, 2013). Memantine, compared to placebo, did not significantly alter the mismatch negativity response (Figure 6.1a). For participants with Alzheimer's disease from the NTAD study, the mismatch negativity was significantly reduced, compared to controls ($t = -2.56$, $p = 0.007$, see supplementary materials). The mismatch negativity response was further reduced over time in people with Alzheimer's disease (baseline *versus* 16-month follow up, $t=2.92$, $p=-.003$, Figure 6.1b) with a medium effect size ($d = 0.60$). For participants with Alzheimer's disease, the MMN amplitude correlated with MMSE: people with lower MMSE (and hence likely to have more severe Alzheimer's disease) had a smaller mismatch negativity response ($r = -0.4$, $p=.01$, Figure 6.1c).

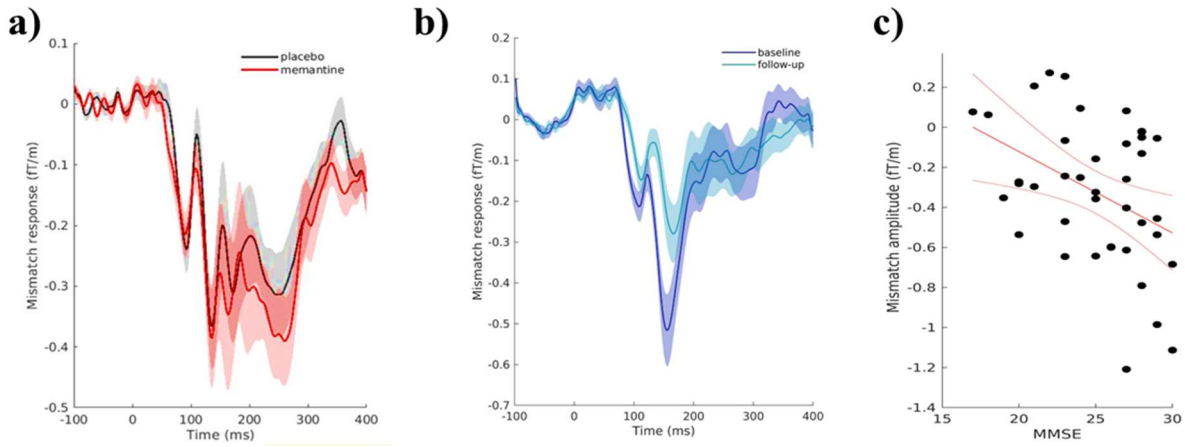


Figure 6.1 Mismatch negativity responses.
a) The mismatch negativity waveform on memantine or placebo in control participants from the memantine-placebo study. There was no significant difference between sessions. **b)** The mismatch negativity waveform for people with Alzheimer's disease from the NTAD study at baseline or follow up. The amplitude was significantly reduced by Alzheimer's disease progression (baseline versus follow up for people with Alzheimer's disease from the NTAD study, t=-2.92, p=.003). **c)** The mismatch negativity amplitude was significantly correlated with MMSE for people with Alzheimer's disease.

6.3.2 The generative model of the mismatch negativity response

Dynamic causal modelling is a standard translational modelling approach which uses variational Bayesian inference to infer synaptic physiology and model evidence from neuroimaging data. Here, a conductance-based canonical microcircuit DCM was modified to allow inference of subject-specific NMDA channel blockade from evoked MEG responses (Figure 2a, see methods section for full details). In brief, the prior distribution of the NMDA channel blockade parameter (blk_{NMDA}) was defined as a normal distribution $blk_{nmda} \sim N(m, \sigma)$, with prior mean of $\text{m} = 0$ and variance of $\sigma = \frac{1}{64}$ (in line with the default variance of other channel time constants in such models). The NMDA blockade parameter is exponentially transformed to assure positivity constraints:

$$\alpha_{NMDA} = \exp\left(blk_{NMDA}\right)$$

The α_{nmda} parameter is scaled by its default physiological value (i.e., -0.06) and modulates the membrane potential V (Figure 2b) through a sigmoid transformation (Moran *et al.*, 2011*b*):

$$m(V) = \frac{1.50265}{1 + 0.33\exp\left(-0.06\alpha_{NMDA}V\right)}$$

A consequence of this model is that the higher the NMDA blockade parameter, the less conductance is mediated by the NMDA channel (Figure 6.2c).

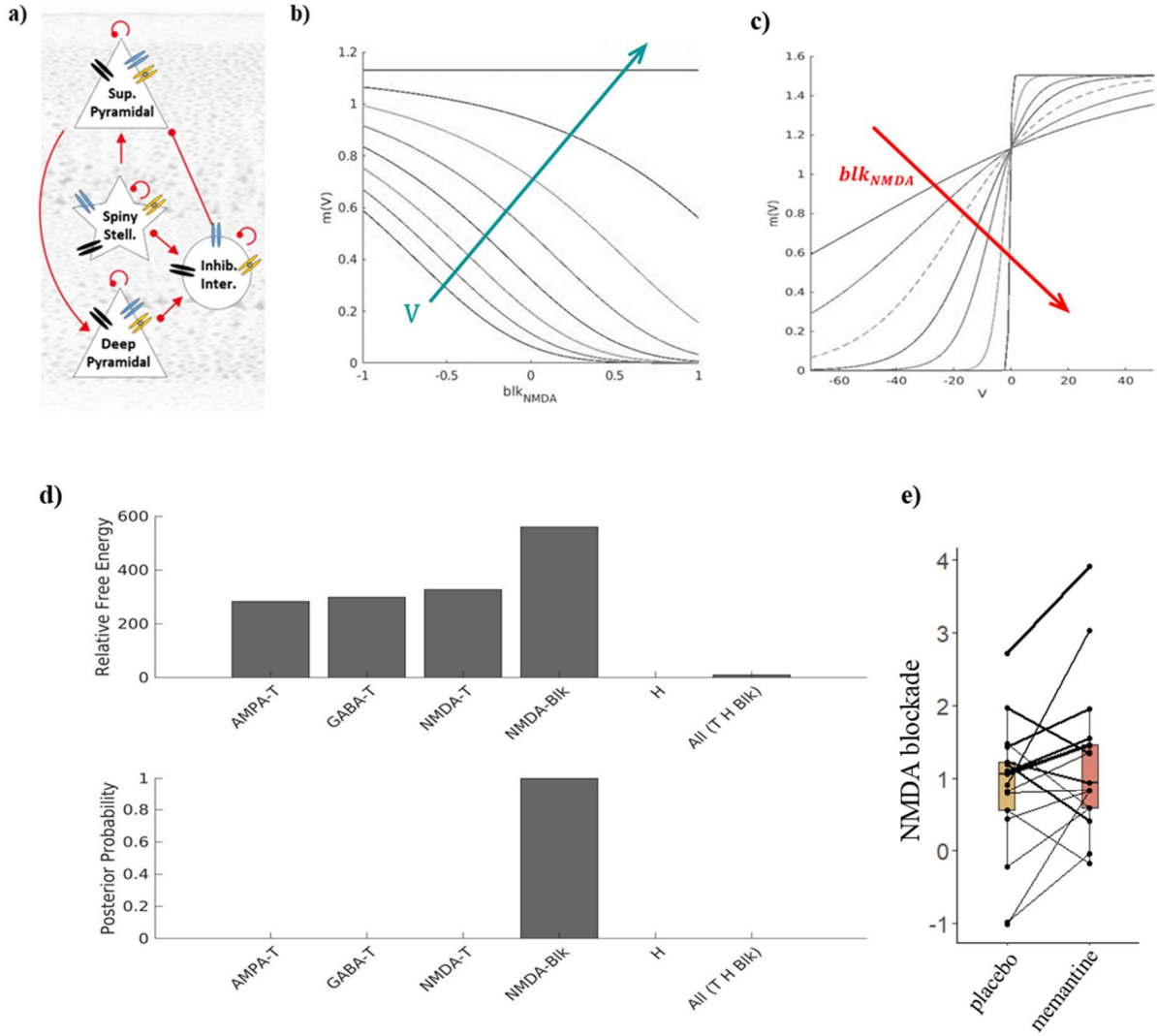


Figure 6.2 The generative canonical microcircuit conductance model with NMDA channel blockade parameters and the mechanism of memantine.

a) The connectivity between cell populations within each region of the model. The NMDA switch function (Equation (3) plotted **b)** against the NMDA blockade parameter shown for increasing voltage values (from -70V to 0V in 10V steps) and **c)** against voltage shown for increasing values of the exponential of the NMDA blockade parameter $\boldsymbol{blk_{NMDA}}$ (-1, -0.5, 0, 0.5, 1, 2 and 4). The dashed line shows the NMDA switch function with the blockade parameter value set at the default value from the original model (Moran *et al.*, 2011*a*). As the blockade parameter increases, the magnesium switch function output, which scales NMDA channel conductance, reduces. **d)** Free energy and posterior probabilities of PEB models explaining the effect of memantine versus placebo. The PEB analysis with the NMDA channel blockade parameters had the highest posterior probability for explaining differences between neurophysiological MMN responses on placebo versus drug; memantine acts primarily on the NMDA blockade parameter. **e)** Memantine increases the NMDA channel blockade parameter with a posterior probability >95% in the left parietal cortex. Lines are weighted by each subject's average precision of NMDA blockade over sessions. Sup., superficial; stell., stellate; inter., interneuron; m(V), the switch function output; blk_{NMDA}, the NMDA blockade parameter; V, voltage; AMPA-T, AMPA channel time constant; GABA-T, GABA channel time constant; NMDA-T; NMDA channel time constant; NMDA-Blk, NMDA channel blockade; H, intrinsic connection strengths.

6.3.3 Increased blockade of NMDA channels explains the memantine effect

Previous application of DCM to the MMN has used a bilateral network of brain regions, including auditory, superior temporal, inferior frontal and parietal cortices (Chapter 4 and Chapter 5). This study focusses on just parietal cortex, given its involvement in Alzheimer's disease, to reduce model complexity (Garrido *et al.*, 2009*a*). The model was fit first to the control participants from the memantine-placebo study. Parametric Empirical Bayes (PEB) was used to compare 6 models, in which memantine affected the NMDA channel blockade parameter (blk_{NMDA}), or the AMPA, GABA or NMDA time constants, or the intrinsic connectivity parameters, or a sixth model in which it affected all of these. The posterior probability was highest for the blk_{NMDA} model (indeed, close to 1), demonstrating that the effect of memantine was most parsimoniously explained by changes in NMDA channel blockade (Figure 6.2d). Memantine increased NMDA channel blockade with a meaningful effect (probability of parameter >95%) in the left parietal cortex (posterior estimate = 0.41, posterior probability, Pp, =1, Figure 6.2e).

6.3.4 Effect of severity and progression of Alzheimer's disease

For the Alzheimer's disease group, PEB analyses were conducted to identify (1) the effect of disease severity (MMSE score) on NMDA channel blockade and (2) the effect of disease progression on NMDA channel blockade (baseline versus follow up). NMDA channel blockade was reduced with more severe Alzheimer's disease (a lower MMSE score) with a meaningful effect (probability of parameter > 95%) in right parietal cortex (posterior estimate = 0.06, posterior probability = 0.99). The NMDA channel blockade further reduced at follow up compared to baseline in the right parietal cortex (posterior estimate = -0.125, posterior probability, Pp=0.97).

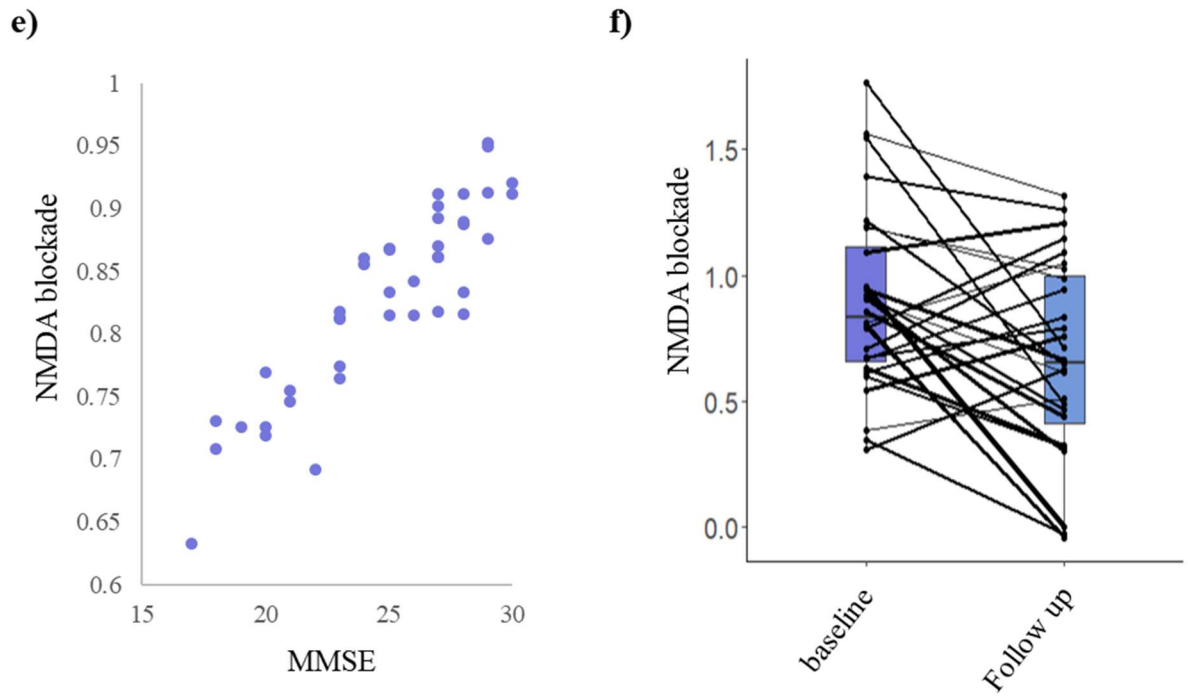


Figure 6.3 NMDA channel blockade is affected by Alzheimer's disease in right parietal cortex. The PEB posterior estimate of the expected value of the NMDA channel blockade parameter for each person with Alzheimer's disease are shown. NMDA channel blockade a) correlates with MMSE (posterior estimate = 0.06, posterior probability = 0.99) and b) reduces further at follow up compared to baseline (posterior estimate = -0.125, posterior probability = 0.97). Lines are weighted by each subject's average precision of NMDA blockade over sessions.

6.4 Discussion

There are three principle results of this study. First, by inversion of a biophysically informed generative model from MEG data, this study confirmed that memantine increases the NMDA blockade parameter, while Alzheimer's disease severity and progression reduce the blockade. The effect of drug and disease on NMDA receptor blockade is not in itself novel; however, this mechanistic inference arises from human, non-invasive brain imaging. As the NMDA blockade parameter increases, conductance through NMDA channels becomes increasingly non-linear, requiring more depolarisation for channel conductance, and this can explain why the mismatch negativity amplitude attenuates with disease severity and with disease progression over 16 months. Thus, this study has shown that this approach to non-invasive neurophysiological data acquired *in vivo* is feasible as a foundation to experimental medicine studies in people with Alzheimer's disease.

To set these disease-specific results in context, clinical trials have lower costs and attrition when target validation is more effective (Paul *et al.*, 2010). Experimental medicines studies can be used to demonstrate pharmacological target engagement and target relevance to a disorder (Emmerich *et al.*, 2020). Target engagement for organs other than the brain can be measured directly, but the blood-brain barrier, skull enclosure, and lack of regenerative capacity make direct brain assays unrealistic. Neurochemical imaging by positron emission tomography and single photon emission computerised tomography with selective tracers are possible for some targets, e.g. for the measurement of dopamine receptor occupancy by dopamine agonists (Deutschländer *et al.*, 2016), but there are relatively few tracer targets, and the spatial resolution is poor. An alternative approach using biophysically informed DCMs has been used to study mechanisms of action of ketamine (Gilbert *et al.*, 2021), galantamine (Moran *et al.*, 2013; Schöbi *et al.*, 2021) and tiagabine (Adams *et al.*, 2020), as well as natural experiments afforded by anti-NMDA antibody mediate encephalitis and inherited channelopathies (Gilbert *et al.*, 2016; Symmonds *et al.*, 2018).

This study confirmed that memantine increases the blockade of NMDA channels. The original direct assays of memantine's blockade of NMDA receptors included patch-clamp recordings (Bormann, 1989) and *post mortem* tissue (Kornhuber *et al.*, 1989). Rodent models with PET imaging confirmed NMDA receptor blockade by a memantine derivative (Ametamey *et al.*, 1999). *In silico* studies suggested that memantine may have a neuroprotective effect on Alzheimer's disease (Świetlik *et al.*, 2022), even if current licenced applications are symptomatic rather than disease modifying in intention. Nonetheless, chronic *in vivo* clinical use of memantine by people with Alzheimer's disease increases cortical metabolism in temporal and parietal regions (Sultzer *et al.*, 2010) along with clinical benefit (Wilkinson, 2012). This study was not designed or powered to show clinical efficacy; rather its aim was to confirm the mechanism of action, as proof of concept for the dynamic causal modelling methodology.

Age has previously been associated with reduced NMDA receptor function (Pegasiou *et al.*, 2020). Here, age was indeed found to increase the block of NMDA receptors (i.e. reduced NMDA receptor function, see supplementary materials). This reduced NMDA receptor function with advancing age may be exacerbated in Alzheimer's disease (Olney *et al.*, 1997). Indeed, compared to control participants, people with Alzheimer's disease had increased functional NMDA receptor blockade (i.e. reduced NMDA receptor function, see supplementary

analysis). This is consistent with previous findings (Dong *et al.*, 2023) from animal-models of Alzheimer's disease (Le Douce *et al.*, 2020) and human *post mortem* studies (Ułas and Cotman, 1997; Mazzo *et al.*, 2016). This is also in line with evidence that therapeutically enhancing NMDA receptor function is beneficial for people with early-stage Alzheimer's disease (Lin *et al.*, 2014; Chang *et al.*, 2021). Yet, as this study shows, Alzheimer's disease severity and progression *increase* relative NMDA receptor function (Hynd *et al.*, 2004; Ittner *et al.*, 2010; Danysz and Parsons, 2012). This apparent contradiction is addressed by Olney and colleagues, who proposed that a disinhibition state triggered by NMDA receptor hypoactivity leads to low-grade chronic excitotoxic activity, exacerbating neuronal degeneration (Olney *et al.*, 1997). Indeed, studies have shown that in response to reduced NMDA receptor function, a typical consequence is excessive glutamate release (Moghaddam *et al.*, 1997; Adams and Moghaddam, 1998; Newcomer *et al.*, 2000).

In Alzheimer's disease, this low but chronic influx of calcium through pathologically-open NMDA receptors may potentiate excitotoxicity (Choi *et al.*, 1988) and cell death (Wang and Reddy, 2017). Although it was theorised that memantine would therefore delay cell death (Danysz and Parsons, 2003), by blocking excitotoxic calcium entry, memantine remains in use as a symptomatic treatment. Note too that memantine is only licenced for moderate to severe Alzheimer's disease (Wilkinson, 2012; McShane *et al.*, 2019), indicating a complex and dynamic evolution of the role NMDA-receptor function in Alzheimer's disease.

An advantage of dynamic causal modelling of evoked neurophysiological responses is the ability to bridge between clinical and preclinical models of disease. It can inform the understanding of the biological processes that generate the neurophysiological responses underlying cognitive task performance. This study found that the mismatch negativity amplitude is significantly correlated with MMSE and significantly reduces with disease progression. This is an important demonstration, given the need for quantitative biological tools to enhance early phase clinical trials. However, the greater value of this study is in the analysis of disease and drug mechanism *in vivo*. Specifically, how NMDA channel blockade relates to the neurophysiological deficit.

A progressive reduction in mismatch negativity amplitude in people with Alzheimer's disease compared to controls has been shown previously in Alzheimer's disease (chapters 4 and 5). Other studies have shown that the mismatch negativity is significantly associated with verbal

learning (Mowszowski *et al.*, 2012), self-reported disability (Mowszowski *et al.*, 2012), cognitive training (Mowszowski *et al.*, 2014) and episodic memory (Laptinskaya *et al.*, 2018) in people with mild cognitive impairment (Mowszowski *et al.*, 2012; Laptinskaya *et al.*, 2018) and Alzheimer's disease (Mowszowski *et al.*, 2014). That the current task (roving mismatch negativity) is sensitive to disease presence, as shown previously (Chapter 4), and disease severity and progression, is especially encouraging given the ease of the task for participants and the robustness of the mismatch negativity waveform (Pruvost-Robieux *et al.*, 2022).

There are nonetheless limitations to this study. First, though the models were informed by human disease, there is no complete model of disease (Friston *et al.*, 2019). Second, only two regions were modelled although the mismatch negativity is generated by a wider network (Garrido *et al.*, 2008; Phillips *et al.*, 2015; Cope *et al.*, 2022). This may have oversimplified and biased interpretations of network activity underlying the neurophysiological deficit. A reduced network was used to reduce model complexity (Garrido *et al.*, 2009*a*) and improve model conversion. This simplified model therefore offers a more parsimonious network for investigating dysfunction of NMDA blockade. Third, there was a relatively small number of participants in the memantine-placebo study (n=19). This may have biased results away from the population the sample represents. Larger studies are required to confirm the mechanism of memantine. Fourth, patient participants were recruited according to clinical diagnoses of Alzheimer's disease, and mild cognitive impairment. However, all patient participants were positive for amyloid biomarkers by cerebrospinal fluid examination or positron emission tomography. Finally, the longitudinal study attracted an attrition rate of 29% over a mean interval of 16 months. This is slightly higher than anticipated (20% per annum), which in part reflects the impact of the COVID-19 pandemic. This may have biased results to the remaining sample.

In conclusion, this dynamic causal modelling approach enabled non-invasive assessment of NMDA-receptor blockade in humans, *in vivo*. Data were recorded during a robust task, the mismatch negativity, which is sensitive to Alzheimer's disease, its disease severity and progression. The biologically-informed generative models reproduced the neurophysiological deficit and indicated appropriate drug target engagement, exemplified by increased NMDA receptor blockade by memantine. Memantine is only licenced for more severe Alzheimer's disease (Wilkinson, 2012; McShane *et al.*, 2019). This is likely due to the complex evolution of NMDA-receptor dynamics (Olney *et al.*, 1997; Danysz and Parsons, 2012). Future studies

could use the techniques illustrated here to assess whether individual participants' NMDA receptor function is abnormally increased or decreased. This information could identify participants who would benefit most from a particular drug. Such techniques could therefore assist treatment decisions in the clinic by informing personalised treatment plans that optimise the patient's NMDA receptor function. NMDA receptor function could be monitored as the disease progresses, and treatments adjusted accordingly. Future studies should assess whether such personalised treatment strategies can improve patient outcomes in clinics. The null effect of memantine on cognition in less severe Alzheimer's disease (Wilkinson, 2012) could be explained using these techniques to assess memantine's effect on NMDA receptor function in less versus more severe disease. Future experimental medicines studies targeting NMDA receptors (Cummings *et al.*, 2024) may therefore have improved outcomes if they select participants according to their NMDA receptor function. For example, future experimental medicine studies looking to increase NMDA receptor function (Chang *et al.*, 2021) to improve cognition in less severe disease, rather than block function in more severe disease, could use these techniques to select participants who would most benefit from the drug mechanism (i.e. those with decreased NMDA receptor function). Future translational studies could tailor generative models to measure other drugs and targets of interest, as part of early-phase clinical trials of much needed novel dementia therapeutics.

Appendix C: Supplementary materials for Chapter 6

Supplementary Methods

Supplementary analysis of people with Alzheimer's disease versus healthy controls

Demographics of the healthy control participants from the NTAD study are detailed in Supplementary Table C.1.

Sex (Male:Female)	Handedness (Right:Left:Both)	Age (yrs)*	Education (yrs)	Baseline MMSE*	Baseline PET	Baseline CSF
09:05	11:03:00	65.3 (±7.29)	16.2 (±3.38)	29.4 (±0.74)	0.98 (± 0)	0.38 (±0.21)

Supplementary Table C.1 NTAD control participant demographics

DCMs were inverted in line with the main analyses.

A PEB analysis was run with a design matrix that comprised of a regressor of ones, a second regressor for group (0 for controls, 1 for patients) and a third regressor to control for age (mean centred and scaled). PEB posterior estimates of the NMDA blockade parameter were extracted and plotted against age.

Fitting first-level DCMs

There were two inversion failures when fitting DCMs to the data from the memantine session of the memantine-placebo study. There was one inversion failure when fitting DCMs to the patient NTAD data. The respective participants were excluded from the PEB analyses.

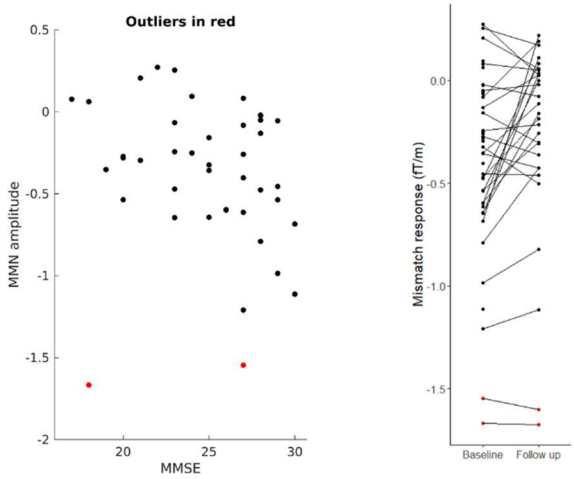
Including age as a covariate in the PEB analysis with MMSE

I reran the PEB analysis investigating the effect of MMSE on NMDA parameter blockade controlling for age (with a third regressor with centred and scaled age of each participant). The effect of MMSE on the NMDA blockade parameters was unchanged when controlling for age. NMDA channel blockade was reduced with more severe Alzheimer's disease (a lower MMSE score) with a meaningful effect (probability of parameter > 95%) in right parietal cortex (posterior estimate = 0.06, posterior probability = 0.99).

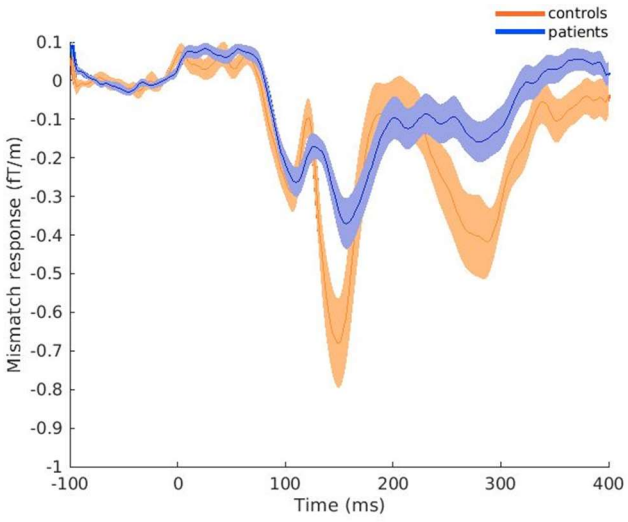
PEB analysis of participants with Alzheimer's disease versus control participants

NMDA channel blockade was higher in patients than controls with a posterior probability > 95% in left (posterior estimate = 0.51, posterior probability = 1) and right (posterior estimate = 0.28, posterior probability = 1) parietal cortices. Age also increased NMDA channel blockade (posterior estimate = 0.17, posterior probability = 1) in the left parietal cortex (see Supplementary Figure C.6).

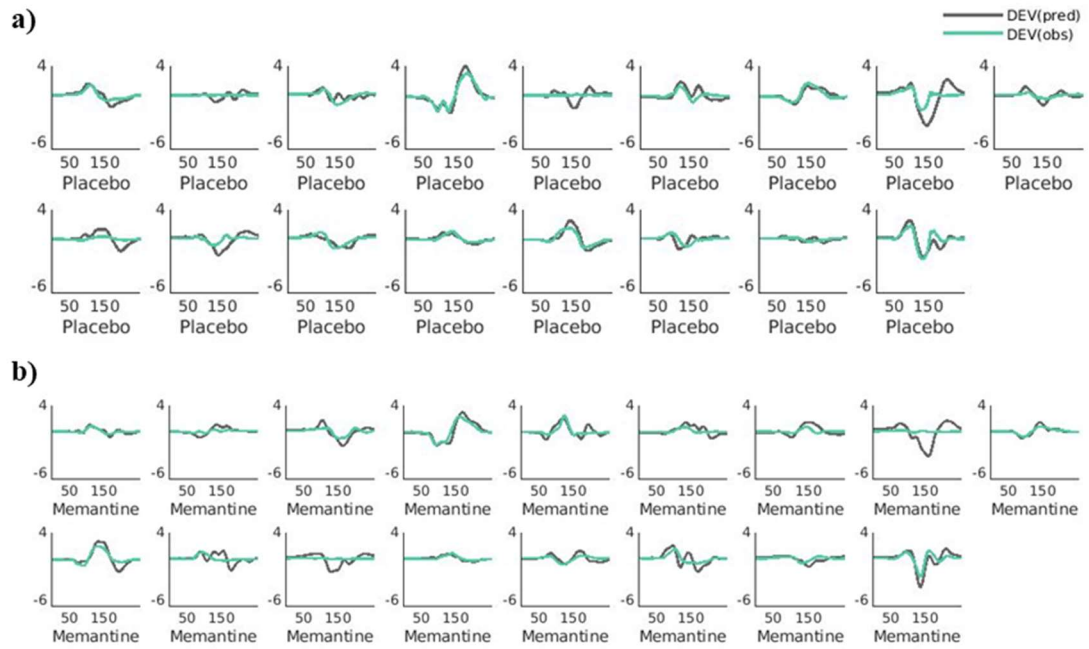
Supplementary Results



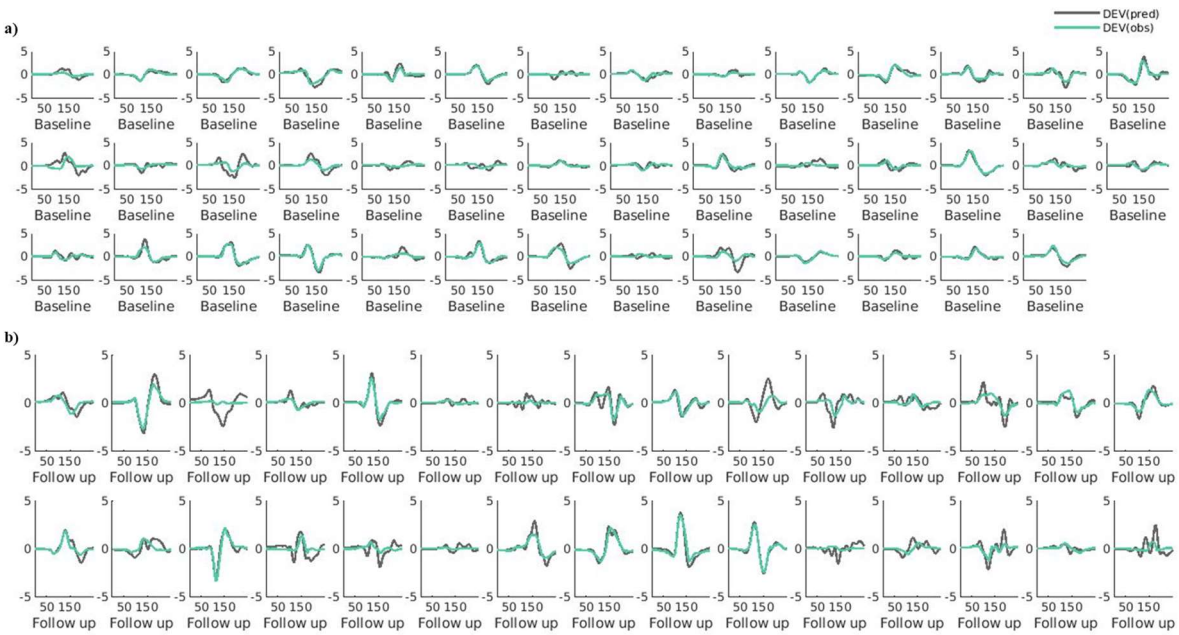
Supplementary Figure C.1 Outliers excluded from sensor level analyses
Scatter plots showing mismatch negativity amplitude for people with Alzheimer's disease, including the two outlier participants (in red) who were excluded from the sensor statistics against a) MMSE and b) session (baseline versus follow up)



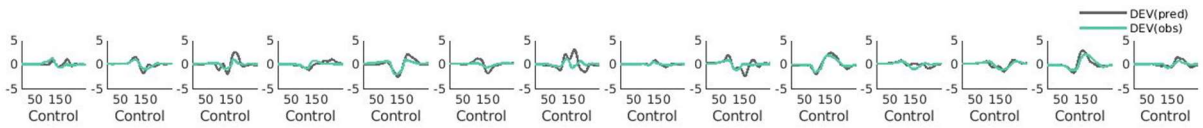
Supplementary Figure C.2 The mismatch response for NTAD participants at baseline.
The amplitude from 140 to 160ms was significantly reduced in patients compared to controls at baseline (t = -2.56, p = 0.007) with a medium effect size (d = 0.76).



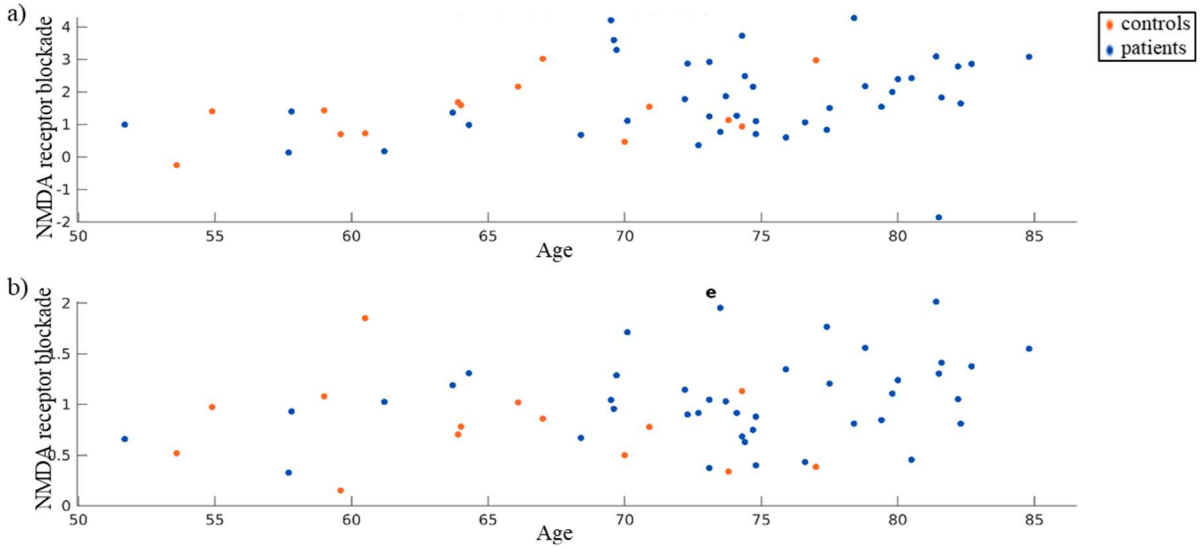
Supplementary Figure C.3 Model fits for the healthy controls from the memantine-placebo study
Observed responses (cyan) and model-generated responses (grey) to the deviant tones of the mismatch negativity paradigm for each participant on **a)** placebo or **b)** memantine.



Supplementary Figure C.4 Model fits for NTAD patient group
Observed responses (cyan) and model-generated responses (grey) to the deviant tones of the Mismatch Negativity paradigm for each participant at **a)** baseline or **b)** follow up sessions.



Supplementary Figure C.5 Model fits for the healthy controls from the NTAD study



Supplementary Figure C.6 The effect of age and group on the NMDA blockade parameter

The PEB posterior estimate of the expected value of the NMDA blockade parameter plotted for controls and patients for the **a)** the left parietal region and **b)** the right parietal region

7 | General Discussion

My work builds on preclinical and *post mortem* findings of disease effects to form and test hypotheses about how cortical microcircuits are affected in people living with Alzheimer's disease. The objectives of this thesis were to identify cellular level effects of Alzheimer's disease on cognition using magnetoencephalography (MEG) to (i) better understand mechanisms of Alzheimer's disease underlying cognitive decline and (ii) to identify mechanistically-informative biomarkers of disease for use in interventional studies.

There are several requirements of a good biomarker. Its measurement must be sufficiently well-tolerated to undertake for participants. The biomarker must also be reliable and sensitive to disease, its severity and progression. There are other measures meeting these criteria, some of which I discuss in chapter 2. The critical difference of the dynamic causal modelling biomarkers identified in this thesis is that they are also informative about disease mechanisms at the level of cortical microcircuits and their cells or receptors.

To address these challenges with respect to MEG biomarkers, I analysed mismatch negativity data from people who participated in the Cambridge NTAD study. I confirmed the reliability and disease-sensitivity of mismatch negativity amplitudes. To explore cellular-level disease effects underlying the observed neurophysiological deficit, I inverted dynamic causal models (DCMs) to mismatch negativity responses. I tested hypotheses based on preclinical models and *post mortem* data about the effect of Alzheimer's disease on cortical microcircuits.

7.1 Summary of the principal findings

7.1.1 Chapter 2

In chapter 2, I described the NTAD study protocol detailing how the data I use throughout this thesis was collected. We recruited people into the study who were neurologically healthy or who had a diagnosis of mild cognitive impairment or Alzheimer's disease. Participants completed a screening session to assess study eligibility. People with a diagnosis of mild cognitive impairment or Alzheimer's disease were required to have an MMSE score > 18, CDR of 0.5 to 1, and a positive amyloid status determined by amyloid-PET or CSF analysis. Neurological-normal people were required to have an MMSE score >24, CDR of 0 and a known amyloid status by amyloid-PET or CSF analysis.

Eligible people proceeded to baseline assessments. These included physiology and blood sampling, MRI, MEG, EEG and neuropsychology assessments. A subset of people with Alzheimer's disease (Alzheimer's dementia or mild cognitive impairment with amyloid biomarkers) had repeat EEG and MEG two-weeks after baseline to assess test-retest reliability of EEG and MEG measures. People with Alzheimer's disease completed annual follow-up 1 sessions of repeat clinical and neuropsychological assessments, blood, MRI, EEG and MEG. Annual follow-up 2 repeated clinical and neuropsychological assessments. I used MEG data from the mismatch negativity task collected at the Cambridge MEG and EEG baseline, test-retest and annual follow up 1 sessions. Before the task, pure tone audiometry assessed hearing thresholds to ensure normal hearing between 45 and 75dB. During the roving mismatch negativity task, participants watched a silent nature documentary (from BBC One's Frozen Planet) while passively listening to tones of different frequencies that repeated in blocks of 3-10 repetitions.

Limitations of this study include that the volunteer panels and clinical services used to recruit participants may not reflect national diversity. People with significant mobility, hearing or visual impairments were ineligible. People were also ineligible if they had contraindications to imaging, such as metallic implants or implanted medical devices. Some participants were on a stable dose of medication. Diagnostic groups were defined by clinical diagnoses with no *post mortem* pathological confirmation of Alzheimer's disease. Clinical diagnoses were however supported by amyloid biomarker status.

7.1.2 Chapter 3

Chapter 3 established clinical and MRI profiles of the NTAD Cambridge cohort. This chapter confirmed that NTAD participants with symptomatic Alzheimer's disease have data features typical of people with sporadic, late-onset Alzheimer's disease. This chapter considered the following, established measures of Alzheimer's disease:

1. Clinical tests: MMSE and ACE-R scores were lower for people with Alzheimer's disease than control participants. MMSE and ACE-R scores of people with Alzheimer's disease were lower at 16-month follow up than baseline sessions.

2. Pathology: People with Alzheimer's disease had increased measures of blood, CSF or amyloid-PET beta-amyloid pathology.

3. Neuropsychology: First principal component scores were calculated using loadings from a principal component analysis of neuropsychological data. First principal component scores were higher for people with Alzheimer's disease than controls. First principal component scores were higher for people with Alzheimer's disease at 16 month follow up than at baseline sessions.

4. MRI: Total brain volume was reduced for people with Alzheimer's disease than control participants and further reduced during 16 month follow up. Voxel-based morphometry showed grey matter atrophy in regions including the hippocampi for people with Alzheimer's disease (1) compared to control participants, (2) that correlated with their neuropsychological severity (first principal component scores) and (3) at annual follow up versus baseline.

I concluded that the patient cohort had features typical of people with amnestic Alzheimer's disease. The analyses had several limitations. There was a significant difference in age between the patient and control groups. Attrition may have limited inferences though there were no significant differences in demographics between participants who completed the annual follow up and those who withdrew from the study. There were missing data and I used imputation for the principal component analysis.

7.1.3 Sensor-level metrics

Chapters 4, 5 and 6 show the sensitivity of sensor-level mismatch negativity MEG responses to the presence of Alzheimer's disease, its severity and progression over 16 months. Chapter 4 analyses used an ANCOVA (with group, tone and age) which showed a main effect of tone

repetition on evoked response amplitudes from 140 to 160ms that interacted with group. A longitudinal repeated-measures ANOVA using evoked responses from 140 to 160ms found a main effect of tone and progression which interacted with each other. An intraclass correlation analysis showed that mismatch negativity waveform amplitudes from 140-160ms have excellent test-retest reliability. Chapters 4 and 5 showed that mismatch negativity waveform amplitudes (from 140-160ms) are progressively attenuated for people with symptomatic Alzheimer's disease. In chapter 6, I showed that mismatch negativity amplitudes correlate with MMSE scores for people with Alzheimer's disease.

These findings confirm the effect of Alzheimer's disease on sensor-level mismatch negativity responses. They indicate that MEG meets the following benchmarks: MEG is sensitive to (1) the presence of Alzheimer's disease, (2) its severity (MMSE scores) and (3) progression and (4) has excellent test-retest reliability.

7.1.4 Chapter 4

Chapter 4 focused on the effect of Alzheimer's disease on pyramidal cell connectivity in hierarchical, cognitive networks. Convolution-based DCMs and parametric empirical Bayesian analyses confirmed the hypothesis that reduced superficial pyramidal cell gain and extrinsic connectivity between pyramidal cells explain neurophysiological differences associated with Alzheimer's disease and its progression.

Cholinergic antagonists attenuate mismatch negativity responses (Pekkonen *et al.*, 2001) and decrease the gain modulation of superficial pyramidal cells (Schöbi *et al.*, 2021). In Alzheimer's disease, there is a loss of cholinergic neurones (Davies and Maloney, 1976). Chapter 4 showed that Alzheimer's disease progressively reduces the gain modulation of superficial pyramidal cells in primary auditory and inferior frontal regions.

Superficial and deep pyramidal cells have abnormal tau deposits (Braak and Tredici, 2018). Tau affects pyramidal cell morphology (Mijalkov *et al.*, 2021) impairing pyramidal cell signalling (Ferrante *et al.*, 2013). People with Alzheimer's disease had reduced connectivity between superficial and deep pyramidal cells, which reduced further during follow up.

The inferences from this chapter may be limited by the models used. The DCM and parametric empirical Bayes models were defined to suit the hypotheses; other models could exist which better explain the data. The impact of treatments such as cholinesterase inhibitors could have

moderated the results. Though I would expect such treatments to reduce rather than exacerbate the differences. There was a difference in age between groups.

7.1.5 Chapter 5

Chapter 5 examined whether Alzheimer's disease affects NMDA channel parameters using conductance-based DCMs and parametric empirical Bayes. I confirmed that abnormal NMDA channel function explains the neurophysiological deficit better than differences in AMPA or GABA channel function, in line with rodent and *post mortem* findings (Carlson *et al.*, 1993; Lai *et al.*, 2019). I found that NMDA channel time constants were altered in all regions of people with symptomatic Alzheimer's disease. Alzheimer's disease progressively increased NMDA time constants in primary auditory regions and progressively decreased NMDA time constants in inferior frontal regions.

This chapter shows changes to NMDA channel time constants in people living with Alzheimer's disease. NMDA channel time constants could be a potential new target for new therapeutics. NMDA receptor function can be facilitated by drugs which alter channel opening times (Perszyk *et al.*, 2020). Further research is needed to assess the potential of such therapeutics for Alzheimer's disease treatment. This chapter demonstrates the potential for dynamic causal modelling to support clinical trials of dementia treatments that target NMDA-receptor activity.

The analyses in this chapter had limitations including group differences in age, attrition at follow up and recruitment according to clinical diagnosis. As in Chapters 4 and 6, it is important to note that these findings of cortical microcircuit changes are from model parameters informed by MEG data and that no model is perfect.

7.1.6 Chapter 6

The final experimental chapter of this thesis showed opposite cortical microcircuit effects of the NMDA antagonist memantine and Alzheimer's disease severity and progression on the cortical microcircuit. In this chapter, I used a conductance-based model adjusted to allow optimisation of NMDA-channel blockade parameters during model inversion (NMDA-channel blockade parameters are fixed in the default model used in chapter 5). As the NMDA-channel blockade parameter increases, conductance through NMDA channels becomes increasingly non-linear, requiring more depolarisation for channel conductance.

I used data from a memantine-placebo crossover study of neurologically-healthy people and data from the Cambridge NTAD study. Parametric empirical Bayes was used to test (1) whether memantine modulates NMDA-channel blockade, and the direction of this pharmacological effect; and (2) the effect of Alzheimer's disease severity and progression on NMDA-channel blockade.

I confirmed opposing effects of the dementia treatment, memantine, and Alzheimer's disease on NMDA-channel blockade. Memantine increased while Alzheimer's disease severity and progression decreased NMDA-channel blockade. I concluded that future clinical studies could similarly tailor biologically-informed models to measure their target-of-interest and so determine the potential of novel, disease-modifying therapeutics.

There are several limitations to this study. A simplified mismatch negativity network with 2 regions was used to reduce model complexity. As above, there is no complete model of disease. There was a relatively small number of participants in the memantine-placebo study. There were two inversion failures when fitting DCMs to data from the memantine session of the memantine placebo study and one failure when fitting DCMs to the NTAD patient data.

7.2 Basic measures of Alzheimer's disease

A good biomarker of Alzheimer's disease must be reliable and sensitive to Alzheimer's disease, its severity and progression. A good biomarker should also be well-tolerated by participants and detectable regardless of disease stage with minimal bias to confounding factors.

In chapter 3, I tested group (patients versus controls) and session (patient baseline versus follow up) differences using established measures of Alzheimer's disease including: (1) MMSE and ACE-R scores (2) measures of Alzheimer pathology, (3) the first component identified by a principal component analysis of neuropsychology scores that loaded onto industry-standard neuropsychological batteries and (4) MRI biomarkers. In Chapters 4, 5 and 6, I showed that mismatch negativity amplitudes are attenuated by Alzheimer's disease, its severity (measured using MMSE scores) and progression. Comparing the efficacy of these basic measures to Alzheimer's disease is beyond the scope of this thesis. However, I can draw some preliminary conclusions. Amyloid-PET had the strongest group effect of all the reported measures ($d = 2.96$). This was followed by cognitive measures: the first principal component and ACE-R memory scores had very large effect sizes ($d > 2$). CSF and plasma measures had large effect

sizes ($d > 0.8$). Differences in mismatch negativity amplitudes between groups had a medium effect size ($0.5 < d < 0.8$). Amyloid-PET has previously been shown to outperform other biomarkers of Alzheimer's disease (Vandenberghe *et al.*, 2013; Ramusino *et al.*, 2020). Neuropathological changes are proposed to occur and progress years before symptom onset (Therriault *et al.*, 2024). Such large effect sizes for established biomarkers of Alzheimer's disease (PET, CSF, plasma and MRI biomarkers) reflect the clinical stage of people with Alzheimer's disease from the NTAD study. This group were symptomatic, with large memory impairments (group differences with $d = 2.19$ for ACE-R memory scores).

The largest effect size reported for longitudinal differences between baseline and 16-month follow up sessions for people with Alzheimer's disease was in mismatch negativity amplitudes (Chapter 6: $d = 0.60$). Differences between baseline and follow-up sessions were stronger when measured with this MEG measure than cognitive test scores (Chapter 3: $d = 0.35$ for PC1 scores and $d = 0.59$ for ACE-R total scores) or total brain volume (Chapter 3: $d = 0.4$). There were no follow-up PET or CSF measures of amyloid pathology, which had the strongest group differences at baseline. I also have not compared longitudinal differences between plasma and MEG biomarkers; however, plasma is arguably more accessible (Hudd et al., 2019).

The NTAD study was designed to test MEG as a potential platform for early-phase clinical trials of short duration rather than to replace established biomarkers. In this thesis, I have shown that mismatch negativity MEG responses are sensitive to disease, its severity and progression over ~16 months and are reliable over test-retest sessions. This thesis shows that mismatch negativity responses are progressively attenuated by Alzheimer's disease. Previous EEG and MEG studies of mismatch negativity paradigms have shown that the mismatch negativity amplitudes of people with Alzheimer's disease are attenuated in comparison to control participants (Savolainen *et al.*, 2001; Cheng *et al.*, 2012; Hsiao *et al.*, 2014; Papadaniil *et al.*, 2016; Jiang *et al.*, 2017), and correlate with disease pathology (Kim *et al.*, 2020; Gjini *et al.*, 2022) and cognitive and clinical severity (Mowszowski *et al.*, 2012, 2014; Gao *et al.*, 2018; Laptinskaya *et al.*, 2018). The mismatch negativity task has several advantages for studying the effect of Alzheimer's disease on cognition compared to cognitive assessments. It is an easy task that participants passively complete with an automatic response. This reduces training and performance confounds and enables high compliance at any disease stage. Indeed, elements of the response are detectable in people who are unconscious (Bekinschtein *et al.*, 2009). This

also largely reduces educational and cultural biases associated with cognitive tests (Stothart *et al.*, 2021).

In conclusion, I propose the mismatch negativity response as an early neurocognitive marker of Alzheimer's disease. My PhD research has shown mismatch negativity amplitudes of people with symptomatic Alzheimer's disease are reliable over test-retest sessions, sensitive to disease (patients vs controls), severity (correlates with MMSE score) and progression (baseline vs follow up, with a higher Cohen's d than the other longitudinal measures used in this thesis).

However, this basic measure gives little information about disease mechanisms. The next section discusses biomarkers of Alzheimer's disease sensitive to disease, its severity and progression that are informative about disease mechanisms underlying dementia.

7.3 Dynamic causal modelling for assessment of cortical microcircuits

For a neurophysiological biomarker to be most beneficial to early-phase clinical trials it must be sensitive to disease and its progression. It must also be sensitive to mechanisms of disease pathology or pharmacology. In this thesis, I assessed disease and pharmacological mechanisms using dynamic causal modelling. This allowed characterisation of neural dynamics by cell type and cortical layer (Friston *et al.*, 2003) from neurophysiological responses (Kiebel *et al.*, 2008, Garrido *et al.*, 2009*a*; Bastos *et al.*, 2012).

Evoked responses generated by the DCMs were highly correlated with observed evoked responses. The observed and model-generated evoked responses were very strongly correlated for the convolution-based DCM used in chapter 4 (mean Pearson's correlation coefficient = 0.86 ± 0.17), for the conductance-based DCMs used in chapter 5 (0.81 ± 0.22) and strongly correlated for the more complex conductance-based model used in chapter 6 (0.71 ± 0.28). This supports the validity of dynamic causal modelling shown by previous studies (Pinotsis *et al.*, 2017; Adams *et al.*, 2021, 2023). The models used in chapters 4 and 5 were the default models within SPM12 (r7771). The model in chapter 6 allowed the voltage-gated blockade of NMDA channels to be optimised during model inversion (rather than fixed as in the default model). This added complexity allowed insight into disease and pharmacological effects on NMDA-channel blockade, with the caveat of having relatively lower correlation between predicted and observed responses.

The differential equations describing neuronal dynamics within DCM canonical microcircuits are based on biology (Douglas and Martin, 1991; Jansen and Rit, 1995; Bastos *et al.*, 2012). DCMs consequently provide cellular-level information about neuronal dynamics generating neurophysiological responses. Specific parameters of interest can be tested for second-level effects according to one's hypotheses. The impact of Alzheimer's disease on cortical microcircuits has been studied with tissue cultures (Kimura *et al.*, 2014; Kaniyappan *et al.*, 2017; Song *et al.*, 2018), animal studies (Lai *et al.*, 2019; Schöbi *et al.*, 2021; Rozumna *et al.*, 2023) and *post mortem* data (Heckers *et al.*, 1992; Ułas and Cotman, 1997; Braak and Tredici, 2018). Such findings provided a basis for my PhD work, allowing development of analytical frameworks and hypotheses to test the impact of Alzheimer's disease on cortical microcircuits in humans, *in vivo*, using dynamic causal modelling. Different DCMs have different model parameters. I used models which best measured the cortical microcircuit parameters required to test my hypotheses.

For chapter 4, I first identified which parameter may be affected by the cholinergic deficit associated with Alzheimer's disease, using literature. I then assessed how Alzheimer's disease affected this parameter using DCMs of the NTAD data. I based my hypothesis on the work of Moran *et al.*, 2013, and Schöbi *et al.*, 2021. Their studies used DCMs of intracranial electrode recordings from rodents (Schöbi *et al.*, 2021) and EEG recordings from humans (Moran *et al.*, 2013). Both studies used convolution-based canonical microcircuit DCMs. They assessed the effects of cholinergic modulation on cortical generators of mismatch negativity responses. They found effects of cholinergic therapeutics on superficial pyramidal cell gain modulation. I assessed this same parameter using the same model in people living with Alzheimer's disease, whose cognitive symptoms are treated by cholinergic modulators (Nagori *et al.*, 2024).

In chapter 6, I followed a similar framework to identify DCM parameters targeted by NMDA-receptor antagonism and assess how disease affects these parameters. In contrast to chapter 4, there were no previous studies that had used DCMs to assess the effects of NMDA-receptor antagonism by Alzheimer treatments on the cortical microcircuit. For this analysis, I therefore first confirmed the mechanisms of the NMDA-receptor antagonist, memantine, using MEG roving MMN data from a placebo-controlled memantine study with neurologically-healthy participants. Comparisons of plausible memantine targets confirmed that memantine blocks NMDA-receptor channels. I used the same model to assess how this parameter was affected by Alzheimer's disease severity and progression. In this way, studies can identify drug

mechanisms using dynamic causal modelling, and then assess whether there is a need for such an intervention in Alzheimer's disease (i.e. whether the mechanism is affected by disease).

Hypotheses can also be informed by *post mortem* findings of disease effects. In chapter 4, I tested a second hypothesis based on *post mortem* findings of pyramidal cell insult by Alzheimer's pathology (Braak and Tredici, 2018). The model included parameters indexing the strength of connections between pyramidal cells of different regions. In chapter 5, I assessed glutamatergic changes associated with Alzheimer's disease (Carlson *et al.*, 1993; Ortiz-Sanz *et al.*, 2022), focusing on the time constant of NMDA channels and NMDA-mediated extrinsic connectivity.

The reported disease effects determined using dynamic causal modelling aligned with the hypotheses based on preclinical and *post mortem* findings. Previous studies have similarly used this approach to study the effects of anti-NMDA autoimmune encephalopathy (Symmonds et al., 2018), inherited channelopathies (Gilbert et al., 2016), ageing (Moran et al., 2014), pathophysiology of non-Alzheimer dementias (Shaw *et al.*, 2019; Adams *et al.*, 2020, 2021, 2023) and confirmatory studies of drug interventions (Moran *et al.*, 2013; Adams *et al.*, 2021).

There are potential limitations to using dynamic causal modelling. Concerns of overfitting have been mitigated through use of a variational Laplace scheme for model inversion which defines the free energy of a model as a trade-off between complexity and accuracy (Zeidman *et al.*, 2023). The reliability (Rowe *et al.*, 2010, Jafarian *et al.*, 2023*a*) and validity (Friston *et al.*, 2003; Penny *et al.*, 2004; Chumbley *et al.*, 2007; Phillips *et al.*, 2016) of related DCMs have been demonstrated. I set up complex, non-linear models requiring analytical methods that adequately consider parameter variances. Therefore, I used parametric empirical Bayesian analysis which operates within a Bayesian framework, incorporating distributions of parameter estimates and accommodating nonlinear models (Friston *et al.*, 2016). In this thesis, I drew as much as possible to a canonical method with minimal tweaking of models. Nevertheless, while some models are useful, no model is perfect.

7.4 Effect of Alzheimer's disease on pyramidal cell connectivity and NMDA channels

In this thesis, the following disease effects on the cortical microcircuit generating mismatch negativity responses were shown: (1) progressively reduced gain modulation of pyramidal

cells, (2) progressively reduced connectivity between pyramidal cells, (3) progressively altered NMDA-channel time constants and (3) increased NMDA-channel blockade with more severe and progressed disease.

This thesis corroborates findings from preclinical and *post mortem* studies that Alzheimer's disease affects superficial and deep layer pyramidal cell connectivity. Chapter 4 analyses revealed that the presence and progression of Alzheimer's disease are associated with reduced superficial pyramidal cell gain and extrinsic connectivity between pyramidal cells. *Post mortem* studies have shown that Alzheimer's pathology is particularly predominant in pyramidal cells (Braak and Tredici, 2018) and correlates with the loss of superficial and deep (Hof *et al.*, 1990) and acetylcholinesterase-rich (Heckers *et al.*, 1992) pyramidal cells. Superficial (layer 3) and deep (layer 5) pyramidal cells of people with Alzheimer's disease have a reduction in acetylcholinesterase activity (Heckers *et al.*, 1992). Cholinergic antagonism (Schöbi *et al.*, 2021), and the presence and progression of Alzheimer's disease (Chapter 4) reduce the gain of superficial pyramidal cells (Schöbi *et al.*, 2021). I suggest this effect of Alzheimer's disease on superficial pyramidal cells is therefore likely due to the cholinergic deficit associated with Alzheimer's disease (Heckers *et al.*, 1992). Superficial pyramidal cell gain (chapter 4) and NMDA-channel kinetics (Chapter 5) were progressively affected by Alzheimer's disease in primary auditory and inferior frontal regions generating mismatch negativity responses. Chapter 4 showed that Alzheimer's disease progressively affects the gain of superficial pyramidal cells in these same regions when generating mismatch negativity responses likely due to disease-related cholinergic deficits (Moran *et al.*, 2013; Schöbi *et al.*, 2021). Changes to NMDA or cholinergic systems affect the other. For example, NMDA hypofunction increases acetylcholine release (Giovannini *et al.*, 1994; Newcomer *et al.*, 2000) and cholinergic antagonism may decrease NMDA-mediated signalling (Chen *et al.*, 2008).

Pyramidal cell death is preceded by disruption of pyramidal cell synaptic function and activity (Oakley *et al.*, 2006) by Alzheimer's pathology (Shankar *et al.*, 2007; Lison *et al.*, 2014). Alzheimer's pathology is present in connections between superficial and deep pyramidal cells (Braak and Tredici, 2018), which have reduced connectivity associated with the presence and progression of Alzheimer's disease (Chapter 3). Alzheimer's pathology may therefore be the cause of this disrupted pyramidal-cell connectivity. Pyramidal cells are the principal source of inter-regional connectivity. Previous studies have shown associations of Alzheimer's pathology with functional connectivity of the frontoparietal and default mode network (Engels *et al.*,

2015; Klaassens *et al.*, 2017; Mandal *et al.*, 2018; Zhao *et al.*, 2019; Wales and Leung, 2021; Yang *et al.*, 2021; Fathian *et al.*, 2022; Moffat *et al.*, 2022; Zhukovsky *et al.*, 2023). The parietal cortex is commonly implicated in connectivity studies of Alzheimer's disease (Wang *et al.*, 2015; Cope *et al.*, 2022). Connectivity between superficial and deep pyramidal cells originating or terminating in the parietal cortex were especially affected by Alzheimer's disease (Chapter 4), in accord with the classical progression of Alzheimer's pathology (Braak and Tredici, 2018).

Loss of pyramidal cell synapses by Alzheimer's pathology is in part modulated by NMDA receptor activity (Shankar *et al.*, 2007). NMDA channel activity is reduced by pathological amyloid beta (Shankar *et al.*, 2007), which also changes proteins moderating NMDA channel kinetics (Ortiz-Sanz et al., 2022). This thesis shows – albeit indirectly - in people living with Alzheimer's disease, that NMDA channel kinetics (opening times, channel 5, and voltage-gating by magnesium ions, channel 6) are progressively affected by Alzheimer's disease. However, the progressive effect of Alzheimer's disease on NMDA receptors has a complex evolution. Early-stage reductions in NMDA-receptor function (Olney *et al.*, 1997; Newcomer *et al.*, 2000) are followed by a compensatory, mild over-activation of NMDA receptors (Hynd *et al.*, 2004; Danysz and Parsons, 2012). In later disease stages, NMDA receptors are reduced in regions most affected by Alzheimer's disease pathology (Sze *et al.*, 2001).

Human *in vivo* studies with SV2a-binding PET ligands confirm loss of synaptic density (Venkataraman *et al.*, 2021). Synaptic function strongly correlates with cognition in Alzheimer's disease (Terry *et al.*, 1991). Synaptic function underlies short-term plasticity, to which changes are an early feature of preclinical models of Alzheimer's disease (Selkoe, 2002; Lee *et al.*, 2012; Chakroborty *et al.*, 2019). The roving mismatch negativity task reflects short-term plasticity as networks learn and adapt to a changing stimulus (Garrido *et al.*, 2009*a*). Chapter 4 showed reductions in the fast phasic response of intrinsic connections to tone repetition. This illustrates an effect of Alzheimer's disease on short-term plasticity.

Dynamic causal modelling of the roving mismatch negativity task can be explained within a predictive coding framework (Garrido *et al.*, 2009*a*). This framework proposes that top-down/backward connections relay predictions from hierarchically-higher to lower cortical regions, and bottom-up/forward connections relay prediction errors from hierarchically-lower to higher cortical regions. Modulation of forward signalling of prediction errors by higher-level

predictions may be mediated by NMDA receptors (Friston, 2005). Indeed, NMDA-receptor disruption (Chapters 5 and 6) increases interference of new with prior information impairing memory updating (Yang *et al.*, 2023). Hierarchically-higher areas may also modulate the precision of prediction errors (Witon *et al.*, 2020) which is proposed to be encoded by superficial pyramidal cell gain (Moran *et al.*, 2013). Alzheimer's disease progressively affects gain modulation of superficial pyramidal cells (chapter 4) and NMDA receptor kinetics (chapter 5 and 6). These changes may therefore interfere with the iterative updating of predictions by prediction error. There is no proof that dynamic causal modelling of the mismatch negativity task represents predictive coding, yet these changes would similarly affect hierarchical processing of information. In addition, there is a mild yet chronic over-activation of NMDA receptors, illustrated with progressively reduced channel blockade (chapter 6). This may increase intracellular calcium at rest (Mazzo *et al.*, 2016) increasing noise leading to impaired signal detection (Danysz and Parsons, 2012). These factors may contribute to abnormal predictive coding in Alzheimer's disease dementia (Kocagoncu *et al.*, 2021; Pérez-González *et al.*, 2022).

This thesis uses dynamic causal modelling to show the effects of Alzheimer's disease on the cortical microcircuit. The changes described underlie attenuation of mismatch negativity responses. These findings consequently improve our understanding of Alzheimer's disease mechanisms underlying dementia.

7.5 Mechanistically-informative biomarkers for clinical trials

In this thesis, I have developed generative models that can quantify potential drug targets in a cortical microcircuit, allowing measures of drug efficacy in future experimental medicines studies or early phase clinical trials. In Alzheimer's disease, acetylcholine and memantine are licenced for symptomatic treatment. Using different DCMs, I showed that one can measure the targets of these drugs, namely superficial pyramidal cell gain (cholinesterase modulators) and NMDA channel blockade (memantine), and how Alzheimer's disease presence, severity and progression affect these targets. This proof of concept provides a framework for future assessment of novel drugs.

Memantine's principal mode of action is to block NMDA channels when they are pathologically open at low-levels of depolarisation, without affecting the neurotransmission

when the post-synaptic membrane is sufficiently depolarised (Parsons *et al.*, 2007). In chapter 6, dynamic causal modelling correctly identified NMDA channel inhibition as best explaining the effect of memantine on neurophysiological responses. In chapter 4, I discuss previous DCM studies that have shown an effect of cholinesterase inhibitors on superficial pyramidal cell gain. In chapter's 4 and 6, I illustrate these drug targets are affected by Alzheimer's disease. Chapter 5 showed that NMDA receptor time constants are affected by Alzheimer's disease. I suggested that as NMDA receptor function can be facilitated by drugs which alter channel opening times (Perszyk *et al.*, 2020), future studies could assess the potential of these therapeutics for treating Alzheimer's disease.

These findings highlight the ability of dynamic causal modelling to make mechanistic inferences using non-invasive imaging. Clinical studies have lower attrition and costs with effective target validation (Paul *et al.*, 2010). Effective target validation demonstrates pharmacological target engagement and relevance to the disease (Emmerich *et al.*, 2020). Here, target engagement of memantine was illustrated. Opposing effects on the cortical microcircuit of Alzheimer's disease and its therapeutics were also illustrated. The ability to infer such receptor dynamics and pharmacology from non-invasive physiological recordings enables assessment of novel drugs of interest, whether candidate symptomatic or disease-modifying treatments. Interventional trials can similarly tailor analytical frameworks to use *a priori* knowledge and dynamic causal modelling to assess target engagement that may improve cognition.

7.6 General limitations and future directions

A limitation of dynamic causal modelling is the conditional dependencies between parameters. I decided to frame my analyses with specific hypotheses to better inform my models with prior knowledge from *post mortem* or preclinical studies of disease. The analyses tested these hypotheses, rather than being data driven. Given this, my findings are only as useful as the hypothesis and alternative hypothesis used. Other parameters, or indeed other combinations of parameters, may better explain the neurophysiological deficit. However, I chose parameters and model comparison methods which best addressed my hypotheses. I used PEB to test second-level effects. PEB is recommended as it considers variances of parameters and reduces conditional dependences of parameters (Jafarian *et al.*, 2023*a*). It is important to note, that no model is good enough. The human brain is complex; DCMs are extremely simple.

Another limitation of my study is that participants were recruited according to clinical diagnoses with no *post mortem* pathological confirmation of disease. Participants may have had comorbidities or other, non-Alzheimer pathological causes of cognitive impairment. To reduce heterogeneity of the sample, clinical diagnoses were supported by a positive amyloid status confirmed using amyloid-PET or CSF analysis.

There was a significant difference in age between people with Alzheimer's disease and control participants precipitated by closure of the MEG facility at short notice for refurbishment and upgrading. People with Alzheimer's disease were on average older and age has previously been shown to affect DCM parameters generating mismatch negativity responses (Moran *et al.*, 2014). Age was included as a covariate in PEB analyses; nevertheless, residual age effects may have affected results.

People were excluded who had mobility, visual or hearing impairments or metallic implants that would cause large MEG artefacts. This may have introduced biases to the data, preventing proper representation of the population. This also raises concerns about inclusivity of imaging research. Other measures could be used in conjunction with MEG measures in later-phase clinical trials to ensure a proper representation of the population. Participants were recruited from memory clinics and volunteer databases which may not reflect national diversity. It is therefore important to consider differences between the study population and the general population when interpreting study findings (Grill and Karlawish, 2010). Future work should prioritise recruitment reflective of national and international diversity. While informal feedback from participants during sessions was positive, there was a lack of formal patient and public involvement evaluation of the NTAD study.

Additionally, the attrition rate of 28% may limit inferences. Attrition may have biased longitudinal results away or towards more severe disease progression. The covid-19 pandemic delayed follow-up assessments. Follow up was extended to 16 months rather than the intended 12 months. This meant that the number needed to recruit to detect effects was reduced. Future studies may need to confirm the sensitivity of MEG to Alzheimer's disease progression over shorter intervals.

Test-retest reliability of patient mismatch negativity amplitudes was excellent; however, we collected no test-retest data for control participants. MEG signal-to-noise is affected by motion, blinking and artefacts from metallic implants. Future studies may utilise optically pumped

magnetometers (OPMs) for better signal sensitivity, motion robustness and hippocampal sensitivity (Tierney *et al.*, 2019). MEG has limited sensitivity to signals from the hippocampus, which is affected early in the progression of Alzheimer's disease. The mismatch negativity response is consequently particularly suitable, as MEG is more sensitive to superficial than deep cortical brain regions. Additionally, the hippocampal signals may be included in the DCMs used in the form of expectancy inputs to the upper layers of the DCM network. The MEG scanner was changed during the follow-up sessions. 76% of follow-up sessions were completed on the MEGIN Triux Neo MEG scanner, while all baseline sessions were completed on the ElektaVectorView system MEG scanner. There is consequently high multicollinearity between scanner and session. For the longitudinal assessments, I compared parameters that were sensitive to disease presence (i.e. differed between baseline groups, collected on the same scanner). Future work should validate the longitudinal findings with the Oxford NTAD cohort. Future work should also establish scanner effects with validation data collected on the old versus new scanners. This study was from data collected at the Cambridge NTAD site. Oxford also collected data; however, data collection was delayed and only completed in October 2023, after my PhD analyses were near complete. Future analyses can assess multi-site scaling of these MEG measures using the Oxford NTAD cohort.

There is a continuous spectrum of Alzheimer's disease, with pre-symptomatic, prodromal, mild cognitive impairment and dementia stages of disease. Future work could look at prodromal and presymptomatic stages of disease. The deep and frequent phenotyping study (Koychev *et al.*, 2019) follows a similar protocol to NTAD, with the roving MMN MEG paradigm, which would enable such work. Both have auditory mismatch negativity paradigms.

Despite these limitations, I propose that the efficacy of treatments for Alzheimer's disease can be assessed using dynamic causal modelling. While I did assess the effect of the Alzheimer treatment memantine, this was in control participants. To build on the findings of this thesis, future work should use these measures, alongside other biomarkers initially, to determine efficacy of disease-modifying or symptomatic treatments in people with Alzheimer's disease.

The NTAD study collected EEG and MEG simultaneously and future work should further explore EEG biomarkers of Alzheimer's disease, which were not covered in this thesis. For early-phase trials, MEG centres are accessible and offer better signal-to-noise than EEG. Nevertheless, one advantage of EEG is at-home measurements of neurophysiology which is

more accessible to participants and cheaper to collect. This allows more frequent assessment to characterise progression with potentially greater temporal resolution (e.g. measurements at 12 timepoints in a year, rather than 2 timepoints in a year). Efforts are underway to assess the sensitivity of home-based measurements of neurophysiology to disease effects.

Future work can aim to detangle whether the physiological changes cause the cognitive deficits, or whether they are merely an epiphenomenon. To do this, mediation and moderation analyses can explore the relationship between physiology and cognition. This will further improve our understanding of the mechanisms underlying dementia. Disease-modifying interventions are ultimately needed in people with Alzheimer's disease to confirm this relationship.

7.7 Concluding remarks

This thesis aimed to improve our understanding of disease and identify mechanistically-informative biomarkers to help facilitate and accelerate disease-modifying treatments for Alzheimer's disease. Mechanistic modelling revealed cellular-level effects of Alzheimer's disease on cognition. Sensor-level mismatch negativity data met the criteria of a good biomarker: it was reliable and sensitive to disease, its severity and progression. MEG measures of mismatch negativity responses may consequently be a good marker of cognitive function for use in future clinical trials. Dynamic causal modelling revealed disease and therapeutic mechanisms. These models replicated findings from preclinical or *post mortem* studies, in people who are living with Alzheimer's disease. They supported the hypotheses of reduced pyramidal cell connectivity, impaired NMDA-channel kinetics and opposing cellular-level effects of disease and its therapeutics. These cellular-level disease effects were associated with disease severity and progression.

Future experimental studies can similarly tailor DCM analyses as illustrated in this thesis. First, identify DCM parameters indexing the target of interest and determine whether this target underlies neurophysiological deficits in people with Alzheimer's disease. Or vice versa: first identify mechanisms underlying deficits, then assess how effectively therapeutics target these mechanisms. A final, and crucial, future step will be to address whether therapeutic modification of these targets will improve cognition and, ultimately, the lives of people affected by Alzheimer's disease.

Bibliography

Adams B, Moghaddam B. Corticolimbic dopamine neurotransmission is temporally dissociated from the cognitive and locomotor effects of phencyclidine. J Neurosci 1998; 18: 5545–54.

Adams JN, Maass A, Harrison TM, Baker SL, Jagust WJ. Cortical tau deposition follows patterns of entorhinal functional connectivity in aging. Elife 2019; 8

Adams NE, Hughes LE, Phillips HN, Shaw AD, Murley AG, Nesbitt D, et al. GABA-ergic Dynamics in Human Frontotemporal Networks confirmed by Pharmaco-Magnetoencephalography. J Neurosci 2020; 40: 1640–9.

Adams NE, Hughes LE, Rouse MA, Phillips HN, Shaw AD, Murley AG, et al. GABAergic cortical network physiology in frontotemporal lobar degeneration. Brain 2021; 144: 2135–45.

Adams NE, Jafarian A, Perry A, Rouse MA, Shaw AD, Murley AG, et al. Neurophysiological consequences of synapse loss in progressive supranuclear palsy. Brain 2023; 146: 2584–94.

Agosta F, Rocca MA, Pagani E, Absinta M, Magnani G, Marcone A, et al. Sensorimotor network rewiring in mild cognitive impairment and Alzheimer's disease. Hum Brain Mapp 2010; 31: 515–25.

Ahmadlou M, Adeli A, Bajo R, Adeli H. Complexity of functional connectivity networks in mild cognitive impairment subjects during a working memory task. Clin Neurophysiol 2014; 125: 694–702.

Ahnaou A, Moechars D, Raeymaekers L, Biermans R, Manyakov N V., Bottelbergs A, et al. Emergence of early alterations in network oscillations and functional connectivity in a tau seeding mouse model of Alzheimer's disease pathology. Sci Rep 2017; 7: 1–14.

Albert MS, DeKosky ST, Dickson D, Dubois B, Feldman HH, Fox NC, et al. The diagnosis of mild cognitive impairment due to Alzheimer's disease: Recommendations from the National Institute on Aging-Alzheimer's Association workgroups on diagnostic guidelines for Alzheimer's disease. Alzheimers Dement 2011; 7: 270.

Allard S, Scardochio T, Cuello AC, Ribeiro-da-Silva A. Correlation of cognitive performance and morphological changes in neocortical pyramidal neurons in aging. Neurobiol Aging 2012; 33: 1466–80.

Alzheimer's Association. NIA-AA Revised Criteria for Diagnosis and Staging of Alzheimer's Disease [Internet]. NIA Alzheimer's Assoc 2023[cited 2024 Mar 18] Available from: https://aaic.alz.org/diagnostic-criteria.asp

Alzheimer A. Uber eine eigenartige Erkrankung der Hirnrinde. Allg Zeitschr f Psychiatr u Psych-Gerichtl Med 1907; 64: 146–8.

Amatniek JC, Hauser WA, DelCastillo-Castaneda C, Jacobs DM, Marder K, Bell K, et al. Incidence and predictors of seizures in patients with Alzheimer's disease. Epilepsia 2006; 47: 867–72.

American Psychiatric Association. Diagnostic and Statistical Manual of Mental Disorders [Internet]. Fifth. American Psychiatric Association; 2013[cited 2020 Apr 2] Available from: https://psychiatryonline.org/doi/book/10.1176/appi.books.9780890425596

Ametamey SM, Samnick S, Leenders KL, Vontobel P, Quack G, Parsons CG, et al. Fluorine-18 radiolabelling, biodistribution studies and preliminary PET evaluation of a new memantine derivative for imaging the NMDA receptor. In: Journal of Receptor and Signal Transduction Research. Taylor & Francis; 1999. p. 129–41

Anderson RM, Hadjichrysanthou C, Evans S, Wong MM. Why do so many clinical trials of therapies for Alzheimer's disease fail? Lancet 2017; 390: 2327–9.

Arriagada P V., Growdon JH, Hedley-Whyte ET, Hyman BT. Neurofibrillary tangles but not senile plaques parallel duration and severity of Alzheimer's disease. Neurology 1992; 42: 631–9.

Ashburner J. A fast diffeomorphic image registration algorithm. Neuroimage 2007; 38: 95–113.

Ashburner J, Friston KJ. Unified segmentation. Neuroimage 2005; 26: 839–51.

Ashton NJ, Brum WS, Molfetta G Di, Benedet AL, Arslan B, Jonaitis E, et al. Diagnostic Accuracy of a Plasma Phosphorylated Tau 217 Immunoassay for Alzheimer Disease Pathology. JAMA Neurol 2024; 81: 255–63.

Auksztulewicz R, Friston K. Attentional enhancement of auditory mismatch responses: A DCM/MEG study. Cereb Cortex 2015; 25: 4273–83.

Auksztulewicz R, Friston K. Repetition suppression and its contextual determinants in predictive coding. Cortex 2016; 80: 125.

Baik K, Jung JH, Jeong SH, Chung SJ, Yoo HS, Lee PH, et al. Implication of EEG theta/alpha and theta/beta ratio in Alzheimer's and Lewy body disease. Sci Reports 2022 121 2022; 12: 1–12.

Baker AP, Brookes MJ, Rezek IA, Smith SM, Behrens T, Smith PJP, et al. Fast transient networks in spontaneous human brain activity. Elife 2014; 2014

Baron JC, Chételat G, Desgranges B, Perchey G, Landeau B, De La Sayette V, et al. In vivo mapping of gray matter loss with voxel-based morphometry in mild Alzheimer's disease. Neuroimage 2001; 14: 298–309.

Barron HC, Auksztulewicz R, Friston K. Prediction and memory: A predictive coding account. Prog Neurobiol 2020; 192: 101821.

Başar E, Femir B, Emek-Savaş DD, Güntekin B, Yener GG. Increased long distance event-related gamma band connectivity in Alzheimer's disease. NeuroImage Clin 2017; 14: 580–90.

Bastin C, Delhaye E, Moulin C, Barbeau EJ. Novelty processing and memory impairment in Alzheimer's disease: A review. Neurosci Biobehav Rev 2019; 100: 237–49.

Bastos AM, Usrey WM, Adams RA, Mangun GR, Fries P, Friston KJ. Canonical Microcircuits for Predictive Coding. Neuron 2012; 76: 695–711.

Bejanin A, Schonhaut DR, La Joie R, Kramer JH, Baker SL, Sosa N, et al. Tau pathology and neurodegeneration contribute to cognitive impairment in Alzheimer's disease. Brain 2017; 140: 3286–300.

Bekinschtein TA, Dehaene S, Rohaut B, Tadel F, Cohen L, Naccache L. Neural signature of the conscious processing of auditory regularities. Proc Natl Acad Sci U S A 2009; 106: 1672–7.

Bennett RE, Robbins AB, Hu M, Cao X, Betensky RA, Clark T, et al. Tau induces blood vessel abnormalities and angiogenesis-related gene expression in P301L transgenic mice and human

Alzheimer's disease. Proc Natl Acad Sci U S A 2018; 115: E1289–98.

Bennys K, Portet F, Touchon J, Rondouin G. Diagnostic value of event-related evoked potentials N200 and P300 subcomponents in early diagnosis of Alzheimer's disease and mild cognitive impairment. J Clin Neurophysiol 2007; 24: 405–12.

Bennys K, Rondouin G, Benattar E, Gabelle A, Touchon J. Can event-related potential predict the progression of mild cognitive impairment? J Clin Neurophysiol 2011; 28: 625–32.

Berger H. Über das Elektrenkephalogramm des Menschen. Dtsch Medizinische Wochenschrift 1934; 60: 1947–9.

Bevan-Jones WR, Surendranathan A, Passamonti L, Rodríguez PV, Arnold R, Mak E, et al. Neuroimaging of inflammation in memory and related other disorders (NIMROD) study protocol: A deep phenotyping cohort study of the role of brain inflammation in dementia, depression and other neurological illnesses. BMJ Open 2017; 7

Billette O V., Ziegler G, Aruci M, Schütze H, Kizilirmak JM, Richter A, et al. Novelty-Related fMRI Responses of Precuneus and Medial Temporal Regions in Individuals at Risk for Alzheimer Disease. Neurology 2022; 99: E775–88.

Blackman J, Morrison HD, Gabb V, Biswas B, Li H, Turner N, et al. Remote evaluation of sleep to enhance understanding of early dementia due to Alzheimer's Disease (RESTED-AD): an observational cohort study protocol. BMC Geriatr 2023; 23

Blackwell AD, Sahakian BJ, Vesey R, Semple JM, Robbins TW, Hodges JR. Detecting dementia: Novel neuropsychological markers of preclinical Alzheimer's disease. Dement Geriatr Cogn Disord 2004; 17: 42–8.

Boly M, Garrido MI, Gosseries O, Bruno MA, Boveroux P, Schnakers C, et al. Preserved feedforward but impaired top-down processes in the vegetative state. Science (80-) 2011; 332: 858–62.

Bormann J. Memantine is a potent blocker of N-methyl-D-aspartate (NMDA) receptor channels. Eur J Pharmacol 1989; 166: 591–2.

Bowie CR, Harvey PD. Administration and interpretation of the Trail Making Test. Nat Protoc 2006; 1: 2277–81.

Braak H, Braak E. Neuropathological stageing of Alzheimer-related changes. Acta Neuropathol 1991; 82: 239–59.

Braak H, Braak E. Frequency of Stages of Alzheimer-Related Lesions in Different Age Categories. Neurobiol Aging 1997; 18: 351–7.

Braak H, Tredici K Del. Spreading of tau pathology in sporadic Alzheimer's disease along cortico-cortical top-down connections. Cereb Cortex 2018; 28: 3372–84.

Brenner RP, Ulrich RF, Spiker DG, Sclabassi RJ, Reynolds CF, Marin RS, et al. Computerized EEG spectral analysis in elderly normal, demented and depressed subjects. Electroencephalogr Clin Neurophysiol 1986; 64: 483–92.

Brito-Moreira J, C. Paula-Lima A, R. Bomfim T, F. Oliveira F, J. Sepulveda F, G. De Mello F, et al. Aβ oligomers induce glutamate release from hippocampal neurons. Curr Alzheimer Res 2011; 8: 552–62.

Bucci M, Chiotis K, Nordberg A. Alzheimer's disease profiled by fluid and imaging markers: tau PET best predicts cognitive decline. Mol Psychiatry 2021; 26: 5888–98.

Budd Haeberlein S, Aisen PS, Barkhof F, Chalkias S, Chen T, Cohen S, et al. Two Randomized Phase 3 Studies of Aducanumab in Early Alzheimer's Disease. J Prev Alzheimer's Dis 2022; 9: 197–210.

Bullich S, Roé-Vellvé N, Marquié M, Landau SM, Barthel H, Villemagne VL, et al. Early detection of amyloid load using 18F-florbetaben PET. Alzheimer's Res Ther 2021; 13: 1–15.

Busche MA, Eichhoff G, Adelsberger H, Abramowski D, Wiederhold KH, Haass C, et al. Clusters of hyperactive neurons near amyloid plaques in a mouse model of Alzheimer's disease. Science (80-) 2008; 321: 1686–9.

Busche MA, Hyman BT. Synergy between amyloid-β and tau in Alzheimer's disease. Nat Neurosci 2020 2310 2020; 23: 1183–93.

Buysse DJ, Reynolds CF, Monk TH, Berman SR, Kupfer DJ. The Pittsburgh sleep quality index: A new instrument for psychiatric practice and research. Psychiatry Res 1989; 28: 193–213.

Buzi G, Fornari C, Perinelli A, Mazza V. Functional connectivity changes in mild cognitive

impairment: A meta-analysis of M/EEG studies. Clin Neurophysiol 2023; 156: 183–95.

Cacciamani F, Salvadori N, Eusebi P, Lisetti V, Luchetti E, Calabresi P, et al. Evidence of practice effect in CANTAB spatial working memory test in a cohort of patients with mild cognitive impairment. Appl Neuropsychol 2018; 25: 237–48.

Cai L, Innis R, Pike V. Radioligand Development for PET Imaging of beta-Amyloid (AD)-Current Status. Curr Med Chem 2006; 14: 19–52.

Calamia M, Markon K, Tranel D. Scoring higher the second time around: Meta-analyses of practice effects in neuropsychological assessment. Clin Neuropsychol 2012; 26: 543–70.

Cambridge Cognition. CANTAB® [Cognitive assessment software]. 2019

Canuet L, Pusil S, López ME, Bajo R, Pineda-Pardo JÁ, Cuesta P, et al. Network disruption and cerebrospinal fluid amyloid-beta and phospho-tau levels in mild cognitive impairment. J Neurosci 2015; 35: 10325–30.

Carlson MD, Penney JB, Young AB. NMDA, AMPA, and benzodiazepine binding site changes in Alzheimer's disease visual cortex. Neurobiol Aging 1993; 14: 343–52.

Casagrande CC, Rempe MP, Springer SD, Wilson TW. Comprehensive review of task-based neuroimaging studies of cognitive deficits in Alzheimer's disease using electrophysiological methods. Ageing Res Rev 2023; 88: 101950.

Van Cauwenberghe C, Van Broeckhoven C, Sleegers K. The genetic landscape of Alzheimer disease: Clinical implications and perspectives. Genet Med 2016; 18: 421–30.

Chakroborty S, Hill ES, Christian DT, Helfrich R, Riley S, Schneider C, et al. Reduced presynaptic vesicle stores mediate cellular and network plasticity defects in an early-stage mouse model of Alzheimer's disease. Mol Neurodegener 2019; 14: 1–21.

Chang CH, Liu CY, Chen SJ, Tsai HC. Effect of N-methyl-d-aspartate receptor enhancing agents on cognition in dementia: an exploratory systematic review and meta-analysis of randomized controlled trials. Sci Rep 2021; 11: 22996.

Chang EH, Savage MJ, Flood DG, Thomas JM, Levy RB, Mahadomrongkul V, et al. AMPA receptor downscaling at the onset of Alzheimer's disease pathology in double knockin mice. Proc Natl Acad Sci U S A 2006; 103: 3410–5.

Chapman RM, McCrary JW, Gardner MN, Sandoval TC, Guillily MD, Reilly LA, et al. Brain ERP components predict which individuals progress to Alzheimer's disease and which do not. Neurobiol Aging 2011; 32: 1742–55.

Chen G, Chen P, Tan H, Ma D, Dou F, Feng J, et al. Regulation of the NMDA receptor-mediated synaptic response by acetylcholinesterase inhibitors and its impairment in an animal model of Alzheimer's disease. Neurobiol Aging 2008; 29: 1795–804.

Chen SD, Huang YY, Shen XN, Guo Y, Tan L, Dong Q, et al. Longitudinal plasma phosphorylated tau 181 tracks disease progression in Alzheimer's disease. Transl Psychiatry 2021; 11

Cheng CH, Wang PN, Hsu WY, Lin YY. Inadequate inhibition of redundant auditory inputs in Alzheimer's disease: An MEG study. Biol Psychol 2012; 89: 365–73.

Chennu S, Noreika V, Gueorguiev D, Blenkmann A, Kochen S, Ibáñez A, et al. Expectation and attention in hierarchical auditory prediction. J Neurosci 2013; 33: 11194–205.

Choi DW, Koh -y. J, Peters S. Pharmacology of glutamate neurotoxicity in cortical cell culture: Attenuation by NMDA antagonists. J Neurosci 1988; 8: 185–96.

Chumbley JR, Friston KJ, Fearn T, Kiebel SJ. A Metropolis-Hastings algorithm for dynamic causal models. Neuroimage 2007; 38: 478–87.

Coben LA, Danziger W, Storandt M. A longitudinal EEG study of mild senile dementia of Alzheimer type: changes at 1 year and at 2.5 years. Electroencephalogr Clin Neurophysiol 1985; 61: 101–12.

Coben LA, Danziger WL, Berg L. Frequency analysis of the resting awake EEG in mild senile dementia of Alzheimer type. Electroencephalogr Clin Neurophysiol 1983; 55: 372–80.

Collingridge GL, Isaac JTR, Yu TW. Receptor trafficking and synaptic plasticity. Nat Rev Neurosci 2004; 5: 952–62.

Coomans EM, Verberk IMW, Ossenkoppele R, Verfaillie SCJ, Visser D, Gouda M, et al. A Head-to-Head Comparison Between Plasma pTau181 and Tau PET Along the Alzheimer's Disease Continuum. J Nucl Med 2023; 64: 437–43.

Cope TE, Hughes LE, Phillips HN, Adams NE, Jafarian A, Nesbitt D, et al. Causal Evidence

for the Multiple Demand Network in Change Detection: Auditory Mismatch Magnetoencephalography across Focal Neurodegenerative Diseases. J Neurosci 2022; 42: 3197–215.

Cope TE, Rittman T, Borchert RJ, Jones PS, Vatansever D, Allinson K, et al. Tau burden and the functional connectome in Alzheimer's disease and progressive supranuclear palsy. Brain 2018; 141: 550–67.

Cuesta P, Garcés P, Castellanos NP, López ME, Aurtenetxe S, Bajo R, et al. Influence of the APOE ε4 allele and mild cognitive impairment diagnosis in the disruption of the MEG resting state functional connectivity in sources space. J Alzheimers Dis 2015; 44: 493–505.

Cummings J, Lee G, Mortsdorf T, Ritter A, Zhong K. Alzheimer's disease drug development pipeline: 2017. Alzheimer's Dement Transl Res Clin Interv 2017; 3: 367–84.

Cummings J, Zhou Y, Lee G, Zhong K, Fonseca J, Cheng F. Alzheimer's disease drug development pipeline: 2023. Alzheimer's Dement Transl Res Clin Interv 2023; 9

Cummings J, Zhou Y, Lee G, Zhong K, Fonseca J, Cheng F. Alzheimer's disease drug development pipeline: 2024. Alzheimer's Dement (New York, N Y) 2024; 10

Cummings JL, Goldman DP, Simmons-Stern NR, Ponton E. The costs of developing treatments for Alzheimer's disease: A retrospective exploration. Alzheimer's Dement 2022; 18: 469–77.

Cummings JL, Morstorf T, Zhong K. Alzheimer's disease drug-development pipeline: Few candidates, frequent failures. Alzheimer's Res Ther 2014; 6: 1–7.

Danysz W, Parsons CG. The NMDA receptor antagonist memantine as a symptomatological and neuroprotective treatment for Alzheimer's disease: Preclinical evidence. In: International Journal of Geriatric Psychiatry. John Wiley & Sons, Ltd; 2003. p. S23–32

Danysz W, Parsons CG. Alzheimer's disease, β-amyloid, glutamate, NMDA receptors and memantine - Searching for the connections. Br J Pharmacol 2012; 167: 324–52.

David O, Guillemain I, Saillet S, Reyt S, Deransart C, Segebarth C, et al. Identifying neural drivers with functional MRI: an electrophysiological validation. PLoS Biol 2008; 6

David O, Maess B, Eckstein K, Friederici AD. Dynamic Causal Modeling of Subcortical

Connectivity of Language. J Neurosci 2011; 31: 2712.

David O, Woźniak A, Minotti L, Kahane P. Preictal short-term plasticity induced by intracerebral 1 Hz stimulation. Neuroimage 2008; 39: 1633–46.

Davies P, Maloney AJF. Selective loss of central cholinergic neurons in Alzheimer's disease. Lancet 1976; 308: 1403.

van Dellen E, de Waal H, van der Flier WM, Lemstra AW, Slooter AJC, Smits LL, et al. Loss of EEG Network Efficiency Is Related to Cognitive Impairment in Dementia With Lewy Bodies. Mov Disord 2015; 30: 1785–93.

Deutschländer A, La Fougère C, Boetzel K, Albert NL, Gildehaus FJ, Bartenstein P, et al. Occupancy of pramipexole (Sifrol) at cerebral dopamine D2/3 receptors in Parkinson's disease patients. Neuroimage (Amst) 2016; 12: 41.

Dietz MJ, Friston KJ, Mattingley JB, Roepstorff A, Garrido MI. Effective connectivity reveals right-hemisphere dominance in audiospatial perception: Implications for models of spatial neglect. J Neurosci 2014; 34: 5003–11.

Dong B, Yue Y, Dong H, Wang Y. N-methyl-D-aspartate receptor hypofunction as a potential contributor to the progression and manifestation of many neurological disorders. Front Mol Neurosci 2023; 16

Donohue MC, Sperling RA, Salmon DP, Rentz DM, Raman R, Thomas RG, et al. The preclinical Alzheimer cognitive composite: Measuring amyloid-related decline. JAMA Neurol 2014; 71: 961–70.

Le Douce J, Maugard M, Veran J, Matos M, Jégo P, Vigneron PA, et al. Impairment of Glycolysis-Derived L-Serine Production in Astrocytes Contributes to Cognitive Deficits in Alzheimer's Disease. Cell Metab 2020; 31: 503-517.e8.

Douglas RJ, Martin KA. A functional microcircuit for cat visual cortex. J Physiol 1991; 440: 735–69.

Drummond E, Wisniewski T. Alzheimer's disease: experimental models and reality. Acta Neuropathol 2017; 133: 155–75.

Duff K, Humphreys Clark JD, O'Bryant SE, Mold JW, Schiffer RB, Sutker PB. Utility of the

RBANS in detecting cognitive impairment associated with Alzheimer's disease: Sensitivity, specificity, and positive and negative predictive powers. Arch Clin Neuropsychol 2008; 23: 603–12.

Dürschmid S, Reichert C, Kuhn J, Freund HJ, Hinrichs H, Heinze HJ. Deep brain stimulation of the nucleus basalis of Meynert attenuates early EEG components associated with defective sensory gating in patients with Alzheimer disease – a two-case study. Eur J Neurosci 2020; 51: 1201–9.

Emmerich CH, Gamboa LM, Hofmann MCJ, Bonin-Andresen M, Arbach O, Schendel P, et al. Improving target assessment in biomedical research: the GOT-IT recommendations. Nat Rev Drug Discov 2020 201 2020; 20: 64–81.

Engels MMA, van der Flier WM, Stam CJ, Hillebrand A, Scheltens P, van Straaten ECW. Alzheimer's disease: The state of the art in resting-state magnetoencephalography. Clin Neurophysiol 2017; 128: 1426–37.

Engels MMA, Stam CJ, van der Flier WM, Scheltens P, de Waal H, van Straaten ECW. Declining functional connectivity and changing hub locations in Alzheimer's disease: An EEG study. BMC Neurol 2015; 15: 1–8.

Erdfelder E, FAul F, Buchner A, Lang AG. Statistical power analyses using G*Power 3.1: Tests for correlation and regression analyses. Behav Res Methods 2009; 41: 1149–60.

Escott-Price V, Sims R, Bannister C, Harold D, Vronskaya M, Majounie E, et al. Common polygenic variation enhances risk prediction for Alzheimer's disease. Brain 2015; 138: 3673–84.

Escudero J, Hornero R, Poza J, Abásolo D, Fernández A. Assessment of classification improvement in patients with Alzheimer's disease based on magnetoencephalogram blind source separation. Artif Intell Med 2008; 43: 75–85.

Evans S, McRae-McKee K, Wong MM, Hadjichrysanthou C, De Wolf F, Anderson R. The importance of endpoint selection: How effective does a drug need to be for success in a clinical trial of a possible Alzheimer's disease treatment? Eur J Epidemiol 2018; 33: 635.

Fagan AM, Roe CM, Xiong C, Mintun MA, Morris JC, Holtzman DM. Cerebrospinal fluid tau/beta-amyloid(42) ratio as a prediction of cognitive decline in nondemented older adults.

Arch Neurol 2007; 64: 343–9.

Fathian A, Jamali Y, Raoufy MR, Weiner MW, Schuf N, Rosen HJ, et al. The trend of disruption in the functional brain network topology of Alzheimer's disease. Sci Reports 2022 121 2022; 12: 1–17.

Felleman DJ, Van Essen DC. Distributed hierarchical processing in the primate cerebral cortex. Cereb Cortex 1991; 1: 1–47.

Fernández A, Hornero R, Gómez C, Turrero A, Gil-Gregorio P, Matías-Santos J, et al. Complexity analysis of spontaneous brain activity in Alzheimer disease and mild cognitive impairment: an MEG study. Alzheimer Dis Assoc Disord 2010; 24: 182–9.

Fernández A, Maestú F, Amo C, Gil P, Fehr T, Wienbruch C, et al. Focal temporoparietal slow activity in Alzheimer's disease revealed by magnetoencephalography. Biol Psychiatry 2002; 52: 764–70.

Fernández A, Turrero A, Zuluaga P, Gil P, Maestú F, Campo P, et al. Magnetoencephalographic Parietal δ Dipole Density in Mild Cognitive Impairment: Preliminary Results of a Method to Estimate the Risk of Developing Alzheimer Disease. Arch Neurol 2006; 63: 427–30.

Ferrante M, Migliore M, Ascoli GA. Functional impact of dendritic branch-point morphology. J Neurosci 2013; 33: 2156–65.

Folch J, Busquets O, Ettcheto M, Sánchez-López E, Castro-Torres RD, Verdaguer E, et al. Memantine for the Treatment of Dementia: A Review on its Current and Future Applications. J Alzheimer's Dis 2018; 62: 1223.

Folstein MF, Folstein SE, McHugh PR. 'Mini-mental state'. A practical method for grading the cognitive state of patients for the clinician. J Psychiatr Res 1975; 12: 189–98.

Fox NC, Schott JM. Imaging cerebral atrophy: normal ageing to Alzheimer's disease. 2004; 363: 392–4.

Friedman LG, Mckeehan N, Hara Y, Cummings JL, Matthews DC, Zhu J, et al. Value-Generating Exploratory Trials in Neurodegenerative Dementias. Neurology 2021; 96: 944.

Frisoni GB, Fox NC, Jack CR, Scheltens P, Thompson PM. The clinical use of structural MRI

in Alzheimer disease. Nat Rev Neurol 2010; 6: 67–77.

Friston K. A theory of cortical responses. Philos Trans R Soc B Biol Sci 2005; 360: 815–36.

Friston K, Mattout J, Trujillo-Barreto N, Ashburner J, Penny W. Variational free energy and the Laplace approximation. Neuroimage 2007; 34: 220–34.

Friston KJ, Harrison L, Penny W. Dynamic causal modelling. Neuroimage 2003; 19: 1273–302.

Friston KJ, Litvak V, Oswal A, Razi A, Stephan KE, Van Wijk BCM, et al. Bayesian model reduction and empirical Bayes for group (DCM) studies. Neuroimage 2016; 128: 413–31.

Friston KJ, Preller KH, Mathys C, Cagnan H, Heinzle J, Razi A, et al. Dynamic causal modelling revisited. Neuroimage 2019; 199: 730–44.

Fruehwirt W, Dorffner G, Roberts S, Gerstgrasser M, Grossegger D, Schmidt R, et al. Associations of event-related brain potentials and Alzheimer's disease severity: A longitudinal study. Prog Neuropsychopharmacol Biol Psychiatry 2019; 92: 31–8.

Gao L, Chen J, Gu L, Shu H, Wang Z, Liu D, et al. Effects of gender and apolipoprotein E on novelty MMN and P3a in healthy elderly and amnestic mild cognitive Impairment. Front Aging Neurosci 2018; 10: 256.

Garcés P, Ángel Pineda-Pardo J, Canuet L, Aurtenetxe S, López ME, Marcos A, et al. The Default Mode Network is functionally and structurally disrupted in amnestic mild cognitive impairment — A bimodal MEG–DTI study. NeuroImage Clin 2014; 6: 214–21.

Garrido MI, Friston KJ, Kiebel SJ, Stephan KE, Baldeweg T, Kilner JM. The functional anatomy of the MMN: A DCM study of the roving paradigm. Neuroimage 2008; 42: 936–44.

Garrido MI, Kilner JM, Kiebel SJ, Stephan KE, Baldeweg T, Friston KJ. Repetition suppression and plasticity in the human brain. Neuroimage 2009; 48: 269–79.

Garrido MI, Kilner JM, Kiebel SJ, Stephan KE, Friston KJ. Dynamic causal modelling of evoked potentials: A reproducibility study. Neuroimage 2007; 36: 571–80.

Garrido MI, Kilner JM, Stephan KE, Friston KJ. The mismatch negativity: A review of underlying mechanisms. Clin Neurophysiol 2009; 120: 453–63.

Genin E, Hannequin D, Wallon D, Sleegers K, Hiltunen M, Combarros O, et al. APOE and

Alzheimer disease: A major gene with semi-dominant inheritance. Mol Psychiatry 2011; 16: 903–7.

Geula C, Mesulam MM. Systematic regional variations in the loss of cortical cholinergic fibers in Alzheimer's disease. Cereb Cortex 1996; 6: 165–77.

Giaquinto S, Nolfe G. The EEG in the normal elderly: a contribution to the interpretation of aging and dementia. Electroencephalogr Clin Neurophysiol 1986; 63: 540–6.

Gilbert JR, Galiano CS, Nugent AC, Zarate CA. Ketamine and Attentional Bias Toward Emotional Faces: Dynamic Causal Modeling of Magnetoencephalographic Connectivity in Treatment-Resistant Depression. Front Psychiatry 2021; 12: 673159.

Gilbert JR, Symmonds M, Hanna MG, Dolan RJ, Friston KJ, Moran RJ. Profiling neuronal ion channelopathies with non-invasive brain imaging and dynamic causal models: Case studies of single gene mutations. Neuroimage 2016; 124: 43–53.

Gilling KE, Jatzke C, Hechenberger M, Parsons CG. Potency, voltage-dependency, agonist concentration-dependency, blocking kinetics and partial untrapping of the uncompetitive N-methyl-d-aspartate (NMDA) channel blocker memantine at human NMDA (GluN1/GluN2A) receptors. Neuropharmacology 2009; 56: 866–75.

Giovannini MG, Mutolo D, Bianchi L, Michelassi A, Pepeu G. NMDA receptor antagonists decrease GABA outflow from the septum and increase acetylcholine outflow from the hippocampus: A microdialysis study. J Neurosci 1994; 14: 1358–65.

Gjini K, Casey C, Tanabe S, Bo A, Parker M, White M, et al. Greater tau pathology is associated with altered predictive coding. Brain Commun 2022; 4

Glenner GG, Wong CW. Alzheimer's disease: Initial report of the purification and characterization of a novel cerebrovascular amyloid protein. Biochem Biophys Res Commun 1984; 120: 885–90.

Goate A. Segregation of a missense mutation in the amyloid β-protein precursor gene with familial Alzheimer's disease. J Alzheimer's Dis 2006; 9: 341–7.

Gómez C, Hornero R, Abásolo D, Fernández A, López M. Complexity analysis of the magnetoencephalogram background activity in Alzheimer's disease patients. Med Eng Phys 2006; 28: 851–9.

Gonçalves MM, Pinho MS, Simões MR. Test–retest reliability analysis of the Cambridge neuropsychological automated tests for the assessment of dementia in older people living in retirement homes. Appl Neuropsychol 2016; 23: 251–63.

Gordon EB, Sim M. The EEG in presenile dementia. J Neurol Neurosurg Psychiatry 1967; 30: 285–91.

Götz J, Halliday G, Nisbet RM. Molecular Pathogenesis of the Tauopathies. Annu Rev Pathol Mech Dis 2019; 14: 239–61.

Govindpani K, Turner C, Waldvogel HJ, Faull RLM, Kwakowsky A. Impaired expression of gaba signaling components in the alzheimer's disease middle temporal gyrus. Int J Mol Sci 2020; 21: 1–19.

Grill JD, Karlawish J. Addressing the challenges to successful recruitment and retention in Alzheimer's disease clinical trials. Alzheimer's Res Ther 2010; 2: 1–11.

Grober E, Dickson D, Sliwinski MJ, Buschke H, Katz M, Crystal H, et al. Memory and mental status correlates of modified Braak staging. Neurobiol Aging 1999; 20: 573–9.

Grober E, Veroff AE, Lipton RB. Temporal unfolding of declining episodic memory on the Free and Cued Selective Reminding Test in the predementia phase of Alzheimer's disease: Implications for clinical trials. Alzheimer's Dement Diagnosis, Assess Dis Monit 2018; 10: 161–71.

De Haan W, Stam CJ, Jones BF, Zuiderwijk IM, Van Dijk BW, Scheltens P. Resting-state oscillatory brain dynamics in Alzheimer disease. J Clin Neurophysiol 2008; 25: 187–93.

Hanseeuw BJ, Betensky RA, Jacobs HIL, Schultz AP, Sepulcre J, Becker JA, et al. Association of Amyloid and Tau with Cognition in Preclinical Alzheimer Disease: A Longitudinal Study. JAMA Neurol 2019; 76: 915–24.

Hardy J, Allsop D. Amyloid deposition as the central event in the aetiology of Alzheimer's disease. Trends Pharmacol Sci 1991; 12: 383–8.

Hardy J, Bogdanovic N, Winblad B, Portelius E, Andreasen N, Cedazo-Minguez A, et al. Pathways to Alzheimer's disease. J Intern Med 2014; 275: 296–303.

Hartley T, Bird CM, Chan D, Cipolotti L, Husain M, Varga-Khadem F, et al. The hippocampus

is required for short-term topographical memory in humans. Hippocampus 2007; 17: 34–8.

Hata M, Kazui H, Tanaka T, Ishii R, Canuet L, Pascual-Marqui RD, et al. Functional connectivity assessed by resting state EEG correlates with cognitive decline of Alzheimer's disease - An eLORETA study. Clin Neurophysiol 2016; 127: 1269–78.

Heckers S, Geula C, Mesulam MM. Acetylcholinesterase-rich pyramidal neurons in alzheimer's disease. Neurobiol Aging 1992; 13: 455–60.

Hedges D, Janis R, Mickelson S, Keith C, Bennett DAVID, Brown BL. P300 Amplitude in Alzheimer's Disease. Clin EEG Neurosci 2016; 47: 48–55.

Henneges C, Reed C, Chen YF, Dell'Agnello G, Lebrec J. Describing the Sequence of Cognitive Decline in Alzheimer's Disease Patients: Results from an Observational Study. J Alzheimer's Dis 2016; 52: 1065–80.

Henstridge CM, Sideris DI, Carroll E, Rotariu S, Salomonsson S, Tzioras M, et al. Synapse loss in the prefrontal cortex is associated with cognitive decline in amyotrophic lateral sclerosis. Acta Neuropathol 2018; 135: 213–26.

Hilgetag CC, Burns GAPC, O'Neill MA, Scannell JW, Young MP. Anatomical connectivity defines the organization of clusters of cortical areas in the macaque monkey and the cat. Philos Trans R Soc B Biol Sci 2000; 355: 91.

Hillebrand A, Barnes GR. A quantitative assessment of the sensitivity of whole-head MEG to activity in the adult human cortex. Neuroimage 2002; 16: 638–50.

Hindriks R, van Putten MJAM. Thalamo-cortical mechanisms underlying changes in amplitude and frequency of human alpha oscillations. Neuroimage 2013; 70: 150–63.

Hodgkin AL, Huxley AF. Action potentials recorded from inside a nerve fibre. Nature 1939; 144: 710–1.

van Hoesen GW, Hyman BT, Damasio AR. Entorhinal cortex pathology in Alzheimer's disease. Hippocampus 1991; 1: 1–8.

Hof PR, Cox K, Morrison JH. Quantitative analysis of a vulnerable subset of pyramidal neurons in Alzheimer's disease: II. Primary and secondary visual cortex. J Comp Neurol 1990; 301: 55–64.

Holland D, Brewer JB, Hagler DJ, Fennema-Notestine C, Dale AM, Initiative the ADN, et al. Subregional neuroanatomical change as a biomarker for Alzheimer's disease. Proc Natl Acad Sci U S A 2009; 106: 20954.

Holland D, McEvoy LK, Dale AM. Unbiased comparison of sample size estimates from longitudinal structural measures in ADNI. Hum Brain Mapp 2012; 33: 2586–602.

Horvath A, Szucs A, Csukly G, Sakovics A, Stefanics G, Kamondi A. EEG and ERP biomarkers of Alzheimer's disease: A critical review. Front Biosci - Landmark 2018; 23: 183–220.

Howe AS, Bani-Fatemi A, De Luca V. The clinical utility of the auditory P300 latency subcomponent event-related potential in preclinical diagnosis of patients with mild cognitive impairment and Alzheimer's disease. Brain Cogn 2014; 86: 64–74.

Hsiao FJ, Chen WT, Wang PN, Cheng CH, Lin YY. Temporo-frontal functional connectivity during auditory change detection is altered in Alzheimer's disease. Hum Brain Mapp 2014; 35: 5565–77.

Hsieh S, Hodges JR, Leyton CE, Mioshi E. Longitudinal changes in primary progressive aphasias: Differences in cognitive and dementia staging measures. Dement Geriatr Cogn Disord 2012; 34: 135–41.

Huang C, Wahlund LO, Dierks T, Julin P, Winblad B, Jelic V. Discrimination of Alzheimer's disease and mild cognitive impairment by equivalent EEG sources: a cross-sectional and longitudinal study. Clin Neurophysiol 2000; 111: 1961–7.

Huang J, Jung JY, Nam CS. Estimating effective connectivity in Alzheimer's disease progression: A dynamic causal modeling study. Front Hum Neurosci 2022; 16

Hudd F, Shiel A, Harris M, Bowdler P, McCann B, Tsivos D, et al. Novel Blood Biomarkers that Correlate with Cognitive Performance and Hippocampal Volumetry: Potential for Early Diagnosis of Alzheimer's Disease. J Alzheimer's Dis 2019; 67: 931–47.

Hughes CP, Berg L, Danziger WL, Coben LA, Martin RL. A new clinical scale for the staging of dementia. Br J Psychiatry 1982; 140: 566–72.

Hughes LE, Henson RN, Pereda E, Bruña R, López-Sanz D, Quinn AJ, et al. Biomagnetic biomarkers for dementia: A pilot multicentre study with a recommended methodological

framework for magnetoencephalography. Alzheimer's Dement Diagnosis, Assess Dis Monit 2019; 11: 450–62.

Hughes LE, Nestor PJ, Hodges JR, Rowe JB. Magnetoencephalography of frontotemporal dementia: Spatiotemporally localized changes during semantic decisions. Brain 2011; 134: 2513–22.

Hughes LE, Rittman T, Regenthal R, Robbins TW, Rowe JB. Improving response inhibition systems in frontotemporal dementia with citalopram. Brain 2015; 138: 1961–75.

Hughes LE, Rittman T, Robbins TW, Rowe JB. Reorganization of cortical oscillatory dynamics underlying disinhibition in frontotemporal dementia. Brain 2018; 141: 2486–99.

Hughes LE, Rittman T, Robbins TW, Rowe JB. Reorganization of cortical oscillatory dynamics underlying disinhibition in frontotemporal dementia. Brain 2018; 141: 2486–99.

Hughes LE, Rowe JB. The impact of neurodegeneration on network connectivity: A study of change detection in frontotemporal dementia. J Cogn Neurosci 2013; 25: 802–13.

Hunt DL, Castillo PE. Synaptic plasticity of NMDA receptors: Mechanisms and functional implications. Curr Opin Neurobiol 2012; 22: 496–508.

Hynd MR, Scott HL, Dodd PR. Glutamate-mediated excitotoxicity and neurodegeneration in Alzheimer's disease. Neurochem Int 2004; 45: 583–95.

Iacobucci GJ, Popescu GK. NMDA receptors: Linking physiological output to biophysical operation. Nat Rev Neurosci 2017; 18: 236–49.

Ishihara T, Terada S. [Geriatric Depression Scale (GDS)]. Nihon Rinsho 2011; 69 Suppl 8: 455–8.

Ismail Z, Agüera-Ortiz L, Brodaty H, Cieslak A, Cummings J, Fischer CE, et al. The Mild Behavioral Impairment Checklist (MBI-C): A Rating Scale for Neuropsychiatric Symptoms in Pre-Dementia Populations. J Alzheimer's Dis 2017; 56: 929–38.

Ittner LM, Ke YD, Delerue F, Bi M, Gladbach A, van Eersel J, et al. Dendritic Function of Tau Mediates Amyloid-β Toxicity in Alzheimer's Disease Mouse Models. Cell 2010; 142: 387–97.

Jack CR, Bennett DA, Blennow K, Carrillo MC, Dunn B, Haeberlein SB, et al. NIA-AA Research Framework: Toward a biological definition of Alzheimer's disease. Alzheimer's

Dement 2018; 14: 535–62.

Jack CR, Knopman DS, Jagust WJ, Shaw LM, Aisen PS, Weiner MW, et al. Hypothetical model of dynamic biomarkers of the Alzheimer's pathological cascade. Lancet Neurol 2010; 9: 119–28.

Jack CR, Petersen RC, Xu Y, O'Brien PC, Smith GE, Ivnik RJ, et al. Rate of medial temporal lobe atrophy in typical aging and Alzheimer's disease. Neurology 1998; 51: 993–9.

Jacobs HIL, Van Boxtel MPJ, Jolles J, Verhey FRJ, Uylings HBM. Parietal cortex matters in Alzheimer's disease: an overview of structural, functional and metabolic findings. Neurosci Biobehav Rev 2012; 36: 297–309.

Jafarian A, Assem MK, Kocagoncu E, Lanskey JH, Williams R, Cheng Y-J, et al. Reliability of dynamic causal modelling of resting state magnetoencephalography. bioRxiv 2023: 2023.10.16.562379.

Jafarian A, Hughes LE, Adams NE, Lanskey JH, Naessens M, Rouse MA, et al. Neurochemistry-enriched dynamic causal models of magnetoencephalography, using magnetic resonance spectroscopy. Neuroimage 2023; 276: 120193.

Jahn H. Memory loss in Alzheimer's disease. Dialogues Clin Neurosci 2013; 15: 445–54.

Jansen BH, Rit VG. Electroencephalogram and visual evoked potential generation in a mathematical model of coupled cortical columns. Biol Cybern 1995; 73: 357–66.

Jeong J. EEG dynamics in patients with Alzheimer's disease. Clin Neurophysiol 2004; 115: 1490–505.

Ji LL, Zhang YY, Zhang LE, He B, Lu GH. Mismatch negativity (MMN) latency as a biomarker of amnestic mild cognitive impairment in Chinese rural elders. Front Aging Neurosci 2015; 7: 22.

Jiang S, Qu C, Wang F, Liu Y, Qiao Z, Qiu X, et al. Using event-related potential P300 as an electrophysiological marker for differential diagnosis and to predict the progression of mild cognitive impairment: a meta-analysis. Neurol Sci 2015; 36: 1105–12.

Jiang S, Yan C, Qiao Z, Yao H, Jiang S, Qiu X, et al. Mismatch negativity as a potential neurobiological marker of early-stage Alzheimer disease and vascular dementia. Neurosci Lett

2017; 647: 26–31.

Jonsson T, Atwal JK, Steinberg S, Snaedal J, Jonsson P V., Bjornsson S, et al. A mutation in APP protects against Alzheimer‘s disease and age-related cognitive decline. Nature 2012; 488: 96.

Jovicich J, Babiloni C, Ferrari C, Marizzoni M, Moretti D V., Del Percio C, et al. Two-Year Longitudinal Monitoring of Amnestic Mild Cognitive Impairment Patients with Prodromal Alzheimer's Disease Using Topographical Biomarkers Derived from Functional Magnetic Resonance Imaging and Electroencephalographic Activity. J Alzheimers Dis 2019; 69: 15–35.

Jürgensen S, Antonio LL, Mussi GEA, Brito-Moreira J, Bomfim TR, De Felice FG, et al. Activation of D1/D5 Dopamine Receptors Protects Neurons from Synapse Dysfunction Induced by Amyloid-β Oligomers. J Biol Chem 2010; 286: 3270.

Jutten RJ, Peeters CFW, Leijdesdorff SMJ, Visser PJ, Maier AB, Terwee CB, et al. Detecting functional decline from normal aging to dementia: Development and validation of a short version of the Amsterdam IADL Questionnaire. Alzheimer's Dement Diagnosis, Assess Dis Monit 2017; 8: 26–35.

Kamenetz F, Tomita T, Hsieh H, Seabrook G, Borchelt D, Iwatsubo T, et al. APP Processing and Synaptic Function. Neuron 2003; 37: 925–37.

Kaniyappan S, Chandupatla RR, Mandelkow EM, Mandelkow E. Extracellular low-n oligomers of tau cause selective synaptotoxicity without affecting cell viability. Alzheimer's Dement 2017; 13: 1270–91.

Karran E, De Strooper B. The amyloid hypothesis in Alzheimer disease: new insights from new therapeutics. Nat Rev Drug Discov 2022; 21: 306–18.

Kashyap G, Bapat D, Das D, Gowaikar R, Amritkar RE, Rangarajan G, et al. Synapse loss and progress of Alzheimer's disease -A network model. Sci Rep 2019; 9: 1–9.

Kaye JA, Swihart T, Howieson D, Dame A, Moore MM, Karnos T, et al. Volume loss of the hippocampus and temporal lobe in healthy elderly persons destined to develop dementia. Neurology 1997; 48: 1297–304.

Kehoe PG, Turner N, Howden B, Jarutyte L, Clegg SL, Malone IB, et al. Safety and efficacy of losartan for the reduction of brain atrophy in clinically diagnosed Alzheimer's disease (the

RADAR trial): a double-blind, randomised, placebo-controlled, phase 2 trial. Lancet Neurol 2021; 20: 895–906.

Kemp JA, McKernan RM. NMDA receptor pathways as drug targets. Nat Neurosci 2002; 5: 1039–42.

Kiebel SJ, Garrido MI, Friston KJ. Dynamic causal modelling of evoked responses: The role of intrinsic connections. Neuroimage 2007; 36: 332–45.

Kiebel SJ, Garrido MI, Moran RJ, Friston KJ. Dynamic causal modelling for EEG and MEG. Cogn Neurodyn 2008; 2: 121–36.

Kim B, Shin J, Kim YS, Choi JH. Destruction of ERP responses to deviance in an auditory oddball paradigm in amyloid infusion mice with memory deficits. PLoS One 2020; 15: e0230277.

Kimura T, Whitcomb DJ, Jo J, Regan P, Piers T, Heo S, et al. Microtubule-associated protein tau is essential for long-term depression in the hippocampus. Philos Trans R Soc B Biol Sci 2014; 369

Klaassens BL, van Gerven JMA, van der Grond J, de Vos F, Möller C, Rombouts SARB. Diminished posterior precuneus connectivity with the default mode network differentiates normal aging from Alzheimer's Disease. Front Aging Neurosci 2017; 9: 97.

Knight MJ, McCann B, Kauppinen RA, Coulthard EJ. Magnetic resonance imaging to detect early molecular and cellular changes in Alzheimer's disease. Front Aging Neurosci 2016; 8: 139.

Knight MJ, Wearn A, Coulthard E, Kauppinen RA. T2 Relaxometry and Diffusion Tensor Indices of the Hippocampus and Entorhinal Cortex Improve Sensitivity and Specificity of MRI to Detect Amnestic Mild Cognitive Impairment and Alzheimer's Disease Dementia. J Magn Reson Imaging 2019; 49: 445–55.

Knopman DS, Petersen RC, Jack CR. A brief history of 'Alzheimer disease': Multiple meanings separated by a common name. Neurology 2019; 92: 1053–9.

Kocagoncu E, Klimovich-Gray A, Hughes LE, Rowe JB. Evidence and implications of abnormal predictive coding in dementia. Brain 2021

Kocagoncu E, Nesbitt D, Emery T, Hughes LE, Henson RN, Rowe JB. Neurophysiological and Brain Structural Markers of Cognitive Frailty Differ from Alzheimer's Disease. J Neurosci 2022; 42: 1362–73.

Kocagoncu E, Quinn A, Firouzian A, Cooper E, Greve A, Gunn R, et al. Tau pathology in early Alzheimer's disease is linked to selective disruptions in neurophysiological network dynamics. Neurobiol Aging 2020; 92: 141–52.

Koelewijn L, Bompas A, Tales A, Brookes MJ, Muthukumaraswamy SD, Bayer A, et al. Alzheimer's disease disrupts alpha and beta-band resting-state oscillatory network connectivity. Clin Neurophysiol 2017; 128: 2347–57.

Koelewijn L, Lancaster TM, Linden D, Dima DC, Routley BC, Magazzini L, et al. Oscillatory hyperactivity and hyperconnectivity in young APOE-ε4 carriers and hypoconnectivity in alzheimer's disease. Elife 2019; 8

Koffie RM, Hyman BT, Spires-Jones TL. Alzheimer's disease: Synapses gone cold. Mol Neurodegener 2011; 6: 1–9.

Koo TK, Li MY. A Guideline of Selecting and Reporting Intraclass Correlation Coefficients for Reliability Research. J Chiropr Med 2016; 15: 155–63.

Koola MM, Nikiforuk A, Pillai A, Parsaik AK. Galantamine-memantine combination superior to donepezil-memantine combination in Alzheimer's disease: critical dissection with an emphasis on kynurenic acid and mismatch negativity. J Geriatr care Res 2018; 5: 57–67.

Kornhuber J, Bormann J, Retz W, Hübers M, Riederer P. Memantine displaces [3H]MK-801 at therapeutic concentrations in postmortem human frontal cortex. Eur J Pharmacol 1989; 166: 589–90.

Kosik KS, Joachim CL, Selkoe DJ. Microtubule-associated protein tau (τ) is a major antigenic component of paired helical filaments in Alzheimer disease. Proc Natl Acad Sci U S A 1986; 83: 4044–8.

Koychev I, Lawson J, Chessell T, Mackay C, Gunn R, Sahakian B, et al. Deep and Frequent Phenotyping study protocol: an observational study in prodromal Alzheimer's disease. BMJ Open 2019; 9: 24498.

Kurimoto R, Ishii R, Canuet L, Ikezawa K, Iwase M, Azechi M, et al. Induced oscillatory

responses during the Sternberg's visual memory task in patients with Alzheimer's disease and mild cognitive impairment. Neuroimage 2012; 59: 4132–40.

Laakso MP, Lehtovirta M, Partanen K, Riekkinen PJ, Soininen H. Hippocampus in Alzheimer's disease: A 3-year follow-up MRI study. Biol Psychiatry 1999; 47: 557–61.

Lacor PN, Buniel MC, Furlow PW, Clemente AS, Velasco PT, Wood M, et al. Aβ oligomer-induced aberrations in synapse composition, shape, and density provide a molecular basis for loss of connectivity in Alzheimer's disease. J Neurosci 2007; 27: 796–807.

LaFerla FM, Green KN. Animal models of Alzheimer disease. Cold Spring Harb Perspect Med 2012; 2: 1–13.

Lai CC, Lo H, Lin HG, Lin HH. Potentiation of NMDA-Mediated Responses by Amyloid-β Peptide 1-40 in Rat Sympathetic Preganglionic Neurons. J Alzheimers Dis 2019; 67: 1291–303.

Lai CL, Lin RT, Liou LM, Liu CK. The role of event-related potentials in cognitive decline in Alzheimer's disease. Clin Neurophysiol 2010; 121: 194–9.

Lansdall CJ, McDougall F, Butler LM, Delmar P, Pross N, Qin S, et al. Establishing Clinically Meaningful Change on Outcome Assessments Frequently Used in Trials of Mild Cognitive Impairment Due to Alzheimer's Disease. J Prev Alzheimer's Dis 2023; 10: 9–18.

Lanskey JH, Jafarian A, Karadag M, Kocagoncu E, Williams R, Yadav P, et al. The effect of Alzheimer's disease and its progression on pyramidal cell gain and connectivity. medRxiv 2024: 2024.04.11.24305662.

Lanskey JH, Kocagoncu E, Quinn AJ, Cheng Y-J, Karadag M, Pitt J, et al. New Therapeutics in Alzheimer's Disease Longitudinal Cohort study (NTAD): study protocol. BMJ Open 2022; 12: e055135.

Lanskey JH, McColgan P, Schrag AE, Acosta-Cabronero J, Rees G, Morris HR, et al. Can neuroimaging predict dementia in Parkinson's disease? Brain 2018

Lappe C, Steinsträter O, Pantev C. Rhythmic and melodic deviations in musical sequences recruit different cortical areas for mismatch detection. Front Hum Neurosci 2013; 7

Laptinskaya D, Thurm F, Küster OC, Fissler P, Schlee W, Kolassa S, et al. Auditory memory

decay as reflected by a new mismatch negativity score is associated with episodic memory in older adults at risk of dementia. Front Aging Neurosci 2018; 10: 5.

Larner AJ. Addenbrooke's Cognitive Examination-Revised (ACE-R) in day-to-day clinical practice [2]. Age Ageing 2007; 36: 685–6.

Lau CG, Zukin RS. NMDA receptor trafficking in synaptic plasticity and neuropsychiatric disorders. Nat Rev Neurosci 2007 86 2007; 8: 413–26.

Lee L, Friston K, Horwitz B. Large-scale neural models and dynamic causal modelling. Neuroimage 2006; 30: 1243–54.

Lee MS, Lee SH, Moon EO, Moon YJ, Kim S, Kim SH, et al. Neuropsychological correlates of the P300 in patients with Alzheimer's disease. Prog Neuro-Psychopharmacology Biol Psychiatry 2013; 40: 62–9.

Lee SH, Kim KR, Ryu SY, Son S, Hong HS, Mook-Jung I, et al. Impaired Short-Term Plasticity in Mossy Fiber Synapses Caused by Mitochondrial Dysfunction of Dentate Granule Cells Is the Earliest Synaptic Deficit in a Mouse Model of Alzheimer's Disease. J Neurosci 2012; 32: 5953.

Lejko N, Larabi DI, Herrmann CS, Aleman A, Ćurčić-Blake B. Alpha Power and Functional Connectivity in Cognitive Decline: A Systematic Review and Meta-Analysis. J Alzheimer's Dis 2020; 78: 1047–88.

Letemendia F, Pampiglione G. Clinical and electroencephalographic observations in Alzheimer's disease. J Neurol Neurosurg Psychiatry 1958; 21: 167–72.

Leung KK, Barnes J, Ridgway GR, Bartlett JW, Clarkson MJ, Macdonald K, et al. Automated cross-sectional and longitudinal hippocampal volume measurement in mild cognitive impairment and Alzheimer's disease. Neuroimage 2010; 51: 1345–59.

Leung KK, Bartlett JW, Barnes J, Manning EN, Ourselin S, Fox NC. Cerebral atrophy in mild cognitive impairment and Alzheimer disease: Rates and acceleration. Neurology 2013; 80: 648–54.

Leuzy A, Chiotis K, Lemoine L, Gillberg PG, Almkvist O, Rodriguez-Vieitez E, et al. Tau PET imaging in neurodegenerative tauopathies—still a challenge. Mol Psychiatry 2019; 24: 1112–34.

Lin CH, Chen PK, Chang YC, Chuo LJ, Chen YS, Tsai GE, et al. Benzoate, a D-amino acid oxidase inhibitor, for the treatment of early-phase Alzheimer disease: A randomized, double-blind, placebo-controlled trial. Biol Psychiatry 2014; 75: 678–85.

Lison H, Happel MFK, Schneider F, Baldauf K, Kerbstat S, Seelbinder B, et al. Disrupted cross-laminar cortical processing in β amyloid pathology precedes cell death. Neurobiol Dis 2014; 63: 62–73.

Litvak V, Jafarian A, Zeidman P, Tibon R, Henson RN, Friston K. There's no such thing as a 'true' model: The challenge of assessing face validity. Conf Proc - IEEE Int Conf Syst Man Cybern 2019; 2019-Octob: 4403–8.

Liu J, Chang L, Song Y, Li H, Wu Y. The role of NMDA receptors in Alzheimer's disease. Front Neurosci 2019; 13: 425433.

Long JM, Holtzman DM. Alzheimer Disease: An Update on Pathobiology and Treatment Strategies. Cell 2019; 179: 312.

Lopes da Silva F. EEG and MEG: Relevance to Neuroscience. Neuron 2013; 80: 1112–28.

López-Sanz D, Bruña R, de Frutos-Lucas J, Maestú F. Magnetoencephalography applied to the study of Alzheimer's disease. In: Progress in Molecular Biology and Translational Science. Academic Press; 2019. p. 25–61

López-Sanz D, Serrano N, Maestú F. The role of magnetoencephalography in the early stages of Alzheimer's disease. Front Neurosci 2018; 12: 1–8.

Louzada PR, Paula Lima AC, De Mello FG, Ferreira ST. Dual role of glutamatergic neurotransmission on amyloid β1-42 aggregation and neurotoxicity in embryonic avian retina. Neurosci Lett 2001; 301: 59–63.

Lu T, Aron L, Zullo J, Pan Y, Kim H, Chen Y, et al. REST and stress resistance in ageing and Alzheimer's disease. Nat 2014 5077493 2014; 507: 448–54.

Mackenzie IRA, Miller LA. Senile plaques in temporal lobe epilepsy. Acta Neuropathol 1994; 87: 504–10.

Maestú F, Cuesta P, Hasan O, Fernandéz A, Funke M, Schulz PE. The importance of the validation of M/EEG with current biomarkers in Alzheimer's disease. Front Hum Neurosci

2019; 13: 1–10.

Maestú F, Fernandez A, Simos PG, López-Ibor MI, Campo P, Criado J, et al. Profiles of brain magnetic activity during a memory task in patients with Alzheimer's disease and in non-demented elderly subjects, with or without depression. J Neurol Neurosurg Psychiatry 2004; 75: 1160–2.

Maestú F, Peña JM, Garcés P, González S, Bajo R, Bagic A, et al. A multicenter study of the early detection of synaptic dysfunction in Mild Cognitive Impairment using Magnetoencephalography-derived functional connectivity. NeuroImage Clin 2015; 9: 103–9.

Maji SK, Anoop A, Singh PK, Jacob RS. CSF biomarkers for Alzheimer's disease diagnosis. Int J Alzheimers Dis 2010; 2010

Malpetti M, Kievit RA, Passamonti L, Simon Jones P, Tsvetanov KA, Rittman T, et al. Microglial activation and tau burden predict cognitive decline in Alzheimer's disease. Brain 2020; 143: 1588–602.

Mandal PK, Banerjee A, Tripathi M, Sharma A. A Comprehensive Review of Magnetoencephalography (MEG) Studies for Brain Functionality in Healthy Aging and Alzheimer's Disease (AD). Front Comput Neurosci 2018; 12: 60.

Di Marco LY, Venneri A, Farkas E, Evans PC, Marzo A, Frangi AF. Vascular dysfunction in the pathogenesis of Alzheimer's disease - A review of endothelium-mediated mechanisms and ensuing vicious circles. Neurobiol Dis 2015; 82: 593–606.

Mazzo F, Zwart R, Serratto GM, Gardinier KM, Porter W, Reel J, et al. Reconstitution of synaptic Ion channels from rodent and human brain in Xenopus oocytes: a biochemical and electrophysiological characterization. J Neurochem 2016; 138: 384–96.

McKhann G, Drachman D, Folstein M, Katzman R, Price D, Stadlan EM. Clinical diagnosis of Alzheimer's disease: report of the NINCDS-ADRDA Work Group under the auspices of Department of Health and Human Services Task Force on Alzheimer's Disease. Neurology 1984; 34: 939–44.

McKhann GM, Knopman DS, Chertkow H, Hyman BT, Jack CR, Kawas CH, et al. The diagnosis of dementia due to Alzheimer's disease: Recommendations from the National Institute on Aging-Alzheimer's Association workgroups on diagnostic guidelines for

Alzheimer's disease. Alzheimer's Dement 2011; 7: 263–9.

McShane R, Westby MJ, Roberts E, Minakaran N, Schneider L, Farrimond LE, et al. Memantine for dementia. Cochrane Database Syst Rev 2019; 2019: 1–446.

Mehta D, Jackson R, Paul G, Shi J, Sabbagh M. Why do trials for Alzheimer's disease drugs keep failing? Expert Opin Investig Drugs 2017; 26: 735–9.

Mendes AJ, Ribaldi F, Lathuiliere A, Ashton NJ, Janelidze S, Zetterberg H, et al. Head-to-head study of diagnostic accuracy of plasma and cerebrospinal fluid p-tau217 versus p-tau181 and p-tau231 in a memory clinic cohort. J Neurol 2024; 3: 1–14.

Menkes-Caspi N, Yamin HG, Kellner V, Spires-Jones TL, Cohen D, Stern EA. Pathological tau disrupts ongoing network activity. Neuron 2015; 85: 959–66.

Merino-Serrais P, Benavides-Piccione R, Blazquez-Llorca L, Kastanauskaite A, Rábano A, Avila J, et al. The influence of phospho-tau on dendritic spines of cortical pyramidal neurons in patients with Alzheimer's disease. Brain 2013; 136: 1913–28.

Mijalkov M, Volpe G, Fernaud-Espinosa I, DeFelipe J, Pereira JB, Merino-Serrais P. Dendritic spines are lost in clusters in Alzheimer's disease. Sci Rep 2021; 11: 12350.

Mintun MA, Lo AC, Duggan Evans C, Wessels AM, Ardayfio PA, Andersen SW, et al. Donanemab in Early Alzheimer's Disease. N Engl J Med 2021; 384: 1691–704.

Mioshi E, Dawson K, Mitchell J, Arnold R, Hodges JR. The Addenbrooke's Cognitive Examination revised (ACE-R): A brief cognitive test battery for dementia screening. Int J Geriatr Psychiatry 2006; 21: 1078–85.

Moffat G, Zhukovsky P, Coughlan G, Voineskos AN. Unravelling the relationship between amyloid accumulation and brain network function in normal aging and very mild cognitive decline: a longitudinal analysis. Brain Commun 2022; 4

Moghaddam B, Adams B, Verma A, Daly D. Activation of glutamatergic neurotransmission by ketamine: a novel step in the pathway from NMDA receptor blockade to dopaminergic and cognitive disruptions associated with the prefrontal cortex. J Neurosci 1997; 17: 2921–7.

Mohammadian F, Noroozian M, Sadeghi AZ, Malekian V, Saffar A, Talebi M, et al. Effective Connectivity Evaluation of Resting-State Brain Networks in Alzheimer's Disease, Amnestic

Mild Cognitive Impairment, and Normal Aging: An Exploratory Study. Brain Sci 2023; 13

Mondadori CRA, Buchmann A, Mustovic H, Schmidt CF, Boesiger P, Nitsch RM, et al. Enhanced brain activity may precede the diagnosis of Alzheimer's disease by 30 years. Brain 2006; 129: 2908–22.

Monsell SE, Kukull WA, Roher AE, Maarouf CL, Serrano G, Beach TG, et al. Characterizing apolipoprotein E ε4 carriers and noncarriers with the clinical diagnosis of mild to moderate Alzheimer dementia and minimal β-amyloid peptide plaques. JAMA Neurol 2015; 72: 1124–31.

Montagne A, Nation DA, Sagare AP, Barisano G, Sweeney MD, Chakhoyan A, et al. APOE4 leads to blood–brain barrier dysfunction predicting cognitive decline. Nature 2020; 581: 71–6.

Moran RJ, Campo P, Symmonds M, Stephan KE, Dolan RJ, Friston KJ. Free energy, precision and learning: The role of cholinergic neuromodulation. J Neurosci 2013; 33: 8227–36.

Moran RJ, Stephan KE, Dolan RJ, Friston KJ. Consistent spectral predictors for dynamic causal models of steady-state responses. Neuroimage 2011; 55: 1694–708.

Moran RJ, Symmonds M, Dolan RJ, Friston KJ. The Brain Ages Optimally to Model Its Environment: Evidence from Sensory Learning over the Adult Lifespan. PLoS Comput Biol 2014; 10

Moran RJ, Symmonds M, Stephan KE, Friston KJ, Dolan RJ. An in vivo assay of synaptic function mediating human cognition. Curr Biol 2011; 21: 1320–5.

Morris JC. The clinical dementia rating (cdr): Current version and scoring rules. Neurology 1993; 43: 2412–4.

Morris JC, Storandt M, Miller JP, McKeel DW, Price JL, Rubin EH, et al. Mild cognitive impairment represents early-stage Alzheimer disease. Arch Neurol 2001; 58: 397–405.

Mowszowski L, Hermens DF, Diamond K, Norrie L, Cockayne N, Ward PB, et al. Cognitive training enhances pre-attentive neurophysiological responses in older adults 'at risk' of dementia. J Alzheimer's Dis 2014; 41: 1095–108.

Mowszowski L, Hermens DF, Diamond K, Norrie L, Hickie IB, Lewis SJG, et al. Reduced mismatch negativity in mild cognitive impairment: Associations with neuropsychological

performance. J Alzheimer's Dis 2012; 30: 209–19.

Murphy DGM, DeCarli CD, Daly E, Gillette JA, McIntosh AR, Haxby J V., et al. Volumetric magnetic resonance imaging in men with dementia of the Alzheimer type: Correlations with disease severity. Biol Psychiatry 1993; 34: 612–21.

Näätänen R, Pakarinen S, Rinne T, Takegata R. The mismatch negativity (MMN): Towards the optimal paradigm. Clin Neurophysiol 2004; 115: 140–4.

Nagori K, Pradhan M, Sharma M, Ajazuddin, Badwaik HR, Nakhate KT. Current Progress on Central Cholinergic Receptors as Therapeutic Targets for Alzheimer's Disease. Curr Alzheimer Res 2024; 21

Naj AC, Schellenberg GD. Genomic variants, genes, and pathways of Alzheimer's disease: An overview. Am J Med Genet Part B Neuropsychiatr Genet 2017; 174: 5–26.

Nakamura A, Cuesta P, Kato T, Arahata Y, Iwata K, Yamagishi M, et al. Early functional network alterations in asymptomatic elders at risk for Alzheimer's disease. Sci Rep 2017; 7

Nelson HE, Willison JR. National Adult Reading Test (NART): Test Manual (2nd edn). 1991

Nelson PT, Alafuzoff I, Bigio EH, Bouras C, Braak H, Cairns NJ, et al. Correlation of alzheimer disease neuropathologic changes with cognitive status: A review of the literature. J Neuropathol Exp Neurol 2012; 71: 362–81.

Neufang S, Akhrif A, Riedl V, Förstl H, Kurz A, Zimmer C, et al. Disconnection of frontal and parietal areas contributes to impaired attention in very early Alzheimer's disease. J Alzheimer's Dis 2011; 25: 309–21.

Newcomer JW, Farber NB, Olney JW. NMDA receptor function, memory, and brain aging. Dialogues Clin Neurosci 2000; 2: 219–32.

Nguyen T, Kim M, Gwak J, Lee JJ, Choi KY, Lee KH, et al. Investigation of brain functional connectivity in patients with mild cognitive impairment: A functional near-infrared spectroscopy (fNIRS) study. J Biophotonics 2019; 12

Niikura T, Tajima H, Kita Y. Neuronal Cell Death in Alzheimers Disease and a Neuroprotective Factor, Humanin. Curr Neuropharmacol 2006; 4: 139–47.

Oakley H, Cole SL, Logan S, Maus E, Shao P, Craft J, et al. Intraneuronal beta-amyloid

aggregates, neurodegeneration, and neuron loss in transgenic mice with five familial Alzheimer's disease mutations: potential factors in amyloid plaque formation. J Neurosci 2006; 26: 10129–40.

Olichney JM, Taylor JR, Gatherwright J, Salmon DP, Bressler AJ, Kutas M, et al. Patients with MCI and N400 or P600 abnormalities are at very high risk for conversion to dementia. Neurology 2008; 70: 1763–70.

Olney JW, Wozniak DF, Farber NB. Excitotoxic neurodegeneration in Alzheimer disease: New hypothesis and new therapeutic strategies. Arch Neurol 1997; 54: 1234–40.

Ortiz-Sanz C, Balantzategi U, Quintela-López T, Ruiz A, Luchena C, Zuazo-Ibarra J, et al. Amyloid β / PKC-dependent alterations in NMDA receptor composition are detected in early stages of Alzheimer´s disease. Cell Death Dis 2022 133 2022; 13: 1–12.

Ortner M, Drost R, Heddderich D, Goldhardt O, Müller-Sarnowski F, Diehl-Schmid J, et al. Amyloid PET, FDG-PET or MRI? - The power of different imaging biomarkers to detect progression of early Alzheimer's disease. BMC Neurol 2019; 19: 1–6.

Ossenkoppele R, Jansen WJ, Rabinovici GD, Knol DL, Van Der Flier WM, Van Berckel BNM, et al. Prevalence of Amyloid PET Positivity in Dementia Syndromes: A Meta-analysis HHS Public Access. JAMA 2015; 313: 1939–49.

Ossenkoppele R, Schonhaut DR, Schö M, Lockhart SN, Ayakta N, Baker SL, et al. Tau PET patterns mirror clinical and neuroanatomical variability in Alzheimer's disease. Brain 2016; 139: 1551–67.

Palmer AM, Gershon S. Is the neuronal basis of Alzheimer's disease cholinergic or glutamatergic? FASEB J 1990; 4: 2745–52.

Palop JJ, Chin J, Roberson ED, Wang J, Thwin MT, Bien-Ly N, et al. Aberrant Excitatory Neuronal Activity and Compensatory Remodeling of Inhibitory Hippocampal Circuits in Mouse Models of Alzheimer's Disease. Neuron 2007; 55: 697–711.

Palop JJ, Mucke L. Amyloid-B-induced neuronal dysfunction in Alzheimer's disease: From synapses toward neural networks. Nat Neurosci 2010; 13: 812–8.

Papadaniil CD, Kosmidou VE, Tsolaki A, Tsolaki M, Kompatsiaris I (Yiannis), Hadjileontiadis LJ. Cognitive MMN and P300 in mild cognitive impairment and Alzheimer's disease: A high

density EEG-3D vector field tomography approach. Brain Res 2016; 1648: 425–33.

Papaliagkas V, Kimiskidis V, Tsolaki M, Anogianakis G. Usefulness of event-related potentials in the assessment of mild cognitive impairment. BMC Neurosci 2008; 9: 1–10.

Papaliagkas VT, Kimiskidis VK, Tsolaki MN, Anogianakis G. Cognitive event-related potentials: Longitudinal changes in mild cognitive impairment. Clin Neurophysiol 2011; 122: 1322–6.

Parra MA, Ascencio LL, Urquina HF, Manes F, Ibáñez AM. P300 and neuropsychological assessment in mild cognitive impairment and alzheimer dementia. Front Neurol 2012; 3 DEC: 31552.

Parsons CG, Stöffler A, Danysz W. Memantine: a NMDA receptor antagonist that improves memory by restoration of homeostasis in the glutamatergic system - too little activation is bad, too much is even worse. Neuropharmacology 2007; 53: 699–723.

Passamonti L, Rodríguez PV, Hong YT, Allinson KSJ, Bevan-Jones WR, Williamson D, et al. PK11195 binding in Alzheimer disease and progressive supranuclear palsy. Neurology 2018; 90: e1989–96.

Passamonti L, Rodríguez PV, Hong YT, Allinson KSJ, Williamson D, Borchert RJ, et al. 18F-AV-1451 positron emission tomography in Alzheimer's disease and progressive supranuclear palsy. Brain 2017; 140: 781–91.

Paul SM, Mytelka DS, Dunwiddie CT, Persinger CC, Munos BH, Lindborg SR, et al. How to improve R&D productivity: the pharmaceutical industry's grand challenge. Nat Rev Drug Discov 2010; 9: 203–14.

Paula-Lima AC, Brito-Moreira J, Ferreira ST. Deregulation of excitatory neurotransmission underlying synapse failure in Alzheimer's disease. J Neurochem 2013; 126: 191–202.

Pegasiou CM, Zolnourian A, Gomez-Nicola D, Deinhardt K, Nicoll JAR, Ahmed AI, et al. Age-dependent changes in synaptic NMDA receptor composition in adult human cortical neurons. Cereb Cortex 2020; 30: 4246–56.

Pekkonen E, Hirvonen J, Jääskeläinen IP, Kaakkola S, Huttunen J. Auditory sensory memory and the cholinergic system: implications for Alzheimer's disease. Neuroimage 2001; 14: 376–82.

Pekkonen E, Jääskeläinen IP, Kaakkola S, Ahveninen J. Cholinergic modulation of preattentive auditory processing in aging. Neuroimage 2005; 27: 387–92.

Penny W, Iglesias-Fuster J, Quiroz YT, Lopera FJ, Bobes MA. Dynamic causal modeling of preclinical autosomal-dominant Alzheimer's disease. J Alzheimer's Dis 2018; 65: 697–711.

Penny WD, Stephan KE, Mechelli A, Friston KJ. Modelling functional integration: A comparison of structural equation and dynamic causal models. Neuroimage 2004; 23: 264–74.

Pérez-González D, Schreiner TG, Llano DA, Malmierca MS. Alzheimer's Disease, Hearing Loss, and Deviance Detection. Front Neurosci 2022; 16

Perry A, Hughes LE, Adams N, Naessens M, Murley AG, Rouse MA, et al. The neurophysiological effect of NMDA-R antagonism of frontotemporal lobar degeneration is conditional on individual GABA concentration. Transl Psychiatry 2022; 12

Perry RJ, Hodges JR. Attention and executive deficits in Alzheimer's disease. A critical review. Brain 1999; 122: 383–404.

Perszyk RE, Swanger SA, Shelley C, Khatri A, Fernandez-Cuervo G, Epplin MP, et al. Biased modulators of NMDA receptors control channel opening and ion selectivity. Nat Chem Biol 2020; 16: 188–96.

Phillips HN, Blenkmann A, Hughes LE, Bekinschtein TA, Rowe JB. Hierarchical Organization of Frontotemporal Networks for the Prediction of Stimuli across Multiple Dimensions. J Neurosci 2015; 35: 9255–64.

Phillips HN, Blenkmann A, Hughes LE, Kochen S, Bekinschtein TA, Cam CAN, et al. Convergent evidence for hierarchical prediction networks from human electrocorticography and magnetoencephalography. Cortex 2016; 82: 192–205.

Piastra MC, Nüßing A, Vorwerk J, Clerc M, Engwer C, Wolters CH. A comprehensive study on electroencephalography and magnetoencephalography sensitivity to cortical and subcortical sources. Hum Brain Mapp 2021; 42: 978–92.

Pinotsis DA, Geerts JP, Pinto L, FitzGerald THB, Litvak V, Auksztulewicz R, et al. Linking canonical microcircuits and neuronal activity: Dynamic causal modelling of laminar recordings. Neuroimage 2017; 146: 355–66.

Pinotsis DA, Schwarzkopf DS, Litvak V, Rees G, Barnes G, Friston KJ. Dynamic causal modelling of lateral interactions in the visual cortex. Neuroimage 2013; 66: 563–76.

Plowey ED, Bussiere T, Rajagovindan R, Sebalusky J, Hamann S, von Hehn C, et al. Alzheimer disease neuropathology in a patient previously treated with aducanumab. Acta Neuropathol 2022; 144: 143–53.

Pontecorvo MJ, Devous MD, Kennedy I, Navitsky M, Lu M, Galante N, et al. A multicentre longitudinal study of flortaucipir (18F) in normal ageing, mild cognitive impairment and Alzheimer's disease dementia. Brain 2019; 142: 1723–35.

Pontecorvo MJ, Devous MD, Navitsky M, Lu M, Salloway S, Schaerf FW, et al. Relationships between flortaucipir PET tau binding and amyloid burden, clinical diagnosis, age and cognition. Brain 2017; 140: 748–63.

Poza J, Hornero R, Abásolo D, Fernández A, García M. Extraction of spectral based measures from MEG background oscillations in Alzheimer's disease. Med Eng Phys 2007; 29: 1073–83.

Price JL, McKeel DW, Buckles VD, Roe CM, Xiong C, Grundman M, et al. Neuropathology of nondemented aging: Presumptive evidence for preclinical Alzheimer disease. Neurobiol Aging 2009; 30: 1026–36.

Price JL, Morris JC. Tangles and plaques in nondemented aging and 'preclinical' alzheimer's disease. Ann Neurol 1999; 45: 358–68.

Pruvost-Robieux E, Marchi A, Martinelli I, Bouchereau E, Gavaret M. Evoked and Event-Related Potentials as Biomarkers of Consciousness State and Recovery. J Clin Neurophysiol 2022; 39: 22–31.

Pusil S, López ME, Cuesta P, Bruña R, Pereda E, Maestú F. Hypersynchronization in mild cognitive impairment: the 'X' model. Brain 2019; 142: 3936–50.

Puttaert D, Coquelet N, Wens V, Peigneux P, Fery P, Rovai A, et al. Alterations in resting-state network dynamics along the Alzheimer's disease continuum. Sci Rep 2020; 10: 1–13.

Quiroz YT, Budson AE, Celone K, Ruiz A, Newmark R, Castrillõn G, et al. Hippocampal hyperactivation in presymptomatic familial Alzheimer's disease. Ann Neurol 2010; 68: 865–75.

Ramusino MC, Garibotto V, Bacchin R, Altomare D, Dodich A, Assal F, et al. Incremental value of amyloid-PET versus CSF in the diagnosis of Alzheimer's disease. Eur J Nucl Med Mol Imaging 2020; 47: 270–80.

Ranasinghe KG, Hinkley LB, Beagle AJ, Mizuiri D, Dowling AF, Honma SM, et al. Regional functional connectivity predicts distinct cognitive impairments in Alzheimer's disease spectrum. NeuroImage Clin 2014; 5: 385–95.

Randolph C, Tierney MC, Mohr E, Chase TN. The Repeatable Battery for the Assessment of Neuropsychological Status (RBANS): Preliminary clinical validity. J Clin Exp Neuropsychol 1998; 20: 310–9.

Rao YL, Ganaraja B, Murlimanju B V., Joy T, Krishnamurthy A, Agrawal A. Hippocampus and its involvement in Alzheimer's disease: a review. 3 Biotech 2022; 12: 55.

Rathore S, Habes M, Iftikhar MA, Shacklett A, Davatzikos C. A review on neuroimaging-based classification studies and associated feature extraction methods for Alzheimer's disease and its prodromal stages. Neuroimage 2017; 155: 530–48.

Raulin AC, Doss S V., Trottier ZA, Ikezu TC, Bu G, Liu CC. ApoE in Alzheimer's disease: pathophysiology and therapeutic strategies. Mol Neurodegener 2022; 17: 1–26.

Razi A, Kahan J, Rees G, Friston KJ. Construct validation of a DCM for resting state fMRI. Neuroimage 2015; 106: 1–14.

Rissman RA, Mobley WC. Implications for treatment: GABAA receptors in aging, Down syndrome and Alzheimer's disease. J Neurochem 2011; 117: 613–22.

Ritchie K, Ropacki M, Albala B, Harrison J, Kaye J, Kramer J, et al. Recommended cognitive outcomes in preclinical Alzheimer's disease: Consensus statement from the European Prevention of Alzheimer's Dementia project. Alzheimer's Dement 2017; 13: 186–95.

Rodríguez MJ, Robledo P, Andrade C, Mahy N. In vivo co-ordinated interactions between inhibitory systems to control glutamate-mediated hippocampal excitability. J Neurochem 2005; 95: 651–61.

Rogaev EI, Sherrington R, Rogaeva EA, Levesque G, Ikeda M, Liang Y, et al. Familial Alzheimer's disease in kindreds with missense mutations in a gene on chromosome 1 related to the Alzheimer's disease type 3 gene. Nature 1995; 376: 775–8.

Rosch RE, Auksztulewicz R, Leung PD, Friston KJ, Baldeweg T. Selective Prefrontal Disinhibition in a Roving Auditory Oddball Paradigm Under N-Methyl-D-Aspartate Receptor Blockade. Biol Psychiatry Cogn Neurosci Neuroimaging 2019; 4: 140–50.

Roselli F, Tirard M, Lu J, Hutzler P, Lamberti P, Livrea P, et al. Soluble β-Amyloid1-40 Induces NMDA-Dependent Degradation of Postsynaptic Density-95 at Glutamatergic Synapses. J Neurosci 2005; 25: 11061.

Rosen WG, Terry RD, Fuld PA, Katzman R, Peck A. Pathological verification of ischemic score in differentiation of dementias. Ann Neurol 1980; 7: 486–8.

Rossini PM, Di Iorio R, Vecchio F, Anfossi M, Babiloni C, Bozzali M, et al. Early diagnosis of Alzheimer's disease: the role of biomarkers including advanced EEG signal analysis. Report from the IFCN-sponsored panel of experts. Clin Neurophysiol 2020; 131: 1287–310.

De Rover M, Pironti VA, McCabe JA, Acosta-Cabronero J, Arana FS, Morein-Zamir S, et al. Hippocampal dysfunction in patients with mild cognitive impairment: A functional neuroimaging study of a visuospatial paired associates learning task. Neuropsychologia 2011; 49: 2060–70.

Rowe CC, Doré V, Jones G, Baxendale D, Mulligan RS, Bullich S, et al. 18F-Florbetaben PET beta-amyloid binding expressed in Centiloids. Eur J Nucl Med Mol Imaging 2017; 44: 2053–9.

Rowe JB, Hughes LE, Barker RA, Owen AM. Dynamic causal modelling of effective connectivity from fMRI: Are results reproducible and sensitive to Parkinson's disease and its treatment? Neuroimage 2010; 52: 1015–26.

Rozumna NM, Hanzha V V., Lukyanetz EA. Memantine protects the cultured rat hippocampal neurons treated by NMDA and amyloid β1-42. Front Neurosci 2023; 17

Rytsar R, Fornari E, Frackowiak RS, Ghika JA, Knyazeva MG. Inhibition in early Alzheimer's disease: An fMRI-based study of effective connectivity. Neuroimage 2011; 57: 1131–9.

Sabri O, Sabbagh MN, Seibyl J, Barthel H, Akatsu H, Ouchi Y, et al. Florbetaben PET imaging to detect amyloid beta plaques in Alzheimer's disease: Phase 3 study. Alzheimer's Dement 2015; 11: 964–74.

Salgado JF. Transforming the area under the normal curve (AUC) into cohen's d, pearson's

rpb, odds-ratio, and natural log odds-ratio: Two conversion tables. Eur J Psychol Appl to Leg Context 2018; 10: 35–47.

Sami S, Williams N, Hughes LE, Cope TE, Rittman T, Coyle-Gilchrist ITS, et al. Neurophysiological signatures of Alzheimer's disease and frontotemporal lobar degeneration: pathology versus phenotype. Brain 2018; 141: 2500–10.

Saransaari P, Oja SS. Taurine release from the developing and ageing hippocampus: Stimulation by agonists of ionotropic glutamate receptors. Mech Ageing Dev 1997; 99: 219–32.

Savolainen S, Karhu J, Pääkkönen A, Paljärvi L, Partanen J, Alafuzoff I, et al. Auditory event-related potentials differentiate patients with normal pressure hydrocephalus and patients with concomitant Alzheimer's disease verified by brain biopsy. Neuroreport 2001; 12: 33–7.

Scheltens P, De Strooper B, Kivipelto M, Holstege H, Chételat G, Teunissen CE, et al. Alzheimer's disease. Lancet 2021; 397: 1577–90.

Schneider LS, Mangialasche F, Andreasen N, Feldman H, Giacobini E, Jones R, et al. Clinical trials and late-stage drug development for Alzheimer's disease: An appraisal from 1984 to 2014. J Intern Med 2014; 275: 251–83.

Schöbi D, Homberg F, Frässle S, Endepols H, Moran RJ, Friston KJ, et al. Model-based prediction of muscarinic receptor function from auditory mismatch negativity responses. Neuroimage 2021; 237

Selkoe DJ. Alzheimer's disease is a synaptic failure. Science (80-) 2002; 298: 789–91.

Serrano N, López-Sanz D, Bruña R, Garcés P, Rodríguez-Rojo IC, Marcos A, et al. Spatiotemporal Oscillatory Patterns during Working Memory Maintenance in Mild Cognitive Impairment and Subjective Cognitive Decline. Int J Neural Syst 2020; 30

Seto M, Weiner RL, Dumitrescu L, Hohman TJ. Protective genes and pathways in Alzheimer's disease: moving towards precision interventions. Mol Neurodegener 2021; 16: 1–16.

Shankar GM, Bloodgood BL, Townsend M, Walsh DM, Selkoe DJ, Sabatini BL. Natural oligomers of the Alzheimer amyloid-β protein induce reversible synapse loss by modulating an NMDA-type glutamate receptor-dependent signaling pathway. J Neurosci 2007; 27: 2866–75.

Shanmugham S, Wetzel LC, Wetzel LC, Bellur S. The Relationship between EEG Changes and Cognitive Functions in Dementia: A Study in a VA Population. Clin EEG Neurosci 1989; 20: 77–85.

Shaw AD, Hughes LE, Moran R, Coyle-Gilchrist I, Rittman T, Rowe JB. In Vivo Assay of Cortical Microcircuitry in Frontotemporal Dementia: A Platform for Experimental Medicine Studies. Cereb Cortex 2019: 1–11.

Shaw AD, Hughes LE, Moran R, Coyle-Gilchrist I, Rittman T, Rowe JB. In vivo assay of cortical microcircuitry in frontotemporal dementia: A platform for experimental medicine studies. Cereb Cortex 2021; 31: 1837–47.

Shaw AD, Muthukumaraswamy SD, Saxena N, Sumner RL, Adams NE, Moran RJ, et al. Generative modelling of the thalamo-cortical circuit mechanisms underlying the neurophysiological effects of ketamine. Neuroimage 2020; 221: 117189.

Sitnikova TA, Hughes JW, Ahlfors SP, Woolrich MW, Salat DH. Short timescale abnormalities in the states of spontaneous synchrony in the functional neural networks in Alzheimer's disease. NeuroImage Clin 2018; 20: 128–52.

Sluimer JD, Van Der Flier WM, Karas GB, Van Schijndel R, Barnes J, Boyes RG, et al. Accelerating regional atrophy rates in the progression from normal aging to Alzheimer's disease. Eur Radiol 2009; 19: 2826–33.

Solomon A, Kivipelto M, Molinuevo JL, Tom B, Ritchie CW. European Prevention of Alzheimer's Dementia Longitudinal Cohort Study (EPAD LCS): Study protocol. BMJ Open 2018; 8

Song X, Jensen MO, Jogini V, Stein RA, Lee CH, McHaourab HS, et al. Mechanism of NMDA receptor channel block by MK-801 and memantine. Nature 2018; 556: 515–9.

Spielberger CD, Gorsuch RL, Lushene RE. Manual for the State-Trait Anxiety Inventory. 1970

Spires-Jones TL, Hyman BT. The Intersection of Amyloid Beta and Tau at Synapses in Alzheimer's Disease. Neuron 2014; 82: 756–71.

Stam CJ, Van Cappellen Van Walsum AM, Micheloyannis S. Variability of EEG synchronization during a working memory task in healthy subjects. Int J Psychophysiol 2002; 46: 53–66.

Stam CJ, Jones BF, Manshanden I, van Cappellen van Walsum AM, Montez T, Verbunt JPA, et al. Magnetoencephalographic evaluation of resting-state functional connectivity in Alzheimer's disease. Neuroimage 2006; 32: 1335–44.

Stanley K, Whitfield T, Kuchenbaecker K, Sanders O, Stevens T, Walker Z. Rate of cognitive decline in Alzheimer's disease stratified by age. J Alzheimer's Dis 2019; 69: 1153–60.

Stephan KE, Kasper L, Harrison LM, Daunizeau J, den Ouden HEM, Breakspear M, et al. Nonlinear dynamic causal models for fMRI. Neuroimage 2008; 42: 649–62.

Stephan KE, Penny WD, Daunizeau J, Moran RJ, Friston KJ. Bayesian model selection for group studies. Neuroimage 2009; 46: 1004–17.

Stothart G, Smith LJ, Milton A, Coulthard E. A passive and objective measure of recognition memory in Alzheimer's disease using Fastball memory assessment. Brain 2021; 144: 2812–25.

Sultzer DL, Melrose RJ, Harwood DG, Campa O, Mandelkern MA. Effect of memantine treatment on regional cortical metabolism in alzheimer's disease. Am J Geriatr Psychiatry 2010; 18: 606–14.

Świetlik D, Kusiak A, Ossowska A. Computational Modeling of Therapy with the NMDA Antagonist in Neurodegenerative Disease: Information Theory in the Mechanism of Action of Memantine. Int J Environ Res Public Health 2022; 19

Symmonds M, Moran CH, Leite MI, Buckley C, Irani SR, Stephan KE, et al. Ion channels in EEG: Isolating channel dysfunction in NMDA receptor antibody encephalitis. Brain 2018; 141: 1691–702.

Sze CI, Bi H, Kleinschmidt-DeMasters BK, Filley CM, Martin LJ. N-Methyl-d-aspartate receptor subunit proteins and their phosphorylation status are altered selectively in Alzheimer's disease. J Neurol Sci 2001; 182: 151–9.

Tait L, Stothart G, Coulthard E, Brown JT, Kazanina N, Goodfellow M. Network substrates of cognitive impairment in Alzheimer's Disease. Clin Neurophysiol 2019; 130: 1581–95.

Talwar P, Kushwaha S, Chaturvedi M, Mahajan V. Systematic Review of Different Neuroimaging Correlates in Mild Cognitive Impairment and Alzheimer's Disease. Clin Neuroradiol 2021; 31: 953–67.

Tampi RR, Forester BP, Agronin M. Aducanumab: Evidence from clinical trial data and controversies. Drugs Context 2021; 10

Tanner JA, Iaccarino L, Edwards L, Asken BM, Gorno-Tempini ML, Kramer JH, et al. Amyloid, tau and metabolic PET correlates of cognition in early and late-onset Alzheimer's disease. Brain 2022; 145: 4489–505.

Teng E, Manser PT, Sanabria Bohorquez S, Wildsmith KR, Pickthorn K, Baker SL, et al. Baseline [18F]GTP1 tau PET imaging is associated with subsequent cognitive decline in Alzheimer's disease. Alzheimer's Res Ther 2021; 13

Terry RD, Masliah E, Salmon DP, Butters N, DeTeresa R, Hill R, et al. Physical basis of cognitive alterations in alzheimer's disease: Synapse loss is the major correlate of cognitive impairment. Ann Neurol 1991; 30: 572–80.

Thangavel R, Sahu SK, Van Hoesen GW, Zaheer A. Modular and laminar pathology of Brodmann's area 37 in Alzheimer's disease. Neuroscience 2008; 152: 50–5.

The MathWorks Inc. Detect and remove outliers in data - MATLAB rmoutliers - MathWorks [Internet]. MathWorks 2023[cited 2024 Jan 4] Available from: https://uk.mathworks.com/help/matlab/ref/rmoutliers.html

Therriault J, Pascoal TA, Lussier FZ, Tissot C, Chamoun M, Bezgin G, et al. Biomarker modeling of Alzheimer's disease using PET-based Braak staging. Nat aging 2022; 2: 526–35.

Therriault J, Schindler SE, Salvadó G, Pascoal TA, Benedet AL, Ashton NJ, et al. Biomarker-based staging of Alzheimer disease: rationale and clinical applications. Nat Rev Neurol 2024 2024: 1–13.

Thijssen EH, La Joie R, Strom A, Fonseca C, Iaccarino L, Wolf A, et al. Plasma phosphorylated tau 217 and phosphorylated tau 181 as biomarkers in Alzheimer's disease and frontotemporal lobar degeneration: a retrospective diagnostic performance study. Lancet Neurol 2021; 20: 739–52.

Thompson PM, Hayashi KM, De Zubicaray G, Janke AL, Rose SE, Semple J, et al. Dynamics of gray matter loss in Alzheimer's disease. J Neurosci 2003; 23: 994–1005.

Tian Hui Kwan A, Arfaie S, Therriault J, Rosa-Neto P, Gauthier S. Lessons Learnt from the Second Generation of Anti-Amyloid Monoclonal Antibodies Clinical Trials. Dement Geriatr

Cogn Disord 2021; 49: 334–48.

Tierney TM, Holmes N, Mellor S, López JD, Roberts G, Hill RM, et al. Optically pumped magnetometers: From quantum origins to multi-channel magnetoencephalography. Neuroimage 2019; 199: 598–608.

Tikhonravov D, Neuvonen T, Pertovaara A, Savioja K, Ruusuvirta T, Näätänen R, et al. Effects of an NMDA-receptor antagonist MK-801 on an MMN-like response recorded in anesthetized rats. Brain Res 2008; 1203: 97–102.

Tomidokoro Y, Ishiguro K, Harigaya Y, Matsubara E, Ikeda M, Park JM, et al. Aβ amyloidosis induces the initial stage of tau accumulation in APPSw mice. Neurosci Lett 2001; 299: 169–72.

Tournier JD, Smith R, Raffelt D, Tabbara R, Dhollander T, Pietsch M, et al. MRtrix3: A fast, flexible and open software framework for medical image processing and visualisation. Neuroimage 2019; 202

Tyrer A, Gilbert JR, Adams S, Stiles AB, Bankole AO, Gilchrist ID, et al. Lateralized memory circuit dropout in Alzheimer's disease patients. Brain Commun 2020; 2

Tzioras M, McGeachan RI, Durrant CS, Spires-Jones TL. Synaptic degeneration in Alzheimer disease. Nat Rev Neurol 2022 191 2022; 19: 19–38.

Ułas J, Cotman CW. Decreased expression of N-methyl-D-aspartate receptor 1 messenger RNA in select regions of Alzheimer brain. Neuroscience 1997; 79: 973–82.

US Food and Drug Administration. FDA Grants Accelerated Approval for Alzheimer's Drug | FDA. FDA News Release 2021: 1–3.

US Food and Drug Administration. FDA Patient-Focused Drug Development Guidance Series for Enhancing the Incorporation of the Patient's Voice in Medical Product Development and Regulatory Decision Making [Internet]. 2022[cited 2024 Feb 19] Available from: https://www.fda.gov/drugs/development-approval-process-drugs/fda-patient-focused-drug-development-guidance-series-enhancing-incorporation-patients-voice-medical

Vandenberghe R, Adamczuk K, Laere K Van. The interest of amyloid PET imaging in the diagnosis of Alzheimer's disease. Curr Opin Neurol 2013; 26: 646–55.

Venegas C, Kumar S, Franklin BS, Dierkes T, Brinkschulte R, Tejera D, et al. Microglia-derived ASC specks crossseed amyloid-β in Alzheimer's disease. Nature 2017; 552: 355–61.

Venkataraman A V, Mansur A, Rizzo G, Bishop C, Lewis Y, Kocagoncu E, et al. Widespread cell stress and mitochondrial dysfunction in early Alzheimer's Disease. medRxiv 2021; 1051: 2021.08.11.21261851.

Verheijen J, Sleegers K. Understanding Alzheimer Disease at the Interface between Genetics and Transcriptomics. Trends Genet 2018; 34: 434–47.

Vidaurre D, Quinn AJ, Baker AP, Dupret D, Tejero-Cantero A, Woolrich MW. Spectrally resolved fast transient brain states in electrophysiological data. Neuroimage 2016; 126: 81–95.

Villemagne VL, Burnham S, Bourgeat P, Brown B, Ellis KA, Salvado O, et al. Amyloid β deposition, neurodegeneration, and cognitive decline in sporadic Alzheimer's disease: A prospective cohort study. Lancet Neurol 2013; 12: 357–67.

Villeneuve S, Rabinovici GD, Cohn-Sheehy BI, Madison C, Ayakta N, Ghosh PM, et al. Existing Pittsburgh Compound-B positron emission tomography thresholds are too high: statistical and pathological evaluation. Brain 2015; 138: 2020–33.

Visser PJ, Verhey FRJ, Hofman PAM, Scheltens P, Jolles J. Medial temporal lobe atrophy predicts Alzheimer's disease in patients with minor cognitive impairment. J Neurol Neurosurg Psychiatry 2002; 72: 491–7.

Wacongne C, Changeux JP, Dehaene S. A neuronal model of predictive coding accounting for the mismatch negativity. J Neurosci 2012; 32: 3665–78.

Wacongne C, Labyt E, Van Wassenhove V, Bekinschtein T, Naccache L, Dehaene S. Evidence for a hierarchy of predictions and prediction errors in human cortex. Proc Natl Acad Sci U S A 2011; 108: 20754–9.

Wales RM, Leung HC. The Effects of Amyloid and Tau on Functional Network Connectivity in Older Populations. Brain Connect 2021; 11: 599–612.

Wang L, Benzinger TL, Su Y, Christensen J, Friedrichsen K, Aldea P, et al. Evaluation of Tau imaging in staging Alzheimer disease and revealing interactions between β-Amyloid and tauopathy. JAMA Neurol 2016; 73: 1070–7.

Wang R, Reddy PH. Role of glutamate and NMDA receptors in Alzheimer's disease. J Alzheimers Dis 2017; 57: 1041.

Wang Z, Xia M, Dai Z, Liang X, Song H, He Y, et al. Differentially disrupted functional connectivity of the subregions of the inferior parietal lobule in Alzheimer's disease. Brain Struct Funct 2015; 220: 745–62.

Washington University Alzheimer's Disease Research Center. The CDR® Dementia Staging Instrument. SCALE 1999: 1.

Wearn AR, Nurdal V, Saunders-Jennings E, Knight MJ, Isotalus HK, Dillon S, et al. T2 heterogeneity: A novel marker of microstructural integrity associated with cognitive decline in people with mild cognitive impairment. Alzheimer's Res Ther 2020; 12: 1–14.

Wechsler D. Wechsler Adult Intelligence Scale - Revised. San Antonio, TX: Psychological Corporation; 1981

Wechsler D. Wechsler Memory Scale - Third UK Edition. London: Harcourt Assessment; 1999

Weggen S, Beher D. Molecular consequences of amyloid precursor protein and presenilin mutations causing autosomal-dominant Alzheimer's disease. Alzheimers Res Ther 2012; 4: 9.

Weiner H, Schuster DB. The electroencephalogram in dementia; some preliminary observations and correlations. Electroencephalogr Clin Neurophysiol 1956; 8: 479–88.

Weintraub S, Wicklund AH, Salmon DP. The neuropsychological profile of Alzheimer disease. Cold Spring Harb Perspect Med 2012; 2

Whitwell JL. Progression of atrophy in Alzheimer's disease and related disorders. Neurotox Res 2010; 18: 339–46.

De Wilde MC, Overk CR, Sijben JW, Masliah E. Meta-analysis of synaptic pathology in Alzheimer's disease reveals selective molecular vesicular machinery vulnerability. Alzheimer's Dement 2016; 12: 633–44.

Wilkinson D. A review of the effects of memantine on clinical progression in Alzheimer's disease. Int J Geriatr Psychiatry 2012; 27: 769–76.

Williams MM, Storandt M, Roe CM, Morris JC. Progression of Alzheimer's disease as measured by Clinical Dementia Rating Sum of Boxes scores. Alzheimer's Dement 2013; 9:

S39.

Witon A, Shirazibehehsti A, Cooke J, Aviles A, Adapa R, Menon DK, et al. Sedation Modulates Frontotemporal Predictive Coding Circuits and the Double Surprise Acceleration Effect. Cereb Cortex 2020; 30: 5204–17.

Woolrich MW, Baker A, Luckhoo H, Mohseni H, Barnes G, Brookes M, et al. Dynamic state allocation for MEG source reconstruction. Neuroimage 2013; 77: 77.

Wu SH, Ma CL, Kelly JB. Contribution of AMPA, NMDA, and GABAA Receptors to Temporal Pattern of Postsynaptic Responses in the Inferior Colliculus of the Rat. J Neurosci 2004; 24: 4625.

Xiao Z, Wu W, Ma X, Wu J, Liang X, Zhou X, et al. Plasma p-tau217, p-tau181, and NfL as early indicators of dementia risk in a community cohort: The Shanghai Aging Study. Alzheimer's Dement Diagnosis, Assess Dis Monit 2023; 15

Xu L, Zhou Y, Hu L, Jiang H, Dong Y, Shen H, et al. Deficits in N-Methyl-D-Aspartate Receptor Function and Synaptic Plasticity in Hippocampal CA1 in APP/PS1 Mouse Model of Alzheimer's Disease. Front Aging Neurosci 2021; 13

Xu M, Sanz DL, Garces P, Maestu F, Li Q, Pantazis Di. A Graph Gaussian Embedding Method for Predicting Alzheimer's Disease Progression with MEG Brain Networks. IEEE Trans Biomed Eng 2021; 68: 1579–88.

Yang FPG, Bal SS, Lee JF, Chen CC. White Matter Differences in Networks in Elders with Mild Cognitive Impairment and Alzheimer's Disease. Brain Connect 2021; 11: 180–8.

Yang L, Liu W, Shi L, Wu J, Zhang W, Chuang YA, et al. NMDA Receptor–Arc Signaling Is Required for Memory Updating and Is Disrupted in Alzheimer's Disease. Biol Psychiatry 2023; 94: 706–20.

Yiannopoulou KG, Anastasiou AI, Zachariou V, Pelidou SH. Reasons for failed trials of disease-modifying treatments for alzheimer disease and their contribution in recent research. Biomedicines 2019; 7

Yu M, Sporns O, Saykin AJ. The human connectome in Alzheimer disease — relationship to biomarkers and genetics. Nat Rev Neurol 2021 179 2021; 17: 545–63.

Zeidman P, Friston K, Parr T. A primer on Variational Laplace (VL). Neuroimage 2023; 279

Zeidman P, Jafarian A, Seghier ML, Litvak V, Cagnan H, Price CJ, et al. A guide to group effective connectivity analysis, part 2: Second level analysis with PEB. Neuroimage 2019; 200: 12–25.

Zhao Q, Sang X, Metmer H, Swati Z nawab NK, Lu J. Functional segregation of executive control network and frontoparietal network in Alzheimer's disease. Cortex 2019; 120: 36–48.

Zhukovsky P, Coughlan G, Buckley R, Grady C, Voineskos AN. Connectivity between default mode and frontoparietal networks mediates the association between global amyloid-β and episodic memory. Hum Brain Mapp 2023; 44: 1147.